TIME-DEPENDENT NONLINEAR CONTROL OF BIPEDAL ROBOTIC WALKING

A Dissertation

Submitted to the Faculty

of

Purdue University

by

Yan Gu

In Partial Fulfillment of the

Requirements for the Degree

of

Doctor of Philosophy

August 2017

Purdue University

West Lafayette, Indiana

THE PURDUE UNIVERSITY GRADUATE SCHOOL
STATEMENT OF DISSERTATION APPROVAL

Dr. Bin Yao, Co-Chair

School of Mechanical Engineering

Dr. C. S. George Lee, Co-Chair

School of Electrical and Computer Engineering

Dr. Gregory M. Shaver

School of Mechanical Engineering

Dr. Inseok Hwang

School of Aeronautics and Astronautics

Approved by:

Dr. Jay P. Gore

Head of the Graduate Program, School of Mechanical Engineering

To my mother, Wei Liao, for her endless love and support.

ACKNOWLEDGMENTS

I would like to first thank my co-advisors, Dr. Bin Yao and Dr. C. S. George Lee. They have given me the independence to discover my passion, the support to explore the beauty of controls and robotics, and the guidance to develop a meaningful career. Dr. Yao's broad, yet in-depth knowledge and understanding of controls and mechatronics has provided continual inspiration and intellectual support for my undergraduate research and my entire Ph.D. study. For creating a unique opportunity for me to work on bipedal robotic walking, for inspiring my interest in a wide range of engineering problems, and for helping me to develop my vision for future research directions, I am deeply grateful for Dr. Lee's advice and mentorship.

I would like to thank my current and former committee members: Dr. Geggory M. Shaver, Dr. Inseok Hwang, and Dr. Justin Seipel. Dr. Shaver has taught me many of the feedback control theories that I needed to shape the foundation of my dissertation research. Dr. Hwang's guidance on hybrid system control has contributed to every major result of my dissertation research. Dr. Seipel's insights on the mechanics of bipedal walking have helped to guide my understanding of biologically inspired robotic locomotion.

I would like to thank Dr. Shirley Rietdyk for many inspiring conversations on stability measure and motor control of human walking. I would like to thank Dr. Cagri A. Savran for providing great support for my career development. I would like to thank Dr. Galen B. King for sharing with me his rich knowledge of control theories and implementation, for inspiring me with his passion for research and teaching, and for many joyful conversations on a variety of topics.

I would like to thank Dr. Carl Zorowski at the North Carolina State University for encouraging me to enter graduate school in the U.S., for inspiring me with his life-long dedication to education, and for showing me what a truly meaningful life is. I would like to thank Dr. Jessy W. Grizzle at the University of Michigan for his valuable comments on

my Ph.D. dissertation research and his advice for my future research directions. I would like to thank Dr. Bo Cheng at the Pennsylvania State University for providing his constant encouragement and constructive guidance during my entire graduate years. I would like to thank Dr. Lu Lu at the New Jersey Institute of Technology for his continuous support for my study and research in the last six years. I would like to thank Dr. Zhenghui Sha at the University of Arkansas for selflessly providing me with his great help for my job searching.

For creating a supportive environment for my Ph.D. study, I would like to thank my labmates of ARTLab: Manas Paldhe, Keerthi Raj Nagaraja, Ashesh Goswami, Dabesmit Das, Rohan Sarkar, Vishveswaran Jothi, Jihoon Moon, Yue Cao, and Joonhyeok Yoon. Special thanks go to Andy Hyungju Park and Roy Kai-Chi Chan for being my fantastic mentors during my early graduate years. I would also like to thank Xingye Da at the University of Michigan for many stimulating conversations on bipedal walking control.

I would like to thank my friends for being my wonderful companions in learning and exploring life. I would like to thank my mother, Wei Liao, who always inspires me with her unparalleled sense of enthusiasm for life. Her unwavering belief in my ability is the greatest gift in my life. I would like to thank my grandparents, Wenbo Gu and Shujie Wang, for their unconditional love and supports.

Finally, I would like to thank Yu Wang for being my best friend and making my life full of joy.

TABLE OF CONTENTS

Page

Page

LIST OF TABLES

LIST OF FIGURES

ABSTRACT

Gu, Yan PhD, Purdue University, August 2017. Time-dependent Nonlinear Control of Bipedal Robotic Walking . Major Professors: Bin Yao, School of Mechanical Engineering and C. S. George Lee, School of Electrical and Computer Engineering.

Although bipedal walking control has been extensively studied for the past forty years, it remains a challenging task. To achieve high-performance bipedal robotic walking, this dissertation studies and investigates control strategies for both fully actuated and underactuated bipedal robots based on nonlinear control theories and formal stability analysis.

Previously, the Hybrid-Zero-Dynamics (HZD) framework, which is a state-based feedback controller design based on the full-order dynamic modeling and the input-output linearization, has successfully realized stable, agile, and efficient bipedal walking for both fully actuated and underactuated bipedal robotic walking. However, the critical issue of achieving high walking versatility has not been fully addressed by the HZD framework. In this dissertation, we propose and develop a time-dependent controller design methodology to achieve not only stable, agile, and efficient but also versatile bipedal walking for fully actuated bipeds. Furthermore, the proposed time-dependent approach can be used to achieve better walking robustness to implementation imperfections for both fully actuated and underactuated bipeds by effectively solving the high-sensitivity issue of the state-based approaches to sensor noises.

In our controller design methodology, the full-order hybrid walking dynamics are first modeled, which consist of both continuous-time dynamics and rigid-body impact dynamics. Then, the desired path/motion for a biped to track is planned, and the output function is designed as the tracking error of the desired path/motion. Based on the full-order model of walking dynamics, the input-output linearization is utilized to synthesize a controller that exponentially drives the output function to zero during continuous phases. Finally, sufficient conditions are developed to evaluate the stability of the hybrid, time-varying

closed-loop control system. By enforcing these conditions, stable bipedal walking can be automatically realized, and the desired motion can be satisfactorily followed.

Both full actuation and underactuation are common in bipedal robotic walking. Full actuation occurs when the number of degrees of freedom equals the number of independent actuators while underactuation occurs when the number of degrees of freedom is greater than the number of independent actuators. Because a fully actuated biped can directly control each of its joints, more objectives may be achieved for a fully actuated biped than an underactuated one. In this dissertation, the exponential tracking of a straight-line contour in Cartesian space is achieved for both planar and three-dimensional (3-D) walking, which greatly improves the versatility of fully actuated bipedal robots. To guarantee the closed-loop stability, the *first* sufficient stability conditions are developed based on the construction of multiple Lyapunov functions.

Underactuated walking is much more difficult to control than fully actuated walking because an underactuated biped cannot directly control each of its joints. In this dissertation, control design of periodic, underactuated walking is investigated, and the *first* set of sufficient conditions for time-dependent orbitally exponential stabilization is established based on time-dependent nonlinear feedback control. Without modifications, the proposed controller design can be directly applied to both planar and 3-D bipeds that are subject to either underactuation or full actuation.

Extensive computer simulation results validated the proposed time-dependent controller design methodology for bipedal robotic walking. Specifically, three bipedal models were simulated: one was a fully actuated, planar bipedal model with three revolute joints, one was a fully actuated, 3-D bipedal model with nine revolute joints, and one was an underactuated, planar bipedal model with five revolute joints.

1. INTRODUCTION

1.1 Motivation

There have been ever increasingly extensive studies on bipedal robotic walking since 1970's [1], and there are several critical reasons for its growing popularity. First, the form of bipedal robotic locomotion can adapt to the human environment without significant modifications of existing facilities [2]. Second, bipedalism is dexterous in addressing uneven terrains, narrow passageways [2], and environments with discontinuous supports [3]. Third, studying bipedal robotic walking may enhance our understanding of human and bipedal animal walking [4]. Finally, bipedal robots are potentially crucial to applications such as entertainment, education, disaster response and rescue [3], and space exploration [5].

Stability, versatility, agility, and efficiency are the four main performance indices that measure the effectiveness of legged locomotion control. For the purpose of operation safety, guaranteeing walking stability has the top priority. Walking stability can be loosely defined as the ability to avoid a fall [6]. Versatility is another important index in evaluating the locomotion capabilities of a legged robot. To accomplish complex tasks such as disaster response and rescue, it is critical that a robot is capable of versatile locomotion such as satisfactorily tracking a planned path on the walking surface. Besides stability and versatility, agility and energy efficiency are also important performance indices because it is desirable that a legged robot can sustain high-speed walking on batteries for a long period. Here, agility is measured by walking velocity, and the energy cost of walking is measured by the integral-squared motor torque per step distance [7].

Impressive bipedal walking performance has been demonstrated on today's most successful bipedal robots, including ATLAS (developed by Boston Dynamics) [8], ATRIAS [9] and MARLO [10] (Oregon State University, University of Michigan, and Carnegie Mellon University), ASIMO (Honda) [11], HRP (AIST) [12], HUBO (KAIST) [13], and Valkyrie

(NASA) [5]. However, their walking performance is still far from satisfactory for completing complex tasks in the real world, and bipedal walking control remains a highly challenging problem.

There are several contributing factors to the difficulty of controller design in achieving stable, versatile, agile, and efficient bipedal robotic walking. First, a bipedal robot typically has high degrees of freedom, which results in a high computational load in both motion planning and control implementation. For example, a HUBO-2 humanoid robot has 38 independent joints. Second, a bipedal robot has a non-fixed base. Its support foot can slip on the walking surface, and it can easily fall over. Therefore, the feasible actuation capacity has to be severely limited to maintain the full, static contact between the support foot and the walking surface [14]. In contrast, an industrial manipulator with its base fixed to the supporting surface never tips over its base edge. Third, bipedal walking dynamics are hybrid, which adds to the complexity of control design. The walking dynamics are described by usual differential equations in the continuous-time domain when one foot swings in the air and the other is in support, and by instantaneous reset maps in the discrete-time domain for impact dynamics during foot landing and switching of support foot. Finally, bipedal robotic walking can sometimes be underactuated. Underactuation occurs when the number of independent actuators is less than that of degrees of freedom. For example, when a biped's support foot rolls about its edge, underactuation happens. The lack of actuators to control each joint may greatly increase the difficulty of controller design for underactuated bipeds.

In this dissertation, our focus centers on the development of a time-dependent controller design methodology that realizes high-performance walking for both fully actuated and underactuated bipedal robots based on full-order dynamic modeling, time-dependent nonlinear control design, and formal stability analysis.

1.2 Literature Survey

To provide a context for the content of this dissertation, a few of the more dominant control strategies of bipedal robotic walking will be reviewed in this section. Because guaranteeing walking stability is the top priority in walking control design, different measures of walking stability have been proposed, and different control strategies have been developed based on these measures [15]. Three groups of such control strategies will be reviewed, including the Zero-Moment Point Approach, the Capture-Point Approach, and the Hybrid-Zero-Dynamics Framework.

As this literature survey is not intended to be exhaustive, we will focus on reviewing three of the most widely applied control strategies for bipedal robotic walking. Some of the other interesting and important bipedal walking control strategies will not be reviewed, including: Marc Raibert's robotic hopper control [16] [17], virtual model control [18], passivity-based walking control [19] [20], learning-based walking control [21] [22], reduction-based walking control [23] [24] [25] [26], intuitive control design based on the spring-loaded inverted pendulum (SLIP) model [27] [28], walking control based on sums of squares [29] [30], and optimization-based planning and control [2] [31] [32] [33] [34] [35] [36].

1.2.1 Definition of Walking Stability

Before reviewing the previous work on stability measure and bipedal walking control, we will first review the previously proposed definition of bipedal walking stability.

Wieber [37] first introduced viability [38] into the research area of legged robotic locomotion. Later on, Pratt and Tedrake [6] introduced the definition of walking stability based on viability.

Fall - When a point on the biped, other than a point on the feet of the biped, touches the ground [6].

Viability - A state is viable if and only if starting from this state the system is able to realize a movement that never gets inside the basin of fall, which is the set of positions where the system is considered as having fallen [37].

Stability - A biped is stable if and only if the state of the robot is not inside the basin of fall [6].

Being equivalent to viability, the above definition essentially states that walking stability is the ability to avoid a fall during the walking process. However, evaluating the viability of a certain state is too computationally expensive to be feasible for the real-world applications [6] [39]. Also, this definition of walking stability is overly vague. It does not explicitly include many factors related to walking stability such as modeling errors, disturbances, controller performance, joint limits, and ground-contact constraints.

In addition to viability, various balance criteria have been proposed for bipedal robotic walking, which will be briefly reviewed next:

1. Among these balance criteria, the most widely used one is the Zero-Moment Point (ZMP) balance criterion [40] [41] [42], which has been utilized to realize bipedal walking on various humanoid robot platforms such as ASIMO [11], HRP [43], and HUBO [13]. There are other point-based balance indicators, including Foot Rotation Indicator (FRI) [44] [45] and Centroidal Moment Pivot (CMP) [46] [47] [48]. However, all of these three balance indicators only evaluate the state of balance for a biped but not a biped's walking stability. Also, previous walking strategies often utilize these balance indicators to guarantee stable walking with accurate joint trajectory tracking, which can only achieve conservative walking performance.

2. Later on, capturability [6] [49] was proposed as a computationally less expensive approximation of viability based on the concept of Capture Point (CP). Because the capturability measure only provides a sufficient condition of walking stability, it is not an ideal stability measure, and it will also lead to conservative walking performance.

3. Stability of periodic walking has been evaluated by the orbital stability of the dynamical walking system. For example, the stability of a passive walker is determined by the stability of the orbit that is generated by the robot's periodic motion [39], and the stability of an actuated biped can be determined by that of the orbit of the closed-loop dynamics [7] [50]. Because this stability evaluation method only applies to periodic walking, its generality is severely limited.

In this dissertation research, a walking process is considered stable if there exists a feasible walking motion that satisfies walking dynamics and necessary constraints (e.g., joint limits, actuation limits, ground-contact constraints) such that a biped, with only its feet touching and detaching from the ground, is able to track this motion in the presence of modeling errors, disturbances, and initial tracking errors.

With this proposed definition of walking stability, we will review the previous walking strategies including the ZMP-based approach, the capturability-based approach, and the Hybrid-Zero-Dynamics framework.

In the following reviews, only horizontal even terrains are considered.

1.2.2 Zero-Moment Point

Before reviewing the previous walking strategies based on the Zero-Moment Point balance criterion, we will first review the definition of Zero-Moment Point and the ZMP balance criterion.

Zero-Moment Point - A Zero-Moment Point (ZMP) is a point about which the sum of all horizontal moments of active forces is equal to zero [41].

ZMP Balance Criterion - A walking robot is balanced when and only when the ZMP trajectory remains strictly within the support polygon [41].

On horizontal even terrains, the equation of motion of a bipedal walker in Cartesian space can be written with respect to the world coordinate frame (See Fig. 1.1):

$$\overrightarrow{OP_{CoP}} \times \mathbf{F}_R + \overrightarrow{OG} \times m\mathbf{g} + \mathbf{M}_z = \overrightarrow{OG} \times m\mathbf{a}_G + \dot{\mathbf{H}}_G, \tag{1.1}$$

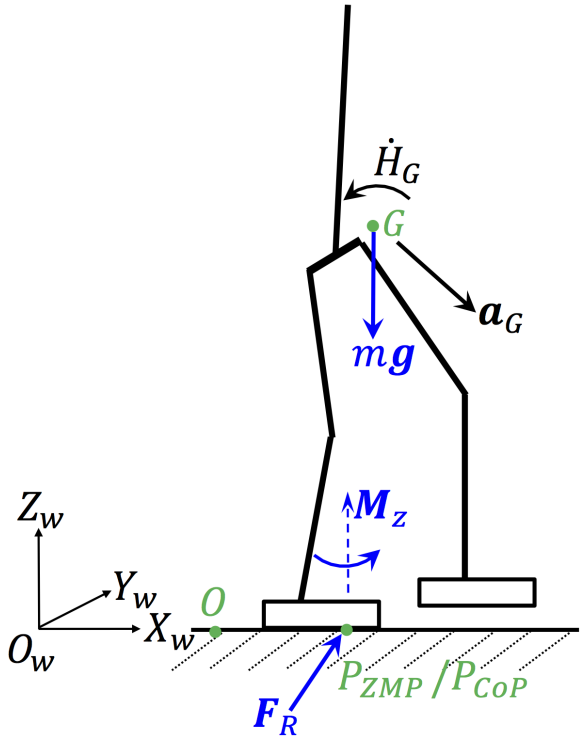

Figure 1.1. An illustration of Zero-Moment Point.

where O is an arbitrary point fixed on the ground, P_{CoP} is the Center of Pressure (CoP), $\overrightarrow{OP_{CoP}} \in \mathbb{R}^3$ is the vector pointing from O to P_{CoP}, G is the whole-body Center of Mass (CoM), $\overrightarrow{OG}$ is the vector pointing from O to G, $\mathbf{M}_z \in \mathbb{R}^3$ is the ground frictional moment about P_{CoP}, $\mathbf{F}_R \in \mathbb{R}^3$ is the ground-reaction force, m is the whole-body mass, $\mathbf{g} \in \mathbb{R}^3$ is the gravitational acceleration, $\mathbf{a}_G \in \mathbb{R}^3$ is the CoM acceleration, and $\mathbf{H}_G \in \mathbb{R}^3$ the whole-body angular momentum about G.

From the definition of ZMP, one has:

$$(\dot{\mathbf{H}}_G + \overrightarrow{P_{ZMP}G} \times m(\mathbf{a}_G - \mathbf{g}))_h = \mathbf{0}, \tag{1.2}$$

where P_{ZMP} is the ZMP, $\overrightarrow{P_{ZMP}G} \in \mathbb{R}^3$ is the vector pointing from P_{ZMP} to G, and the subscript h represents the components in the horizontal plane.

Comparing Eqs. (1.1) and (1.2), one has:

$$\overrightarrow{P_{ZMP}P} = \mathbf{0}, \tag{1.3}$$

which proves that ZMP and CoP always coincide on a horizontal even terrain. Also, both ZMP and CoP only exist within the support polygon. Their difference is that ZMP is defined by dynamic forces but CoP is defined by ground-reaction forces. On horizontal even terrains, CoP is a point about which the horizontal moment of the ground-reaction force is zero. This point is often used in biomechanics for postural and gait stability analysis [51] [52] [53] [54]. The ZMP balance criterion is sometimes referred to as the CoP constraint in biomechanics [51].

According to our proposed definition of walking stability, the ZMP balance criterion is a sufficient condition for stable walking when applied with accurate joint trajectory tracking. For bipedal robots with flat feet, keeping ZMP strictly within the support polygon ensures that the support foot does not tip over its edge and that the underactuation caused by foot rotation about the edge is avoided. Hence, a walking robot essentially becomes a fully actuated, fixed-based robotic manipulator under ZMP-based walking control, which enables high walking versatility [55] [56] [57] [58] [59] [60] [61] [62] [63] [64].

Despite the high walking versatility, conservative walking performance is the major disadvantage of the ZMP-based accurate trajectory tracking. The ZMP balance criterion requires flat-footed walking and prohibits a biped's support foot from rotating about its edge. However, a foot rotation does not necessarily lead to a fall. Thus, enforcing the ZMP balance criterion with accurate joint trajectory tracking is not a necessary condition for guaranteeing walking stability [6]. In summary, stable walking realized through ZMP-based accurate joint-trajectory tracking is highly conservative; i.e., the achievable walking speed of the ZMP approach is highly limited.

Also, high energy consumption is another undesirable feature of the ZMP approach, which is partly caused by accurate joint-trajectory tracking [65]. Furthermore, the ZMP approach cannot deal with underactuated bipedal robotic walking.

1.2.3 Foot Rotation Indicator

The concept of Foot Rotation Indicator is very similar to ZMP in the sense that they are both indicators of support foot rotation. Therefore, using Foot Rotation Indicator as a balance indicator suffers from the same problems as ZMP.

Foot Rotation Indicator - A Foot Rotation Indicator (FRI) is a point at which the ground-reaction force would have to act to keep the support foot stationary [44] [45].

FRI Criterion - The support foot does not rotate if and only if the FRI and the CoP coincide [44] [45]. *Foot rotation occurs only when FRI deviates from CoP.*

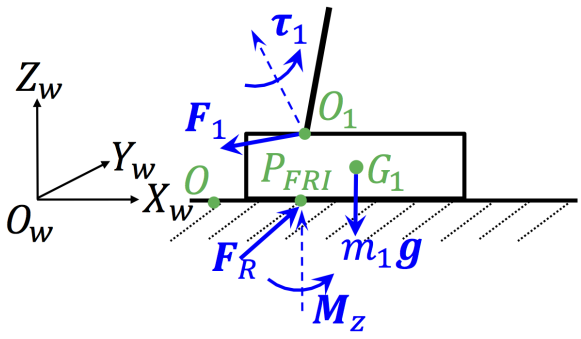

Figure 1.2. An illustration of Foot Rotation Indicator.

First, let us consider the dynamic equilibrium of the support foot (see Fig. 1.2). The force and the torque applied to the support foot by the rest of the links can be denoted as $\mathbf{F}_{R1}$ and $\boldsymbol{\tau}_1$, respectively, which act at the center of the ankle, O_1. With respect to the world coordinate frame, the equation of the support foot's dynamic equilibrium can be written as:

$$\overrightarrow{OP_{FRI}} \times \mathbf{F}_R + \mathbf{M}_z + \overrightarrow{OG_1} \times m_1\mathbf{g} + \boldsymbol{\tau}_1 + \overrightarrow{OO_1} \times \mathbf{F}_{R1} = \overrightarrow{OG_1} \times m_1\mathbf{a}_1 + \dot{\mathbf{H}}_{G1}, \tag{1.4}$$

where O is an arbitrary point fixed on the ground, P_{FRI} is the FRI, $\overrightarrow{OP_{FRI}} \in \mathbb{R}^3$ is the vector pointing from O to P_{FRI}, G_1 is the CoM of the support foot, $\overrightarrow{OG_1} \in \mathbb{R}^3$ is the vector pointing from O to G_1, m_1 is the mass of the support foot, $\overrightarrow{OO_1} \in \mathbb{R}^3$ is the vector pointing from O to O_1, $\mathbf{a}_1$ is the acceleration of the support foot, and $\mathbf{H}_{G1}$ is the angular momentum of the

support foot about its CoM. Because the foot will be stationary when the ground-reaction force acts at the FRI, one has

$$(\overrightarrow{OP_{FRI}} \times \mathbf{F}_R + \overrightarrow{OG}_1 \times m_1\mathbf{g} + \boldsymbol{\tau}_1 + \overrightarrow{OO}_1 \times \mathbf{F}_{R1})_h = \mathbf{0} \tag{1.5}$$

and

$$\mathbf{F}_R + \mathbf{F}_{R1} + m_1\mathbf{g} = \mathbf{0}. \tag{1.6}$$

Also, considering

$$\overrightarrow{OG}_1 = \overrightarrow{OP_{FRI}} + \overrightarrow{P_{FRI}G}_1 \tag{1.7}$$

and

$$\overrightarrow{OO}_1 = \overrightarrow{OP_{FRI}} + \overrightarrow{P_{FRI}O}_1, \tag{1.8}$$

one has

$$(\overrightarrow{P_{FRI}G}_1 \times m_1\mathbf{g} + \boldsymbol{\tau}_1 + \overrightarrow{P_{FRI}O}_1 \times \mathbf{F}_{R1})_h = \mathbf{0}. \tag{1.9}$$

For bipedal robots with rigid, flat feet walking on a horizontal even terrain, FRI and ZMP coincide only when the support foot is stationary. When the support foot tips over its edge, the ZMP will stay at the edge of the support polygon while the FRI will be outside the support polygon. For robots walking on horizontal even terrains with flexible or multi-joint feet, the support foot can tip over its edge while both ZMP and FRI are strictly within the support polygon. Because support foot rotation does not necessarily imply unstable walking [66], the FRI may not be a good indicator of bipedal walking stability.

1.2.4 Centroidal Moment Pivot

Centroidal Moment Pivot has been used to indicate the whole-body angular momentum about a biped's CoM. It has been verified that the whole-body angular momentum with respect to the whole-body CoM is strictly regulated in normal human walking [48]. However, this strict regulation is not a necessary condition for guaranteeing walking stability, which, similar to the ZMP balance criterion, can lead to conservative walking performance.

Centroidal Moment Pivot - A Centroidal Moment Pivot (CMP) is a point at which the ground-reaction force would have to act to keep the rate of the whole-body angular momentum about CoM to be zero [46] [47].

CMP Criterion - CMP coincides with ZMP/CoP only when the rate of change of the whole-body angular momentum about CoM is zero [46] [47].

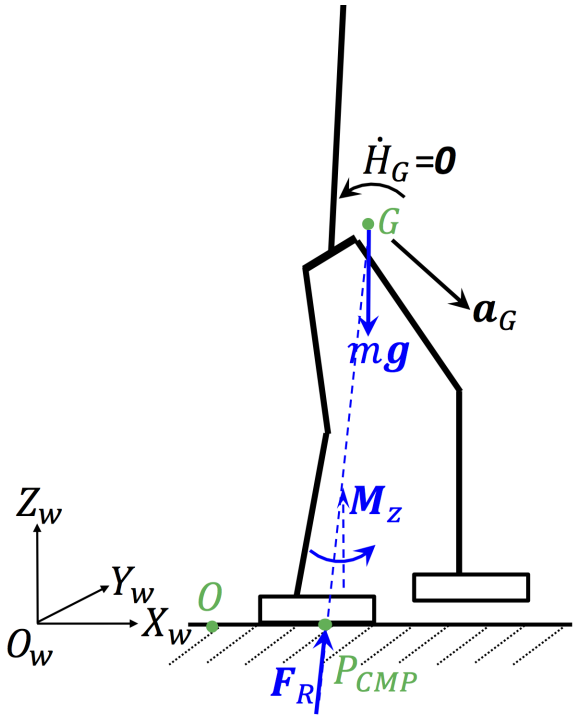

Figure 1.3. An illustration of Centroidal Moment Pivot.

From Eq. (1.2) and Fig. 1.3, and by the definition of CMP, one obtains:

$$(\overrightarrow{P_{CMP}G} \times m(\mathbf{g} - \mathbf{a}_G))_h = \mathbf{0}, \tag{1.10}$$

where P_{CMP} is the CMP and $\overrightarrow{P_{CMP}G} \in \mathbb{R}^3$ is the vector pointing from P_{CMP} to G.

The coincidence of CMP with ZMP/CoP is not a necessary condition for balance/stability. For example, the rate of change of angular momentum is typically not zero during a sit-to-stand motion of a human, but the motion can still be stable.

A few facts about ZMP, FRI, and CMP are summarized as follows:

1. On horizontal even terrains, ZMP always coincides with CoP and thus only exists within the support polygon;

2. On horizontal even terrains, FRI coincides with ZMP/CoP only when the support foot does not tip over its edge, and the ZMP criterion and the FRI criterion are equivalent for robots with rigid, flat feet walking on horizontal even terrains;

3. On horizontal even terrains, CMP coincides with ZMP/CoP if the rate of change of the whole-body angular momentum about the whole-body CoM is zero.

According to our proposed definition of walking stability, the above balance indicators when applied with accurate joint trajectory tracking are not necessary stability measures, although they have been successfully implemented on many bipedal robots:

1. The three balance criteria (i.e., ZMP, FRI, CMP) are essentially three different constraints, and they are not ideal stability criteria because the key factors to walking stability are not considered such as joint motion range, joint actuation limits, and controller performance limits.

2. The ZMP balance criterion is essentially a constraint, which requires that ZMP/CoP should never move to the edge of the support foot.

3. The FRI criterion requires no foot rotation of the support foot, which is overly conservative, and, in fact, previous studies have found that support foot rotation during the single-support phase contributes to the high efficiency of human walking [67].

4. The CMP criterion is also overly conservative as strict regulation of the whole-body angular momentum about the whole-body CoM is not necessary for guaranteeing stable walking.

When these balance criteria are utilized to guarantee walking stability with accurate joint trajectory tracking, the resulting walking performance will be highly conservative and energy consuming.

1.2.5 Capture Point and Capturability

As discussed previously, the complete set of viability is too computationally expensive to calculate. Capturability, proposed by Pratt and Tedrake [6] [68], provides a reasonable approximation of viability, and it has been successfully implemented on real walking robots for push recovery tasks and walking tasks [69] [70]. Because capturability-based walking strategies no longer require flat-footed walking, the achievable walking performance may be less conservative than ZMP-based approaches. However, there are other critical problems associated with this walking control method. Before reviewing its advantages and disadvantages in greater detail, we will first review the definition of Capture Point and capturability.

Capture Point - A Capture Point is a point on the ground where the biped can step to in order to bring itself to a complete stop [49].

N-step Capture Point - An N-Step Capture Point is a point on the ground where the biped can step to in order to bring itself to a complete stop in N steps [49].

N-step Capturability - N-Step Capturability is informally defined as the ability of a biped to come to a stop without falling by taking N or fewer steps, given its dynamics and actuation limits [68] [6].

The Extrapolated CoM [71] [72] was independently proposed in the area of biomechanics, which has the same mathematical expression as a Capture Point when derived based on a linear inverted pendulum model with point feet. In addition, the concept of feasible stability region proposed in the area of biomechanics [51] is closely related to the concepts of capture point and capturability. In fact, stability measure of human walking has been extensively studied in the area of biomechanics [51] [52] [54] [71] [73] [74].

The derivation of the capture point utilizes simplified dynamic models of walking robots [6] [49] [68], for example, a three-dimensional Linear Inverted Pendulum Model (3-D LIPM) with point feet. The 3-D LIPM was first proposed by Kajita, et.al, [55], and it has then been widely used for ZMP-based bipedal walking control as well. In a 3-D LIPM, a walking robot is modeled as a point mass with a massless leg. The point mass is

assumed to move on a constant horizontal plane. Equations of motion with respect to the world coordinate frame can be derived based on Eq. (1.1) with $\mathbf{M}_z$ and $\dot{\mathbf{H}}_G$ both equal to zero:

$$\overrightarrow{OP_{CoP}} \times \mathbf{F}_R + \overrightarrow{OG} \times M\mathbf{g} = \overrightarrow{OG} \times m\mathbf{a}_G, \tag{1.11}$$

$$\mathbf{F}_R + m\mathbf{g} = m\mathbf{a}_G. \tag{1.12}$$

Denote the projection of G on the horizontal plane as G', and define $\mathbf{r}_G := \overrightarrow{OG'}$ and $\mathbf{r}_{CoP} := \overrightarrow{OP_{CoP}}$. Combining Eqs. (1.11) and (1.12), one has:

$$\ddot{\mathbf{r}}_G = \frac{g}{c_{z0}}(\mathbf{r}_G - \mathbf{r}_{CoP}). \tag{1.13}$$

Since the system dynamics in the X_w- and the Y_w-directions are decoupled under the constant CoM height assumption, Eq. (1.13) can be written as:

$$\ddot{x}_G = \frac{g}{c_{z0}}(x_G - x_P) \text{ and } \ddot{y}_G = \frac{g}{c_{z0}}(y_G - y_P), \tag{1.14}$$

where x_G and y_G are the x- and y- coordinates of $\mathbf{r}_G$, and x_P and y_P are the x- and y-coordinates of $\mathbf{r}_{CoP}$.

Because the dynamics in the X_w- and the Y_w-directions are identical, without loss of generality, only the X_w-direction component of dynamics is considered and rewritten as:

$$\begin{bmatrix} \dot{\tilde{x}}_G \\ \ddot{\tilde{x}}_G \end{bmatrix} = \begin{bmatrix} 0 & 1 \\ \frac{g}{c_{z0}} & 0 \end{bmatrix} \begin{bmatrix} \tilde{x}_G \\ \dot{\tilde{x}}_G \end{bmatrix}, \tag{1.15}$$

where $\tilde{x}_G := x_G - x_P$.

The equilibrium point of the system Eq. (1.15) is a saddle point, which proves that a walking robot is essentially unstable. The two eigenvalues of the system in Eq. (1.15) are $\pm\sqrt{\frac{g}{c_{z0}}}$, and the corresponding eigenvectors are determined by $\sqrt{\frac{g}{c_{z0}}}\tilde{x}_G \mp \dot{\tilde{x}}_G = 0$. The negative eigenvalue $-\sqrt{\frac{g}{c_{z0}}}$ corresponds to the stable eigenvector $\sqrt{\frac{g}{c_{z0}}}\tilde{x}_G + \dot{\tilde{x}}_G = 0$ (see Fig. 1.4). The states that lie along the stable eigenvector in the phase plane will eventually converge to the equilibrium; i.e. the robot will come to a complete stop. If an unstable state can be instantaneously moved to a point that is along the stable eigenvector in the state

space, the biped will come to a complete stop [55]. The point that the support foot should instantaneously move to is called a *Capture Point* [49], which is defined as $\mathbf{r}_{CP}$:

$$\mathbf{r}_{CP} = \mathbf{r}_G + \sqrt{\frac{c_{z0}}{g}}\dot{\mathbf{r}}_G. \tag{1.16}$$

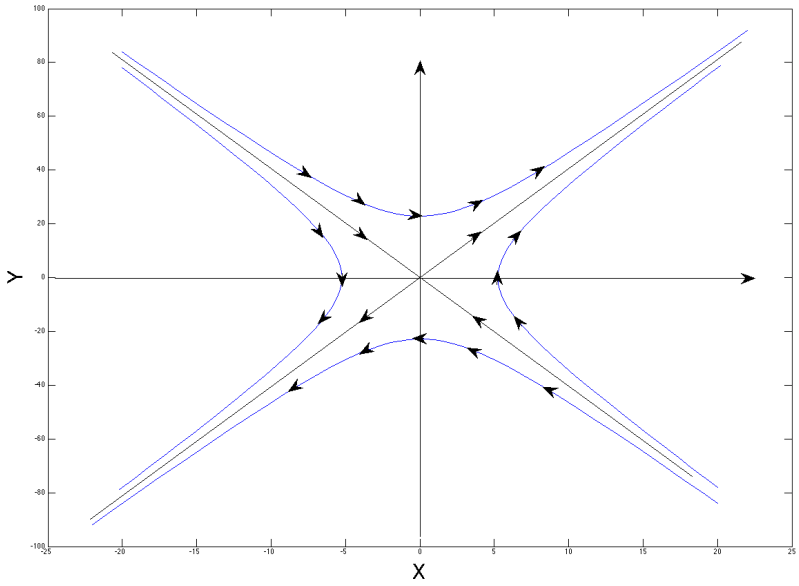

Figure 1.4. Phase portrait of Eq. (1.15). (The x-axis and the y-axis represent $\tilde{x}_G$ and $\dot{\tilde{x}}_G$, respectively.)

Taking the first derivative of Eq. (1.16) yields

$$\dot{\mathbf{r}}_{CP} = \sqrt{\frac{g}{c_{z0}}}(\mathbf{r}_{CP} - \mathbf{r}_P). \tag{1.17}$$

Equation (1.17) shows an important property of a capture point; that is, the capture point diverges from the CoP exponentially fast with a diverging velocity always pointing from the CoP towards the capture point. Thus, the swing time and the swing length of the stepping foot are important for push recovery strategies that utilize the capture-point approach. In human walking, push recovery can be achieved by the hip strategy that regulates the rate of change of the whole-body angular momentum to bring the human body to come to a

stop [75]. Accordingly, a reaction mass was incorporated in the 3-D LIPM to emulate this strategy [68].

Although modeling simplification such as the 3-D LIPM helps to reduce the computational burden of motion planning and control of bipedal robotic walking, some key elements of bipedal walking are omitted when a simplified model is utilized in the development of walking strategies. For example, due to modeling simplification, a controller design based on capturability ignores variations of the CoM height during walking, the performance limitations of a controller design, and the internal kinematics and dynamics during bipedal walking.

1.2.6 The Hybrid-Zero-Dynamics Framework

The last group of walking strategies that will be reviewed in this Chapter is the Hybrid-Zero-Dynamics (HZD) framework. Instead of relying on a ground-reference point to indicate walking stability, the HZD framework approaches the problem of bipedal walking control through full-order dynamic modeling, nonlinear feedback control design, and formal closed-loop stability analysis. As the HZD framework does not enforce overly conservative walking criteria such as no foot rotation or strict regulation of the whole-body angular motion, it has enabled much higher walking performance in terms of agility and energy efficiency as compared with the ZMP approach and the capturability based walking strategies. Furthermore, the HZD framework can realize high-performance walking for underactuated bipeds.

However, the HZD framework has been largely focused on bipedal periodic gaits. According to our proposed definition of walking stability, periodic gaits are not a necessary requirement for stable walking. Therefore, walking control performance of the HZD framework lacks gait versatility.

As the HZD framework focuses on feedback control of periodic gaits, we will first review a few concepts related to the definition and evaluation of the stability of a periodic solution of a dynamical system.

The stability of a periodic gait can be determined by the stability of the orbit generated by the periodic gait.

Let χ be the n^{th}-dimensional, full state space of a dynamical system. Let $\mathbf{x} \in \chi$ be a state of the system. Suppose that the system dynamics are autonomous:

$$\dot{\mathbf{x}} = \mathbf{f}(\mathbf{x}), \tag{1.18}$$

where $\mathbf{f} : \chi \to T\chi$ is continuously differentiable on $\mathbf{x} \in \chi$. Suppose that the dynamic system in Eq. (1.18) has a nontrivial periodic solution $\mathbf{p}(t)$ for $t \geq 0$ and that

$$\mathbf{p}(t+T) = \mathbf{p}(t), \forall t \geq 0, \tag{1.19}$$

where T is a finite positive number, which represents the least gait period of $\mathbf{p}(t)$. Then, the periodic orbit Γ generated by $\mathbf{p}(t)$ can be formally defined as:

$$\Gamma := \{\mathbf{x} \in \chi : \mathbf{x} = \mathbf{p}(t), \forall t \geq 0\}. \tag{1.20}$$

Define an δ-neighborhood of Γ by $U_\delta := \{\mathbf{x} \in \chi : \text{dist}(\mathbf{x}, \Gamma) < \delta\}$, where $\text{dist}(\mathbf{x}, \Gamma)$ represents the distance between $\mathbf{x}$ and Γ. The stability definition of the orbit Γ will be reviewed as follows.

Stability - The orbit Γ *is stable if, for each* $\varepsilon > 0$*, there is* $\delta > 0$ *such that* [76]

$$\mathbf{x}(0) \in U_\delta \Rightarrow \mathbf{x}(t) \in U_\varepsilon, \ \forall t \geq 0. \tag{1.21}$$

Asymptotic Stability - The orbit Γ *is asymptotically stable if it is stable and* δ *can be chosen such that* [76]

$$\mathbf{x}(0) \in U_\delta \Rightarrow \lim_{t \to \infty} \text{dist}(\mathbf{x}(t), \Gamma) = 0. \tag{1.22}$$

Exponential Stability - The orbit Γ *is exponentially stable if there exist* $\delta > 0$*,* $k > 0$*, and* $c > 0$ *such that* [77]

$$\mathbf{x}(0) \in U_\delta \Rightarrow \text{dist}(\mathbf{x}(t), \Gamma) < ke^{-ct}, \ \forall t \geq 0. \tag{1.23}$$

A nontrivial periodic solution $\mathbf{p}(t)$ of Eq. (1.18) is called:

- *Orbitally stable* if the orbit Γ generated by $\mathbf{p}(t)$ is stable;

- *Orbitally asymptotically stable* if the orbit Γ generated by $\mathbf{p}(t)$ is asymptotically stable;

- *Orbitally exponentially stable* if the orbit Γ generated by $\mathbf{p}(t)$ is exponentially stable.

The orbital stability of a periodic solution can be numerically evaluated by the following equivalent conditions:

- The eigenvalues of the linearized Poincaré return map at the fixed point [50];

- The eigenvalues of the monodromy matrix of the variational equation [39] [78] [79].

There are two groups of bipedal walking whose stability can be determined by this stability measure [39]. The first group is passive walkers that utilize the natural dynamics of a biped to achieve stable walking and thus consume very low to zero actuation power [80] [81] [82] [83] [84] [85] [86] [87] [88] [39] [78] [89] [90] [91]. During flat-terrain walking, only a small amount of energy needs to be injected into the system to compensate for the energy loss caused by impact and friction. During down-hill walking, the external energy consumption can be zero. Although passive walkers are highly energy-efficient, they severely lack versatility because the orbitally stable gait is mainly determined by the mechanical design, which leaves little freedom to achieve different types of gaits, not to mention to negotiate unstructured environments.

The second group is the actuated bipeds, and the most successful and dominant trend in this group is the Hybrid-Zero-Dynamics (HZD) framework [50]. Orbital stabilization of bipedal walking can also be realized through oscillator-based stabilization [92] and transverse linearization [77] [93] [94] [95]. For transverse linearization, a transverse coordinate along a curve, not necessarily an orbit, in the state space is constructed analytically, and the transverse dynamics is linearized. Convergence to the curve in the state space is then guaranteed through receding-horizon control of the linearized transverse dynamics. Besides closed-loop feedback control, stable periodic walking has also been realized based on open-loop optimal control [96] [97] [98].

As this dissertation research is largely inspired by the HZD framework, it will be reviewed in greater detail next.

The Hybrid-Zero-Dynamics Framework (HZD) was first introduced for feedback control of underactuated bipedal walking by Grizzle *et al.* [3] [7] [50]. Instead of focusing on a ground-reference point or utilizing the natural dynamics of a bipedal robot, this approach stabilizes a walking process by stabilizing the closed-loop control system based on nonlinear feedback control and formal stability analysis. This is the first time that the provably stable walking was achieved for bipedal robots based on feedback control, and the HZD framework has achieved high walking speed and high energy efficiency [99] [100] [101].

In the HZD framework, the walking process is modeled as a hybrid dynamical system, which captures the full-order walking dynamics and consists of continuous phases and impulse rigid-body impacts of foot landings:

$$\begin{cases} \dot{\mathbf{x}} = \mathbf{f}(\mathbf{x}) + \boldsymbol{g}(\mathbf{x})\mathbf{u}, & \text{for } \mathbf{x}^- \notin S(\mathbf{x}); \\ \mathbf{x}^+ = \boldsymbol{\Delta}(\mathbf{x}^-), & \text{for } \mathbf{x}^- \in S(\mathbf{x}); \end{cases} \tag{1.24}$$

where $\mathbf{f} : \chi \to T\chi$, $\mathbf{g} : \chi \to T\chi$, $\mathbf{u} \in \mathbb{R}^k$ ($k \leq n$) represents the control input, $S(\mathbf{x}) := \{\mathbf{x} \in \chi : z_{sw}(\mathbf{x}) = 0,\ \dot{z}_{sw}(\mathbf{x}) < 0\}$ is the switching surface that defines the moment of a swing-foot touchdown (z_{sw} represents the swing foot height above the ground), the symbols $+$ and $-$ represent the moments right before and after an impact, respectively, and $\boldsymbol{\Delta}(\mathbf{x})$ is the reset map that represents the landing impact dynamics.

The controller design utilized in the HZD framework is state feedback control based on input-output linearization. The output functions are defined as virtual constraints, and they are asymptotically driven to zero by the controller during continuous phases. The virtual constraints were initially defined as functions of a biped's generalized coordinates alone [50] [102] [103]. Specifically, the virtual constraints are defined as the tracking error of the desired walking pattern that defines the desired evolution of the directly actuated joint variables with respect to a reference joint in a complete gait cycle. The Beziér curves [104] have been used for defining the walking pattern:

$$\boldsymbol{\Phi}(s) := \sum_{m=0}^{K} \mathbf{a}_m \frac{K!}{k!(K-m)!} s^m (1-s)^{K-m}, \tag{1.25}$$

where s represents the encoding variable of the walking pattern, $\mathbf{a}_m \in \mathbb{R}^k$ is the parameter of the Beziér curves (recall that k is the number of independently actuated joints and $k \leq n$),

and K is the order of the Beziér curves. Later on, angular momentum and velocity have been used to define the virtual constraints [105] [106]. Recently, the virtual constraints have been defined as time-dependent functions to solve some implementation issues caused by sensor noise, which is associated with the state-based definition [107].

Based on the concept of virtual constraints, hybrid zero dynamics is introduced to reduce the dimension of stability analysis. In the early exploration, underactuated walking with a single degree of underactuated is studied, and the convergence of the output function to zero during a continuous phase is assumed to be finite-time. Under this assumption, the continuous-time zero dynamics are invariant with respect to the impact event, and thus the orbital stability of the closed-loop system can be inferred from that of the hybrid zero dynamics, which greatly reduces the stability analysis dimension [50]. Later on, the finite-time convergence is relaxed to be exponential convergence, and the hybrid zero dynamics can be constructed by properly defining the virtual constraints [102]. If there exists an exponentially stable orbit in the hybrid invariance manifold and the convergence rate to the hybrid invariance manifold is sufficiently fast, then the closed-loop system is exponentially orbitally stable. However, hybrid invariance fails to hold for high degrees of underactuation. To extend the construction of hybrid zero dynamics from a single degree of underactuation to higher degrees of underactuation for underactuated walking, an update law of the output function definition was developed to be applied at the moment right after a landing impact [103] [108] [109]. Recently, rapidly exponential stabilization has been developed to deal with the potentially expansive effect of the reset map based on control Lyapunov functions [110].

In addition to underactuated walking, the HZD framework of orbital stabilization has also been extended to fully actuated bipedal walking [111]. With the advantage of full actuation, velocity tracking in Cartesian space has been realized. Human-like walking has been achieved by extracting human walking patterns from experimental data and then using it to define the output function [111] [112] [113]. Furthermore, the HZD framework has been extended to compliant HZD [114] [115] [116], planar bipedal running [117] [118], three-dimensional walking [10] [119] [120] [121] [122] [123] [124], aperiodic walking [125],

uneven terrain walking [105] [126] [127] [128] [129], multi-domain gait control [130], walking with nontrivial foot motion [131] [132] [133] [134], control of prosthetic devices [135] [136], and control of exoskeletons [137]. Barrier functions have also been extended to bipedal walking control based on the HZD framework [138].

1.2.7 Summary

To tackle the challenging problem of bipedal walking control, different walking control strategies have been proposed based on different measures of walking stability. Among them, the most widely used approaches are the ZMP Approach, the Capture-Point approach, and the HZD framework.

The ZMP approach relies on a highly conservative stability criterion and accurate joint trajectory tracking to guarantee walking stability. One of the main advantages of the ZMP approach is its high versatility. The ZMP approach has been utilized to realize a variety of walking motions, such as climbing stairs, making turns, and dancing [55] [56] [57] [58] [59] [60] [61] [62] [63] [64]. However, the achievable walking speed of the ZMP approach is limited, and the resulting energy consumption of walking is high. For example, the energy consumption of ASIMO's walking is ten times higher than human walking [65]. Furthermore, the ZMP approach cannot handle underactuation well.

The walking strategy design based on the Capturability suffers from the same limitations as the ZMP approach, i.e., limited walking speed and high energy consumption. Similar to the ZMP approach, the Capture-Point approach can realize highly versatile walking for bipedal robots.

In contrast with the ZMP and the Capture-Point approaches, the HZD framework can achieve bipedal robotic walking with provable stability, high walking speed, and high efficiency. This is because the controller design is established based on the full-order hybrid dynamics of bipedal walking and the formal stability analysis of the closed-loop control system. However, the major limitation of the HZD framework is its low walking versatility. As reviewed previously, the HZD framework focuses on periodic walking, which

severely limits its potentials in real-world applications. Although the HZD framework has been extended to aperiodic walking [139], the resulting walking motions are not truly versatile. For example, position tracking in Cartesian space has not been fully addressed by the HZD framework, but the capability of satisfactorily controlling a biped's position on the walking surface is critical to real-world applications such as multi-agent coordination.

1.3 Objectives and Proposed Approaches

Although various controller design methodologies have been previously developed to enable impressive walking motions, the performance of today's bipedal robotic walking is still far from satisfactory for real-world applications. Therefore, the objective of this dissertation is to develop a model-based controller design methodology that realizes stable, versatile, agile, and efficient bipedal robotic walking based on nonlinear control theories and formal stability proof. Specifically, we will focus on achieving stable, agile, and efficient walking for both fully actuated and underactuated bipeds. In addition, the proposed controller design methodology will be utilized to achieve high walking versatility for fully actuated bipeds and improved walking robustness for both fully actuated and underactuated bipeds.

Inspired by the HZD framework, we will synthesize state feedback controllers that utilize full-order dynamic modeling and input-output linearization. Therefore, similar to the HZD framework, the proposed controller design methodology can realize stable, fast, and efficient walking because of its model-based nature. However, different from the HZD framework that utilizes state-based control design, we will explicitly define the output function as time-dependent, which will not only significantly improve walking versatility for fully actuated bipeds [140] [141] but also greatly enhance walking robustness for both fully actuated and underactuated bipeds [142] [143]. High walking versatility is critical for accomplishing complex tasks in the real-world environments, and the lack of versatility has been a major problem of the HZD framework because this state-based approach has been limited to realizing periodic gaits. High robustness is also a desirable feature for real-world

applications, and experimental results have shown that walking robustness can be greatly improved by time-dependent control design as compared with the state-based HZD framework [107]. Despite these advantages of time-dependent approaches, they have not been fully explored for bipedal walking control based on nonlinear control theories and formal stability proof.

Because full actuation and underactuation are both common in bipedal robotic walking, we will apply the time-dependent controller design methodology to both fully actuated and underactuated bipeds. A bipedal robot is fully actuated if the number of independent actuators equals the number of degrees of freedom, and a bipedal robot is underactuated if the number of independent actuators is less than the number of degrees of freedom. For fully actuated bipeds, we will investigate both planar and three-dimensional (3-D) walking for versatility improvement. For underactuated bipeds, improving walking versatility may not be realistic due to the lack of actuators to control each joint. Instead, we will develop a time-dependent feedback controller to improve walking robustness for underactuated periodic walking, and we will show that our proposed controller design can be directly applied to fully actuated bipeds as well.

In this dissertation, controller designs for three types of bipedal robots will be proposed and developed based on the same time-dependent controller design methodology, which consists of the following four steps:

Step 1: The full-order, hybrid walking dynamics will be modeled;

Step 2: The desired motions will be planned such that the energy consumption of walking is minimized and that necessary constraints and conditions are satisfied;

Step 3: The tracking error of the desired motions will be utilized to design a time-dependent output function;

Step 4: The input-output linearization will be utilized to synthesize the needed control law;

Step 5: The sufficient stability conditions for the hybrid, time-varying closed-loop system will be established based on nonlinear control theories and formal stability analysis.

Based on this controller design methodology, three types of bipeds will be studied: a) a fully actuated planar biped, b) a fully actuated 3-D biped, and c) an underactuated planar biped. Because of the differences in actuation types and control objectives, the controller designs for these three types of bipeds will be distinctively different from one another, and they are summarized next.

a) **Walking Control of Fully Actuated Planar Bipeds for Improved Walking Versatility**: High walking versatility is potentially achievable for a fully actuated biped because such a biped can directly control each of its joints. High walking versatility is important for accomplishing complex tasks in real-world applications. For example, realizing aperiodic, asymmetric gaits may become necessary when a biped operates in a complex environment, and satisfactory position tracking in Cartesian space is critical for complex tasks such as multi-agent coodination. However, previous work such as the HZD framework has been heavily focused on achieving periodic gaits for fully actuated walking, and position tracking in Cartesian space has not been fully studied. To improve the walking versatility of a fully actuated planar biped as compared with previous studies, we will develop a controller design that can achieve exponential tracking of aperiodic, asymmetric gaits and the desired position trajectory in Cartesian space. To our best knowledge, it is the *first* time that satisfactory position tracking in Cartesian space has been realized for fully actuated planar biped through model-based feedback control design and formal stability analysis. This controller design will be introduced in Chapter 3.

b) **Walking Control of Fully Actuated Three-dimensional Bipeds for Improved Walking Versatility**: Because real-world applications of bipedal robots typically require three-dimensional (3-D) walking, we will extend our controller design for fully actuated planar bipeds to fully actuated 3-D bipeds in this project. Our main goal is to achieve exponential tracking of the desired position trajectory in Cartesian space. Due to the complexity of 3-D bipedal walking, position tracking in Cartesian space is much more difficult for 3-D walking than planar walking. Position tracking in Carte-

sian space for 3-D bipeds includes both the convergence to the planned path on the walking surface and the convergence to the desired motion along the path. However, convergence to the planned path on the walking surface is a trivial task for planar walking because a planar biped is confined to only moving in the sagittal plane. In this project, we will utilize our proposed time-dependent design methodology to synthesize a walking controller that achieves exponential tracking of the desired path on the walking surface as well as the desired motion along the path. As the first step of our ongoing research, only straight-line paths will be considered as the desired path in this project. The details of control design will be presented in Chapter 4.

c) **Walking Control of Underactuated Bipeds for Improved Walking Robustness**: As previously explained, underactuation is a common phenomenon in bipedal robotic walking, and thus it is necessary to investigate controller designs for underactuated walking. Because it is difficult to handle underactuation due to the lack of actuators to control each joint, achieving high versatility such as position tracking in Cartesian space will not be addressed in this project. Instead, we will focus on time-dependent orbital stabilization of underactuated, periodic walking. Orbital stabilization of underactuated walking has been extensively studied under the state-based HZD framework. However, experimental results have shown that, as compared with the state-based HZD framework, a time-dependent approach can effectively improve walking robustness by effectively solving the implementation issue caused by sensor noise [107]. Although time-dependent walking control is advantageous in achieving high walking robustness for underactuated, periodic walking, it has not been fully studied. In this project, we will establish the *first* time-dependent feedback controller design that can achieve orbitally exponential stabilization of underactuated bipedal walking. The details of control design will be presented in Chapter 5.

1.4 Organization of Dissertation

The organization of the remainder of the thesis is listed as follows.

In Chapter 2, two common gait characterizations will be first explained. The first gait characterization describes a bipedal gait by the support and the swing legs, which can be used to compactly express walking dynamics. The second gait characterization describes a bipedal gait by the left and the right legs, which can be used to conveniently define a symmetric gait. Then, the full-order, hybrid dynamics of bipedal robotic walking will be presented, which include both continuous-time dynamics and impulsive rigid-body impact dynamics. Based on the full-order, continuous-phase dynamic model, we will introduce and develop the measure of Feasible Center of Mass Dynamic Manipulability (FCDM), which can be utilized to explain some of the contributing factors to the difficulty of bipedal walking control.

Chapter 3 presents the controller design for fully actuated planar walking with the exponential global position tracking capabilities. Following the proposed time-dependent controller design methodology, the output function is designed as time-dependent, which represents the tracking error of the desired time-varying global position trajectory as well as the desired state-based walking pattern. Based on the full-order walking dynamics, an input-output linearizing controller is synthesized to drive the time-dependent output function exponentially to zero during continuous phases. Also, we will introduce a new method of walking pattern design to guarantee the hybrid invariance of the desired motion, and we will develop sufficient conditions of the closed-loop stability based on the construction of multiple Lyapunov functions. Finally, the proposed controller design will be validified on a simulated planar biped with three revolute joints.

Chapter 4 provides the controller design for fully actuated three-dimensional (3-D) walking. To accomplish the task of exponential position tracking on the walking surface, we will develop a contouring control strategy that decomposes this task into two subtasks. One subtask is the exponential convergence to the desired path (i.e., contour), and the other subtask is the exponential convergence to the desired motion along the path. Similar to Chapter 3, sufficient stability conditions for the closed-loop system will be developed based on the construction of multiple Lyapunov functions. Finally, a 3-D biped with nine revolute joints will be simulated to validate the proposed controller design.

Chapter 5 introduces the time-dependent orbitally exponential stabilization of underactuated bipedal robotic walking. The objective of the controller design is to realize exponential convergence to the desired orbit in the state space. The desired motion to be tracked by the controller design is defined by modifying the periodic joint trajectories that reside on the desired orbit, and the output function is designed as the tracking error of the desired motion. Based on the full-order walking dynamics presented in Chapter 2, input-output linearization will be utilized to synthesize a feedback control law that drives the output function exponentially to zero during continuous phases. In the closed-loop stability analysis, we will first transform the hybrid, time-varying closed-loop system into a time-invariant one, and then we will establish the closed-loop stability conditions based on the variational equation of the transformed system. Furthermore, we will introduce a systematic motion planning method such that walking stability can be guaranteed through integrated motion planning and control. The results of this Chapter will be tested on a simulated underactuated biped with five revolute joints. Through discussions, it is concluded that the results of this Chapter can also be directly applied to underactuated bipeds with high degrees of underactuation as well as fully actuated bipeds.

Chapter 6 presents concluding remarks and briefly introduces potential directions for future work.

2. MODELING AND ANALYSIS OF BIPEDAL ROBOTIC WALKING

2.1 Introduction

Before introducing the walking controller designs in Chapters 3 - 5, we will first review and study dynamic modeling of bipedal robotic walking. Dynamic modeling is critical to the performance of a model-based controller design. For the purpose of achieving high-performance walking, all of our controller designs in this dissertation will utilize the full-order dynamic model of bipedal robotic walking. Specifically, the walking process will be modeled as a hybrid dynamical system that consists of both continuous phases and impulse rigid-body impacts.

In this Chapter, we will first describe and compare two common bipedal gait characterizations. Then, we will present the dynamic model of bipedal robotic walking. Both gait characterization and dynamic modeling will be used for controller designs in Chapters 3 - 5. Finally, to analyze the contributing factors to the difficulties in bipedal walking control, the measure of Feasible Center of Mass Dynamic Manipulability (FCDM) will be proposed and analyzed.

2.2 Bipedal Gait Characterization

There are two common types of bipedal gait characterization. The first one utilizes the support and the swing legs to describe a bipedal gait, which will be called the support-swing gait characterization in this dissertation [50] [77] [110]. A leg/foot that moves in the air is called a swing leg/foot, and a leg/foot that contacts the ground is called a support leg/foot. During bipedal walking, a swing leg and a support leg switch their roles when the swing foot touches the ground. Therefore, when a bipedal gait is described by the support-swing characterization, the states that represent positions and velocities of the support and the swing legs are always discontinuous at a swing-foot touchdown.

The second gait characterization utilizes the left and the right legs to describe a bipedal gait, which will be called the left-right gait characterization in this dissertation [9] [124] [144]. It is straightforward to know that the states representing joint positions will be continuous and well-defined at a swing-foot landing. The states representing joint velocities will still experience sudden jumps at an impulse rigid-body landing impact, but the definition of these states will be consistent throughout a walking process.

As compared with the support-swing characterization, the expression of dynamics is more complicated under the left-right characterization. However, the left-right gait characterization can be used to conveniently define both symmetric and asymmetric gaits, and the support-swing characterization can only conveniently define symmetric gaits. The advantage of the left-right gait characterization in defining asymmetric gaits will be detailed in Chapter 3, and the support-swing gait characterization will be utilized for the controller designs in Chapters 4 and 5 for simplicity of expressions.

2.3 Hybrid Dynamics of Bipedal Robotic Walking

A complete bipedal step typically consists of two phases – a single-support phase (SSP) and a double-support phase (DSP). During a SSP, one foot is the support foot, and the other is the swing foot. During a DSP, both feet are support feet. A SSP and a DSP are connected by the switching event of a swing-foot landing. If a biped has full-sized feet, each of the two phases can be further decomposed into several subphases depending on the movement of both feet [111].

In this dissertation, the following model assumptions are considered [7] [50]:

1. The mass of each link is lumped at the center of the link;
2. The two legs are identical;
3. The walking surface is flat, horizontal;
4. During a SSP, the support foot is in static, full contact with the walking surface;

5. The landing impact at a swing-foot touchdown is modeled as a contact between rigid bodies;

6. At the impact event, the former swing foot neither slips nor rotates upon touching the walking surface, and the former support foot releases from the walking surface right after the impact;

7. A DSP is instantaneous.

Based on these model assumptions, we will present the full-order dynamic model of bipedal robotic walking.

Consider a bipedal robot with n revolute joints and k ($k \leq n$) independent actuators. Let Q be the n-dimensional configuration space of the bipedal robot when the support leg is in static, full contact with the walking surface and the joint position limits are satisfied. Let $\chi = TQ \subset \mathbb{R}^{2n}$ be the full state space.

Under the assumption that the support leg is in static, full contact with the walking surface, the bipedal robot during a single-support phase will have n degrees of freedom (DOFs). The single-support-phase dynamics can be obtained with Lagrange's method, which can be expressed in terms of the joint positions $\mathbf{q} \in Q$ and the joint torques $\mathbf{u} \in \mathbb{R}^k$ [7] [50]:

$$\mathbf{M}(\mathbf{q})\ddot{\mathbf{q}} + \mathbf{c}(\mathbf{q}, \dot{\mathbf{q}}) = \mathbf{B}_u \mathbf{u}, \tag{2.1}$$

where $\mathbf{M} : Q \to \mathbb{R}^{n \times n}$ is the inertia matrix, $\mathbf{c} : TQ \to \mathbb{R}^n$ is the sum of the gravitational, the Coriolis, and the centrifugal terms, and $\mathbf{B}_u \in \mathbb{R}^{n \times k}$ is full column rank.

Let $z_{sw}(\mathbf{q}) : Q \to \mathbb{R}$ represent the height of the swing foot above the walking surface, and then the occurrence of a swing-foot landing can be determined by the switching surface $S_q(\mathbf{q}, \dot{\mathbf{q}})$ [7]:

$$S_q(\mathbf{q}, \dot{\mathbf{q}}) := \{(\mathbf{q}, \dot{\mathbf{q}}) \in TQ : z_{sw}(\mathbf{q}) = 0,\ \dot{z}_{sw}(\mathbf{q}, \dot{\mathbf{q}}) < 0\}. \tag{2.2}$$

When the swing foot hits the walking surface, an impact occurs. The impact dynamics can be modeled as:

$$[\mathbf{q}^+; \dot{\mathbf{q}}^+] = \begin{bmatrix} \boldsymbol{\Delta}_q(\mathbf{q}^-) \\ \boldsymbol{\Delta}_{\dot{q}}(\mathbf{q}^-)\dot{\mathbf{q}}^- \end{bmatrix} := \boldsymbol{\Delta}(\mathbf{q}^-, \dot{\mathbf{q}}^-), \tag{2.3}$$

where $\mathbf{\Delta} : TQ \to \mathbb{R}^{2n}$ is the reset map.

The details of dynamic modeling can be found in the reference [50].

2.4 Feasible Center of Mass Dynamic Manipulability of Bipedal Robots

Locomotion stability of a bipedal robot is closely related to the capacity to regulate its Center of Mass (CoM) motion. In this section, the concept of Feasible Center of Mass Dynamic Manipulability (FCDM) is introduced and analyzed as a measure of this capacity. The FCDM measure indicates the ability of a bipedal robot to regulate its CoM motion at a given posture (i.e., joint position $\mathbf{q}$) under ground-contact constraints. Specifically, three common and important ground-contact constraints – the unilateral contact-force constraint, the friction constraint, and the Center of Pressure constraint – are incorporated in the derivation of FCDM. It geometrically shows how each of the three constraints reduces the original torque-bounded manipulability polytope and affects the maximum achievable CoM acceleration in different directions. Finally, we will investigate the effects of postures on the maximum feasible CoM acceleration in a specific direction.

2.4.1 Center of Mass Dynamic Manipulability

Before introducing the FCDM measure, the concept of CoM dynamic manipulability (CDM) [145] [146] is first revisited. The CDM measure is developed based on Dynamic Manipulability, which was originally introduced for robotic manipulators [147] [148] [149] [150] [151] [152] [153] [154].

Here, only the flat-footed single-support phase in Eq. (2.1) is considered.

The relationship between the CoM velocity and the joint velocities via the CoM Jacobian can be expressed as:

$$\dot{\mathbf{r}}_c = \mathbf{J}_c(\mathbf{q})\dot{\mathbf{q}}, \tag{2.4}$$

where $\mathbf{r}_c = [x_c, y_c, z_c]^T \in \mathbb{R}^3$ is the CoM position and $\mathbf{J}_c : Q \to \mathbb{R}^{3\times n}$ is the CoM Jacobian. Taking the time derivative of Eq. (2.4) and combining it with the single-support-phase dynamics in Eq. (2.1), the CoM acceleration can be obtained as:

$$\ddot{\mathbf{r}}_c = \mathbf{J}_c\mathbf{M}^{-1}(\mathbf{B}_u\mathbf{u} - \mathbf{c}) + \dot{\mathbf{J}}_c\dot{\mathbf{q}}. \tag{2.5}$$

To analyze the effect of the joint-torque limit, we consider

$$\mathbf{u} \in [-\mathbf{u}_{max}, \mathbf{u}_{max}],$$

where $\mathbf{u}_{max} = [u_{max1}, u_{max2}, ..., u_{maxn}]^T \in \mathbb{R}^n$, and $\mathbf{J}_c\mathbf{M}^{-1}\mathbf{B}_u\mathbf{u}$ can be rewritten as:

$$\mathbf{J}_c\mathbf{M}^{-1}\mathbf{B}_u\mathbf{u} = \mathbf{J}_c\mathbf{M}^{-1}\mathbf{B}_u\mathbf{W}\mathbf{u}_N,$$

where

$$\mathbf{W} := \text{diag}[u_{max1}, u_{max2}, ..., u_{maxn}] \in \mathbb{R}^{n\times n}$$

is a scaling matrix and

$$\mathbf{u}_N = [u_{N1}, u_{N2}, ..., u_{Nn}]^T \in \mathbb{R}^n$$

is the normalized joint-torque vector with

$$|u_{Ni}| \leq 1$$

for $i \in \{1, 2, \ldots, n\}$.

Denoting $\tilde{\mathbf{J}} = \mathbf{J}_c\mathbf{M}^{-1}\mathbf{B}_u\mathbf{W}$ and applying singular value decomposition, $\tilde{\mathbf{J}}$ can be decomposed as

$$\tilde{\mathbf{J}} = \mathbf{U}\Sigma\mathbf{V}^T,$$

where

$$\mathbf{U} := [\boldsymbol{\mu}_1, \boldsymbol{\mu}_2, \boldsymbol{\mu}_3] \in \mathbb{R}^{3\times 3}$$

and

$$\mathbf{V} := [\boldsymbol{\nu}_1, \boldsymbol{\nu}_2, \ldots, \boldsymbol{\nu}_n] \in \mathbb{R}^{n\times n}$$

are orthogonal matrices and

$$\Sigma := \left[\begin{array}{ccc|c} \sigma_1 & 0 & 0 & \\ 0 & \sigma_2 & 0 & \mathbf{0}_{3\times(n-3)} \\ 0 & 0 & \sigma_3 & \end{array}\right] \in \mathbb{R}^{3\times n}.$$

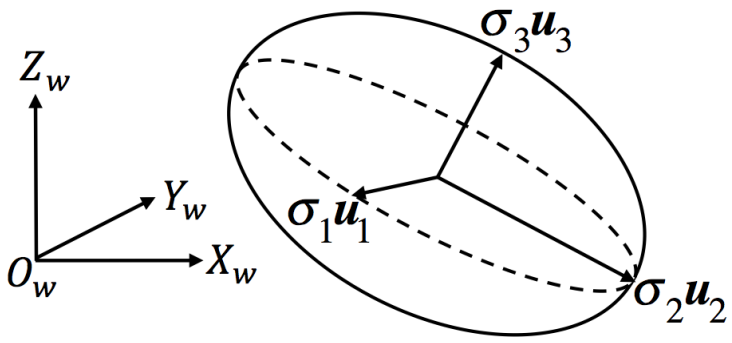

Figure 2.1. A CoM dynamic manipulability ellipsoid.

$\tilde{\mathbf{J}}$ maps the sphere $\|\mathbf{u}_N\| \leq 1$ onto an ellipsoid (see Fig. 2.1) in the CoM acceleration space, which is the CoM Dynamic Manipulability Ellipsoid. The ellipsoid semi-principal axes are of length σ_1, σ_2 and σ_3 in the directions of $\mathbf{u}_1$, $\mathbf{u}_2$ and $\mathbf{u}_3$, respectively. Although the complete torque-bounded set of CoM acceleration at a given posture with given joint velocities is not an ellipsoid but a polytope, which is bounded by $|u_{Ni}| \leq 1$ for $i \in \{1,2,\ldots,n\}$, the ellipsoid is a reasonable approximation [147] and it shares the same center as the polytope.

2.4.2 Feasible Center of Mass Dynamic Manipulability

Different from a fixed-based robot manipulator, bipedal locomotion is subject to various ground-contact constraints. These constraints decide the feasible subset of the torque-bounded CoM dynamic manipulability polytope. This feasible subset is defined as the Feasible CoM Dynamic Manipulability (FCDM) Polytope. Here, three common ground-contact constraints in bipedal robotic walking are considered, including: 1) the unilateral

ground-contact constraint, 2) the friction constraint, and 3) the CoP constraint (i.e., the ZMP balance criterion). They are mathematically and respectively described as:

$$\begin{aligned} &1) \quad F_z \geq 0; \\ &2) \quad \sqrt{F_x^2 + F_y^2} \leq \mu |F_z|; \\ &3) \quad \mathbf{r}_p \in \{SP\} \setminus \partial\{SP\}; \end{aligned} \tag{2.6}$$

where F_x, F_y and F_z are the x-, y- and z-components of the ground-reaction force $\mathbf{F}_R$, respectively, μ is the friction coefficient, $\mathbf{r}_p = [x_p, y_p, 0]^T$ is the CoP/ZMP position on the horizontal even terrain, $\{SP\}$ is the support polygon, and $\partial\{SP\}$ is the boundary of $\{SP\}$.

To analyze the effects of the above constraints, a planar bipedal robot (see Fig. 2.2) is considered.

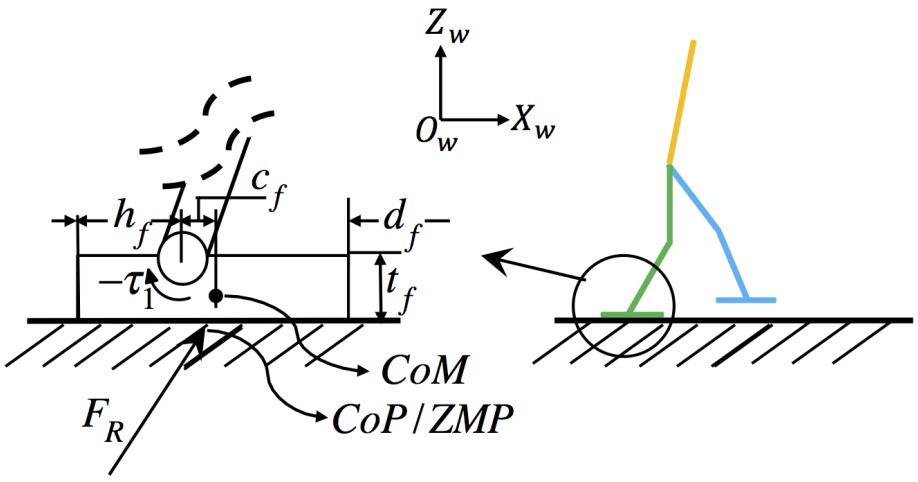

Figure 2.2. Support foot geometry ($t_f = 0$).

Combined with the unilateral constraint, the friction constraint becomes

$$-\mu F_z \leq F_x \leq \mu F_z. \tag{2.7}$$

Since $F_x = M\ddot{x}_c$ and $F_z = M\ddot{z}_c + Mg$ ($g = 9.81$ m/s^2 and M is the total mass), the set of achievable CoM acceleration bounded by the friction constraint is then described by

$$-\mu(\ddot{z}_c + g) \leq \ddot{x}_c \leq \mu(\ddot{z}_c + g). \tag{2.8}$$

For a planar robot, the CoP constraint becomes

$$x_0 < x_p < x_0 + d_f,$$

where x_0 is the heel location and d_f is the length of the support foot. The CoP position along the X_w-axis of the world coordinate frame $O_w X_w Z_w$ is [155]

$$x_p = x_0 + h_f + \frac{m_f g c_f - \tau_1 - M\ddot{x}_c t_f}{M(g + \ddot{z}_c)}, \tag{2.9}$$

where m_f, c_f, h_f and t_f are the mass, ankle-CoM distance, ankle-heel distance, and height of the support foot, respectively, and -τ_1 is the joint torque applied to the support foot (see Fig. 2.2). Combined with the unilateral constraint, the subset of the achievable CoM acceleration bounded by the CoP constraint then becomes

$$0 < \frac{m_f g c_f - \tau_1 - M\ddot{x}_c t_f}{M(g + \ddot{z}_c)} + h_f < d_f. \tag{2.10}$$

2.4.3 Effects of Ground-Contact Constraints on Achievable Center of Mass Acceleration at a Given Posture

From Eq. (2.8), it is clear that the subset bounded by the friction constraint only depends on the friction coefficient. However, Eq. (2.10) indicates that the subset bounded by the CoP constraint is dependent on the given posture and the torque limit. Therefore, it is not straightforward to determine how the CoP constraint shrinks the original torque-bounded polytope geometrically. The FCDM polytopes for two planar robots with zero joint velocities are shown in Fig. 2.3. The planar biped corresponding to Fig. 2.3(a) has two revolute joints – an ankle joint and a hip joint. The planar biped corresponding to Fig. 2.3(b) has three revolute joints – an ankle joint, a knee joint, and a hip joint.

Figure 2.3 shows that the friction constraint is indeed not affected by the torque constraint or the posture because the corresponding boundaries in two cases are the same. Also, the 3-DOF robot at the given posture has a relatively larger subset bounded by the CoP constraint as compared with the 2-DOF robot. It indicates that the higher DOFs may have the higher capacity to regulate CoM acceleration.

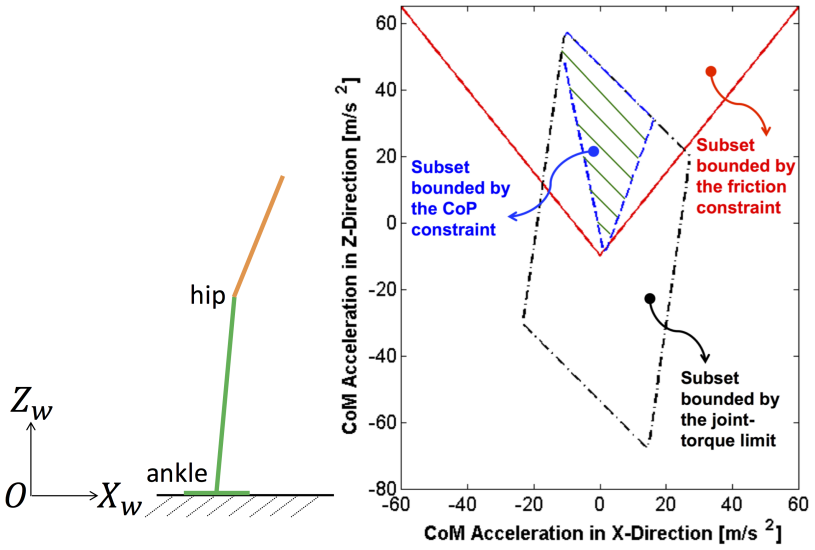

(a)

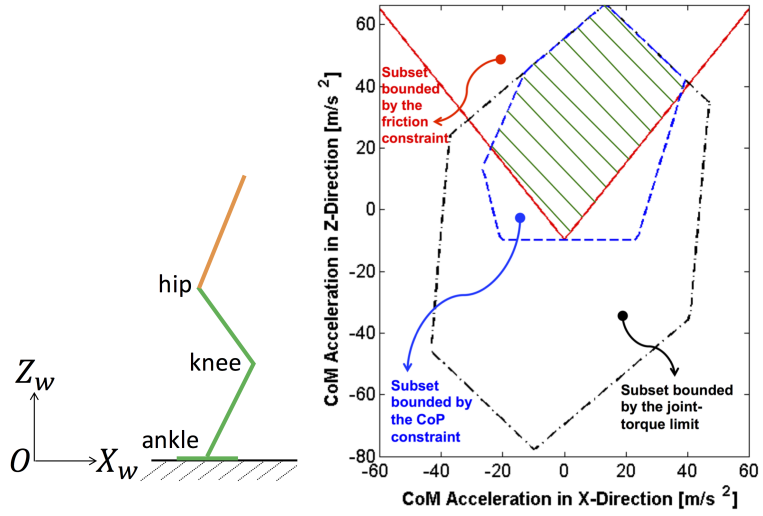

(b)

Figure 2.3. Feasible CoM dynamic manipulability polytopes (FCMP). (a): FCDM of a planar biped with an ankle joint and a hip joint. (b): FCDM of a planar biped with an ankle joint, a knee joint, and a hip joint. Black dot-dashed: the boundary of the subset bounded by the joint-torque limit. Red solid: the boundary of the subset bounded by the friction constraint (implicitly with the unilateral constraint). Blue dashed: the boundary of the subset bounded by the CoP constraint (implicitly with the unilateral constraint and the joint-torque limit). Green shaded: the subset bounded by the joint-torque limit and the three ground-contact constraints; that is, FCMP).

From Fig. 2.3 we can also see that the achievable CoM acceleration in different directions is drastically different due to the existence of the ground-contact constraints. Previous research on evaluation of a robot's dynamic performance is more focused on the global performance [148] [152]. Here, our interest is in the maximum achievable CoM acceleration in a specific direction. Thus, it is necessary to first analyze the effects of ground-contact constraints on the maximum achievable CoM acceleration in different directions. The following analysis is based on Fig. 2.3(b).

- **Horizontal Direction**: When the CoM acceleration is exactly horizontal, its magnitude is at most μg due to the friction constraint. It also indicates that the CoM acceleration, in this case, may be realized by an infinite number of postures for a redundant robot.

- **Downward Direction**: The vertical downward CoM acceleration is at most g in magnitude, which is determined by the unilateral constraint. For general downward acceleration, its magnitude is bounded by the friction constraint (implicitly with the unilateral constraint). There may exist infinitely many postures for CoM acceleration maximization.

- **Upward Direction**: The upward CoM acceleration is bounded by the CoP constraint (implicitly with the joint-torque constraint) and the friction constraint. For the directions bounded by the friction constraint, an infinite number of postures may exist for maximization of CoM acceleration. For the directions bounded by the CoP constraint, a unique optimal posture may exist.

2.4.4 Effects of Postures on Achievable Maximum CoM Acceleration in Different Directions

From Eq. (2.5), it is clear that the shape and the orientation of the CoM dynamic ellipsoid/polytope are affected by the robot's posture; that is, a biped's posture can affect the maximum feasible CoM acceleration in different directions. Maximizing the feasible

CoM acceletion is desirable for bipedal walking control because walking stabilty is closely related to a biped's capcity to regulate its CoM motion. Therefore, it is necessary to investigate the effects of postures on a biped's maximum feasible CoM acceleration.

To help understand the effects of postures on a biped's maximum feasible CoM acceleration, we will first utilize the numerical search to obtain the optimal posture that results in the maximum CoM acceleration in a specified direction:

$$\begin{aligned} \max \ & \|\ddot{\mathbf{r}}_c(\mathbf{q},\boldsymbol{\tau})\| \\ \text{subject to } & \mathbf{q} \in [\mathbf{q}_{min},\mathbf{q}_{max}] \\ & \mathbf{u} \in [-\mathbf{u}_{max},\mathbf{u}_{max}] \\ & \dot{\mathbf{q}} = \dot{\mathbf{q}}_0 \\ & \ddot{\mathbf{r}}_c = \mathbf{J}_c\mathbf{M}^{-1}(\mathbf{B}_u\mathbf{u}-\mathbf{c}) + \dot{\mathbf{J}}_c\dot{\mathbf{q}} \\ & F_z \geq 0 \\ & \sqrt{F_x^2+F_y^2} \leq \mu|F_z| \\ & \mathbf{r}_p \in \{SP\} \setminus \partial\{SP\} \\ & \angle(\ddot{\mathbf{r}}_c) = \gamma \end{aligned} \tag{2.11}$$

where γ specifies the desired direction of the CoM acceleration and $\dot{\mathbf{q}}_0$ is the given joint velocities.

Simulation results on a planar robot confirmed the previous analysis. The maximum feasible CoM acceleration bounded by the friction constraint can be achieved by an infinite number of postures. For each of the other directions, there exists a unique optimal posture. Figure 2.4(a) shows the optimal postures for seven of those directions. Figure 2.4(b) shows the corresponding CoM dynamic ellipses.

From Fig. 2.4, we discover that:

1. The maximum CoM acceleration in the upward direction as shown in Fig. 2.4(a) seems to be achieved when the hip joint is close to singularity;

2. Because the changes of both the knee and the hip angles are relatively small at different optimal postures as shown in Fig. 2.4(a), the ellipse orientation seems to change with the ankle angle monotonically;

3. The major axis of the torque-bounded ellipse aligns approximately with the specified CoM acceleration direction (see Fig. 2.4(b)).

From the simulation results, it is clear that the posture affects a biped's feasible CoM acceleration range. Hence, a biped's posture can be optimized in motion planning so as to maximize its feasible CoM acceleration capacity.

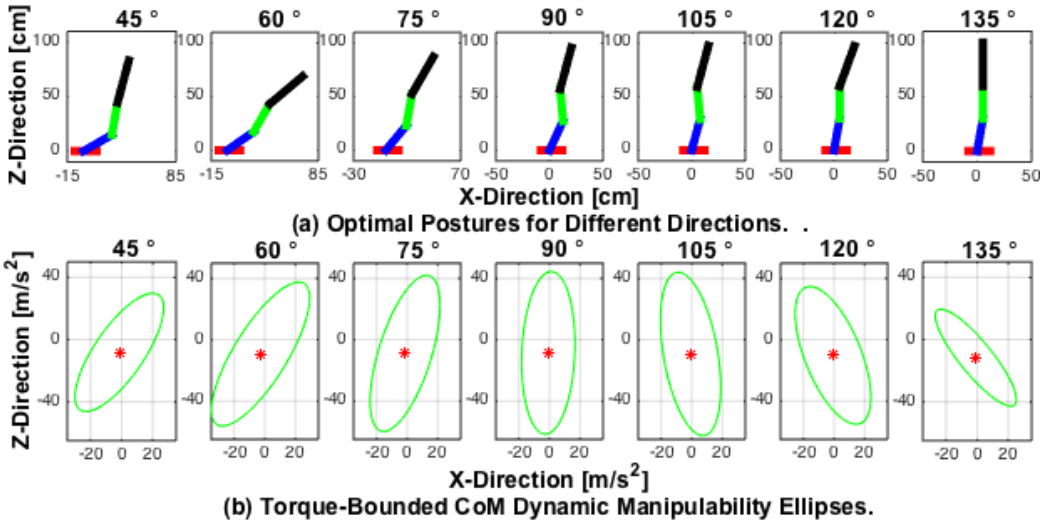

Figure 2.4. Optimal postures for achieving maximum feasible CoM acceleration in different directions and the corresponding torque-bounded CoM dynamic manipulability ellipses (specified CoM acceleration directions (from left to right): 45°, 60°, 75°, 90°, 105°, 120°, 135°).

2.5 Summary

In this Chapter, two types of bipedal gait characterization are described, the hybrid dynamics of bipedal robotic walking are modeled, and the stability measure of FCDM is introduced for walking analysis.

A bipedal gait can be typically characterized in two ways, one by the support and the swing legs and the other one by the left and the right legs. The support-swing characterization yields compact expressions of bipedal walking dynamics when symmetric gaits are of interest. But it cannot be conveniently used for characterization of asymmetric gaits. In contrast, the left-right characterization can be utilized to conveniently describe asymmetric gaits, but the resulting dynamic model is not as compact as the support-swing characterization. In this dissertation, both characterizations will be utilized to describe bipedal gaits. The dynamic model presented in this Chapter will be used in the model-based feedback controller designs for different bipedal models and control objectives in later Chapters. With the analysis based on the FCDM measure, one can visualize the limiting effects of ground-contact constraints on the feasible Center of Mass (CoM) accelerations, which also explains one of the main contributing factors to the difficulties in bipedal walking control. This measure can also be used in motion planning for selecting the desired postures to maximize a biped's feasible CoM acceleration capacity.

3. EXPONENTIAL TRACKING OF GLOBAL POSITION TRAJECTORY FOR FULLY ACTUATED PLANAR WALKING

3.1 Introduction

This Chapter and Chapter 4 focus on the study and development of model-based feedback controllers for fully actuated bipedal robotic walking, and Chapter 5 investigates walking control of underactuated bipeds. A bipedal robot is fully actuated if its number of degrees of freedom (DOFs) matches the number of independent actuators. Compared with underactuated walking, control design for fully actuated walking is relatively straightforward, which opens up opportunities for designing advanced controllers to achieve more control objectives. One such control objective that will be investigated in this Chapter is to achieve high versatility of walking. Specifically, exponential tracking of the desired global position trajectory in Cartesian space will be explored for planar bipedal robotic walking.

Controlling a biped's global position trajectory in Cartesian space is desirable because it enables planning and control of high-level tasks such as multi-agent coordination and obstacle avoidance. Previously, the HZD framework has been extended to realize the exponential tracking of the desired walking pattern as well as the desired walking speed for fully actuated bipedal walking [7] [111]. Because only velocity tracking has been addressed in those studies, satisfactory position tracking is not guaranteed, thus limiting the walking versatility of previous studies.

In this Chapter, we focus on achieving high versatility for fully actuated planar walking by realizing exponential position tracking in Cartesian space. Furthermore, the left-right gait characterization is utilized to describe a bipedal gait and express the dynamic model such that asymmetric gaits can be conveniently planned and controlled. Although this type of gait characterization has been previously utilized [124], the planning and control of asymmetric gaits have not been fully studied.

To achieve exponential tracking of the desired global position trajectory as well as the desired walking pattern, input-output linearization is utilized to synthesize a feedback controller, and the closed-loop stability conditions are derived based on the construction of multiple Lyapunov functions [156]. In the controller design, the full-order walking dynamics are considered, and the time-dependent output function is designed as the global position tracking error and the walking pattern tracking error. By driving the output function to zero, exponential tracking of the desired global position trajectory can be realized along with that of the desired walking pattern. Moreover, a new method of walking pattern design is presented, which guarantees that the planned motion respects the impact events and enables decoupled planning of the desired global position trajectory and the desired walking pattern. The proposed walking strategy was validated through simulated walking of a planar biped model with full-sized feet and three revolute joints. Simulation results showed that exponential tracking of the desired global position trajectory in Cartesian space, as well as the desired walking pattern in the configuration space, was satisfactorily realized. A comparison with previous studies on orbital stabilization is also presented to show the improved versatility.

3.2 Problem Formulation

This chapter explores the control strategies to achieve exponentially stable walking with improved versatility for a fully actuated, planar biped as compared with previous studies on orbital stabilization. To improve walking versatility, we will focus on realizing exponential tracking of the desired walking pattern, both symmetric and asymmetric, as well as the desired global position trajectory in Cartesian space. With this goal in mind, we will formulate the control design problem by utilizing the left-right gait characterization to conveniently define asymmetric walking patterns, modeling the hybrid walking dynamics of a fully actuated, planar biped, and deriving the mathematical expression of the position tracking error in Cartesian space as well as the walking pattern tracking error. Based on the proposed problem formulation, we will develop a model-based feedback control law, a

new method of desired gait design, and a set of sufficient conditions for guaranteeing the closed-loop stability.

3.2.1 Planar Walking Dynamics under Left-Right Gait Characterization

A planar bipedal robot with three revolute joints and finite-sized feet are shown in Fig. 3.1. In addition to the model assumptions listed in Section 2.3, it is assumed that the feet are massless, thin and that the swing foot always lands flat. Suppose that the actuator of the support leg's ankle is activated and that the actuator of the swing leg's ankle is not activated. Then, the bipedal robot is fully actuated. Its model parameters are given in Table 3.1.

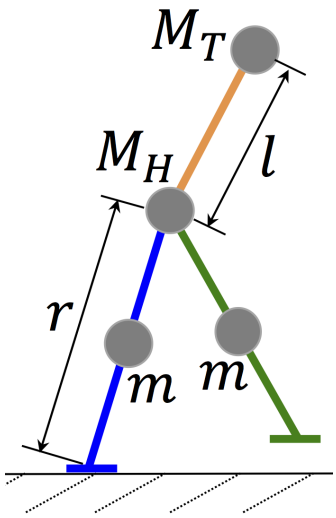

Figure 3.1. A planar biped with three revolute joints. (l and r are the lengths of the trunk and the legs, respectively. M_T, M_H, and m are the masses of the trunk, the hip, and the legs, respectively.)

To conveniently define asymmetric gaits as explained in Chapter 2, we use the left and the right legs to characterize the biped's gaits (see Fig. 3.2).

Table 3.1.
Mass and length parameters of the planar biped model in Fig. 3.1.

m (kg)	M_H (kg)	M_T (kg)	l, $\frac{r}{2}$ (m)
10	5	5	0.5

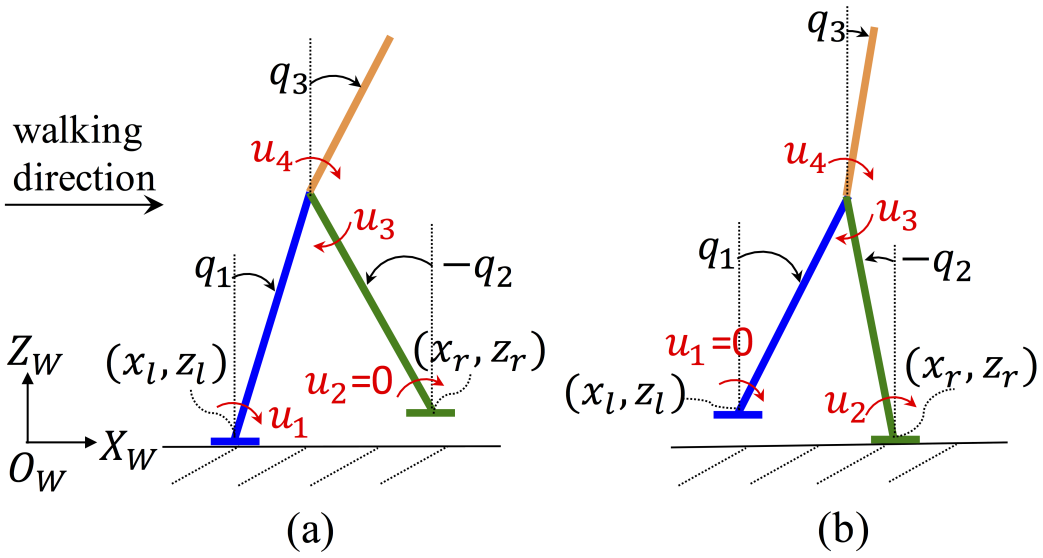

Figure 3.2. A fully actuated planar biped represented by the left-right gait characterization. (The left leg, the right leg, and the trunk are represented in blue, green, and orange colors, respectively.) (a): Left leg in support. (b): Right leg in support.

Under the left-right characterization, the joint position $\mathbf{q}$ is defined as

$$\mathbf{q} = \begin{bmatrix} q_1 \\ q_2 \\ q_3 \end{bmatrix} \in Q, \tag{3.1}$$

where $Q \subset \mathbb{R}^3$ is the configuration space of the bipedal robot when the support leg is in static, full contact with the walking surface and the joint position limits are satisfied, q_1 is the joint position of the left leg, q_2 is the joint position of the right leg, and q_3 is the joint

position of the trunk. The joint position $\mathbf{q}$ is defined with respect to the world coordinate frame $O_wX_wZ_w$ as shown in Fig. 3.2. Let

$$\mathbf{u} = \begin{bmatrix} u_1 \\ u_2 \\ u_3 \\ u_4 \end{bmatrix} \in \mathbb{R}^4$$

denote the joint-torque vector as illustrated in Fig. 3.2.

When the roles of the left and the right legs are differentiated, a complete gait cycle will include four subphases: a) left-in-support single-support phase (SSP), b) left-in-support double-support phase (DSP), c) right-in-support SSP, and d) right-in-support DSP.

Let $S_L(\mathbf{q}, \dot{\mathbf{q}})$ denote the switching surface that connects the left-in-support DSP and the right-in-support SSP:

$$S_L(\mathbf{q}, \dot{\mathbf{q}}) := \{(\mathbf{q}, \dot{\mathbf{q}}) \in TQ : z_{swL}(\mathbf{q}) = 0,\ \dot{z}_{swL}(\mathbf{q}, \dot{\mathbf{q}}) < 0\}, \tag{3.2}$$

where $z_{swL}(\mathbf{q})$ is the height of the swing foot during a left-in-support SSP and $z_{swL}(\mathbf{q}) := l\cos(q_1) - l\cos(q_2)$.

Let $S_R(\mathbf{q}, \dot{\mathbf{q}})$ denote the switching surface that connects the right-in-support DSP and the left-in-support SSP:

$$S_R(\mathbf{q}, \dot{\mathbf{q}}) := \{(\mathbf{q}, \dot{\mathbf{q}}) \in TQ : z_{swR}(\mathbf{q}) = 0,\ \dot{z}_{swR}(\mathbf{q}, \dot{\mathbf{q}}) < 0\}, \tag{3.3}$$

where $z_{swR}(\mathbf{q})$ is the height of the swing foot during a right-in-support SSP and $z_{swR}(\mathbf{q}) := l\cos(q_2) - l\cos(q_1)$.

Based on the dynamics equations in Section 2.3 and under the left-right characterization, the hybrid walking dynamics can be expressed as:

$$\begin{aligned}
\Sigma_L : &\begin{cases} \mathbf{M}_L(\mathbf{q})\ddot{\mathbf{q}} + \mathbf{c}_L(\mathbf{q}, \dot{\mathbf{q}}) = \mathbf{B}_{uL}\mathbf{u}_L, & \text{if } (\mathbf{q}^-, \dot{\mathbf{q}}^-) \notin S_L(\mathbf{q}, \dot{\mathbf{q}}); \\ [\mathbf{q}^+; \dot{\mathbf{q}}^+] = \boldsymbol{\Delta}_L(\mathbf{q}^-, \dot{\mathbf{q}}^-), & \text{if } (\mathbf{q}^-, \dot{\mathbf{q}}^-) \in S_L(\mathbf{q}, \dot{\mathbf{q}}); \end{cases} \\
\Sigma_R : &\begin{cases} \mathbf{M}_R(\mathbf{q})\ddot{\mathbf{q}} + \mathbf{c}_R(\mathbf{q}, \dot{\mathbf{q}}) = \mathbf{B}_{uR}\mathbf{u}_R, & \text{if } (\mathbf{q}^-, \dot{\mathbf{q}}^-) \notin S_R(\mathbf{q}, \dot{\mathbf{q}}); \\ [\mathbf{q}^+; \dot{\mathbf{q}}^+] = \boldsymbol{\Delta}_R(\mathbf{q}^-, \dot{\mathbf{q}}^-), & \text{if } (\mathbf{q}^-, \dot{\mathbf{q}}^-) \in S_R(\mathbf{q}, \dot{\mathbf{q}}); \end{cases}
\end{aligned} \tag{3.4}$$

where $i \in \{L,R\}$ indicates whether the left (L) or the right (R) leg is in support, $\mathbf{M}_i : Q \to \mathbb{R}^{3\times 3}$ is the inertia matrix, $\mathbf{c}_i : Q \to \mathbb{R}^3$ is the sum of the Coriolis, the centrifugal, and the gravitational terms, $\mathbf{B}_{ui} : \mathbb{R}^{3\times 3}$ is the nonsingular input matrix, $\mathbf{u}_i \in \mathbb{R}^3$ is the torque vector of the active joints, and $\boldsymbol{\Delta}_i : TQ \to \mathbb{R}^6$ is the reset map. The expressions of $\mathbf{M}_i$, $\mathbf{c}_i$, $\mathbf{B}_{ui}$, and $\mathbf{u}_i$ are given in Appendix A.1, and the expression of $\boldsymbol{\Delta}_i$ is given in Appendix A.2.

From the expression of $\boldsymbol{\Delta}_i$ in Appendix A.2, it can be known that

$$\boldsymbol{\Delta}_i(\mathbf{q},\dot{\mathbf{q}}) := \begin{bmatrix} \mathbf{q} \\ \boldsymbol{\Delta}_{\dot{q}i}(\mathbf{q})\dot{\mathbf{q}} \end{bmatrix}, \tag{3.5}$$

where the expression of $\boldsymbol{\Delta}_{\dot{q}i} : Q \to \mathbb{R}^{3\times 3}$ can be obtained from that of $\boldsymbol{\Delta}_i$ in Appendix A.2. Equation (3.5) indicates that the states representing joint velocities may experience a sudden jump at the switching event, but the states representing joint positions are always continuous because of the left-right gait characterization.

3.2.2 Tracking Error of the Desired Position Trajectory in Cartesian Space

To accomplish tasks such as multi-agent coordination and obstacle avoidance, it is necessary for a biped to follow the desired travel path with desired motion in Cartesian space, which can be formulated as a contouring control problem in general. By constructing an orthogonal global task coordinate frame along the desired travel path, the contour error and the motion along the desired travel path can be separately represented in two sets of coordinates, based on which contour error minimization and desired motion following along the contour can be decoupled into a stabilization problem and a trajectory tracking problem [157]. In this Chapter, we want to solve this contouring control problem for the planar biped model in Fig. 3.1, which reduces to the problem of position trajectory tracking along the X_w-axis because the X_w-axis is the only feasible travel path for the planar biped. The complete problem of straight-line contouring control will be considered for a three-dimensional (3-D) biped in Chapter 4.

A biped's global position in Cartesian space is needed in order to define its desired motion along the travel path. With reference to Fig. 3.2, let the biped's hip position $s(t)$

along the X_w-axis represent its global position in Cartesian space. Let (x_l, z_l) and (x_r, z_r) represent the positions of the left and the right feet with respect to the world coordinate frame, respectively. The hip position s can then be expressed as:

$$s = \begin{cases} x_l + l\sin(q_1) & \text{(left-leg-in-support);} \\ x_r + l\sin(q_2) & \text{(right-leg-in-support).} \end{cases} \tag{3.6}$$

Accordingly, let $s_d(t)$ denote the desired hip position trajectory along the X_w-axis.

Hence, the global position tracking error can be expressed as $s - s_d(t)$.

Let

$$q_{st} := \begin{cases} q_1 & \text{(left-in-support)} \\ q_2 & \text{(right-in-support)} \end{cases}$$

be the support-leg angle. Under the assumption that the support foot position is known, the desired position trajectory of the support leg can be obtained from $s_d(t)$ as:

$$q_{std}(t) := \begin{cases} q_{1d}(t) := sin^{-1}(\frac{s_d(t)-x_l}{l}) & \text{(left-in-support);} \\ q_{2d}(t) := sin^{-1}(\frac{s_d(t)-x_r}{l}) & \text{(right-in-support).} \end{cases} \tag{3.7}$$

Then, the tracking error of $q_{st} - q_{std}(t)$ can be used to indicate the global position tracking error $s - s_d(t)$. If a control law is synthesized such that $q_{st} - q_{std}(t)$ is driven to zero exponentially, then the exponential tracking of the desired global position trajectory $s_d(t)$ is realized.

3.2.3 Tracking Error of the Desired Walking Pattern

A walking pattern represents the relative evolution of a biped's joint positions with respect to a reference (or, encoding) variable in a complete walking cycle [50]. Note that a complete cycle under the left-right characterization includes two successive steps. Tracking a preplanned walking pattern is desirable not only because the joint motion can be synchronized with respect to the reference variable but also because a proper walking pattern design will lead to some advantages in motion planning and control design. The latter will be explored and explained in Sections 3.4 and 3.5.

To integrate walking pattern encoding with a biped's global motion, the relative position of the hip with respect to the support ankle, denoted as $\bar{s}$, is used as the encoding variable:

$$\bar{s} = \begin{cases} s - x_l & \text{(left-leg-in-support);} \\ s - x_r & \text{(right-leg-in-support).} \end{cases} \tag{3.8}$$

Note that $\bar{s}(t)$ increases monotonically in time during a forward step.

The desired motion of the swing leg and the trunk can then be encoded by $\bar{s}$, and the corresponding desired walking pattern is introduced as

$$\mathbf{g}_i(\bar{s}, q_{sw}, q_3) = \mathbf{0},\ i \in \{L, R\},$$

where $\mathbf{g}_i(\bar{s}, q_{sw}, q_3)$ is defined as:

$$\begin{cases} \text{left-leg-in-support:} & \mathbf{g}_L(\bar{s}, q_{sw}, q_3) := \begin{bmatrix} q_2 - \phi_{1L}(\bar{s}) \\ q_3 - \phi_{2L}(\bar{s}) \end{bmatrix}; \\ \text{right-leg-in-support:} & \mathbf{g}_R(\bar{s}, q_{sw}, q_3) := \begin{bmatrix} q_1 - \phi_{1R}(\bar{s}) \\ q_3 - \phi_{2R}(\bar{s}) \end{bmatrix}. \end{cases} \tag{3.9}$$

Hence, the walking pattern tracking error is simply $\mathbf{g}_i(\bar{s}, q_{sw}, q_3),\ i \in \{L, R\}$. The function $\phi_{ji}(\bar{s})$ $(i \in \{L, R\},\ j \in \{1, 2\})$ will be determined with a new method of walking pattern design in Section 3.4.

From Eqs. (3.6) and (3.8),

$$\bar{s} = l \sin(q_{st}).$$

Hence, one has

$$\tilde{\phi}_{ji}(q_{st}) := \phi_{ji}(\bar{s}) = \phi_{ji}(l \sin(q_{st})) \tag{3.10}$$

for $i \in \{L, R\}$ and $j \in \{1, 2\}$. Also, by the definition in Eq. (3.9), $\begin{bmatrix} \bar{s} \\ \mathbf{g}_L(\bar{s}, q_{sw}, q_3) \end{bmatrix}$ and $\begin{bmatrix} \bar{s} \\ \mathbf{g}_R(\bar{s}, q_{sw}, q_3) \end{bmatrix}$ are both local diffeomorphisms on $\mathbf{q}$.

With the above walking encoding method, the walking pattern in terms of the swing-leg joint position is represented by

$$\begin{cases} \text{left-leg-in-support:} & q_2 - \tilde{\phi}_{1L}(q_1) = 0 \\ \text{right-leg-in-support:} & q_1 - \tilde{\phi}_{1R}(q_2) = 0. \end{cases} \tag{3.11}$$

Such a walking pattern is also shown in Fig. 3.3 in terms of the support-leg angle q_{st} and the swing-leg angle q_{sw}. From Fig. 3.3, an asymmetric gait can be conveniently defined by differentiating the left and the right legs because $\tilde{\phi}_{1L}(q_{st})$ and $\tilde{\phi}_{1R}(q_{st})$ can be chosen independently. However, as shown by the dashed line in Fig. 3.3, the traditional walking characterization based on the support and the swing legs can at most represent a symmetric walking pattern where $\tilde{\phi}_{1L}(q_{st}) = \tilde{\phi}_{1R}(q_{st}) = \tilde{\phi}_1(q_{st})$.

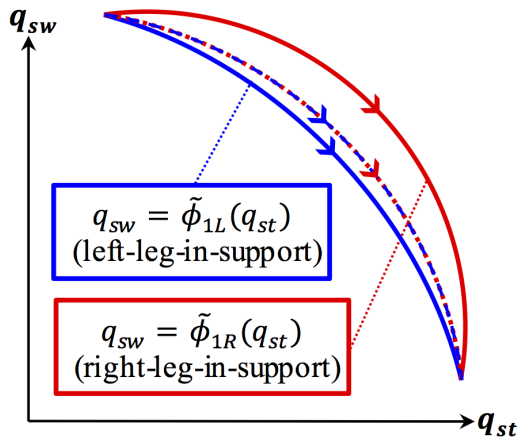

Figure 3.3. Encoding the swing-leg pattern using the support-leg angle q_{st} and the swing-leg angle q_{sw}.

3.3 Model-based Feedback Control through Input-Output Linearization

The control objective of this Chapter is to realize exponential tracking of the desired walking pattern in the configuration space as well as the desired position trajectory in Cartesian space. Under the assumption that there are no modeling errors or disturbances, input-

output linearization is utilized to synthesize the needed controller to achieve these objectives. Specifically, the swing leg and the trunk are driven to realize exponential tracking of the desired walking pattern encoded by the support-leg angle, and the support leg is controlled to realize exponential tracking of the desired motion in Cartesian space.

From Eqs. (3.7), (3.9), and (3.10), the output function is designed as:

$$\begin{cases} \text{left-leg-in-support:} & \mathbf{y}_L := \mathbf{q} - \mathbf{q}_{Ld}(t, q_1); \\ \text{right-leg-in-support:} & \mathbf{y}_R := \mathbf{q} - \mathbf{q}_{Rd}(t, q_2); \end{cases} \tag{3.12}$$

where

$$\mathbf{q}_{Ld}(t, q_1) := \begin{bmatrix} q_{1d}(t) \\ \tilde{\phi}_{1L}(q_1) \\ \tilde{\phi}_{2L}(q_1) \end{bmatrix} \text{ and } \mathbf{q}_{Rd}(t, q_2) := \begin{bmatrix} \tilde{\phi}_{1R}(q_2) \\ q_{2d}(t) \\ \tilde{\phi}_{2R}(q_2) \end{bmatrix}.$$

Then, by driving the output function $\mathbf{y}_i(t)$ ($i \in \{L, R\}$) to zero exponentially fast, exponential tracking of the desired global motion $s_d(t)$ and the desired walking pattern $\mathbf{g}_i(\bar{s}, q_{sw}, q_3) = \mathbf{0}$ can be realized simultaneously.

From Eq. (3.12), one obtains

$$\ddot{\mathbf{y}}_i = \mathbf{P}_i(q_{st})\ddot{\mathbf{q}} - \mathbf{z}_i(t, q_{st}, \dot{q}_{st}) \ , \ i \in \{L, R\}, \tag{3.13}$$

where $\mathbf{P}_i(q_{st})$ is proved to be always invertible. The expressions of $\mathbf{P}_i(q_{st})$ and $\mathbf{z}_i(t, q_{st}, \dot{q}_{st})$ are given in Appendix B.

Under the holonomic constraints in Eq. (3.2), motion during each continuous phase can be completely characterized by the reduced-dimensional generalized coordinates $\mathbf{q}$, and the ground-reaction force $\mathbf{F}_i$ ($i \in \{L, R\}$) can be eliminated from the continuous-phase dynamics in Eq. (3.2). Accordingly, one has

$$\ddot{\mathbf{q}} = \mathbf{M}_i(\mathbf{q})^{-1}(\mathbf{B}_{ui}i\mathbf{u}_i - \mathbf{c}_i(\mathbf{q}, \dot{\mathbf{q}})) \ , \ i \in \{L, R\}. \tag{3.14}$$

From Eqs. (3.13) and (3.14), one has

$$\ddot{\mathbf{y}}_i = \mathbf{N}_i(\mathbf{q})\mathbf{u}_i - \mathbf{L}_i(t, \mathbf{q}, \dot{\mathbf{q}}) \ , \ i \in \{L, R\}, \tag{3.15}$$

where $\mathbf{N}_i = \mathbf{P}_i\mathbf{M}_i^{-1}\mathbf{B}_{ui}$ is proved to be invertible and $\mathbf{L}_i = \mathbf{P}_i\mathbf{M}_i^{-1}\mathbf{c}_i + \mathbf{z}_i$.

Therefore, the feedback control law based on input-output linearization is defined as:

$$\mathbf{u}_i = \mathbf{N}_i^{-1}(\mathbf{v}_i + \mathbf{L}_i), \tag{3.16}$$

which results in a linear system:

$$\ddot{\mathbf{y}}_i = \mathbf{v}_i \ , \ i \in \{L,R\}. \tag{3.17}$$

If $\mathbf{v}_i$ is chosen as a proportional-derivative (PD) controller,

$$\mathbf{v}_i = -\mathbf{K}_{Pi}\mathbf{y}_i - \mathbf{K}_{Di}\dot{\mathbf{y}}_i, \ , \ i \in \{L,R\}, \tag{3.18}$$

where $\mathbf{K}_{Pi}$ and $\mathbf{K}_{Di}$ are both nonsingular diagonal matrices, one then obtains the following linear system:

$$\dot{\mathbf{x}} = \mathbf{A}_i(\mathbf{K}_{Pi}, \mathbf{K}_{Di})\mathbf{x} \ , \ i \in \{L,R\} \tag{3.19}$$

with

$$\mathbf{x} := \begin{bmatrix} x_1 \\ x_2 \\ x_3 \\ x_4 \\ x_5 \\ x_6 \end{bmatrix} := \begin{bmatrix} \mathbf{y}_i \\ \dot{\mathbf{y}}_i \end{bmatrix} \in \chi \tag{3.20}$$

and

$$\mathbf{A}_i(\mathbf{K}_{Pi}, \mathbf{K}_{Di}) := \begin{bmatrix} \mathbf{0}_{3\times 3} & \mathbf{I}_{3\times 3} \\ -\mathbf{K}_{Pi} & -\mathbf{K}_{Di} \end{bmatrix}, \tag{3.21}$$

where $\chi \subset \mathbb{R}^6$ is the full state space and $\mathbf{I}_{3\times 3} \in \mathbb{R}^5$ is an identity matrix.

If $\mathbf{K}_{Pi}$ and $\mathbf{K}_{Di}$ are chosen such that $\mathbf{A}_i(\mathbf{K}_{Pi}, \mathbf{K}_{Di})$ is Hurwitz, then there exists a real positive-definite-symmetric matrix $\mathbf{W}_i$ such that $V_i(\mathbf{x}) = \mathbf{x}^T\mathbf{W}_i\mathbf{x}$ is a Lyapunov function candidate for the continuous-phase dynamics in Eq. (3.19) and there exist positive constants c_{1i}, c_{2i}, and c_{3i} ($i \in \{L,R\}$) such that $V_i(\mathbf{x})$ satisfies

$$c_{1i}\|\mathbf{x}\|^2 \leq V_i(\mathbf{x}) \leq c_{2i}\|\mathbf{x}\|^2 \text{ and } \dot{V}_i(\mathbf{x}) \leq -c_{3i}V_i(\mathbf{x}) \tag{3.22}$$

for all $\mathbf{x}$ during continuous phases [76].

3.4 Desired Walking Pattern Design for the Construction of Hybrid Invariance

The desired walking motion $\mathbf{q}_{id}(t, q_{st})$ ($i \in \{L, R\}$) is completely defined by the desired global position trajectory and the desired walking pattern. Suppose that the desired global position trajectory $s_d(t)$ is determined by the high-level task planner, which is continuously differentiable and monotonically increasing for $t > 0$. Then, the remaining task of motion planning is walking pattern design, which should guarantee that the desired motion $\mathbf{q}_{id}(t, q_{st})$ will satisfy the following conditions:

(C1) $\mathbf{\Delta}_L(\tau_K^-, \mathbf{0}) = \mathbf{0}$ and $\mathbf{\Delta}_R(\tau_{K+1}^-, \mathbf{0}) = \mathbf{0}$, $\forall\, K \in \{1, 3, 5, ...\}$;

(C2) Joint position and velocity limits;

(C3) Joint-torque limits;

(C4) Ground-contact constraints including the friction cone and the unilateral constraint.

Since the last four conditions (C2) - (C4) can be easily met through trajectory optimization, they are not further discussed here. The first condition (C1) essentially states that the desired gait should respect the reset map; that is, if $\mathbf{x}(\tau_K^-) = \mathbf{0}$, then $\mathbf{x}(\tau_K^+) = \mathbf{0}$ should always hold. As will be presented in Section 3.5, the first condition (C1) is important because it can greatly simplify the stability analysis of the hybrid closed-loop control system. However, the satisfaction of (C1) is not straightforward as it involves both the desired global position trajectory and the desired walking pattern. In this section, a new method of walking pattern design is proposed, which guarantees that (C1) is always satisfied for any $s_d(t)$ that is continuously differentiable and monotonically increasing for $t > 0$. This is advantageous because the high-level planning of the desired global position trajectory $s_d(t)$ and the low-level planning of the desired walking pattern represented by $\tilde{\phi}_{ji}(q_{st})$ are decoupled for the satisfaction of (C1).

To minimize the energy cost of walking, the integral-squared motor torque per step distance can be minimized with the cost function J defined as [7]:

$$J = \frac{1}{d} \int_0^{\tau} \|\mathbf{u}_d(t)\|^2 dt, \tag{3.23}$$

where d is the planned step distance and $\mathbf{u}_d$ is motor torque corresponding to the desired walking motion. This constrained nonlinear optimization problem can be solved by the MATLAB command $fmincon$.

3.4.1 Invariance of $\mathbf{x} = \mathbf{0}$ upon Impacts for Desired Motion

The condition (C1) can be decomposed into two parts. One part requires that the desired walking pattern should respect the reset map, which can be satisfied based on the same method of walking pattern design for constructing HZD [103]. The other part is tricky to meet, which requires that the desired position trajectory of the support leg should respect the reset map. As indicated in Eq. (3.7), the desired support-leg trajectory is updated at the beginning of each step and depends on when and where the last actual swing-foot touchdown occurs. In the following, a new walking pattern design is presented, which guarantees that (C1) is always satisfied for any $s_d(t)$ that is continuously differentiable and monotonically increasing for $t > 0$.

Without loss of generality, suppose that the walking process begins with the left-leg-in-support continuous phase. Then, the K^{th} step ($K \in \{1,3,5...\}$) is a left-leg-in-support phase and the K^{th} switching is a left-to-right-support switching. For any $K \in \{1,3,5,...\}$, the assumption that $\mathbf{x} = \mathbf{0}$ during the K^{th} continuous phase and the definition of switching surface in Eq. (3.2) indicate that there may exist a positive number q_1^*, which satisfies

$$q_1^* + \tilde{\phi}_{1L}(q_1^*) = 0, \tag{3.24}$$

such that the K^{th} switching aways occurs at the fixed support-leg angle q_1^*. Because $s_d(t)$ increases monotonically, $q_{1d}(t)$ also increases monotonically within the K^{th} step. Hence, for any $K \in \{1,3,5,...\}$, $q_{1d}(\tau_K) = q_1^*$ always holds and uniquely determines the desired K^{th} impact time τ_K.

Assuming $\mathbf{x}(\tau_K^-) = \mathbf{0}$, one has

$$\mathbf{q}(\tau_K^-) = \mathbf{H}_{qL}(q_1^*) \text{ and } \dot{\mathbf{q}}(\tau_K^-) = \mathbf{H}_{\dot{q}L}(q_1^*)\dot{q}_{1d}(\tau_K^-), \tag{3.25}$$

where

$$\mathbf{H}_{qL}(q_1) := \begin{bmatrix} q_1 \\ \tilde{\phi}_{1L}(q_1) \\ \tilde{\phi}_{2L}(q_1) \end{bmatrix} \text{ and } \mathbf{H}_{\dot{q}L}(q_1) := \begin{bmatrix} 1 \\ \frac{d\tilde{\phi}_{1L}}{dq_1}(q_1 \\ \frac{d\tilde{\phi}_{2L}}{dq_1}(q_1) \end{bmatrix}. \tag{3.26}$$

Then, at $t = \tau_K^+$, due to the continuity in joint positions and the reset map on joint velocities,

$$\begin{aligned} &\mathbf{q}(\tau_K^+) = \mathbf{q}(\tau_K^-) = \mathbf{H}_{qL}(q_1^*), \\ &\dot{\mathbf{q}}(\tau_K^+) = \mathbf{\Delta}_{\dot{q}L}(\mathbf{q}(\tau_K^-))\dot{\mathbf{q}}(\tau_K^-) = \tilde{\mathbf{\Delta}}_{\dot{q}L}(q_1^*)\mathbf{H}_{\dot{q}L}(q_1^*)\dot{q}_{1d}(\tau_K^-), \end{aligned} \tag{3.27}$$

where $\tilde{\mathbf{\Delta}}_{\dot{q}L}(q_1^*) := \mathbf{\Delta}_{\dot{q}L}(\mathbf{H}_{qL}(q_1^*)) = \mathbf{\Delta}_{\dot{q}L}(\mathbf{q}(\tau_K^-))$.

Assuming $\mathbf{x}(\tau_K^+) = \mathbf{0}$, one has

$$\mathbf{q}(\tau_K^+) = \mathbf{H}_{qR}(q_{2d}(\tau_K^+)) \text{ and } \dot{\mathbf{q}}(\tau_K^+) = \mathbf{H}_{\dot{q}R}(q_{2d}(\tau_K^+))\dot{q}_{2d}(\tau_K^+), \tag{3.28}$$

where

$$\mathbf{H}_{qR}(q_2) := \begin{bmatrix} \tilde{\phi}_{1R}(q_2) \\ q_2 \\ \tilde{\phi}_{2R}(q_2) \end{bmatrix} \text{ and } \mathbf{H}_{\dot{q}R}(q_2) := \begin{bmatrix} \frac{d\tilde{\phi}_{1R}}{dq_2}(q_2) \\ 1 \\ \frac{d\tilde{\phi}_{2R}}{dq_2}(q_2) \end{bmatrix}. \tag{3.29}$$

Because $s_d(t)$ is continuously differentiable for $t > 0$, one has

$$s_d(\tau_K^+) = s_d(\tau_K^-) \tag{3.30}$$

and

$$\dot{s}_d(\tau_K^+) = \dot{s}_d(\tau_K^-). \tag{3.31}$$

Also, $s(t)$ is continuous for $t > 0$. Therefore, considering Eqs. (3.7) and (3.24), one obtains

$$q_{2d}(\tau_K^+) = \tilde{\phi}_{1L}(q_1^*) \tag{3.32}$$

and

$$\dot{q}_{2d}(\tau_K^+) = \frac{\cos(q_1^*)}{\cos(\tilde{\phi}_{1L}(q_1^*))}\dot{q}_{1d}(\tau_K^-) := \gamma_L(q_1^*)\dot{q}_{1d}(\tau_K^-). \tag{3.33}$$

where

Therefore, if $\tilde{\phi}_{ji}$ ($i \in \{L,R\}$, $j \in \{1,2\}$) can be designed to satisfy

$$\mathbf{H}_{qL}(q_1^*) = \mathbf{H}_{qR}(\tilde{\phi}_{1L}(q_1^*)) \tag{3.34}$$

and

$$\tilde{\mathbf{\Delta}}_{\dot{q}L}(q_1^*)\mathbf{H}_{\dot{q}L}(q_1^*) = \mathbf{H}_{\dot{q}R}(\tilde{\phi}_{1L}(q_1^*))\gamma_L(q_1^*), \tag{3.35}$$

then $\mathbf{x}(\tau_K^+) = \mathbf{\Delta}_L(\tau_K^-, \mathbf{0}) = \mathbf{0}$ holds for any $K \in \{1,3,5,...\}$.

Similarly, assume that $\mathbf{x} = \mathbf{0}$ holds during the $(K+1)^{th}$ ($K \in \{1,3,5,...\}$) continuous phase and that the $(K+1)^{th}$ impact occurs at the fixed support-leg angle $q_2 = q_2^*$. If $\tilde{\phi}_{ji}$ ($i \in \{L,R\}$, $j \in \{1,2\}$) is designed to satisfy

$$\mathbf{H}_{qR}(q_2^*) = \mathbf{H}_{qL}(\tilde{\phi}_{1R}(q_2^*)) \tag{3.36}$$

and

$$\tilde{\mathbf{\Delta}}_{\dot{q}R}(q_2^*)\mathbf{H}_{\dot{q}R}(q_2^*) = \mathbf{H}_{\dot{q}L}(\tilde{\phi}_{1R}(q_2^*))\gamma_R(q_2^*) \tag{3.37}$$

with

$$\tilde{\mathbf{\Delta}}_{\dot{q}R}(q_2^*) := \mathbf{\Delta}_{\dot{q}R}(\mathbf{H}_{qR}(q_2^*))$$

and

$$\gamma_R(q_2^*) := \frac{\cos(q_1^*)}{\cos(\tilde{\phi}_{1R}(q_2^*))},$$

then $\mathbf{\Delta}_R(\tau_{K+1}^-, \mathbf{0}) = \mathbf{0}$ for any $K \in \{1,3,5,...\}$.

3.4.2 Walking Pattern Parameterization with Beziér Curves

Introduce the reference variables as:

$$\lambda_L(q_1) = \frac{q_1 - q_{10}}{q_1^* - q_{10}} \text{ and } \lambda_R(q_2) = \frac{q_2 - q_{20}}{q_2^* - q_{20}}, \tag{3.38}$$

where q_{10} and q_{20} are the initial support-leg angles of the left-leg-in-support and the right-leg-in-support phases, respectively, determined by the desired walking pattern and the switching surfaces.

Similar to the previous study [102], the function $\tilde{\phi}_{ji}$ ($i \in \{L,R\},\ j \in \{1,2\}$), which defines the desired walking pattern, can be parameterized by the M^{th}-order Beziér curves:

$$\begin{aligned}
\tilde{\phi}_{1L}(q_1) &:= \bar{\phi}_{1L}(\lambda_L) = \sum_{p=0}^{M} \alpha_{Lp} \frac{M!}{p!(M-p)!} \lambda_L^p (1-\lambda_L)^{M-p}, \\
\tilde{\phi}_{2L}(q_1) &:= \bar{\phi}_{2L}(\lambda_L) = \sum_{p=0}^{M} \beta_{Lp} \frac{M!}{p!(M-p)!} \lambda_L^p (1-\lambda_L)^{M-p}, \\
\tilde{\phi}_{1R}(q_2) &:= \bar{\phi}_{1R}(\lambda_R) = \sum_{p=0}^{M} \alpha_{Rp} \frac{M!}{p!(M-p)!} \lambda_R^p (1-\lambda_R)^{M-p}, \\
\tilde{\phi}_{2R}(q_2) &:= \bar{\phi}_{2R}(\lambda_R) = \sum_{p=0}^{M} \beta_{Rp} \frac{M!}{p!(M-p)!} \lambda_R^p (1-\lambda_R)^{M-p},
\end{aligned} \tag{3.39}$$

where α_{ip} and β_{ip} ($i \in \{L,R\}$) are parameters of the Beziér curves.

Because Beziér curves are chosen to define $\bar{\phi}_{ji}(\lambda_i)$ ($i \in \{L,R\},\ j \in 1,2$), the desired function $\bar{\phi}_{ji}(\lambda_i)$ has the following properties:

1. $\bar{\phi}_{1i}(0) = \alpha_{i0}$, $\bar{\phi}_{2i}(0) = \beta_{i0}$;
2. $\bar{\phi}_{1i}(1) = \alpha_{iM}$, $\bar{\phi}_{2i}(1) = \beta_{iM}$;
3. $\frac{d\bar{\phi}_{1i}}{d\lambda_i}(0) = M\alpha_{i1} - \alpha_{i0}$, $\frac{d\bar{\phi}_{2i}}{d\lambda_i}(0) = M\beta_{i1} - \beta_{i0}$;
4. $\frac{d\bar{\phi}_{1i}}{d\lambda_i}(1) = M\alpha_{iM} - \alpha_{i(M-1)}$, $\frac{d\bar{\phi}_{2i}}{d\lambda_i}(1) = M\beta_{iM} - \beta_{i(M-1)}$.

These properties can be utilized to construct the desired walking pattern that satisfies the hybrid invariance conditions in Eqs. (3.34) - (3.39), which will be explained with an example next.

3.4.3 A Walking Pattern Design Example with Third-order Beziér Curves

In this subsection, the procedure of obtaining the unknown parameters of $\tilde{\phi}_{ji}$ ($i \in \{L,R\}$, $j \in \{1,2\}$) in Eq. (3.39) is explained. Suppose $M = 3$. From Eqs. (3.34) - (3.38) and the properties of $\tilde{\phi}_{ji}$ ($i \in \{L,R\}$, $j \in \{1,2\}$), one has:

$$q_1^* = \alpha_{R0},\ q_2^* = \alpha_{L0},\ q_{10} = \alpha_{R3},\ q_{20} = \alpha_{L3}, \tag{3.40}$$

$$\lambda_L(q_1) = \frac{q_1 - \alpha_{R3}}{\alpha_{R0} - \alpha_{R3}},\ \lambda_R(q_2) = \frac{q_2 - \alpha_{L3}}{\alpha_{L0} - \alpha_{L3}}, \tag{3.41}$$

$$\beta_{L3} = \beta_{R0},\ \beta_{L0} = \beta_{R3}, \tag{3.42}$$

$$\gamma_L(\alpha_{R0}) \begin{bmatrix} \frac{3\alpha_{R1}-\alpha_{R0}}{\alpha_{L0}-\alpha_{L3}} \\ 1 \\ \frac{3\beta_{R1}-\beta_{R0}}{\alpha_{L0}-\alpha_{L3}} \end{bmatrix} = \tilde{\mathbf{I}}_L(\alpha_{R0}) \begin{bmatrix} 1 \\ \frac{3\alpha_{L3}-\alpha_{L2}}{\alpha_{R0}-\alpha_{R3}} \\ \frac{3\beta_{L3}-\beta_{L2}}{\alpha_{R0}-\alpha_{R3}} \end{bmatrix}, \tag{3.43}$$

$$\gamma_R(\alpha_{L0}) \begin{bmatrix} 1 \\ \frac{3\alpha_{L1}-\alpha_{L0}}{\alpha_{R0}-\alpha_{R3}} \\ \frac{3\beta_{L1}-\beta_{L0}}{\alpha_{R0}-\alpha_{R3}} \end{bmatrix} = \tilde{\mathbf{I}}_R(\alpha_{L0}) \begin{bmatrix} \frac{3\alpha_{R3}-\alpha_{R2}}{\alpha_{L0}-\alpha_{L3}} \\ 1 \\ \frac{3\beta_{R3}-\beta_{R2}}{\alpha_{L0}-\alpha_{L3}} \end{bmatrix}. \tag{3.44}$$

When the desired walking direction is forward, the function $\tilde{\phi}_{ji}$ ($i \in \{L,R\}$, $j \in \{1,2\}$) should satisfy the following switching conditions:

$$\begin{aligned} & l\cos(\alpha_{R0}) - l\cos(\alpha_{L3}) = 0, \\ & l(-\sin(\alpha_{R0}) + \sin(\alpha_{L3})\frac{3\alpha_{L3} - \alpha_{L2}}{\alpha_{R0} - \alpha_{R3}}) < 0, \\ & l\cos(\alpha_{L0}) - l\cos(\alpha_{R3}) = 0, \\ & l(-\sin(\alpha_{L0}) + \sin(\alpha_{R3})\frac{3\alpha_{R3} - \alpha_{R2}}{\alpha_{L0} - \alpha_{L3}}) < 0. \end{aligned} \tag{3.45}$$

There are 16 unknown parameters of the eight 3^{rd}-order Beziér curves, and there are 10 equations and 2 inequality constraints in Eqs. (3.42) - (3.45). Therefore, the function $\tilde{\phi}_{ji}$ ($i \in \{L,R\}$, $j \in \{1,2\}$) can be determined through numerical search in order to satisfy the first condition (C1).

3.5 Closed-Loop Stability Analysis

Based on previous analysis, the closed-loop walking dynamics can be compactly written as

$$\begin{cases} \dot{\mathbf{x}} = \mathbf{A}_L \mathbf{x}, & \text{if } (t^-, \mathbf{x}^-) \notin S_{L\to R}(t, \mathbf{x}) \\ \mathbf{x}^+ = \mathbf{\Delta}_{L\to R}(t^-, \mathbf{x}^-), & \text{if } (t^-, \mathbf{x}^-) \in S_{L\to R}(t, \mathbf{x}) \end{cases} \tag{3.46}$$

during the left-leg-in-support phase and

$$\begin{cases} \dot{\mathbf{x}} = \mathbf{A}_R \mathbf{x}, & \text{if } (t^-, \mathbf{x}^-) \notin S_{R\to L}(t, \mathbf{x}) \\ \mathbf{x}^+ = \mathbf{\Delta}_{R\to L}(t^-, \mathbf{x}^-), & \text{if } (t^-, \mathbf{x}^-) \in S_{R\to L}(t, \mathbf{x}) \end{cases} \tag{3.47}$$

during the right-leg-in-support phase, where the expression of $\mathbf{\Delta}_i(t^-, \mathbf{x}^-)$ ($i \in \{L, R\}$) can be derived from Eqs. (3.4) and (3.12). The switching surfaces $S_{L\to R}(t, \mathbf{x})$ and $S_{R\to L}(t, \mathbf{x})$ can be obtained from Eqs. (3.2) and (3.3) as:

$$\begin{aligned} S_{L\to R}(t, \mathbf{x}) &:= \{(t, \mathbf{x}) : h_L(t, \mathbf{x}) = 0, \dot{h}_L(t, \mathbf{x}) < 0\}, \\ S_{R\to L}(t, \mathbf{x}) &:= \{(t, \mathbf{x}) : h_R(t, \mathbf{x}) = 0, \dot{h}_R(t, \mathbf{x}) < 0\}, \end{aligned} \tag{3.48}$$

where the expression of $h_i(t, \mathbf{x})$ ($i \in \{L, R\}$) can be derived from $z_{swi}(\mathbf{q})$.

Suppose that the walking process begins with the left-leg-in-support continuous phase at $t = t_0$. Without loss of generality, suppose $t_0 = 0$. Let T_{L_k} and T_{R_k}, $k \in \{1, 2, ...\}$, represent the actual moments of the k^{th} left-to-right-support and the k^{th} right-to-left-support impacts, respectively. Without loss of generality, assume $T_{R_0} = t_0$. Let τ_{L_k} and τ_{R_k}, $k \in \{1, 2, ...\}$, denote the desired moments of the k^{th} left-to-right impact assuming $\mathbf{x}(t) = 0 \; \forall t > T_{R_{k-1}}$ and the k^{th} right-to-left impact assuming $\mathbf{x}(t) = 0 \; \forall t > T_{L_k}$, respectively.

Properties of T_{L_k} and T_{R_k} are summarized in Theorem 3.1, which is introduced based on Lemma 2 in [79].

Theorem 3.1 Consider the fully actuated walking system in Eqs. (3.46) and (3.47). Let the following conditions hold:

(A1) There is no beating effect at impacts;

(A2) The desired global position trajectory $s_d(t)$ is continuously differentiable and monotonically increasing for $t > 0$;

(A3) The function $\tilde{\phi}_{ji}(q_{st})$ ($i \in \{L,R\}$, $j \in \{1,2\}$) that represents the desired walking pattern is continuously differentiable in q_{st}.

Then, there exists a small neighborhood U of the point $(\tau_{i_k}, \mathbf{0})$, $i \in \{L,R\}$, $k \in \{1,2,...\}$, such that $T_{i_k}(\tau_{i_k}, \mathbf{p}_{i_k}(\tau_{i_k}))$ is a unique continuously differentiable function in U, where $\mathbf{p}_{L_k}(t)$ is the solution of $\dot{\mathbf{x}} = \mathbf{A}_L\mathbf{x}$ on $t \in (T_{R_{k-1}}, +\infty)$ with initial condition $\mathbf{p}_{L_k}(T^+_{R_{k-1}}) = \mathbf{x}(T^+_{R_{k-1}})$ and $\mathbf{p}_{R_k}(t)$ is the solution of $\dot{\mathbf{x}} = \mathbf{A}_R\mathbf{x}$ on $t \in (T_{L_k}, +\infty)$ with initial condition $\mathbf{p}_{R_k}(T^+_{L_k}) = \mathbf{x}(T^+_{L_k})$. Also, T_{i_k} has the following properties:

(P1) $T_{L_k}(\tau_{L_k}, \mathbf{0}) = \tau_{L_k}$, $T_{R_k}(\tau_{R_k}, \mathbf{0}) = \tau_{R_k}$;

(P2) There exists a positive number L_τ such that $|T_{i_k}(\tau, \mathbf{w}) - T_{i_k}(\tau, \mathbf{u})| \leq L_\tau \|\mathbf{w} - \mathbf{u}\|$, $\forall (\tau, \mathbf{w})$, $(\tau, \mathbf{u}) \in U$.

■

Proof: By the definitions of T_{i_k} and τ_{i_k}, (P1) holds. From the conditions (A1) - (A3) and Eqs. (3.46), (3.47), and (3.48), it is easy to know that the functions that define the continuous dynamics, the reset maps, and the switching surfaces are all continuously differentiable in t and $\mathbf{x}$. Then, by the implicit function theorem, (P2) holds. ■

We are now ready to present the main theorem of this study.

Theorem 3.2 Let the conditions (A1) - (A3) hold. Assume that $\mathbf{\Delta}_L(\tau^-_{L_k}, \mathbf{0}) = \mathbf{0}$ and $\mathbf{\Delta}_R(\tau^-_{R_k}, \mathbf{0}) = \mathbf{0}$ for any $k \in \{1,2,...\}$. There exist sufficiently large $\mathbf{K}_{Pi}$ and $\mathbf{K}_{Di}$ ($i \in \{L,R\}$) and a positive number δ such that for any $\mathbf{x}(0) \in B_\delta(\mathbf{0}) := \{\mathbf{x} \in \chi : \|\mathbf{x}\| < \delta\}$ the hybrid closed-loop system in Eqs. (3.46) and (3.47) is locally exponentially stable. ■

Proof: Without loss of generality, suppose that the walking process begins with the left-leg-in-support continuous phase.

Let $V_L(\mathbf{x})$ and $V_R(\mathbf{x})$ be the Lyapunov functions associated with the left-leg-in-support and the right-leg-in-support phases, respectively. Let $V_R|^+_K$ and $V_L|^+_{K+1}$ ($K \in \{1,3,5,...\}$) denote the values of Lyapunov functions right after the K^{th} and the $(K+1)^{th}$ impacts, respectively. By stability analysis via multiple Lyapunov functions [156], the overall system is exponentially stable if $V_L(\mathbf{x})$ and $V_R(\mathbf{x})$ are exponentially decreasing in the left-leg-in-

support and the right-leg-in-support phases, respectively, and if $\{V_R|_1^+, V_R|_3^+, V_R|_5^+ ...\}$ and $\{V_L|_2^+, V_L|_4^+, V_L|_6^+ ...\}$ are both strictly decreasing sequences.

As explained in Section 3.3, if $\mathbf{K}_{Pi}$ and $\mathbf{K}_{Di}$ ($i \in \{L,R\}$) are chosen such that $\mathbf{A}_i(\mathbf{K}_{Pi}, \mathbf{K}_{Di})$ is Hurwitz then the continuous-phase subsystems are exponentially stabilized. Therefore, the remaining task is to derive stability conditions so that the sequences $\{V_R|_1^+, V_R|_3^+, V_R|_5^+ ...\}$ and $\{V_L|_2^+, V_L|_4^+, V_L|_6^+ ...\}$ are both strictly decreasing. This requirement can be rewritten as:

$$V_R|_{K+2}^+ < V_R|_K^+ \text{ and } V_L|_{K+3}^+ < V_L|_{K+1}^+, \tag{3.49}$$

for any $K \in \{1,3,5,...\}$.

First, we prove that there exist positive-definite diagonal matrices $\mathbf{K}_{Pi}$, $\mathbf{K}_{Di}$ ($i \in \{L,R\}$), and a positive number δ_R such that $V_R|_{K+2}^+ < V_R|_K^+$ for any $\mathbf{x}(0) \in B_{\delta_R}(\mathbf{0})$.

From Eq. (3.22), one has

$$V_R(\mathbf{x}) \leq e^{-c_{3R}(t-T_K)} V_R|_K^+ \tag{3.50}$$

during the continuous phase right after the K^{th} impact and

$$V_L(\mathbf{x}) \leq e^{-c_{3L}(t-T_{K+1})} V_L|_{K+1}^+ \tag{3.51}$$

during the continuous phase right after the $(K+1)^{th}$ impact.

Because of the assumption $\boldsymbol{\Delta}_R(\tau_{K+1}^-, \mathbf{0}) = \mathbf{0}$,

$$\begin{aligned} \|\mathbf{x}|_{K+1}^+\| &= \|\boldsymbol{\Delta}_R(T_{K+1}^-, \mathbf{x}|_{K+1}^-)\| \\ &\leq \|\boldsymbol{\Delta}_R(T_{K+1}^-, \mathbf{x}|_{K+1}^-) - \boldsymbol{\Delta}_R(\tau_{K+1}^-, \mathbf{x}|_{K+1}^-)\| \\ &+ \|\boldsymbol{\Delta}_R(\tau_{K+1}^-, \mathbf{x}|_{K+1}^-) - \boldsymbol{\Delta}_R(\tau_{K+1}^-, \mathbf{0})\|, \end{aligned} \tag{3.52}$$

where T_{K+1} is the moment of the actual $(K+1)^{th}$ impact, $\mathbf{x}|_{K+1}^-$ and $\mathbf{x}|_{K+1}^+$ represent the values of $\mathbf{x}$ right before and after the $(K+1)^{th}$ impact, respectively, and τ_{K+1} is the moment of the desired $(K+1)^{th}$ impact assuming $\mathbf{x}(t) = 0 \; \forall t > T_K$.

Because the reset map $\boldsymbol{\Delta}_i(t, \mathbf{x})$, $i \in \{L,R\}$, is continuously differentiable in t and $\mathbf{x}$, it is locally Lipschitz continuous in t and $\mathbf{x}$. Hence, there exists $r_R^* > 0$ such that for any $\mathbf{x}(0) \in B_{r_R^*}(\mathbf{0})$, one has

$$\|\boldsymbol{\Delta}_R(\tau_{K+1}^-, \mathbf{x}|_{K+1}^-) - \boldsymbol{\Delta}_R(\tau_{K+1}^-, \mathbf{0})\| \leq L_{\Delta_{Rx}} \|\mathbf{x}|_{K+1}^-\| \tag{3.53}$$

and

$$\|\mathbf{\Delta}_R(T_{K+1}^-, \mathbf{x}|_{K+1}^-) - \mathbf{\Delta}_R(\tau_{K+1}^-, \mathbf{x}|_{K+1}^-)\| \leq L_{\Delta_{Rt}}|T_{K+1} - \tau_{K+1}| \tag{3.54}$$

for some Lipschitz constants L_{Δ_x} and L_{Δ_t}.

Define

$$\tilde{\mathbf{x}}_R(t) := e^{\mathbf{A}_R(t-T_K)}\mathbf{x}|_K^+, \ \forall t > T_K, \tag{3.55}$$

and then by Theorem 3.1 there exist positive numbers h_R^* and L_τ such that

$$\begin{aligned} |T_{K+1} - \tau_{K+1}| &= |T_{K+1}(\tau_{K+1}, \tilde{\mathbf{x}}_R(\tau_{K+1})) - T_{K+1}(\tau_{K+1}, \mathbf{0})| \\ &\leq L_\tau \|\tilde{\mathbf{x}}_R(\tau_{K+1})\| \end{aligned} \tag{3.56}$$

for any $\mathbf{x}(0) \in B_{h_R^*}(\mathbf{0})$.

From Eqs. (3.52), (3.53), (3.54), and (3.56), one has

$$\|\mathbf{x}|_{K+1}^+\|^2 \leq L_{\Delta_R}(\|\mathbf{x}|_{K+1}^-\|^2 + \|\tilde{\mathbf{x}}_R(\tau_{K+1})\|^2), \tag{3.57}$$

where $L_{\Delta_R} := \max\{2L_{\Delta_{Rx}}^2, 2L_{\Delta_{Rt}}^2 L_\tau^2\}$.

Similarly,

$$\|\mathbf{x}|_{K+2}^+\|^2 \leq L_{\Delta_L}(\|\mathbf{x}|_{K+2}^-\|^2 + \|\tilde{\mathbf{x}}_L(\tau_{K+2})\|^2), \tag{3.58}$$

where L_{Δ_L} is a constant and can be obtained similarly to L_{Δ_R} and $\tilde{\mathbf{x}}_L(t)$ is defined as

$$\tilde{\mathbf{x}}_L(t) := e^{\mathbf{A}_L(t-T_{K+1})}\mathbf{x}|_{K+1}^+, \ \forall t > T_{K+1}. \tag{3.59}$$

According to Eq. (3.22), the following inequalities hold:

$$\begin{aligned} &V_R|_{K+1}^- \geq c_{1R}\|\mathbf{x}|_{K+1}^-\|^2, \ V_R(\tilde{\mathbf{x}}_R(\tau_{K+1})) \geq c_{1R}\|\tilde{\mathbf{x}}_R(\tau_{K+1})\|^2, \\ &V_L|_{K+2}^- \geq c_{1L}\|\mathbf{x}|_{K+2}^-\|^2, \ V_L(\tilde{\mathbf{x}}_L(\tau_{K+2})) \geq c_{1L}\|\tilde{\mathbf{x}}_L(\tau_{K+2})\|^2, \\ &V_L|_{K+1}^+ \leq c_{2L}\|\mathbf{x}|_{K+1}^+\|^2, \ V_R|_{K+2}^+ \leq c_{2R}\|\mathbf{x}|_{K+2}^+\|^2. \end{aligned} \tag{3.60}$$

Furthermore, from Eqs. (3.50), (3.51), (3.55), and (3.59), one has

$$V_R(\tilde{\mathbf{x}}_R(\tau_{k+1})) \leq e^{-c_{3R}(\tau_{k+1}-T_K)}V_R|_K^+ \tag{3.61}$$

and

$$V_L(\tilde{\mathbf{x}}_L(\tau_{k+2})) \leq e^{-c_{3L}(\tau_{k+2}-T_{K+1})}V_L|_{K+1}^+. \tag{3.62}$$

Combining Eqs. (3.57) - (3.62), one obtains

$$\begin{aligned} V_R|_{K+2}^{+} \leq & \frac{c_{2L}c_{2R}}{c_{1R}c_{1L}} L_{\Delta_L} L_{\Delta_R} (e^{-c_{3L}\Delta\tau_{K+1}} (e^{-c_{3L}(T_{K+2}-\tau_{K+2})} + 1) \\ & + e^{-c_{3R}\Delta\tau_K} (e^{-c_{3R}(T_{K+1}-\tau_{K+1})} + 1)) V_R|_K^{+}, \end{aligned} \tag{3.63}$$

where $\Delta\tau_K := \tau_{K+1} - T_K$ and $\Delta\tau_{K+1} := \tau_{K+2} - T_{K+1}$, $K \in \{1,3,5,...\}$. Note that $\Delta\tau_K$ is the desired duration of the $(K+1)^{th}$ step, which is known right after the K^{th} actual impact occurs.

From Eqs. (3.22) and (3.55),

$$\|\tilde{\mathbf{x}}_R(\tau_{k+1})\| \leq \sqrt{\frac{c_{2R}}{c_{1R}}} e^{-\frac{c_{3R}}{2c_{2R}}\Delta\tau_k} \|\mathbf{x}|_K^{+}\|, \tag{3.64}$$

holds, and thus from Eqs. (3.56) and (3.64) one has

$$|T_{K+1} - \tau_{K+1}| \leq L_\tau \sqrt{\frac{c_{2R}}{c_{1R}}} e^{-\frac{c_{3R}}{2c_{2R}}\Delta\tau_K} \|\mathbf{x}|_K^{+}\|. \tag{3.65}$$

Similarly,

$$|T_{K+2} - \tau_{K+2}| \leq L_\tau \sqrt{\frac{c_{2L}}{c_{1L}}} e^{-\frac{c_{3L}}{2c_{2L}}\Delta\tau_{K+1}} \|\mathbf{x}|_{K+1}^{+}\|. \tag{3.66}$$

Therefore, it is easy to know that for any $\varepsilon_R > 0$ there exist sufficiently large c_{3R} and c_{3L} and a positive number l^* such that

$$e^{-c_{3R}(T_{K+1}-\tau_{K+1})} \leq 1+\varepsilon \text{ and } e^{-c_{3L}(T_{K+2}-\tau_{K+2})} \leq 1+\varepsilon \tag{3.67}$$

hold for all $\mathbf{x}(0) \in B_{l^*}(\mathbf{0})$.

Then, it can be obtained from Eqs. (3.63) and (3.67) that

$$V_R|_{K+2}^{+} \leq \frac{c_{2L}c_{2R}}{c_{1L}c_{1R}} L_{\Delta_L} L_{\Delta_R} (1+\varepsilon)^2 e^{-(c_{3L}\Delta\tau_{K+1} + c_{3R}\Delta\tau_K)} V_R|_K^{+} \tag{3.68}$$

holds for any $\mathbf{x}(0) \in B_{\delta_R}(\mathbf{0})$ where $\delta_R := \min\{r_R^*, h_R^*, l^*\}$.

Similarly,

$$V_L|_{K+3}^{+} \leq \frac{c_{2L}c_{2R}}{c_{1L}c_{1R}} L_{\Delta_L} L_{\Delta_R} (1+\varepsilon)^2 e^{-(c_{3L}\Delta\tau_{K+3} + c_{3R}\Delta\tau_{K+2})} V_L|_{K+1}^{+}, \tag{3.69}$$

holds for any $\mathbf{x}(0) \in B_{\delta_L}(\mathbf{0})$ where δ_L can be found similarly to the above analysis.

Note that c_{3i} is determined by $\mathbf{K}_{Pi}$ and $\mathbf{K}_{Di}$, $i \in \{L,R\}$. Hence, if the PD gains are sufficiently large such that $\mathbf{A}_i$ is Hurwitz and that there exists a positive number $\delta < \min\{\delta_L, \delta_R\}$ such that

$$c_{3L}\Delta\tau_{K+1} + c_{3R}\Delta\tau_K > 2\ln(\frac{c_{2L}c_{2R}}{c_{1L}c_{1R}}L_{\Delta_L}L_{\Delta_R}(1+\varepsilon)) \tag{3.70}$$

and

$$c_{3L}\Delta\tau_{K+3} + c_{3R}\Delta\tau_{K+2} > 2\ln(\frac{c_{2L}c_{2R}}{c_{1L}c_{1R}}L_{\Delta_L}L_{\Delta_R}(1+\varepsilon)) \tag{3.71}$$

hold for any $\mathbf{x}(0) \in B_\delta(\mathbf{0})$ and any $K \in \{1,3,5,...\}$, then $V_R|^+_{K+2} < V_R|^+_K$ and $V_L|^+_{K+3} < V_L|^+_{K+1}$ hold for any $\mathbf{x}(0) \in B_\delta(\mathbf{0})$ and any $K \in \{1,3,5,...\}$; that is, the closed-loop system in Eqs. (3.46) and (3.47) is locally exponentially stable. ■

The stability conditions in Eqs. (3.70) and (3.71) indicate that the output function should converge to zero sufficiently fast so as to diminish the divergence caused by reset maps. Note that gait recharacterization does not affect the expansiveness of a reset map. In previous studies, rapidly exponential convergence of output function has been proposed to deal with the expansiveness of a landing impact [110], which can also be applied here to further increase the convergence rate.

Also, note that the assumptions $\mathbf{\Delta}_L(\tau_K^-, \mathbf{0}) = \mathbf{0}$ and $\mathbf{\Delta}_R(\tau_{K+1}^-, \mathbf{0}) = \mathbf{0}$ in Theorem 3.2 will always hold for any $K \in \{1,3,5,...\}$ if the desired walking pattern is designed properly as introduced in Section 3.4.

3.6 Simulation Results

Computer simulations are carried out on a fully actuated, planar biped (see Fig. 3.2) to show the validity of the proposed walking strategy. We first compare our proposed gait design and control with previous studies based on the same desired symmetric walking pattern to show that we can achieve exponential tracking of the desired global position trajectory $s_d(t)$ but the previous study can only track a constant walking speed. Moreover, an asymmetric walking pattern, which cannot be realized based on previous gait characterization, is simulated with two different desired global position trajectories $s_d(t)$ – one with a constant walking speed and the other with a time-varying walking speed – to further show the

versatility of the proposed walking strategy. Simulation results show that the desired gait respects the reset map regardless of the choice of $s_d(t)$ when the desired walking pattern is designed as introduced in Section 3.4. Finally, effects of the continuous-phase convergence rate on the closed-loop stability are analyzed through simulations, which validates the stability conditions in Section 3.5.

A symmetric walking pattern and an asymmetric walking pattern are generated through the proposed gait design in Section 3.4. For the purpose of illustration, the symmetric walking pattern of the swing-leg angle q_{sw} with respect to the support-leg angle q_{st} is shown in Fig. 3.4 (a), and the asymmetric one is shown in Fig. 3.4 (b).

3.6.1 Comparison with Orbitally Exponential Stabilization

In the previous work on orbital stabilization [111], the bipedal gait is characterized by the support and the swing legs. Thus, only a symmetric walking pattern can be exponentially tracked. Besides walking pattern tracking, another control objective of the previous work is velocity tracking in Cartesian space.

In order to compare our proposed walking strategy with the previous orbital stabilization [111], the desired walking pattern is chosen as the symmetric walking pattern in Fig. 3.4(a). The desired global position trajectory $s_d(t)$ is defined as monotonically increasing with a constant speed. Because the previous walking strategy focuses on velocity tracking in Cartesian space, its desired global motion is defined as $\dot{s}_d(t)$.

The simulation results corresponding to the previous work are shown in Fig. 3.5. From Fig. 3.5, it is clear to see that exponential tracking of the desired symmetric walking pattern is achieved. However, there is always a nonzero steady-state tracking error of the desired global position trajectory $s_d(t)$, although the desired global velocity trajectory $\dot{s}_d(t)$ can be exponentially tracked.

In contrast, with our proposed walking strategy, we can realize exponential walking pattern tracking and exponential global position tracking, as shown in Fig. 3.6.

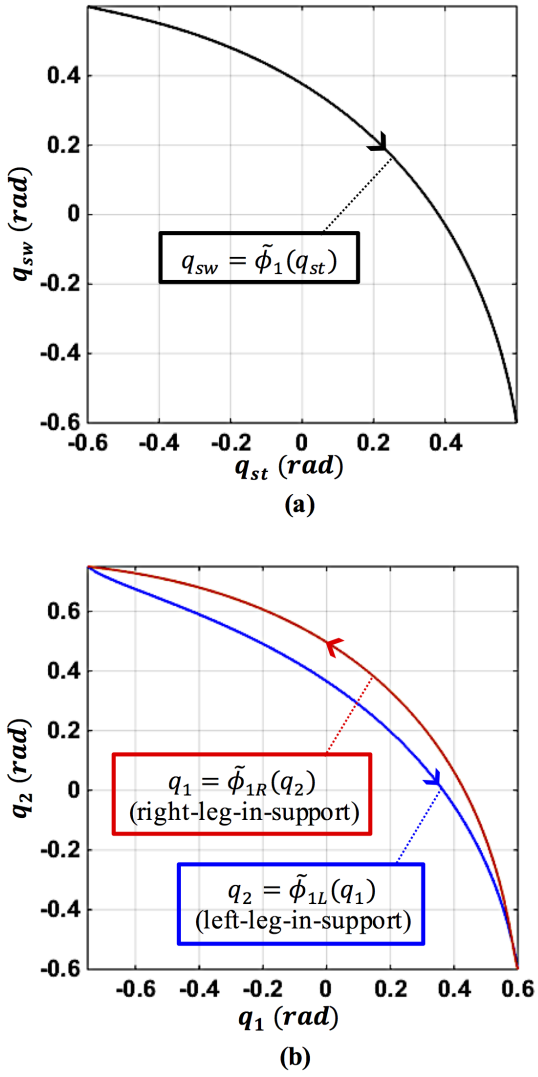

Figure 3.4. Desired walking patterns of swing-leg angle q_{sw} with respect to support-leg angle q_{st}. (a): Symmetric. (b): Asymmetric.

This comparison clearly illustrates that our proposed walking strategy can greatly improve walking versatility as compared with the previous work on orbital stabilization.

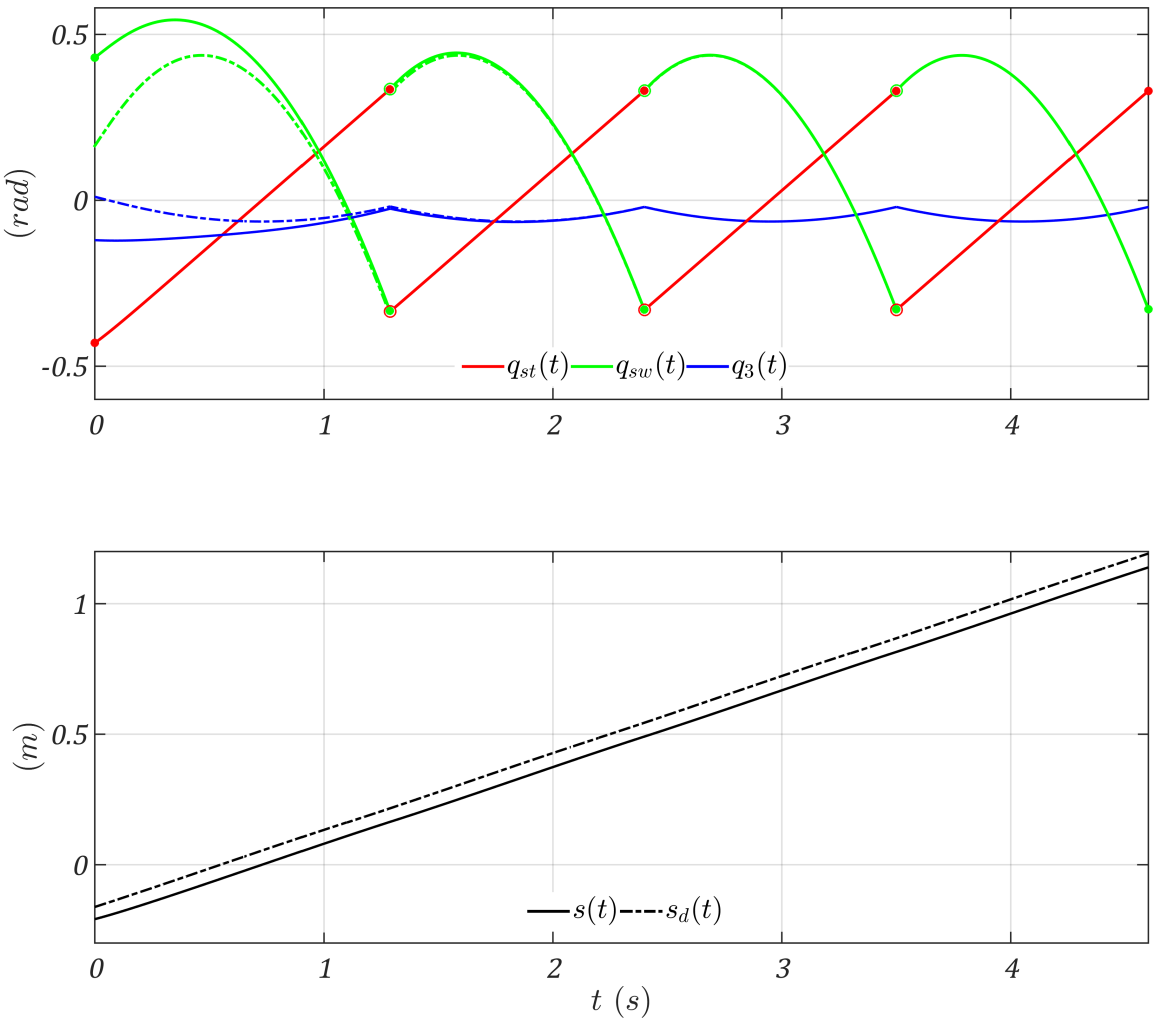

Figure 3.5. Simulation results of previous studies with walking characterization by support leg and swing leg. Green (blue) dashed: desired swing-leg (trunk) trajectory determined by the desired walking pattern.

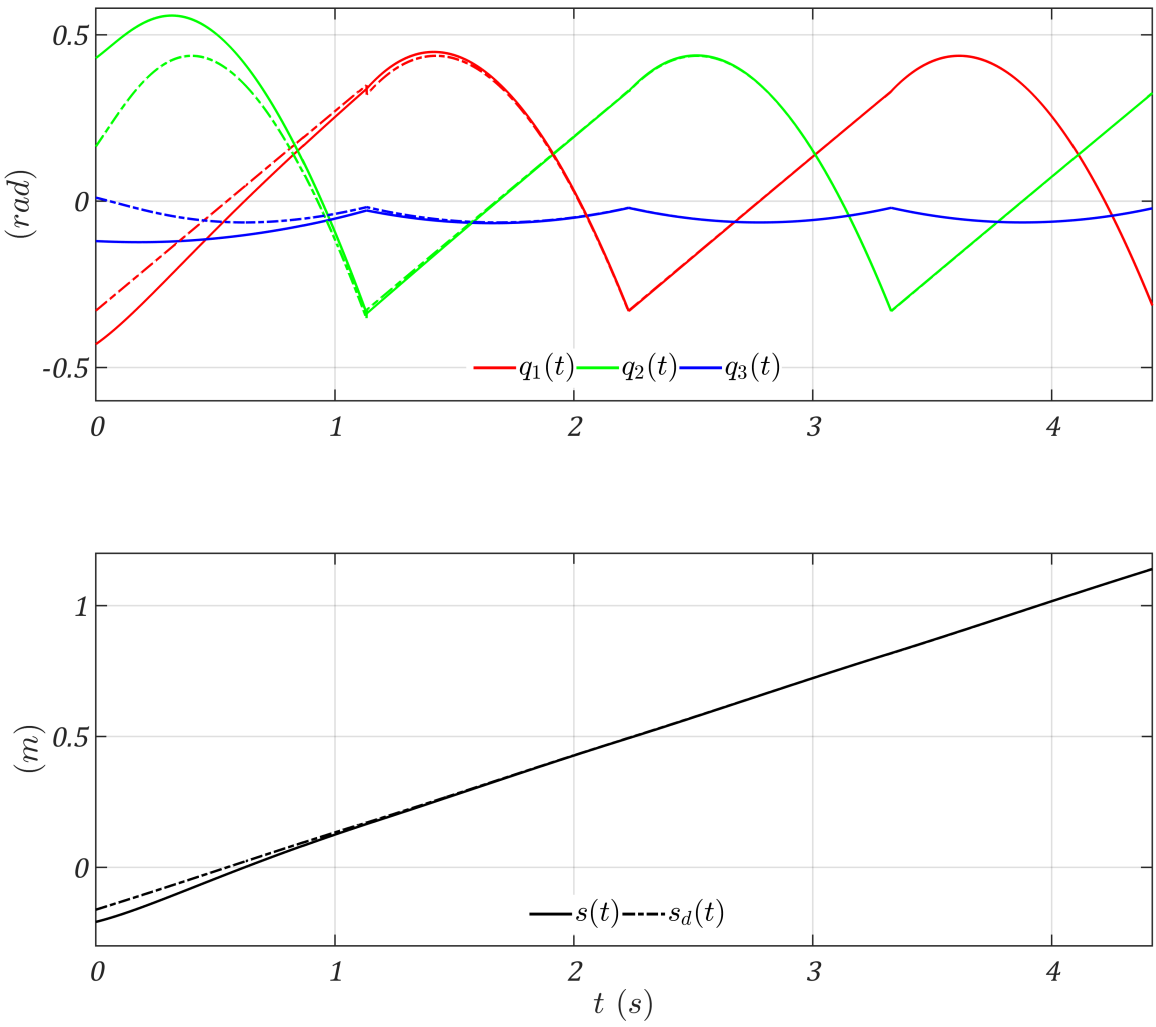

Figure 3.6. Simulation results of proposed desired gait design and control with walking characterized by left leg and right leg. Dashed lines (red, green, blue): desired trajectories determined by $\mathbf{g}_i(\bar{s}, q_{sw}, q_3) = \mathbf{0}$ ($i \in \{L, R\}$) and $s_d(t)$.

3.6.2 Stable Symmetric Walking

In this subsection, we will show two sets of bipedal walking with the same desired symmetric walking pattern (see Fig. 3.4(a)) but different desired hip trajectories $s_d(t)$. Without loss of generality, the control gains are chosen the same for both cases: $\mathbf{K}_{PL} = \mathbf{K}_{PR} = \text{diag}[28, 28, 28]$, $\mathbf{K}_{DL} = \mathbf{K}_{DR} = \text{diag}[11, 11, 11]$. These control gains are chosen such that the matrices $\mathbf{A}_L$ and $\mathbf{A}_R$ in Eq. (3.19) are both Hurwitz and that the conditions in Eqs. (3.70)

and (3.71) are met under relatively large initial tracking errors. These two sets of bipedal walking also share the same initial conditions:

$$\begin{aligned}
&s(0) - s_d(0) = -0.1(\text{m}),\ \dot{s}(0) - \dot{s}_d(0) = 0.1(\text{m/s}),\\
&q_2(0) - \tilde{\phi}_{1L}(q_1(0)) = 0.1(\text{rad}),\\
&q_3(0) - \tilde{\phi}_{2L}(q_1(0)) = -0.1(\text{rad}),\\
&\dot{q}_2(0) - \tfrac{d\tilde{\phi}_{1L}}{dq_1}(q_1(0))\dot{q}_1(0) = -0.1(\text{rad/s}),\\
&\dot{q}_3(0) - \tfrac{d\tilde{\phi}_{2L}}{dq_1}(q_1(0))\dot{q}_1(0) = 0.1(\text{rad/s}).
\end{aligned} \tag{3.72}$$

Due to the identical control gains, $\mathbf{A} = \mathbf{A}_L = \mathbf{A}_R$. Then, without loss of generality, the Lyapunov functions during the left-leg-in-support and the right-leg-in-support phases are chosen to be the same:

$$V_L(\mathbf{x}) = V_R(\mathbf{x}) = \mathbf{x}^T \mathbf{W} \mathbf{x}, \tag{3.73}$$

where $\mathbf{W}$ is the solution of the Lyapunov equation $\mathbf{AW} + \mathbf{WA}^T + \mathbf{Q} = \mathbf{0}$ with $\mathbf{Q} = \mathbf{I}_{6\times 6}$ [76].

Figure 3.7 shows the results with $s_d(t) = 0.6t - 0.1(\text{m})$, and Fig. 3.8 corresponds to $s_d(t) = 2.3e^{-0.3(t+0.5)} + 0.6t - 2.1(\text{m})$. From the plots, we can see that exponential tracking of the desired hip trajectory $s_d(t)$ with either constant or time-varying walking speed is achieved under the same desired walking pattern. It confirms that a walking pattern generated through the proposed gait design method in Section 3.4 can be automatically incorporated with an arbitrary hip trajectory $s_d(t)$ that is differentiable and monotonically increasing. Note that the Lyapunov function plot in Fig. 3.7 shows a relatively large jump at the first impact at $t = 0.5$ (s) while the one in Fig. 3.8 shows no significant jump at the first landing impact at $t = 2$ (s). Because the desired global position trajectory in Fig. 3.8 has a much lower velocity in the first few seconds than that in Fig. 3.7, the duration of the first step is much longer in Fig. 3.8, which results in the much smaller trajectory tracking error right before the first impact and the much smaller jump of the Lyapunov function right after the first impact in Fig. 3.8.

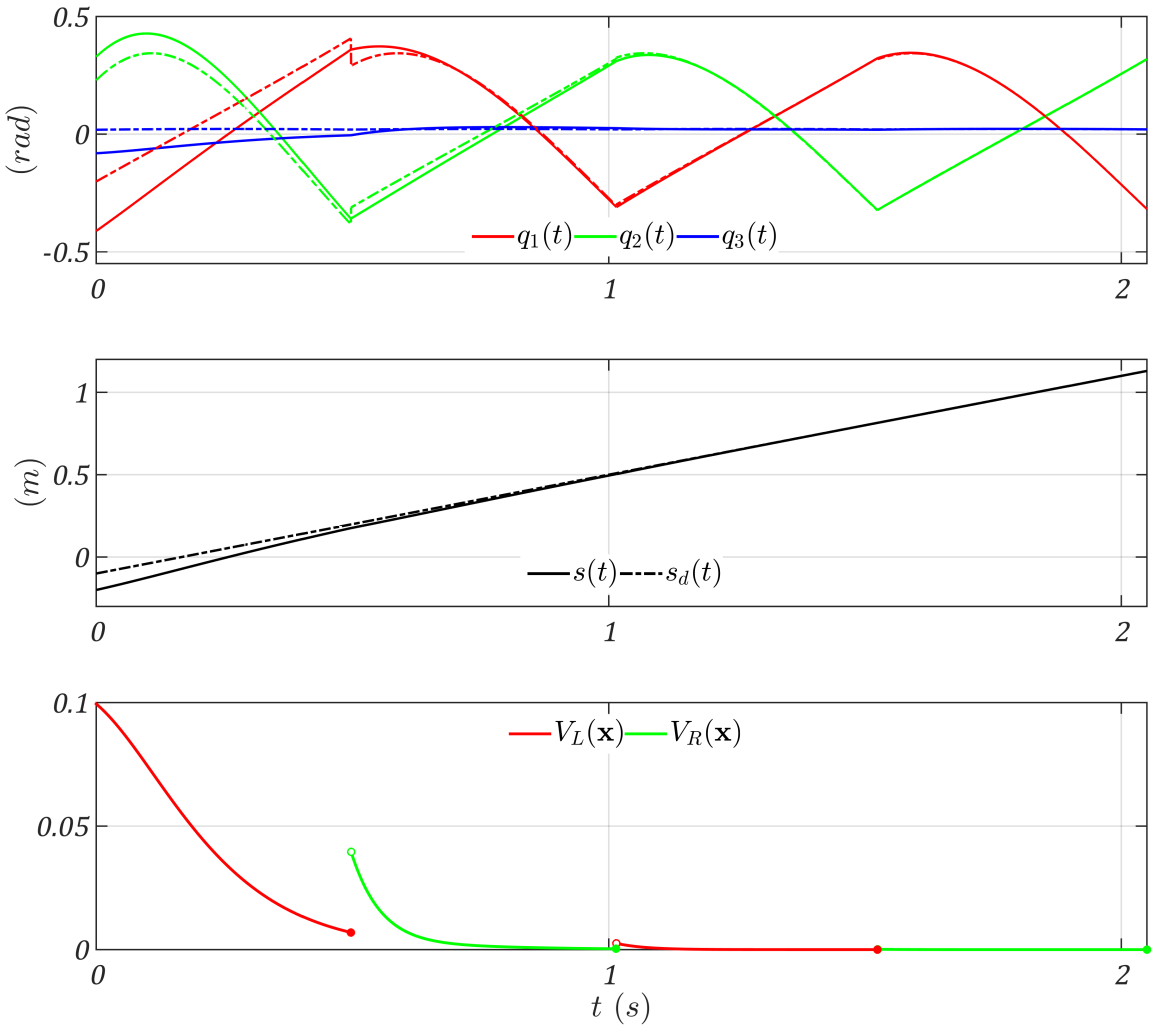

Figure 3.7. Symmetric walking with $s_d(t) = 0.6t - 0.1$(m), $\mathbf{K}_{Pi}$= diag[28,28,28,28,28], and $\mathbf{K}_{Di}$= diag[11,11,11,11,11]. Dashed lines (red, green, blue): desired joint trajectories determined by $\mathbf{g}_i(\bar{s}, q_{sw}, q_3) = \mathbf{0}$ ($i \in \{L,R\}$) and $s_d(t)$.

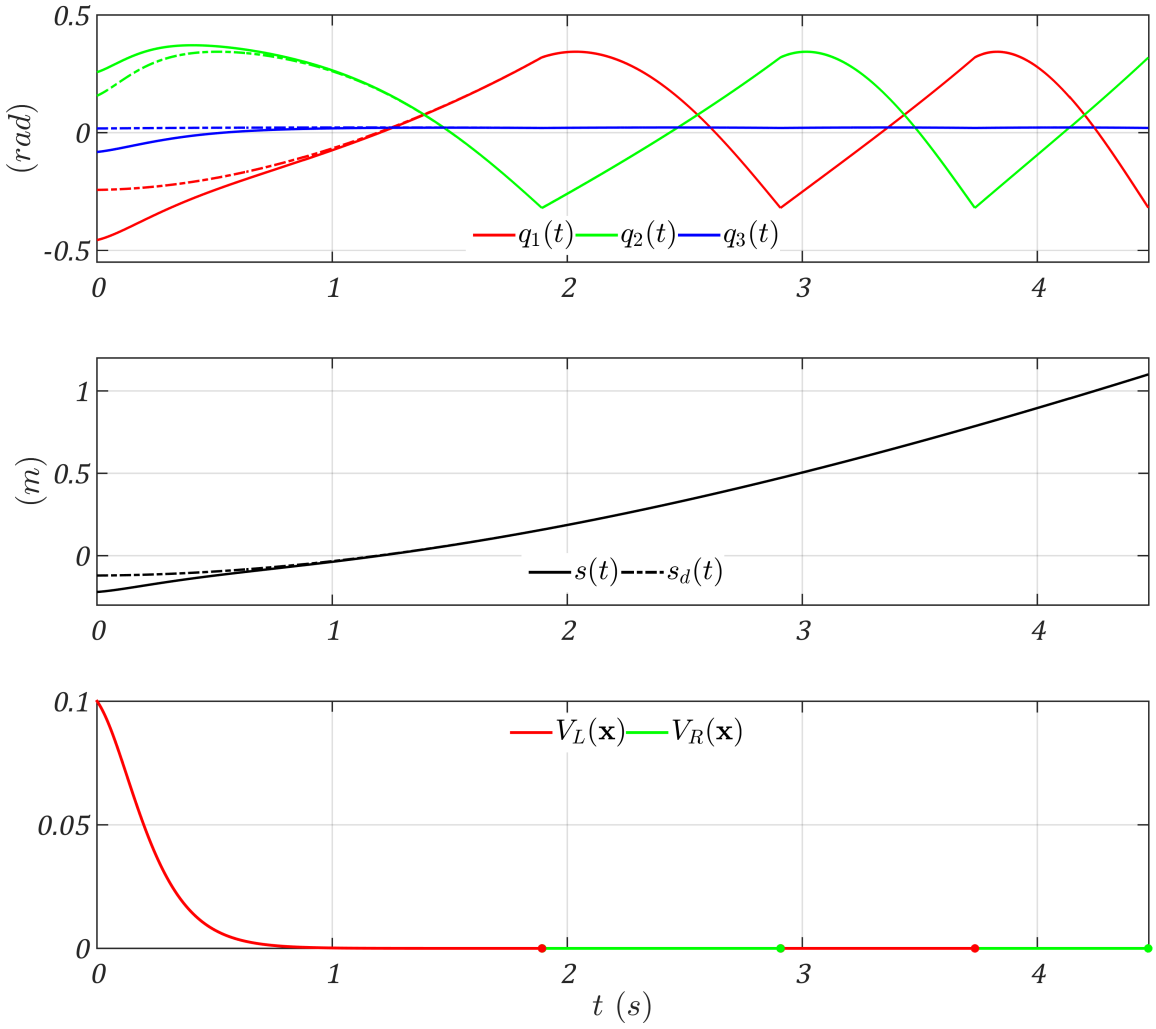

Figure 3.8. Symmetric walking with $s_d(t) = 2.3e^{-0.3(t+0.5)} + 0.6t - 2.1$(m), $\mathbf{K}_{Pi}$= diag[28, 28,28,28,28], and $\mathbf{K}_{Di}$=diag[11,11,11,11,11]. Dashed lines (red, green, blue): desired joint trajectories determined by $\mathbf{g}_i(\bar{s}, q_{sw}, q_3) = \mathbf{0}$ ($i \in \{L,R\}$) and $s_d(t)$.

3.6.3 Stable Asymmetric Walking

As stated earlier, the left-right gait characterization enables planning and tracking of an asymmetric walking pattern, which is illustrated with two sets of simulation results in Figs 3.9 and 3.10. Except for the desired global position trajectories $s_d(t)$, these two sets of

simulations share the same desired asymmetric walking pattern as in Fig. 3.4(b), the same control parameters $\mathbf{K}_{PL} = \mathbf{K}_{PR} = \text{diag}[12,12,12,12,12]$ and $\mathbf{K}_{DL} = \mathbf{K}_{DR} = \text{diag}[7,7,7,7,7]$, and the same initial conditions and definitions of Lyapunov functions as in Section 3.6.2.

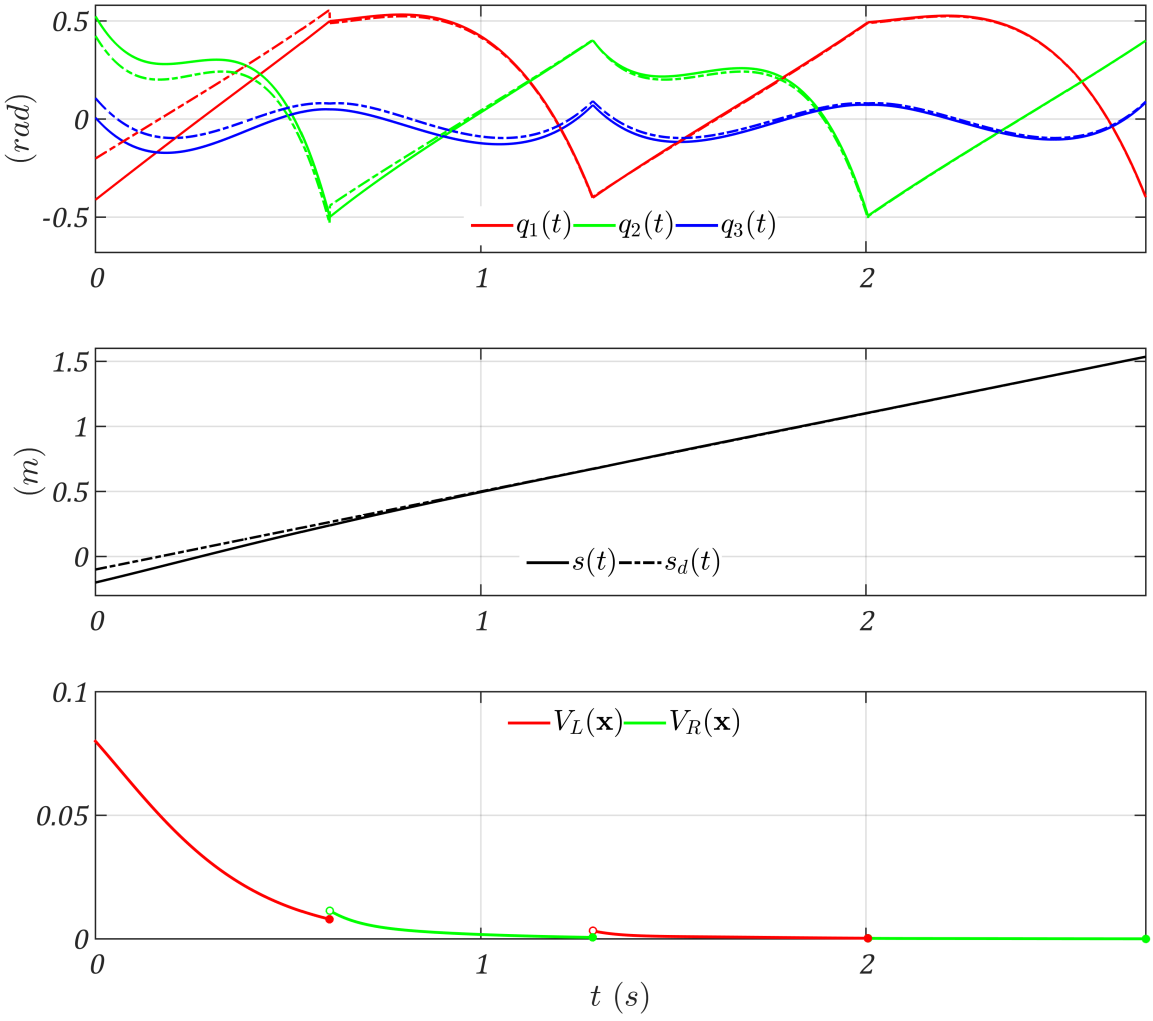

Figure 3.9. Asymmetric walking with $s_d(t) = 0.6t - 0.1$(m), $\mathbf{K}_{Pi}$=diag[12,12,12,12,12], and $\mathbf{K}_{Di}$=diag[7,7,7,7,7]. Dashed lines (red, green, blue): desired joint trajectories determined by $\mathbf{g}_i(\bar{s}, q_{sw}, q_3) = \mathbf{0}$ ($i \in \{L,R\}$) and $s_d(t)$.

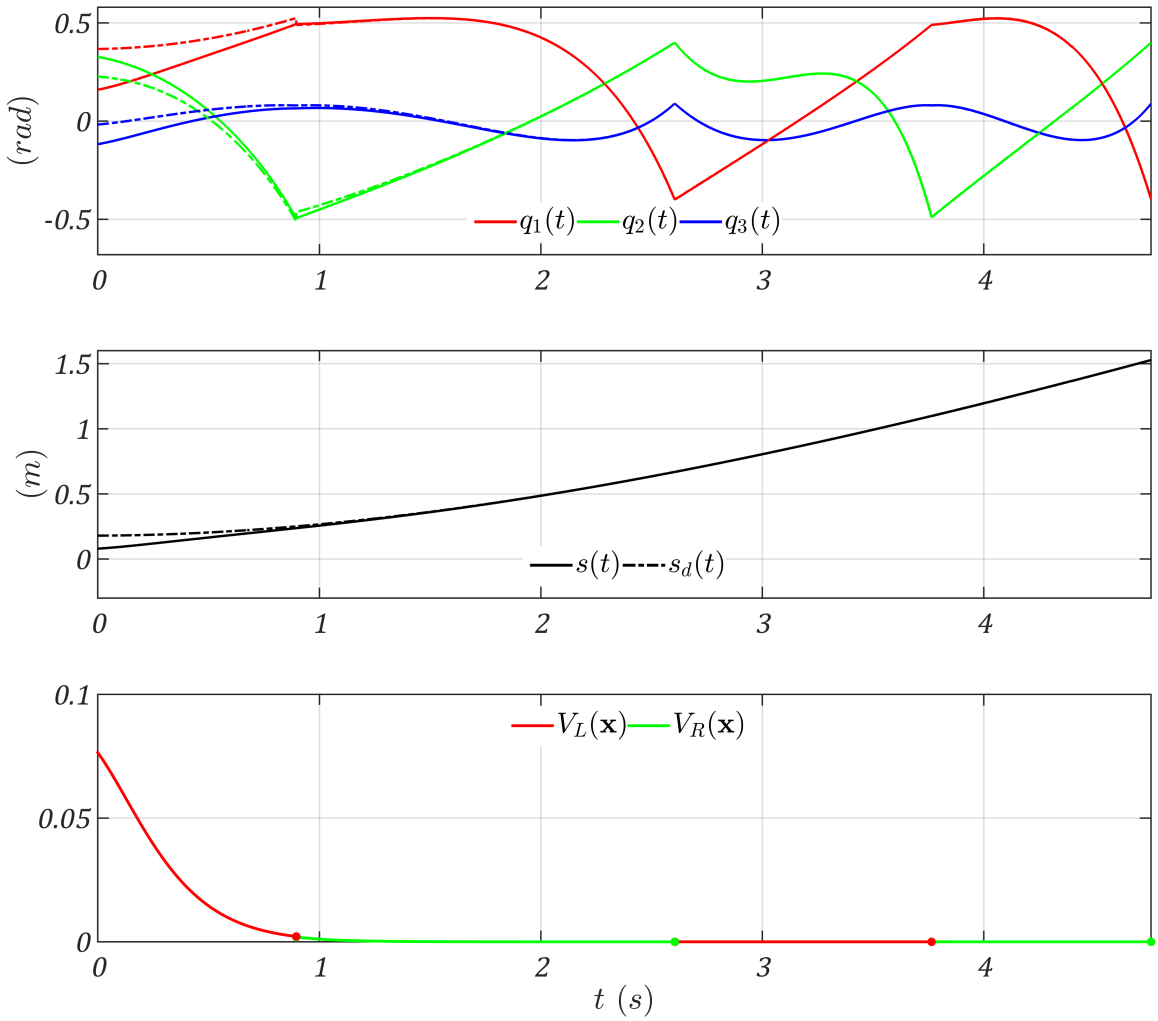

Figure 3.10. Asymmetric walking with $s_d(t) = 2.3e^{-0.3(t+0.5)} + 0.6t - 2.1$(m), $\mathbf{K}_{Pi}$=diag[12, 12,12,12,12], and $\mathbf{K}_{Di}$=diag[7,7,7,7,7]. Dashed lines (red, green, blue): desired joint trajectories determined by $\mathbf{g}_i(\bar{s}, q_{sw}, q_3) = \mathbf{0}$ ($i \in \{L, R\}$) and $s_d(t)$.

3.6.4 Effects of Proportional-derivative Control Gains on Closed-Loop Stability

Theorem 3.2 introduced in Section 3.5 indicates that the continuous-phase convergence rate determined by the PD gains should be sufficiently fast to guarantee the stability of the closed-loop hybrid dynamical system in Eqs. (3.46) and (3.47). Here, two sets of simulated bipedal walking (see Figs. 3.11 and 3.12) are presented under different PD gains but

with the same initial conditions, desired walking pattern, and desired hip trajectory as in Fig. 3.9. Definitions of the Lyapunov functions are the same as in Eq. (3.73). The PD gains corresponding to Fig. 3.11 is larger than those that correspond to Fig. 3.12. Accordingly, the actual joint trajectories $\mathbf{q}(t)$, as well as the hip position $s(t)$, converge to the desired motions faster in Fig. 3.11 than in Fig. 3.12. This trend is also shown by the plots of Lyapunov functions. This comparison illustrates Theorem 3.2 and shows that a higher convergence rate during the continuous phases results in faster closed-loop convergence.

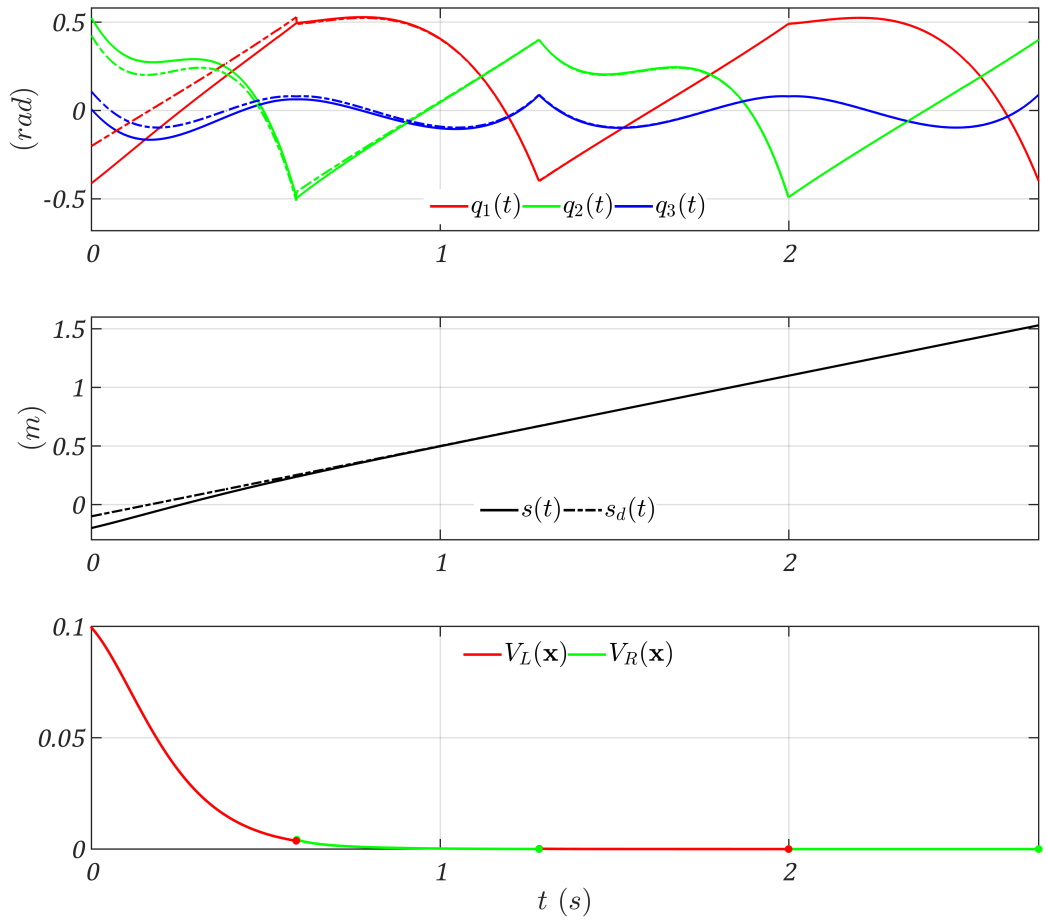

Figure 3.11. Asymmetric walking with $s_d(t) = 0.6t - 0.1$(m), $\mathbf{K}_{PL}$=$\mathbf{K}_{PR}$=diag[28,28,28,28, 28], and $\mathbf{K}_{DL}$= $\mathbf{K}_{DR}$= diag[11,11,11,11,11]. Dashed lines (red, green, blue): desired joint trajectories determined by $\mathbf{g}_i(\bar{s}, q_{sw}, q_3) = \mathbf{0}$ ($i \in \{L,R\}$) and $s_d(t)$.

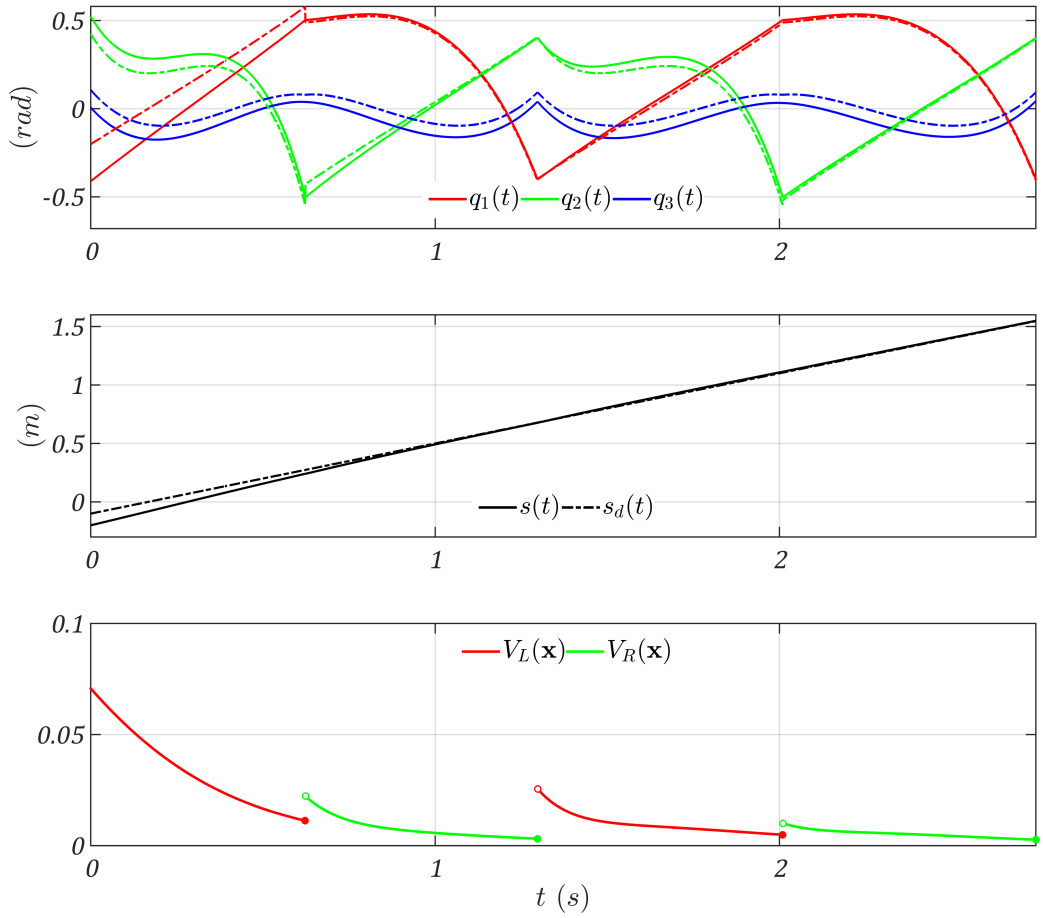

Figure 3.12. Asymmetric walking with $s_d(t) = 0.6t - 0.1$(m), $\mathbf{K}_{Pi}$=diag[6,6,6,6,6], and $\mathbf{K}_{Di}$=diag[5,5,5,5,5]. Dashed lines (red, green, blue): desired joint trajectories determined by $\mathbf{g}_i(\bar{s}, q_{sw}, q_3) = \mathbf{0}$ ($i \in \{L, R\}$) and $s_d(t)$.

3.7 Summary

In this Chapter, provably stable, fully actuated, planar bipedal robotic walking has been achieved with improved versatility as compared with previous studies. In order to define both symmetric and asymmetric walking patterns, the left and the right legs were used to characterize a bipedal gait. A feedback controller was then synthesized in order to realize exponential tracking of the desired global position trajectory in Cartesian space as well as the desired walking pattern, both symmetric and asymmetric, in the configuration

space. Closed-loop stability conditions were analyzed based on the construction of multiple Lyapunov functions, which essentially require that the continuous-phase convergence rate of the output function should be sufficiently fast in order to overcome the possibility of divergence caused by landing impacts. A new method of walking pattern design was proposed, which guarantees that the low-level planning of the desired walking pattern can be decoupled from the high-level planning of the desired global motion. Provably exponential stabilization and versatility of the proposed walking strategy were confirmed with simulated bipedal walking.

The result of this Chapter will be extended to a fully actuated three-dimensional (3-D) biped for contouring control in Chapter 4.

4. EXPONENTIAL TRACKING OF GLOBAL POSITION TRAJECTORY FOR FULLY ACTUATED THREE-DIMENSIONAL WALKING

4.1 Introduction

In Chapter 3, exponential tracking of the desired global position trajectory was investigated for fully actuated planar bipedal robotic walking. To our best knowledge, it is the first time that global position tracking of planar bipedal robotic walking has been addressed based on nonlinear feedback control and formal stability analysis. However, the walking strategy developed in Chapter 3 is for planar bipedal robots that are confined to moving in the sagittal plane. In this Chapter, the controller synthesis in Chapter 3 will be extended to the global position tracking problem for fully actuated three-dimensional (3-D) bipedal robotic walking.

For many complex tasks such as multi-agent coordination, it is important that a bipedal robot can satisfactorily track the desired global position trajectory on the walking surface. This problem has been studied mainly by the Zero-Moment Point (ZMP) approach, which utilizes the ZMP balance criterion to stabilize bipedal walking and track the desired motion [41] [158]. However, it has not been fully explored using model-based feedback control that utilizes full-order dynamic modeling and formal stability analysis. Velocity tracking in Cartesian space has been studied for fully actuated walking based on the concept of partial hybrid zero dynamics [111], but global position tracking for 3-D bipedal robots has not been addressed under the HZD framework.

The objective of this Chapter is to realize exponential tracking of the desired position trajectory in Cartesian space as well as the desired walking pattern for 3-D bipedal robotic walking. The desired walking pattern is defined as the desired relative evolution of joint positions with respect to a phase variable that represents how far a step has progressed [50]. The desired position trajectory in Cartesian space is defined as the planned

path on the walking surface along with the desired motion along the path. The problem of position tracking in Cartesian space will be formulated as a contouring control problem. Contouring control has been extensively studied for machining tasks such as cutting and milling [157] [159] [160]. Here, the concept is adapted to legged robotic locomotion. A contour is defined as a 1-D geometric path on the walking surface, and the contouring control problem will be decomposed into two subproblems. One is a stabilization problem, and the objective is to realize exponential convergence to the shape of the desired contour. The other is a position tracking problem, and the objective is to realize exponential convergence to the desired position trajectory along the desired contour. In this Chapter, the desired paths/contours on the walking surface are limited to straight-line paths/contours.

4.2 Problem Formulation

The controller design in this Chapter focuses on the realization of exponential tracking of the desired position trajectory in Cartesian space as well as the desired walking pattern for fully actuated, 3-D bipedal robotic walking. For simplicity, only symmetric gaits are considered here, which will be described using the support-swing gait characterization. The first step of the proposed controller design is to model the full-order hybrid dynamics of 3-D bipedal robotic walking under the support-swing gait characterization. Then, we will derive the mathematical expression of the tracking error of the desired walking pattern as well as the desired contour and motion.

4.2.1 Three-dimensional Walking Dynamics under Support-Swing Gait Characterization

A 3-D bipedal robot with nine revolute joints is shown in Fig. 4.1 [121]. Different from the planar biped model in Chapter 3 that only has pitch joints (see Fig. 3.1), the 3-D biped model as shown in Fig. 4.1 also has roll joints. To clearly show the distribution of joint actuators, their arrangement is illustrated in Fig. 4.1.

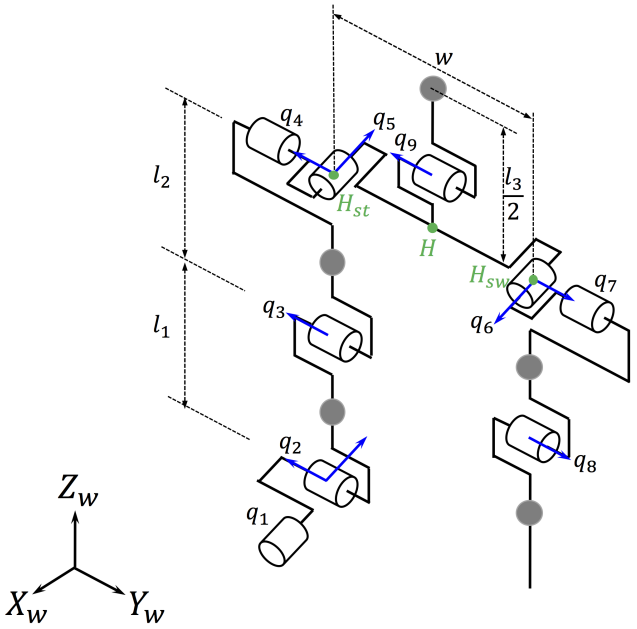

(a)

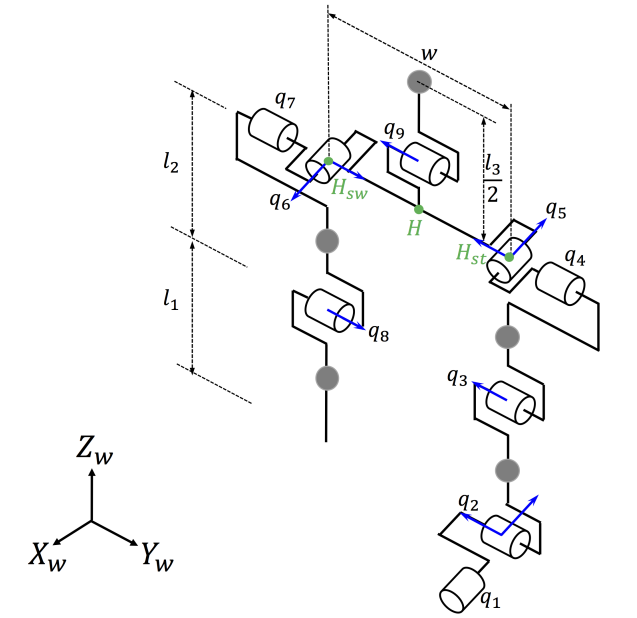

(b)

Figure 4.1. A fully actuated 3-D biped represented by the support-swing gait characterization. (a): The right leg is in support. (b): The left leg is in support.

In addition to the model assumptions listed in Section 2.3, it is assumed that the biped's feet are massless, thin. Also, for simplicity and without loss of generality, it is assumed that the swing foot always lands flat pointing towards the positive direction of the X_w-axis. Hence, the orientation of the support foot coordinate frame $O_f X_f Y_f Z_f$ is always aligned with the world coordinate frame $O_w X_w Y_w Z_w$. This 3-D biped model is fully actuated because it is supposed that the actuator of the support ankle is activated and that the actuator of the swing ankle is not.

Parameters of the simulated biped model are shown in Table 4.1.

Table 4.1.
Mass and length parameters of the three-dimensional biped model in Fig. 4.1.

m_1 (kg)	m_2 (kg)	m_T (kg)	l_1, l_2, $\frac{l_3}{2}$ (m)	w (m)
3	6	20	0.4	0.3

For the simplicity of expression, only the support-swing characterization will be considered here to describe a 3-D bipedal gait. Therefore, a complete gait cycle consists of a SSP and an instantaneous DSP.

Under the support-swing characterization, the joint position $\mathbf{q}$ is defined as:

$$\mathbf{q} = \begin{bmatrix} q_1 \\ q_2 \\ q_3 \\ q_4 \\ q_5 \\ q_6 \\ q_7 \\ q_8 \\ q_9 \end{bmatrix} \in Q, \tag{4.1}$$

where $Q \subset \mathbb{R}^9$ is the configuration space of the bipedal robot when the support leg is in static, full contact with the walking surface and the joint position limits are satisfied, q_1, q_2, q_3, q_4, and q_5 are joint positions of the support leg, q_6, q_7, and q_8 are joint positions of the swing leg, and q_9 is the joint position of the trunk. Let

$$\mathbf{u} = \begin{bmatrix} u_1 \\ u_2 \\ u_3 \\ u_4 \\ u_5 \\ u_6 \\ u_7 \\ u_8 \\ u_9 \end{bmatrix} \in \mathbb{R}^9$$

represent the joint-torque vector.

Although a complete gait of the 3-D biped in Fig. 4.1 consists of a SSP and an instantaneous DSP under the support-swing characterization, the expressions of the dynamic matrices for the left-in-support phases are different from the right-in-support phases.

Let $S_L(\mathbf{q}, \dot{\mathbf{q}})$ represent the switching surface that connects the left-in-support DSP and the right-in-support SSP:

$$S_L(\mathbf{q}, \dot{\mathbf{q}}) := \{(\mathbf{q}, \dot{\mathbf{q}}) \in TQ : z_{swL}(\mathbf{q}) = 0, \dot{z}_{swL}(\mathbf{q}, \dot{\mathbf{q}}) < 0\}, \tag{4.2}$$

where $z_{swL}(\mathbf{q})$ is the height of the swing foot when the left leg is in support.

Let $S_R(\mathbf{q}, \dot{\mathbf{q}})$ denote the switching surface that connects the right-in-support DSP and the left-in-support SSP:

$$S_R(\mathbf{q}, \dot{\mathbf{q}}) := \{(\mathbf{q}, \dot{\mathbf{q}}) \in TQ : z_{swR}(\mathbf{q}) = 0, \dot{z}_{swR}(\mathbf{q}, \dot{\mathbf{q}}) < 0\}, \tag{4.3}$$

where $z_{swR}(\mathbf{q})$ is the height of the swing foot when the right leg is in support.

The hybrid walking dynamics for the 3-D biped in Fig. 4.1 under the support-swing characterization can be expressed as:

$$\Sigma_L : \begin{cases} \mathbf{M}_L(\mathbf{q})\ddot{\mathbf{q}} + \mathbf{c}_L(\mathbf{q},\dot{\mathbf{q}}) = \mathbf{B}_u\mathbf{u}, & \text{if } (\mathbf{q}^-,\dot{\mathbf{q}}^-) \notin S_L(\mathbf{q},\dot{\mathbf{q}}); \\ [\mathbf{q}^+;\dot{\mathbf{q}}^+] = \boldsymbol{\Delta}_L(\mathbf{q}^-,\dot{\mathbf{q}}^-), & \text{if } (\mathbf{q}^-,\dot{\mathbf{q}}^-) \in S_L(\mathbf{q},\dot{\mathbf{q}}); \end{cases}$$
$$\Sigma_R : \begin{cases} \mathbf{M}_R(\mathbf{q})\ddot{\mathbf{q}} + \mathbf{c}_R(\mathbf{q},\dot{\mathbf{q}}) = \mathbf{B}_u\mathbf{u}, & \text{if } (\mathbf{q}^-,\dot{\mathbf{q}}^-) \notin S_R(\mathbf{q},\dot{\mathbf{q}}); \\ [\mathbf{q}^+;\dot{\mathbf{q}}^+] = \boldsymbol{\Delta}_R(\mathbf{q}^-,\dot{\mathbf{q}}^-), & \text{if } (\mathbf{q}^-,\dot{\mathbf{q}}^-) \in S_R(\mathbf{q},\dot{\mathbf{q}}); \end{cases} \tag{4.4}$$

where $i \in \{L,R\}$ indicates whether the left (L) or the right (R) leg is in support, $\mathbf{M}_i : Q \to \mathbb{R}^{9\times 9}$ is the inertia matrix, $\mathbf{c}_i : Q \to \mathbb{R}^9$ is the sum of the Coriolis, the centrifugal, and the gravitational terms, $\mathbf{B}_u : \mathbb{R}^{9\times 9}$ is the nonsingular input matrix, $\mathbf{u} \in \mathbb{R}^9$ is the torque vector of the active joints, and $\boldsymbol{\Delta}_i : TQ \to \mathbb{R}^{18}$ is the reset map. The expressions of $\mathbf{M}_i$, $\mathbf{c}_i$, $\mathbf{B}_u$ and $\boldsymbol{\Delta}_i$ will not be given in the Appendices due to space limitations. Once the expressions of $\mathbf{M}_L$, $\mathbf{c}_L$, and $\boldsymbol{\Delta}_L$ are determined, the expressions of $\mathbf{M}_R$, $\mathbf{c}_R$, and $\boldsymbol{\Delta}_R$ can be obtained by replacing w with $-w$ in $\mathbf{M}_L$, $\mathbf{c}_L$, and $\boldsymbol{\Delta}_L$, respectively [122].

4.2.2 Tracking Error of the Desired Walking Pattern

A walking pattern represents the relative evolution of joint positions with respect to a phase variable within a complete walking cycle [50]. Denote the desired walking pattern as:

$$\mathbf{h}_1(\mathbf{q}) := \mathbf{h}_c(\mathbf{q}) - \boldsymbol{\phi}(\theta(\mathbf{q})) = \mathbf{0}, \tag{4.5}$$

where $\theta : Q \to Q_f \subset \mathbb{R}$ is a phase variable, which is monotonically increasing during a step and used to encode the walking pattern, $\mathbf{h}_c : Q \to Q_c \subset \mathbb{R}^7$ is continuously differentiable in $\mathbf{q}$, and $\boldsymbol{\phi}(\theta) : Q_f \to \mathbb{R}^7$ is continuously differentiable in θ. The desired walking pattern in Eq. (4.5) is also called virtual constraints [50].

The function $\mathbf{h}_c(\mathbf{q})$ is defined as follows:

$$\mathbf{h}_c(\mathbf{q}) = \begin{bmatrix} q_9 \\ \theta_{r,h}(\mathbf{q}) \\ \theta_{p,h}(\mathbf{q}) \\ x_{h2sw}(\mathbf{q}) \\ y_{h2sw}(\mathbf{q}) \\ z_{sw}(\mathbf{q}) \\ z_h(\mathbf{q}) \end{bmatrix}, \tag{4.6}$$

where q_9 is already define, z_{sw} is the swing foot height, and the rest of the elements are defined with respect to the world coordinate frame as follows:

- $\theta_{r,h}(\mathbf{q})$ is the angle from the horizontal plane to the vector $\overrightarrow{H_{st}H_{sw}}$ where H_{st} and H_{sw} represent the hip points of the support and the swing legs, respectively (see Fig. 4.1);
- $\theta_{p,h}(\mathbf{q})$ is the angle from the z_f-axis to the trunk link;
- $(x_{h2sw}(\mathbf{q}),y_{h2sw}(\mathbf{q}))$ is the relative position of the swing foot with respect to the pelvis H, projected on the walking surface;
- $z_h(\mathbf{q})$ is the height of the pelvis H above the walking surface.

The desired function $\boldsymbol{\phi}(\theta)$ is defined as:

$$\boldsymbol{\phi} := [\phi_1(\theta), \phi_2(\theta), \phi_3(\theta), \phi_4(\theta), \phi_5(\theta), \phi_6(\theta), \phi_7(\theta)]^T. \tag{4.7}$$

Similar to the HZD framework [102] and our previous work [140] [141] [142] [143], Bezier Curves are used to define the desired function $\boldsymbol{\phi}(\theta)$:

$$\boldsymbol{\phi}(\theta) := \sum_{k=0}^{M} \mathbf{a}_k \frac{M!}{k!(M-k)!} s(\theta)^k (1-s(\theta))^{M-k} \tag{4.8}$$

with

$$s(\theta) := \frac{\theta - \theta_0}{\theta^* - \theta_0}, \tag{4.9}$$

where $k \in \{0,1,...,M\}$,

$$\mathbf{a}_k := \begin{bmatrix} a_{k1} \\ a_{k2} \\ a_{k3} \\ a_{k4} \\ a_{k5} \\ a_{k6} \\ a_{k7} \end{bmatrix} \in \mathbb{R}^7$$

is the unknown vector to be optimized in Section 4.5, and θ_0 and θ^* are the planned values of θ at the beginning and the end of a step, respectively.

For simplicity, only symmetric gaits are discussed in this Chapter. Therefore, the desired function $\boldsymbol{\phi}(\theta)$ is the same for both the left-in-support and the right-in-support phases except for the desired function $\phi_5(\theta)$ that defines the desired pattern for y_{h2sw}. Define $\phi_5(\theta)$ as:

$$\phi_5(\theta) := \begin{cases} \phi_{5L}(\theta) & \text{(left-in-support) ;} \\ \phi_{5R}(\theta) & \text{(right-in-support) .} \end{cases} \tag{4.10}$$

Because of the left-right symmetry, $\phi_{5L}(\theta) = -\phi_{5R}(\theta)$.

4.2.3 Tracking Error of the Desired Contour and Position Trajectory in Cartesian Space

Suppose the walking process begins with the continuous phase. Let $(x_{st,k}, y_{st,k}, 0)$ denote the the support foot position right after the k^{th} ($k \in \{1,2,...\}$) swing-foot touchdown, which is defined with respect to the world coordinate frame. Without loss of generality, $(x_{st,0}, y_{st,0}, 0)$ represents the initial support foot position at $t = 0$. During the k^{th} step, the horizontal hip position (x_h, y_h) with respect to the world coordinate frame can be expressed as:

$$\begin{aligned} x_h &= x_{st,k-1} + \bar{x}_h(\mathbf{q}); \\ y_h &= y_{st,k-1} + \bar{y}_h(\mathbf{q}), \end{aligned} \tag{4.11}$$

where $\bar{x}_h : Q \to Q_x \subset \mathbb{R}$ and $\bar{y}_h : Q \to Q_y \subset \mathbb{R}$, defined with respect to the world coordinate frame, represent the x- and y-coordinates of the relative position of the hip with respect to the support foot, respectively.

Let Γ_d be the desired contour. An orthogonal coordinate frame can be established along the desired contour [157]: the curvilinear coordinate r_c along the normal direction of the desired contour represents the contour error, and the curvilinear coordinate r_m represents the motion along the desired contour. Define the desired motion along Γ_d as $s_d(t)$, which is monotonically increasing and continuously differentiable in t. The objectives of contouring control are then:

1. To drive r_c to zero, and
2. To drive r_m to $s_d(t)$.

For simplicity, we consider a straight-line contour on the walking surface and define the contour as the Y_w-axis:

$$\Gamma_d = \{(x_h, y_h) \in \mathbb{R}^2 : y_h = 0\}. \tag{4.12}$$

Then,

$$\begin{cases} r_c = y_h; \\ r_m = x_h. \end{cases} \tag{4.13}$$

4.3 Model-based Feedback Control through Input-Output Linearization

Similar to Chapter 3, a model-based feedback controller will be designed to achieve exponential tracking of the desired walking pattern and the desired global position trajectory in Cartesian space. It is then natural to define the output function $\mathbf{y}$ as the tracking error derived in Section 4.2. Because the biped in Fig. 4.1 has nine independent actuators, nine output functions can be designed.

First, the output function $\mathbf{y}_1$ is designed as the walking pattern tracking error:

$$\mathbf{y}_1 = \mathbf{h}_1(\mathbf{q}). \tag{4.14}$$

If $\mathbf{y}_1$ is exponentially driven to zero, $\mathbf{h}_c(\mathbf{q})$ will accordingly converge to the desired function $\boldsymbol{\phi}(\theta(\mathbf{q}))$ exponentially, and the desired walking pattern will be exactly followed at the steady state.

Second, the output function $\mathbf{y}_2$ during the k^{th} ($k \in \{1,2,...\}$) step is designed as:

$$\mathbf{y}_2 = \mathbf{h}_2(t,\mathbf{q}) = \begin{bmatrix} \bar{x}_h(\mathbf{q}) \\ \bar{y}_h(\mathbf{q}) \end{bmatrix} - \begin{bmatrix} s_d(t) - x_{st,k-1} \\ -y_{st,k-1} \end{bmatrix}, \tag{4.15}$$

where $(x_{st,k-1}, y_{st,k-1})$ is the projection of the support-foot position on the walking surface during the k^{th} step and $s_d(t)$ is a monotonically increasing and continuously differentiable function that defines the desired motion along the desired contour.

Finally, the output function $\mathbf{y}$ can be compactly written as:

$$\mathbf{y} = \mathbf{h}(t,\mathbf{q}), \tag{4.16}$$

where

$$\mathbf{y} := \begin{bmatrix} \mathbf{y}_1 \\ \mathbf{y}_2 \end{bmatrix} \tag{4.17}$$

and

$$\mathbf{h}(t,\mathbf{q}) := \begin{bmatrix} \mathbf{h}_1(\mathbf{q}) \\ \mathbf{h}_2(t,\mathbf{q}) \end{bmatrix}. \tag{4.18}$$

As a straight-line contour is of interest and the desired motion along the contour is defined as monotonically increasing in this study, $\bar{x}_h(\mathbf{q})$ will be chosen as the phase variable to encode the desired function $\boldsymbol{\phi}$ in Eq. (4.5); that is,

$$\theta := \bar{x}_h(\mathbf{q}). \tag{4.19}$$

To drive the output function $\mathbf{y}$ to zero such that the desired position trajectory in Cartesian space and the desired walking pattern are both satisfactorily followed, a feedback controller is synthesized based on input-output linearization.

The feedback control law is chosen as [76]

$$\mathbf{u} = (\tfrac{\partial \mathbf{h}}{\partial \mathbf{q}} \mathbf{M}_L^{-1} \mathbf{B})^{-1} (\mathbf{v} + \tfrac{\partial \mathbf{h}}{\partial \mathbf{q}} \mathbf{M}_L^{-1} \mathbf{c}_L - \tfrac{\partial^2 \mathbf{h}}{\partial t^2} - \tfrac{\partial}{\partial \mathbf{q}} (\tfrac{\partial \mathbf{h}}{\partial \mathbf{q}} \dot{\mathbf{q}}) \dot{\mathbf{q}}) \tag{4.20}$$

when the left leg is in support and

$$\mathbf{u} = (\frac{\partial \mathbf{h}}{\partial \mathbf{q}}\mathbf{M}_R^{-1}\mathbf{B})^{-1}(\mathbf{v} + \frac{\partial \mathbf{h}}{\partial \mathbf{q}}\mathbf{M}_R^{-1}\mathbf{c}_R - \frac{\partial^2 \mathbf{h}}{\partial t^2} - \frac{\partial}{\partial \mathbf{q}}(\frac{\partial \mathbf{h}}{\partial \mathbf{q}}\dot{\mathbf{q}})\dot{\mathbf{q}}) \tag{4.21}$$

when the right leg is in support.

The continuous-phase dynamics then become:

$$\ddot{\mathbf{y}} = \mathbf{v}. \tag{4.22}$$

Choosing $\mathbf{v}$ as the following proportional-derivative (PD) control law:

$$\mathbf{v} = -\mathbf{K}_P\mathbf{y} - \mathbf{K}_D\dot{\mathbf{y}}, \tag{4.23}$$

where $\mathbf{K}_P \in \mathbb{R}^{9\times 9}$ and $\mathbf{K}_D \in \mathbb{R}^{9\times 9}$ are positive-definite diagonal matrices, one then obtains the following linear dynamics of output function:

$$\begin{bmatrix} \dot{\mathbf{y}} \\ \ddot{\mathbf{y}} \end{bmatrix} = \begin{bmatrix} \mathbf{0}_{9\times 9} & \mathbf{I}_{9\times 9} \\ -\mathbf{K}_P & -\mathbf{K}_D \end{bmatrix} \begin{bmatrix} \mathbf{y} \\ \dot{\mathbf{y}} \end{bmatrix} := \mathbf{A}(\mathbf{K}_P, \mathbf{K}_D) \begin{bmatrix} \mathbf{y} \\ \dot{\mathbf{y}} \end{bmatrix}, \tag{4.24}$$

where $\mathbf{0}_{9\times 9} \in \mathbb{R}^{9\times 9}$ is a zero matrix and $\mathbf{I}_{9\times 9} \in \mathbb{R}^{9\times 9}$ is an identity matrix.

Defining

$$\mathbf{x} := \begin{bmatrix} \mathbf{y} \\ \dot{\mathbf{y}} \end{bmatrix} \in \chi,$$

where $\chi \subset \mathbb{R}^{18}$ is the full state space, one can compactly rewrite the closed-loop dynamics as:

$$\begin{aligned} \Sigma_L : \begin{cases} \dot{\mathbf{x}} = \mathbf{A}(\mathbf{K}_P, \mathbf{K}_D)\mathbf{x}, & \text{if } (t^-, \mathbf{x}^-) \notin S_{L\to R}(t, \mathbf{x}); \\ \mathbf{x}^+ = \mathbf{\Delta}_{L\to R}(t, \mathbf{x}^-), & \text{if } (t^-, \mathbf{x}^-) \in S_{L\to R}(t, \mathbf{x}); \end{cases} \\ \Sigma_R : \begin{cases} \dot{\mathbf{x}} = \mathbf{A}(\mathbf{K}_P, \mathbf{K}_D)\mathbf{x}, & \text{if } (t^-, \mathbf{x}^-) \notin S_{R\to L}(t, \mathbf{x}); \\ \mathbf{x}^+ = \mathbf{\Delta}_{R\to L}(t, \mathbf{x}^-), & \text{if } (t^-, \mathbf{x}^-) \in S_{R\to L}(t, \mathbf{x}); \end{cases} \end{aligned} \tag{4.25}$$

where the expressions of $S_{L\to R}(t, \mathbf{x})$ and $S_{R\to L}(t, \mathbf{x})$ can be obtained from Eqs. (4.2) and (4.3), respectively.

If $\mathbf{K}_P$ and $\mathbf{K}_D$ are chosen such that $\mathbf{A}(\mathbf{K}_P, \mathbf{K}_D)$ is Hurwitz, then there exists a real positive-definite-symmetric matrix $\mathbf{W}$ such that $V(\mathbf{x}) = \mathbf{x}^T \mathbf{W} \mathbf{x}$ is a Lyapunov function candidate for the continuous-phase dynamics. Furthermore, there exist positive constants c_1, c_2, and c_3 such that $V(\mathbf{x})$ satisfies

$$c_1 \|\mathbf{x}\|^2 \leq V_i(\mathbf{x}) \leq c_2 \|\mathbf{x}\|^2 \text{ and } \dot{V}(\mathbf{x}) \leq -c_3 V(\mathbf{x}) \tag{4.26}$$

for all $\mathbf{x}$ during continuous phases [76].

4.4 Closed-Loop Stability Analysis

In this section, the closed-loop stability of the hybrid time-varying system is analyzed. Before introducing the main theorem on the closed-loop stability of this study, we first present some properties of the system.

Suppose that the walking process begins with the left-in-support continuous phase at $t = 0$.

Let T_k be the moment of the k^{th} ($k \in \{1, 2, ...\}$) actual impact, which is defined as the moment of the first intersection with the k^{th} switching surface $S_k(t, \mathbf{x})$ on $t > T_{k-1}^+$. Without loss of generality, define $T_0 = 0$. The k^{th} switching surface S_k is defined as:

$$S_k(t, \mathbf{x}) := \begin{cases} S_{L \to R}(t, \mathbf{x}), & \text{if } k \in \{1, 3, 5, ...\}; \\ S_{R \to L}(t, \mathbf{x}), & \text{if } k \in \{2, 4, 6, ...\}. \end{cases} \tag{4.27}$$

In the following, $\star(T_{k-1}^-)$ and $\star(T_{k-1}^+)$ will be denoted as $\star|_{k-1}^-$ and $\star|_{k-1}^+$, respectively, when notational simplicity is preferred.

Let $\tilde{\mathbf{x}}(t; t_0, \lambda_0) = [\tilde{\mathbf{q}}(t; t_0, \lambda_0); \dot{\tilde{\mathbf{q}}}(t; t_0, \lambda_0)]$ denote a solution of $\dot{\tilde{\mathbf{x}}} = \mathbf{A}(\mathbf{K}_p, \mathbf{K}_d)\tilde{\mathbf{x}}$ with the initial condition $\tilde{\mathbf{x}}(t_0) = \lambda_0$, $\forall t > t_0$. Note that a solution $\mathbf{x}(t)$ of the hybrid dynamics in Eq. (4.25) with impact moments T_k ($k \in \{1, 2, ...\}$ satisfies

$$\mathbf{x}(t) = \tilde{\mathbf{x}}(t; T_{k-1}^+, \mathbf{x}|_{k-1}^+), \ \forall t \in (T_{k-1}, T_k]. \tag{4.28}$$

Let τ_k denote the k^{th} ($k \in \{1, 2, ...\}$) desired impact moment, which is defined as the moment of the first intersection with the k^{th} switching surface $S_k(t, \mathbf{x})$ on $t > T_{k-1}^+$ assumsing $\mathbf{x} = 0 \ \forall t > T_{k-1}^+$.

Theorem 5.1 Consider the following assumptions:

1. The desired function $\phi_6(\theta)$ has at least one intersection with zero for both $\theta < 0$ and $\theta > 0$ (denote the interaction for $\theta < 0$ that is nearest to zero as θ_0);

2. The phase variable θ increases monotonically from θ_0 to a positive number during a step.

Then, there exists a constant θ^* such that $\theta(\tau_k^-) = \theta^*$ always holds under the assumption that $\mathbf{x} = 0\ \forall t > T_{k-1}^+$. Therefore, $\mathbf{h}_c(\tau_k^-) = \boldsymbol{\phi}(\theta^*)$. Furthermore, if $\phi_1(\theta) = 0$, $\phi_2(\theta) = 0$, $\phi_3(\theta) = 0$, and $y_{st,k-1} = y_{std} := \phi_5(\theta^*)$, then $\mathbf{q}(\tau_k^-) \in Q$, if exists, is also fixed and equal to a unique value, denoted as $\mathbf{q}^*$. ■

Proof: By the definitions of τ_k and the switching surface, one has

$$z_{sw}(\tau_k^-) = 0. \tag{4.29}$$

By the definition of $\mathbf{y}_1$ and under the assumption that $\mathbf{x} = 0\ \forall t > T_{k-1}^+$, one has

$$z_{sw}(\tau_k^-) = \phi_6(\theta). \tag{4.30}$$

Therefore,

$$\phi_6(\theta(\tau_k^-)) = 0 \tag{4.31}$$

holds. Because θ increases monotonically from a negative number during a step and $\phi_6(\theta)$ has at least one intersection with zero for $\theta > 0$, Eq. (4.31) indicates that $\theta(\tau_k^-)$ is fixed; that is, there exists a constant θ^* such that

$$\theta(\tau_k^-) = \theta^* \tag{4.32}$$

always holds. Accordingly, $\mathbf{h}_c(\tau_k^-) = \boldsymbol{\phi}(\theta^*)$ always holds.

When $y_{st,k-1} = y_{std} := \phi_5(\theta^*)$ and the desired function is chosen such that $\phi_1(\theta) = 0$, $\phi_2(\theta) = 0$, and $\phi_3(\theta) = 0$, it can be proved that the following equation

$$\begin{bmatrix} \mathbf{h}_c(\mathbf{q}) \\ \bar{x}_h(\mathbf{q}) \\ \bar{y}_h(\mathbf{q}) \end{bmatrix} = \begin{bmatrix} \boldsymbol{\phi}(\theta^*) \\ \theta^* \\ -y_{std} \end{bmatrix}$$

has a unique solution for $\mathbf{q} \in Q$. ■

In fact, when $q_9 = 0$, $\theta_{r,h}(\mathbf{q}) = 0$, and $\theta_{p,h}(\mathbf{q}) = 0$, it can be proved that there exists a diffeomorphism $D : Q_c \times Q_f \times Q_y \to Q$.

Theorem 5.2 (Convergence of the Support Foot Position along Y_w-Axis) Define $y_{std} := \phi_5(\theta^*)$. Then there exists positive numbers β_{st} and r_2 such that

$$|y_{st,k} - y_{std}| \leq \|\mathbf{x}|_k^-\| + \beta_{st}\|\tilde{\mathbf{x}}(\tau_k; T_{k-1}^+, \mathbf{x}|_{k-1}^-)\| \tag{4.33}$$

holds for any $\mathbf{x}(0^+) \in B_{r_2}(\mathbf{0}) := \{\mathbf{x} \in \mathbb{R}^{18} : \|\mathbf{x}\| \leq r_2\}$ and $k \in \{1, 2, ...\}$. ■

Proof:

The y-coordinate of the support-foot position during the $(k+1)^{th}$ ($k \in \{1, 2, ...\}$) step can be expressed as

$$y_{st,k} = y_h(T_k^-) + y_{h2sw}(T_k^-). \tag{4.34}$$

Therefore,

$$|y_{st,k} - y_{std}| = |y_h(T_k^-) + y_{h2sw}(T_k^-) - y_{std}| \leq |y_h(T_k^-)| + |y_{h2sw}(T_k^-) - y_{std}|. \tag{4.35}$$

Because $y_{std} = \phi_5(\theta^*)$, one has:

$$\begin{aligned} |y_{h2sw}(T_k^-) - y_{std}| \leq & |y_{h2sw}(T_k^-) - \phi_5(\theta(T_k^-))| \\ & + |\phi_5(\theta(T_k^-)) - \phi_5(\tilde{\theta}(\tau_k; T_{k-1}^+, \mathbf{x}|_{k-1}^+))| \\ & + |\phi_5(\tilde{\theta}(\tau_k; T_{k-1}^+, \mathbf{x}|_{k-1}^+)) - \phi_5(\theta^*)|. \end{aligned} \tag{4.36}$$

By the definition of $\mathbf{y}_1$,

$$|y_{h2sw}(T_k^-) - \phi_5(\theta(T_k^-))| \leq \|\mathbf{x}(T_k^-)\|.$$

Recall that $\theta(T_k^-) = \tilde{\theta}(T_k; T_{k-1}^+, \mathbf{x}|_{k-1}^+))$. Because $\phi_5(\theta)$ and $\theta(\mathbf{q}(t))$ are continuously differentiable in θ and t, respectively, there exists a positive number r_1 and Lipschitz constants L_{ϕ_5} and L_{θ_t} such that

$$\|\phi_5(\theta(T_k^-)) - \phi_5(\tilde{\theta}(\tau_k; T_{k-1}^+, \mathbf{x}|_{k-1}^+))\| \leq L_{\phi_5}\|\theta(T_k^-) - \tilde{\theta}(\tau_k; T_{k-1}^+, \mathbf{x}|_{k-1}^+)\| \tag{4.37}$$

and

$$\|\theta(T_k^-) - \tilde{\theta}(\tau_k; T_{k-1}^+, \mathbf{x}|_{k-1}^+)\| \leq L_{\theta_t}|T_k - \tau_k|$$

hold for any $\mathbf{x}(0^+) \in B_{r_1}(\mathbf{0})$ Also, by [Theorem 1, [141]], there exists a positive number r_2 and a Lipschitz constant L_{T_x} such that

$$|T_k - \tau_k| \leq L_{T_x}\|\tilde{\mathbf{x}}(\tau_k; T_{k-1}^+, \mathbf{x}|_{k-1}^+)\| \tag{4.38}$$

for any $\mathbf{x}(0^+) \in B_{r_2}(\mathbf{0})$.

Because $\theta^* = \tilde{\theta}(\tau_k^-; T_{k-1}^+, \mathbf{0}) = s_d(\tau_k) - x_{st,k-1}$, one has

$$\begin{aligned} |\tilde{\theta}(\tau_k^-; T_{k-1}^+, \mathbf{x}|_{k-1}^+) - \theta^*| =& \|\tilde{\mathbf{x}}_h(\tau_k^-; T_{k-1}^+, \mathbf{x}|_{k-1}^+) - (s_d(\tau_k) - x_{st,k-1})\| \\ \leq& \|\tilde{\mathbf{x}}(\tau_k; T_{k-1}^+, \mathbf{x}|_{k-1}^+)\|. \end{aligned} \tag{4.39}$$

Let $\beta = L_{\phi_5}(L_{\theta_t}L_{T_x} + 1)$ and $d_1 = \min(r_1, r_2)$. Then, from Eqs. (4.36)-(4.39), one obtains

$$|y_{st,k} - y_{std}| \leq \|\mathbf{x}|_k^-\| + \beta_{st}\|\tilde{\mathbf{x}}(\tau_k; T_{k-1}^+, \mathbf{x}|_{k-1}^-)\| \tag{4.40}$$

for any $\mathbf{x}(0^+) \in B_{d_1}(\mathbf{0})$. ■

Theorem 5.3 (Hybrid Invariance under $y_{st,k-1} = y_{std}$) Denote

$$\mathbf{H}_v(\mathbf{q}) := \begin{bmatrix} \frac{d\mathbf{h}_c}{d\mathbf{q}}(\mathbf{q}) \\ \frac{d\bar{x}_h}{d\mathbf{q}}(\mathbf{q}) \\ \frac{d\bar{y}_h}{d\mathbf{q}}(\mathbf{q}) \end{bmatrix}. \tag{4.41}$$

If the desired function $\boldsymbol{\phi}(\theta)$ is designed such that the following conditions are satisfied:

(A1) $\mathbf{h}_c(\boldsymbol{\Delta}_q(\mathbf{q}^*)) = \boldsymbol{\phi}(\bar{x}_h(\boldsymbol{\Delta}_q(\mathbf{q}^*)))$;

(A2) $\frac{d\bar{x}_h}{d\mathbf{q}}(\boldsymbol{\Delta}_q(\mathbf{q}^*))\boldsymbol{\Delta}_{\dot{q}}(\mathbf{q}^*)\mathbf{H}_v^{-1}(\mathbf{q}^*)\begin{bmatrix} \frac{d\boldsymbol{\phi}}{d\theta}(\theta^*) \\ 1 \\ 0 \end{bmatrix} = 1$;

(A3) $\mathbf{H}_v(\boldsymbol{\Delta}_q(\mathbf{q}^*))\boldsymbol{\Delta}_{\dot{q}}(\mathbf{q}^*)\mathbf{H}_v^{-1}(\mathbf{q}^*)\begin{bmatrix} \frac{d\boldsymbol{\phi}}{d\theta}(\theta^*) \\ 1 \\ 0 \end{bmatrix} = \begin{bmatrix} \frac{d\boldsymbol{\phi}}{d\theta}(\bar{x}_h(\boldsymbol{\Delta}_q(\mathbf{q}^*))) \\ 1 \\ 0 \end{bmatrix}$.

Then, under the condition $y_{st,k-1} = y_{std}$, the hybrid invariance holds; that is, if $\mathbf{x}(\tau_k^-) = \mathbf{0}$ then $\mathbf{x}(\tau_k^+) = \boldsymbol{\Delta}_i(\tau_k^-, \mathbf{0}) = \mathbf{0}$. ■

Proof: From Theorem 5.1 and $\mathbf{x}(\tau_k^-) = \mathbf{0}$, one has

$$\mathbf{q}(\tau_k^+) = \mathbf{q}_0 := \boldsymbol{\Delta}_q(\mathbf{q}^*), \quad \theta(\tau_k^+) = \theta_0 := \bar{x}_h(\mathbf{q}_0). \tag{4.42}$$

Then, from (A1), one has

$$\mathbf{y}_1(\tau_k^+) = \mathbf{h}_c(\mathbf{q}_0) - \boldsymbol{\phi}(\theta_0) = \mathbf{0}. \tag{4.43}$$

Because $\mathbf{x}(\tau_k^-) = \mathbf{0}$ and x_h, y_h, and $s_d(t)$ are all continuous in t, one has

$$\mathbf{y}_2(\tau_k^+) = \mathbf{y}_2(\tau_k^-) = \mathbf{0}. \tag{4.44}$$

Therefore, from Eqs. (4.43) and (4.44), $\mathbf{y}(\tau_k^+) = \mathbf{0}$ holds.

Now, because $\dot{\mathbf{y}}(\tau_k^-) = \mathbf{0}$, one has

$$\mathbf{H}_v(\mathbf{q}^*)\dot{\mathbf{q}}(\tau_k^-) = \begin{bmatrix} \frac{d\boldsymbol{\phi}}{d\theta}(\theta^*) \\ 1 \\ 0 \end{bmatrix} \dot{\theta}(\tau_k^-). \tag{4.45}$$

Without loss of generality, suppose that $\mathbf{H}_v(\mathbf{q})$ is locally invertible within a small neighborhood about $\mathbf{q}^*$. One obtains

$$\dot{\mathbf{q}}(\tau_k^-) = \mathbf{H}_v(\mathbf{q}^*)^{-1} \begin{bmatrix} \frac{d\boldsymbol{\phi}}{d\theta}(\theta^*) \\ 1 \\ 0 \end{bmatrix} \dot{\theta}(\tau_k^-). \tag{4.46}$$

Then, from the reset map in Eq. (2.3), one has:

$$\dot{\mathbf{q}}(\tau_k^+) = \boldsymbol{\Delta}_{\dot{q}}(\mathbf{q}^*)\dot{\mathbf{q}}(\tau_k^-). \tag{4.47}$$

Because $\dot{x}_{hd}^+ - \dot{x}_{st,k} = \dot{x}_{hd}^+ = \dot{x}_{hd}^- = \dot{x}_{hd}^- - \dot{x}_{st,k-1}^- = \dot{\theta}(\tau_k^-)$ and by the definition of $\mathbf{y}$, one has:

$$\dot{\mathbf{y}}(\tau_k^+) = \mathbf{H}_v(\mathbf{q}_0)\dot{\mathbf{q}}(\tau_k^+) - \begin{bmatrix} \frac{d\boldsymbol{\phi}}{d\theta}(\theta_0)\dot{\theta}(\tau_k^+) \\ \dot{\theta}(\tau_k^-) \\ 0 \end{bmatrix}. \tag{4.48}$$

From (A2), one has:

$$\dot{\theta}^{+} = \frac{d\bar{x}_h}{d\mathbf{q}}(\mathbf{q}_0)\dot{\mathbf{q}}(\tau_k^{+}) = \dot{\theta}^{-}. \tag{4.49}$$

Then, from (A3) and Eq. (4.49), one has

$$\dot{\mathbf{y}}^{+} = \mathbf{0}. \tag{4.50}$$

■

Theorem 5.4 (Closed-Loop Stability Conditions) Let the conditions (A1) - (A3) in Theorem 5.3 hold. The closed-loop control system in Eq. (4.25) is locally exponentially stable if the PD gains in Eq. (4.23) are chosen such that $\mathbf{A}(\mathbf{K}_p, \mathbf{K}_d)$ is Hurwitz and that the continuous-phase convergence rate is sufficiently fast. ■

Proof: Let $V(\mathbf{x})$ be the Lyapunov function candidate. By stability analysis based on the construction of multiple Lyapunov functions [156], the hybrid time-varying system in Eq. (4.25) is locally exponentially stable if there exists a positive number d_2 such that $V(\mathbf{x})$ is exponentially decreasing during each continuous phase and that $\{V|_1^+, V|_2^+, V|_3^+ ...\}$ is a strictly decreasing sequence for any $\mathbf{x}(0^+) \in B_{d_2}(\mathbf{0})$.

If the PD gains $\mathbf{K}_P$ and $\mathbf{K}_D$ are chosen such that the matrix $\mathbf{A}$ in Eq. (4.25) is Hurwitz, then, from Eq. (4.26), one has

$$V|_k^- \leq e^{-c_3(T_{k+1}-T_k)} V|_{k-1}^+, \tag{4.51}$$

during the k^{th} ($k \in \{1,2,...\}$) step.

Now, consider the k^{th} ($k \in \{1,2,...\}$) impact event. The corresponding k^{th} reset map $\mathbf{\Delta}_k$ is defined as

$$\mathbf{\Delta}_k(t,\mathbf{x}) := \begin{cases} \mathbf{\Delta}_{L\to R}(t,\mathbf{x}), & \text{if } k \in \{1,3,5,...\}; \\ \mathbf{\Delta}_{R\to L}(t,\mathbf{x}), & \text{if } k \in \{2,4,6,...\}. \end{cases} \tag{4.52}$$

To explicitly discuss the effect of $y_{st,k-1}$ on the reset map, the reset map is rewritten as:

$$\mathbf{\Delta}_k(T_k^-, \mathbf{x}|_k^-) = \mathbf{\Delta}_k(T_k^-, \mathbf{x}|_k^-, y_{st,k-1}).$$

Because $x|_k^+ = \boldsymbol{\Delta}_k(T_k^-, \mathbf{x}|_k^-)$, one has

$$\begin{aligned}\|x|_k^+\| = \|\boldsymbol{\Delta}_k(T_k^-, \mathbf{x}|_k^-, y_{st,k-1})\| \leq & \|\boldsymbol{\Delta}_k(T_k^-, \mathbf{x}|_k^-, y_{st,k-1}) - \boldsymbol{\Delta}_k(\tau_k^-, \mathbf{x}|_k^-, y_{st,k-1})\| \\ & + \|\boldsymbol{\Delta}_k(\tau_k^-, \mathbf{x}|_k^-, y_{st,k-1}) - \boldsymbol{\Delta}_k(\tau_k^-, \mathbf{0}, y_{st,k-1})\| \\ & + \|\boldsymbol{\Delta}_k(\tau_k^-, \mathbf{0}, y_{st,k-1}) - \boldsymbol{\Delta}_k(\tau_k^-, \mathbf{0}, y_{std})\| \\ & + \|\boldsymbol{\Delta}_k(\tau_k^-, \mathbf{0}, y_{std})\|.\end{aligned} \tag{4.53}$$

As the desired function $\boldsymbol{\phi}(\theta)$ satisfies the conditions (A1) - (A3) in Theorem 5.3, one has

$$\|\boldsymbol{\Delta}_k(\tau_k^-, \mathbf{0}, y_{std})\| = \mathbf{0}. \tag{4.54}$$

Because the reset map $\boldsymbol{\Delta}_k(t, \mathbf{x}, y_{st,k-1})$ is continuously differentiable in t, $\mathbf{x}$, and $y_{st,k-1}$, there exist a positive number r_3 and Lipschitz constants L_{Δ_t}, L_{Δ_x}, and $L_{\Delta_{st}}$ such that the following inequalities hold for any $\mathbf{x}(0^+) \in B_{r_3}(\mathbf{0})$:

$$\begin{aligned}&\|\boldsymbol{\Delta}_k(T_k^-, \mathbf{x}|_k^-, y_{st,k-1}) - \boldsymbol{\Delta}_k(\tau_k^-, \mathbf{x}|_k^-, y_{st,k-1})\| \leq L_{\Delta_t}\|T_k - \tau_k\|; \\ &\|\boldsymbol{\Delta}_k(\tau_k^-, \mathbf{x}|_k^-, y_{st,k-1}) - \boldsymbol{\Delta}_k(\tau_k^-, \mathbf{0}, y_{st,k-1})\| \leq L_{\Delta_x}\|x|_k^-\|; \\ &\|\boldsymbol{\Delta}_k(\tau_k^-, \mathbf{0}, y_{st,k-1}) - \boldsymbol{\Delta}_k(\tau_k^-, \mathbf{0}, y_{std})\| \leq L_{\Delta_{st}}|y_{st,k-1} - y_{st,d}|.\end{aligned} \tag{4.55}$$

From Eqs. (4.38) and (4.55), one has

$$\|\boldsymbol{\Delta}_k(T_k^-, \mathbf{x}|_k^-, y_{st,k-1}) - \boldsymbol{\Delta}_k(\tau_k^-, \mathbf{x}|_k^-, y_{st,k-1})\| \leq L_{\Delta_t}L_{T_x}\|\tilde{\mathbf{x}}(\tau_k; T_{k-1}^+, \mathbf{x}|_{k-1}^+)\| \tag{4.56}$$

for any $\mathbf{x}(0^+) \in B_{d_2}(\mathbf{0})$, where $d_2 = \min\{r_2, r_3\}$.

From Theorem 5.2 and Eq. (4.55), one has

$$\|\boldsymbol{\Delta}_k(\tau_k^-, \mathbf{0}, y_{st,k-1}) - \boldsymbol{\Delta}_k(\tau_k^-, \mathbf{0}, y_{std})\| \leq L_{\Delta_{st}}(\|\mathbf{x}|_k^-\| + \beta_{st}\|\tilde{\mathbf{x}}(\tau_k; T_{k-1}^+, \mathbf{x}|_{k-1}^-)\|) \tag{4.57}$$

for any $\mathbf{x}(0^+) \in B_{d_2}(\mathbf{0})$.

Therefore, from Eqs. (4.53) - (4.57), one has, for any $\mathbf{x}(0^+) \in B_{d_2}(\mathbf{0})$,

$$\begin{aligned}\|x|_k^+\| = \|\boldsymbol{\Delta}_k(T_k^-, \mathbf{x}|_k^-, y_{st,k-1})\| &\leq (L_{\Delta_t}L_{T_x} + L_{\Delta_{st}}\beta_{st})\|\tilde{\mathbf{x}}(\tau_k; T_{k-1}^+, \mathbf{x}|_{k-1}^-)\| + (L_{\Delta_x} + L_{\Delta_{st}})\|x|_k^-\| \\ &:= \tilde{L}(\|\tilde{\mathbf{x}}(\tau_k; T_{k-1}^+, \mathbf{x}|_{k-1}^-)\| + \|x|_k^-\|),\end{aligned} \tag{4.58}$$

where $\tilde{L} := \max(L_{\Delta_t}L_{T_x} + L_{\Delta_{st}}\beta_{st}, L_{\Delta_x} + L_{\Delta_{st}})$.

From Eq. (4.26), one has:

$$\begin{aligned} \|x|_k^-\| &\leq \sqrt{\frac{c_2}{c_1}} e^{-\frac{c_3}{2c_2}(T_k - T_{k-1})} \|x|_{k-1}^+\|; \\ \|\tilde{\mathbf{x}}(\tau_k; T_{k-1}^+, \mathbf{x}|_{k-1}^-)\| &\leq \sqrt{\frac{c_2}{c_1}} e^{-\frac{c_3}{2c_2}(\tau_k - T_{k-1})} \|x|_{k-1}^+\|. \end{aligned} \tag{4.59}$$

Therefore, from Eqs. (4.58) and (4.59), one has

$$\|x|_k^+\| \leq 2\tilde{L}\sqrt{\frac{c_2}{c_1}} e^{-\frac{c_3}{2c_2}(\tau_k - T_{k-1})} (1 + e^{-\frac{c_3}{2c_2}(T_k - \tau_k)}) \|x|_{k-1}^+\|. \tag{4.60}$$

For any $\varepsilon > 0$ there exist PD gains $\mathbf{K}_P$ and $\mathbf{K}_D$ that correspond to sufficiently high continuous-phase convergence rate $\frac{c_3}{2c_2}$ such that

$$e^{-\frac{c_3}{2c_2}(T_k - \tau_k)} \leq 1 + \varepsilon. \tag{4.61}$$

Hence, from Eqs. (4.60) and (4.61), one has

$$\|x|_k^+\| \leq B e^{-\frac{c_3}{2c_2}\Delta\tau_k} \|x|_{k-1}^+\|, \tag{4.62}$$

with $B := 2\tilde{L}\sqrt{\frac{c_2}{c_1}}(2+\varepsilon)$ and $\Delta\tau_k := \tau_k - T_{k-1}$ for any $\mathbf{x}(0) \in B_{d_2}(\mathbf{0})$.

If $\mathbf{K}_P$ and $\mathbf{K}_D$ are chosen such that

$$B e^{-\frac{c_3}{2c_2}\Delta\tau_k} < 1 \tag{4.63}$$

holds, then the sequence $\{V|_1^+, V|_2^+, V|_3^+ ...\}$ is strictly decreasing for any $\mathbf{x}(0^+) \in B_{d_2}(\mathbf{0})$.

Therefore, if the PD gains are chosen such that $\mathbf{A}(\mathbf{K}_P, \mathbf{K}_D)$ is Hurwitz and that Eq.(4.63) is satisfied for any $\mathbf{x}(0^+) \in B_{d_2}(\mathbf{0})$, then the closed-loop hybrid system is locally exponentially stable. ■

4.5 Simulation Results

Computer simulations on a 3-D bipedal robot with nine revolute joints (see Fig. 4.1) was performed to validate the proposed walking strategy. Motion planning of $\boldsymbol{\phi}(\theta)$ is developed to find the desired function $\boldsymbol{\phi}$ such that necessary constraints are satisfied. To demonstrate the high versatility of the proposed walking strategy, two sets of desired position trajectory

on the walking surface are chosen for simulations along with a symmetric walking pattern. The first desired position trajectory has a constant velocity, and the second one has a time-varying velocity. For both cases, the proposed walking strategy can realize exponential tracking of the desired position trajectory in Cartesian space as well as the desired motion along the contour. Furthermore, the effects of the continuous-phase convergence rate on the closed-loop stability are illustrated through simulations.

4.5.1 Motion Planning

The objective of motion planning here is to find the desired function $\boldsymbol{\phi}(\theta)$ such that necessary constraints and conditions are satisfied. Planning of the desired position trajectory $s_d(t)$ is not addressed in this Chapter, which is monotonically increasing and continuously differentiable in t and assumed to be provided by a high-level planner.

Similar to our desired gait design for a fully actuated, planar biped in Chapter 3, optimization is utilized to find the desired function $\boldsymbol{\phi}(\theta)$ that defines the desired walking pattern (i.e., virtual constraints). In addition to the conditions (A1) - (A3), the following constraints are considered in the motion planning:

(B1) Feasibility constraints:

- (a) Joint position limits;
- (b) Joint velocity limits;
- (c) No scuffing the ground of the swing leg.

(B2) Performance specifications:

- (a) The desired step distance.

As the focus of this Chapter is on control design and stability analysis, the above list is not intended to be exhaustive. The Matlab command *fmincon* is used to search for the desired function $\boldsymbol{\phi}(\theta)$ such that the constraints (B1) - (B2) are satisfied. The optimization variables are $\mathbf{a}_k$ ($k \in \{0,1,2,...,6\}$) as defined in Eq. (4.8).

In the following, three sets of 3-D bipedal walking will be simulated, and they share the same desired walking pattern. The desired contour is chosen as the Y_w-axis. The initial conditions are chosen such that the tracking errors projected on the joint position and velocity are the same for three cases:

$$\begin{aligned} \mathbf{e}_q &= 0.1 \times [-1,1,-1,1,-1,1,-1,-1,-1](\text{rad}); \\ \dot{\mathbf{e}}_q &= 0.2 \times [1,1,1,1,1,1,1,1,1](\text{rad/s}). \end{aligned} \tag{4.64}$$

4.5.2 Exponential Tracking of a Straight-Line Contour with Constant Velocity

The desired motion along the straight-line contour $y_h = 0$ is chosen as:

$$s_d(t) = 0.5t - 0.16 \text{ (m)}.$$

Without loss of generality, the PD gains are chosen the same for all output functions, and their values are denoted as K_p and K_d, respectively. Choosing

$$K_p = 841 \text{ and } K_d = 58,$$

we obtain a pair of real closed-loop poles at $p_{1,2} = -29$ for the continuous dynamics. Therefore, $\mathbf{A}(\mathbf{K}_P, \mathbf{K}_D)$ in Eq. (4.25) is Hurwitz.

Figure 4.2 shows the tracking of the desired walking pattern as defined in Eq. (4.5). As clearly shown in the graph, the actual gait converges to the desired walking pattern exponentially. The exponential convergence of y_h to the Y_w-axis, which is the desired contour, is shown in Fig. 4.3. Also, the desired motion along the Y_w-axis is exponentially tracked (see Fig. 4.4). These two plots clearly show the exponential tracking of the desired contour and the desired motion along the contour is realized. Figure 4.5 shows that the actual support foot position along the Y_w-axis converges to a constant value as predicted by Theorem 5.2.

4.5.3 Exponential Tracking of a Straight-Line Contour with Time-varying Velocity

One of the main advantages of the proposed walking strategy is that it decouples the higher-level planning of the desired motion along the desired contour from the lower-level

planning of the desired walking pattern. The walking pattern encoded and planned as in this study can be automatically used in the contouring tracking of an arbitrary, feasible motion along the contour. This argument is illustrated with the simulation results in Figs. 4.6 - 4.9.

The same desired function $\boldsymbol{\phi}(\theta)$ as in the last set of simulations is used here. The desired position trajectory along the straight-line contour $y_h = 0$ is chosen as:

$$s_d(t) = 2.3e^{-0.3(t+0.5)} + 0.6t - 2.2 \text{ (m)}. \tag{4.65}$$

The PD gains K_p and K_d are chosen as:

$$K_p = 625 \text{ and } K_D = 50. \tag{4.66}$$

These values yield a pair of real closed-loop poles at $p_{1,2} = -25$ for the continuous dynamics. Therefore, $\mathbf{A}$ in Eq. (4.25) is Hurwitz.

Figures 4.7 and 4.8 show that the biped exponentially converges to the desired contour as well as the desired motion along the contour. Also, the desired walking pattern is exponentially followed as shown in Fig. 4.6. These simulation results validate the high versatility of the proposed walking strategy.

4.5.4 Effects of Proportional-derivative Control Gains on Closed-Loop Stability

To analyze the effects of PD gains on the closed-loop stability through simulation results, this set of simulation shares the same conditions as the first set except for the PD gains. Here, higher PD gains are chosen as compared with the first set of simulations, and they are selected as:

$$K_p = 6400 \text{ and } K_D = 160. \tag{4.67}$$

The corresponding closed-loop poles for the continuous phase are then $p_{1,2} = -80$, which are much faster than the first simulations. Accordingly, the overall convergence rate is much faster than the first simulations, as shown in Figs. 4.10 - 4.13.

4.6 Summary

Based on nonlinear feedback control and formal stability analysis, this Chapter has proposed and developed a controller design that can realize exponential tracking of a straight-line contour for fully actuated 3-D bipedal robots. With the output function designed as the tracking error of the desired straight-line contour, the desired motion along the contour, and the desired walking pattern, an input-output linearizing controller was synthesized to drive the output function exponentially to zero during continuous phases. By carefully selecting and encoding the walking pattern, hybrid invariance was constructed for the desired motion at the steady state. The sufficient stability conditions for the hybrid time-varying closed-loop system were established, and the simulation results on a 9-DOF, 3-D biped confirmed the effectiveness of the proposed walking strategy in improving walking versatility for fully actuated bipedal robots.

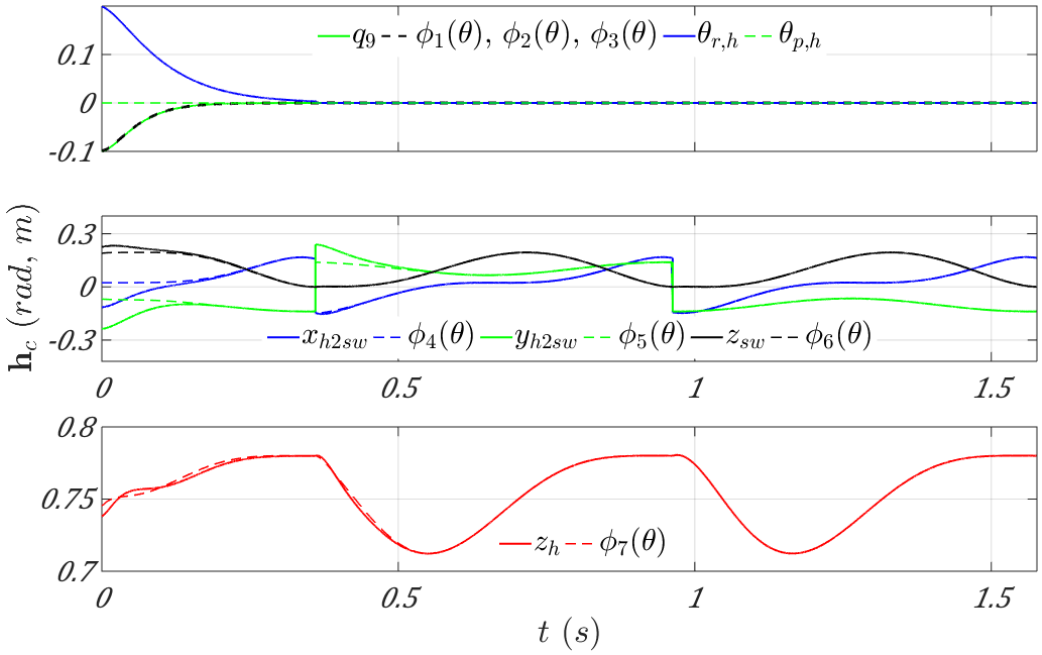

Figure 4.2. Exponential tracking of the desired walking pattern $\mathbf{h}_c = \mathbf{0}$. Desired contour Γ_d: Y_w-axis. Desired position trajectory along Γ_d: $s_d(t) = 0.5t - 0.16$(m). Control gains: $K_p = 841$; $K_d = 58$. Initial conditions: $\mathbf{e}_q = 0.1 \times [-1,1,-1,1,-1,1,-1,-1,-1]$(rad); $\dot{\mathbf{e}}_q = 0.2 \times [1,1,1,1,1,1,1,1,1]$(rad/s).

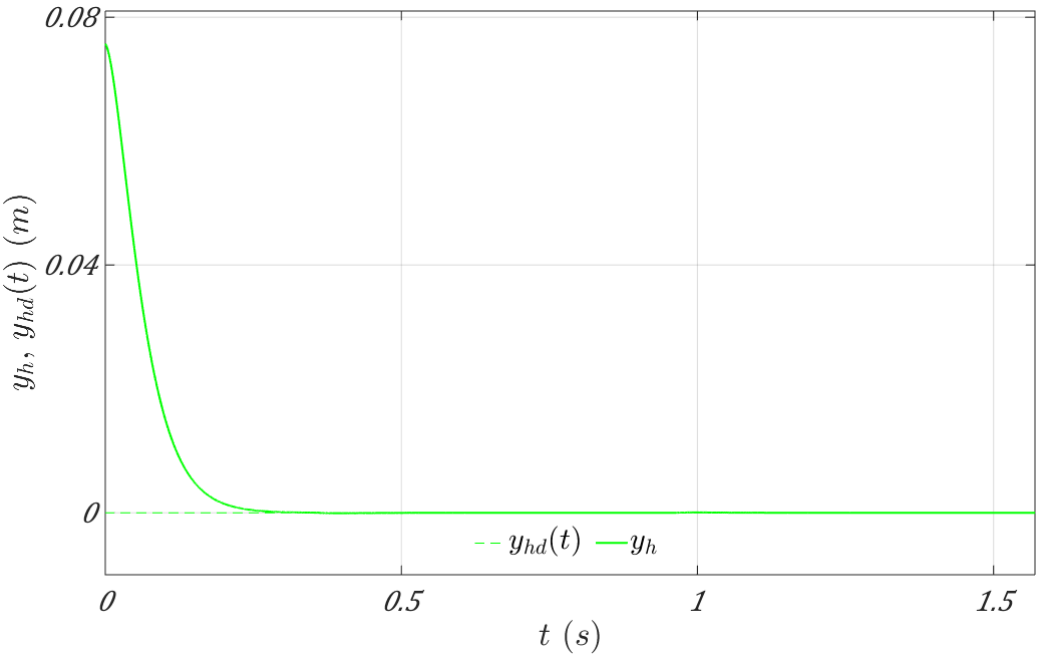

Figure 4.3. Exponential tracking of a straight-line contour ($y_h = 0$). Desired contour Γ_d: Y_w-axis. Desired position trajectory along Γ_d: $s_d(t) = 0.5t - 0.16$(m). Control gains: $K_p = 841$; $K_d = 58$. Initial conditions: $\mathbf{e}_q = 0.1 \times [-1,1,-1,1,-1,1,-1,-1,-1,-1]$((rad)); $\dot{\mathbf{e}}_q = 0.2 \times [1,1,1,1,1,1,1,1,1,1]$((rad/s)).

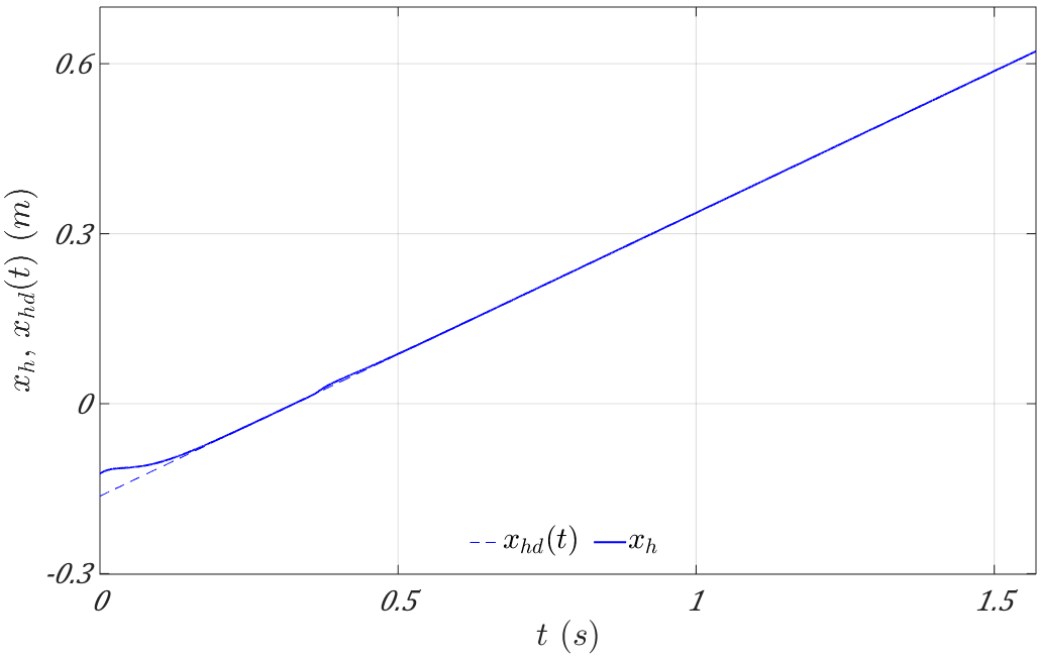

Figure 4.4. Exponential tracking of the desired motion $s_d(t)$ along the contour. Desired contour Γ_d: Y_w-axis. Desired position trajectory along Γ_d: $s_d(t) = 0.5t - 0.16$(m). Control gains: $K_p = 841$; $K_d = 58$. Initial conditions: $\mathbf{e}_q = 0.1 \times [-1,1,-1,1,-1,1,-1,-1,-1]$(rad); $\dot{\mathbf{e}}_q = 0.2 \times [1,1,1,1,1,1,1,1,1]$(rad/s).

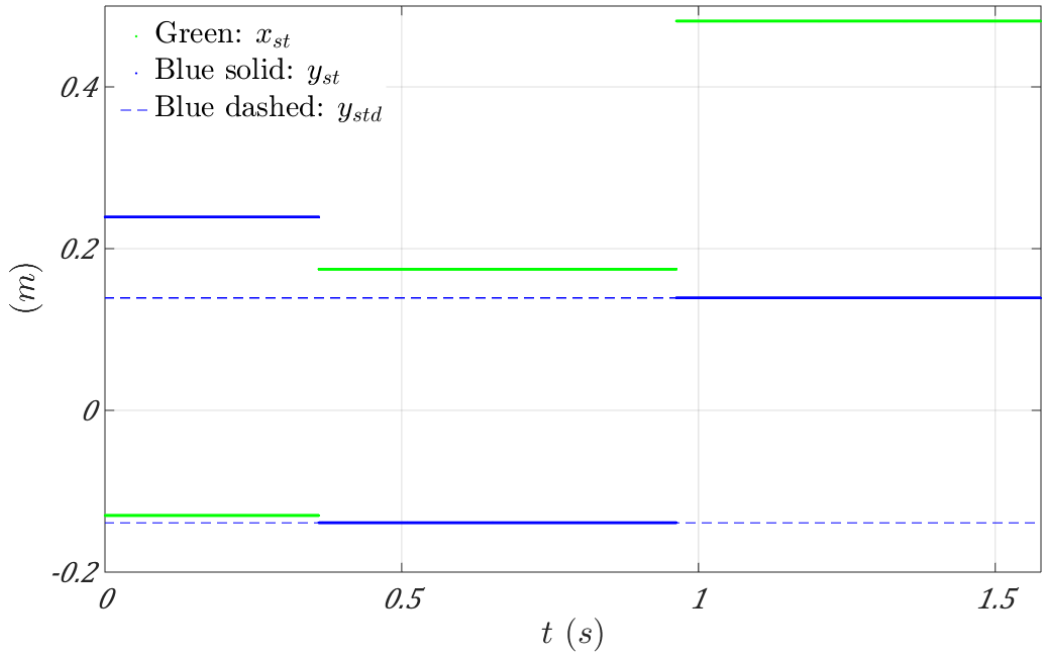

Figure 4.5. Support foot position (x_{st}, y_{st}). Desired contour Γ_d: Y_w-axis. Desired position trajectory along Γ_d: $s_d(t) = 0.5t - 0.16$(m). Control gains: $K_p = 841$; $K_d = 58$. Initial conditions: $\mathbf{e}_q = 0.1 \times [-1,1,-1,1,-1,1,-1,-1,-1]$(rad); $\dot{\mathbf{e}}_q = 0.2 \times [1,1,1,1,1,1,1,1,1]$(rad/s).

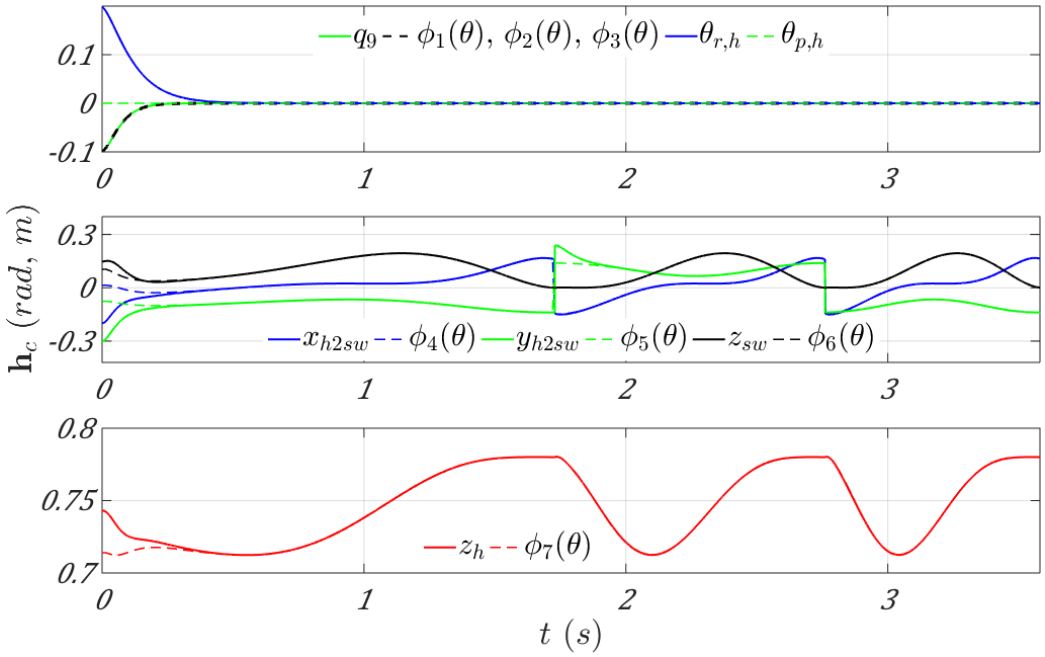

Figure 4.6. Exponential tracking of the desired walking pattern $\mathbf{h}_c = \mathbf{0}$. Desired contour Γ_d: Y_w-axis. Desired position trajectory along Γ_d: $s_d(t) = 2.3e^{-0.3(t+0.5)} + 0.6t - 2.2$(m). Control gains: $K_p = 625$; $K_d = 50$. Initial conditions: $\mathbf{e}_q = 0.1 \times [-1,1,-1,1,-1,1,-1,-1,-1]$(rad); $\dot{\mathbf{e}}_q = 0.2 \times [1,1,1,1,1,1,1,1,1]$(rad/s).

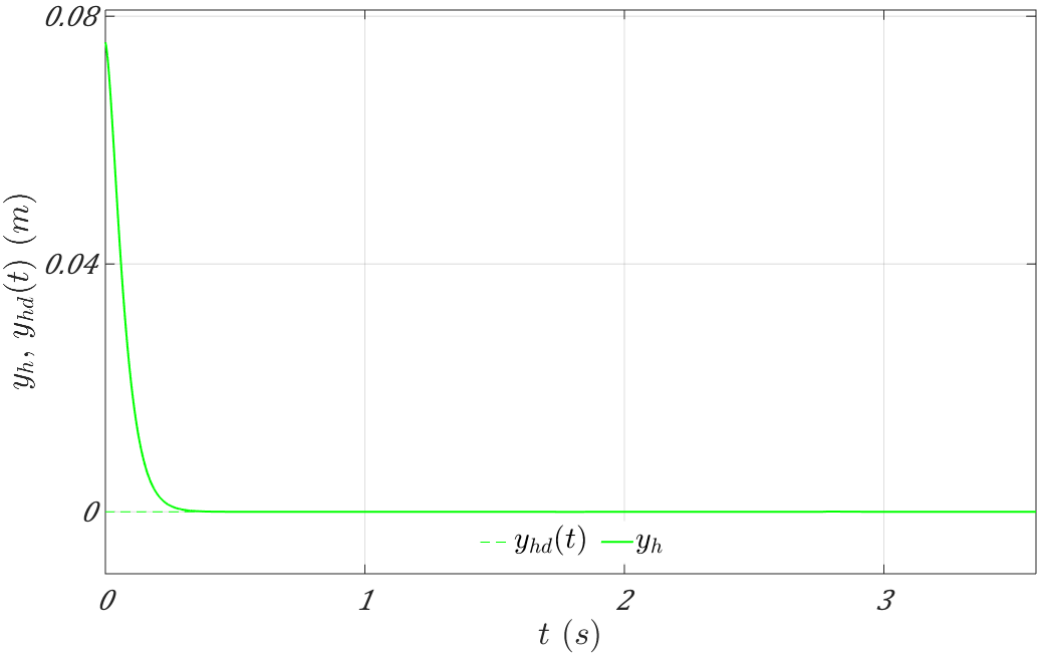

Figure 4.7. Exponential tracking of a straight-line contour ($y_h = 0$). Desired contour Γ_d: Y_w-axis. Desired position trajectory along Γ_d: $s_d(t) = 2.3e^{-0.3(t+0.5)} + 0.6t - 2.2$(m). Control gains: $K_p = 625$; $K_d = 50$. Initial conditions: $\mathbf{e}_q = 0.1 \times [-1,1,-1,1,-1,1,-1,-1,-1]$(rad/s); $\dot{\mathbf{e}}_q = 0.2 \times [1,1,1,1,1,1,1,1,1]$(rad/s).

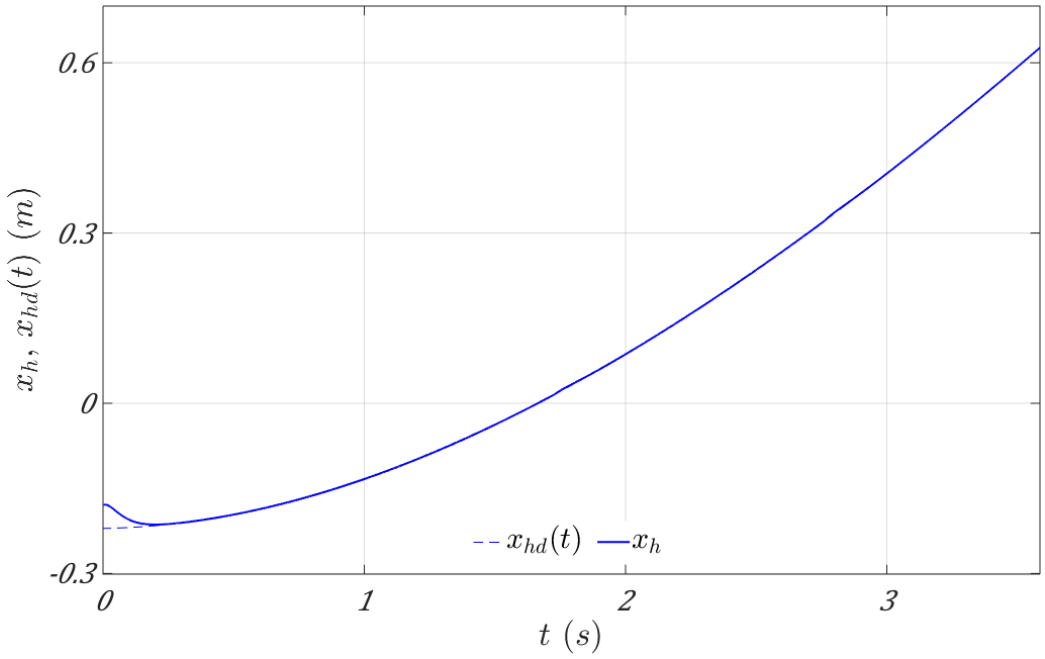

Figure 4.8. Exponential tracking of the desired motion $s_d(t)$ along the contour. Desired contour Γ_d: Y_w-axis. Desired position trajectory along Γ_d: $s_d(t) = 2.3e^{-0.3(t+0.5)} + 0.6t - 2.2$(m). Control gains: $K_p = 625$; $K_d = 50$. Initial conditions: $\mathbf{e}_q = 0.1 \times [-1,1,-1,1,-1,1,-1,-1,-1]$(rad); $\dot{\mathbf{e}}_q = 0.2 \times [1,1,1,1,1,1,1,1,1]$(rad/s).

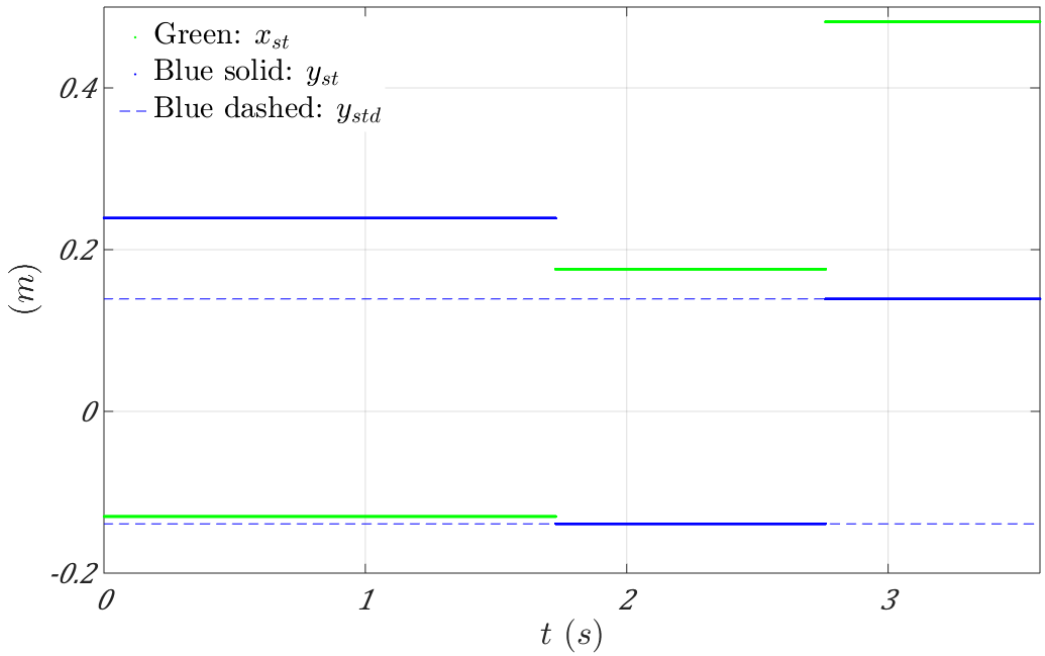

Figure 4.9. Support foot position (x_{st}, y_{st}). Desired contour Γ_d: Y_w-axis. Desired position trajectory along Γ_d: $s_d(t) = 2.3e^{-0.3(t+0.5)} + 0.6t - 2.2$(m). Control gains: $K_p = 625$; $K_d = 50$. Initial conditions: $\mathbf{e}_q = 0.1 \times [-1,1,-1,1,-1,1,-1,-1,-1]$(rad); $\dot{\mathbf{e}}_q = 0.2 \times [1,1,1,1,1,1,1,1,1]$(rad/s).

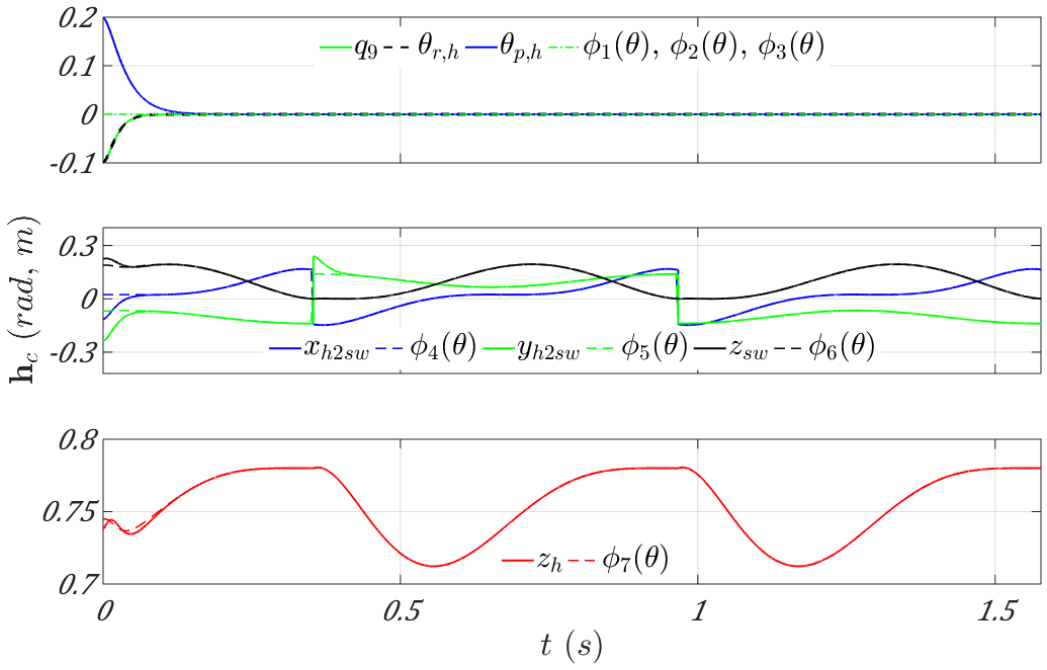

Figure 4.10. Exponential tracking of the desired walking pattern $\mathbf{h}_c = \mathbf{0}$. Desired contour Γ_d: Y_w-axis. Desired position trajectory along Γ_d: $s_d(t) = 0.5t - 0.16$(m). Control gains: $K_p = 6400$; $K_d = 160$. Initial conditions: $\mathbf{e}_q = 0.1 \times [-1,1,-1,1,-1,1,-1,-1,-1]$(rad); $\dot{\mathbf{e}}_q = 0.2 \times [1,1,1,1,1,1,1,1,1]$(rad/s).

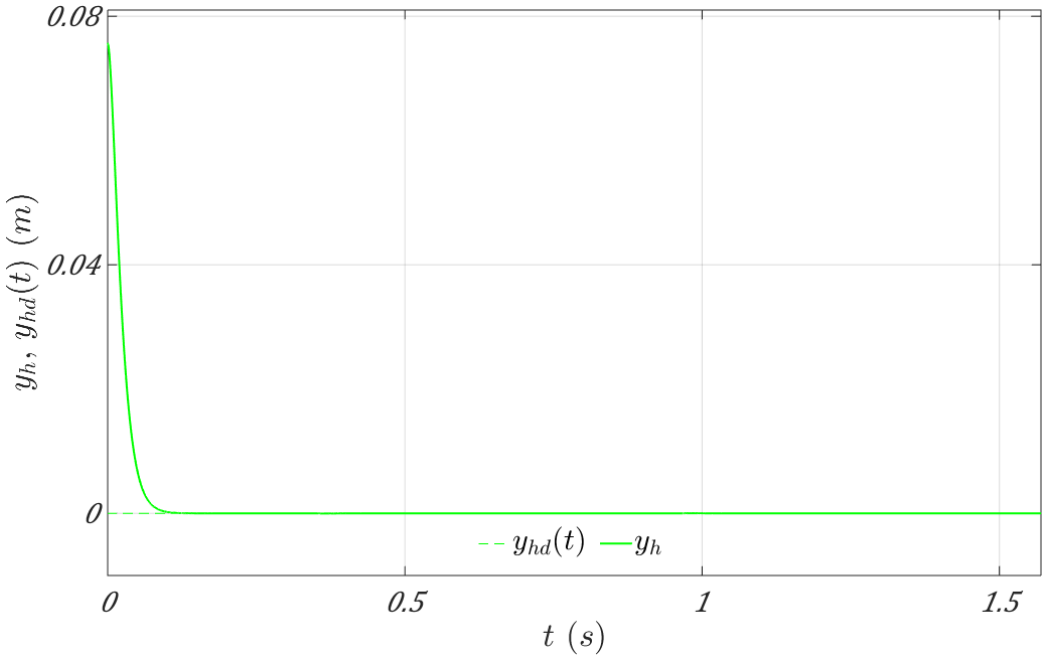

Figure 4.11. Exponential tracking of a straight-line contour ($y_h = 0$). Desired contour Γ_d: Y_w-axis. Desired position trajectory along Γ_d: $s_d(t) = 0.5t - 0.16$(m). Control gains: $K_p = 6400$; $K_d = 160$. Initial conditions: $\mathbf{e}_q = 0.1 \times [-1,1,-1,1,-1,1,-1,-1,-1]$(rad); $\dot{\mathbf{e}}_q = 0.2 \times [1,1,1,1,1,1,1,1,1]$(rad/s).

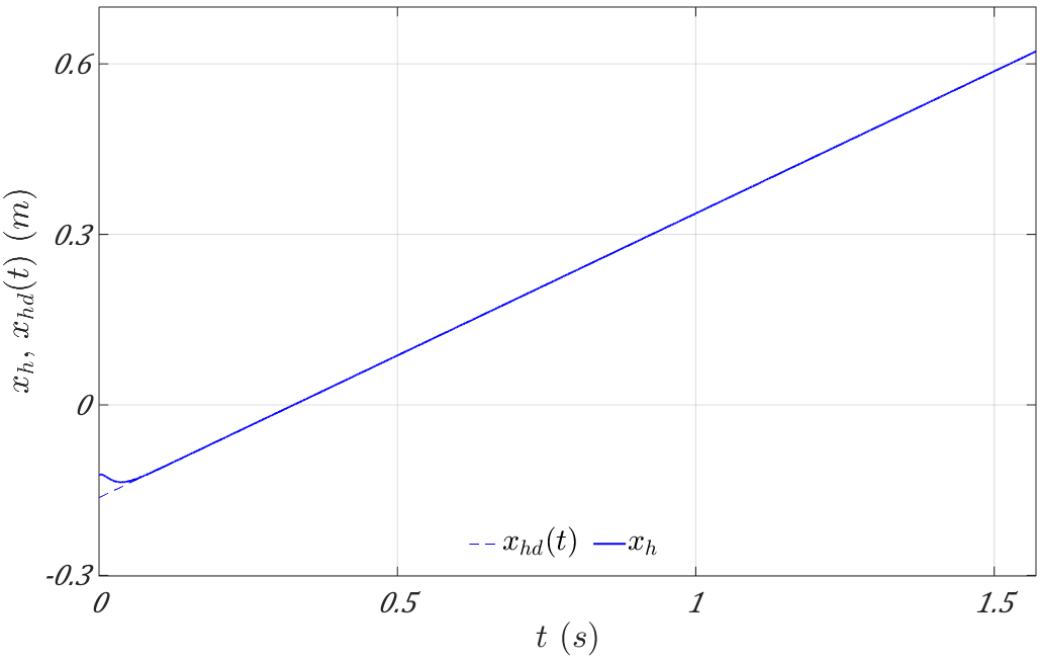

Figure 4.12. Exponential tracking of the desired motion $s_d(t)$ along the contour. Desired contour Γ_d: Y_w-axis. Desired position trajectory along Γ_d: $s_d(t) = 0.5t - 0.16$(m). Control gains: $K_p = 6400$; $K_d = 160$. Initial conditions: $\mathbf{e}_q = 0.1 \times [-1,1,-1,1,-1,1,-1,-1,-1]$(rad); $\dot{\mathbf{e}}_q = 0.2 \times [1,1,1,1,1,1,1,1,1]$(rad/s).

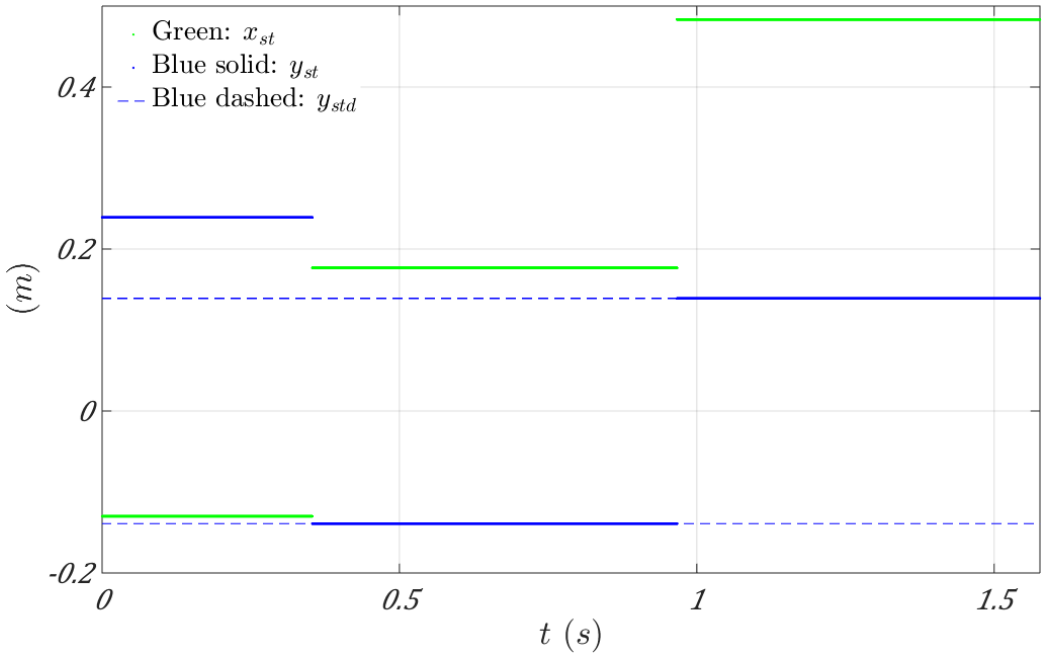

Figure 4.13. Support foot position (x_{st}, y_{st}). Desired contour Γ_d: Y_w-axis. Desired position trajectory along Γ_d: $s_d(t) = 0.5t - 0.16$(m). Control gains: $K_p = 6400$; $K_d = 160$. Initial conditions: $\mathbf{e}_q = 0.1 \times [-1,1,-1,1,-1,1,-1,-1,-1]$(rad); $\dot{\mathbf{e}}_q = 0.2 \times [1,1,1,1,1,1,1,1,1]$(rad/s).

5. TIME-DEPENDENT ORBITALLY EXPONENTIAL STABILIZATION OF UNDERACTUATED WALKING

5.1 Introduction

Underactuation is a common phenomenon in both human walking and bipedal robotic walking [111]. When a biped has higher degrees of freedom than the number of actuators, underactuation occurs. For example, bipedal robots with point feet are underactuated because they have no ankle actuators. Even for bipedal robots with full-sized feet, underactuation may occur when the support foot rolls about its edge. Robots with compliant transmission systems are also underactuated [28] [109]. Hence, it is important to study walking control for underactuated bipedal robots.

Underactuation is more difficult to handle than full actuation due to the lack of actuators to control each joint. Thus, it is challenging to improve the walking versatility of underactuated walking by utilizing a controller design that is based on full-order dynamic modeling and formal stability analysis. Instead, we will focus on improving the robustness of underactuated periodic walking by developing a time-dependent feedback controller that orbitally exponentially stabilizes underactuated walking. This Chapter focuses on the more difficult problem of stabilizing underactuated walking, and the result of this Chapter can be applied to fully actuated walking as well.

Motion control of underactuated bipedal robotic walking has been extensively studied [9] [10] [28] [50] [77] [102] [103] [105] [110] [138] [161] [162]. Because of the cyclic nature of normal bipedal walking, periodic gaits are the focus of these studies. As reviewed in Chapter 1, the HZD framework has been heavily focused on orbital stabilization of underactuated walking. Besides the HZD framework, the stabilization of underactuated bipedal robotic walking has also been studied based on transverse linearization and optimal control [77] [93] [95]. A transverse coordinate is analytically constructed along a

periodic orbit in the state space, and the transverse dynamics are linearized based on which a receding-horizon controller is synthesized to stabilize the orbit. In addition, stable underactuated walking has been achieved based on reduced-order dynamic modeling and energy regulation as well [28].

In all of the above-mentioned studies that are developed based on the HZD framework, the output function is defined by the tracking error of the desired walking pattern, which can be encoded by functions of joint positions [50] [102] [103], angular momentum [106], velocity [105], and/or time [107] [162]. Previous studies have shown that state-based encoding can cause implementation issues due to sensor noise and that the time-dependent encoding can solve that problem effectively by improving the robustness of the closed-loop control system [107]. Therefore, it is meaningful to investigate time-dependent control and provide stability conditions for the closed-loop system.

When states such as joint positions, angular momentum, and/or joint velocities are used to define the output function, the resulting closed-loop system is autonomous whose stability can be evaluated by the first approximation of the Poincaré return map at the fixed-point on the Poincaré section [7]. However, when the encoding variable is chosen as time, the output function becomes an explicit function of time, and the closed-loop dynamics will be aperiodically time-varying with internal dynamics caused by underactuation. Since it is not straightforward to evaluate the stability of a periodic orbit for such a system, no explicit conditions for orbitally exponential stability are provided in the previous studies on time-dependent feedback control [107] [162]. Sufficient conditions for exponentially stabilizing underactuated bipedal walking have also been developed based on time-dependent open-loop control [98], but open-loop control is problematic when dealing with uncertainties and modeling errors in the real-world environment.

In this Chapter, sufficient conditions for orbitally exponential stabilization of underactuated walking are developed based on time-dependent feedback control. The output function is designed as linear combinations of the actual joint positions and some desired time functions, which leads to an aperiodically varying closed-loop system. To evaluate the stability of the nonautonomous closed-loop system, a new state variable is introduced

and used to define an augmented set of states. The system dynamics in terms of the augmented states are autonomous whose stability is more straightforward to evaluate than that of the original, aperiodically varying system and is thus used to determine the closed-loop stability conditions. Because the stability of the zero dynamics caused by underactuation can only be affected by the definition of output function but not the control law, the definition of output function is systematically optimized in motion planning so as to satisfy the proposed stability conditions and create an exponentially stable orbit of the closed-loop system.

5.2 Problem Formulation

In this Chapter, a feedback control law based on input-output linearization will be proposed to stabilize the walking process for an underactuated biped model. In problem formulation, the full-order dynamics of underactuated bipedal robotic walking will be first established, which will be utilized in the proposed model-based controller design. For notational simplicity and without loss of generality, the support-swing gait characterization is utilized to describe the gait. Then, the desired gait is presented, which is periodic and symmetric.

5.2.1 Planar Walking Dynamics under Support-Swing Gait Characterization

A planar bipedal robot with five revolute joints and point feet is shown in Fig. 5.1. Because this biped has point feet instead of finite-sized feet, its ankles are not actuated. Hence, this biped has four actuators, and it is underactuated. Also, this planar biped satisfies all of the model assumptions listed in Section 2.3. Its model parameters are given in Table 5.1.

Without loss of generality, we only consider symmetric gaits in this Chapter, and the robot's gait is characterized by the support and the swing legs. When the support-swing gait characterization is used to describe a bipedal gait, a complete gait cycle will consist of two subphases – a single-support phase (SSP) and an instantaneous double-support phase (DSP) (see Fig. 5.2).

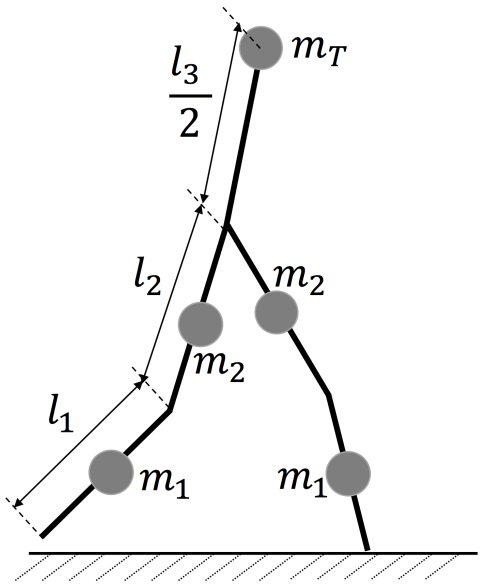

Figure 5.1. A planar biped with five revolute joints. (l_1, l_2 and l_3 are the lengths of the lower limbs, the upper limbs, and the trunk, respectively.)

Table 5.1.
Mass and length parameters of the planar biped model in Fig. 5.1.

m_1 (kg)	m_2 (kg)	m_T (kg)	$l_1, l_2, \frac{l_3}{2}$ (m)
3	6	20	0.4

Define the joint position $\mathbf{q}$ as

$$\mathbf{q} = \begin{bmatrix} q_1 \\ q_2 \\ q_3 \\ q_4 \\ q_5 \end{bmatrix} \in Q, \tag{5.1}$$

where $Q \subset \mathbb{R}^5$ is the configuration space of the bipedal robot when the support leg is in static, full contact with the walking surface and the joint position limits are satisfied, q_1

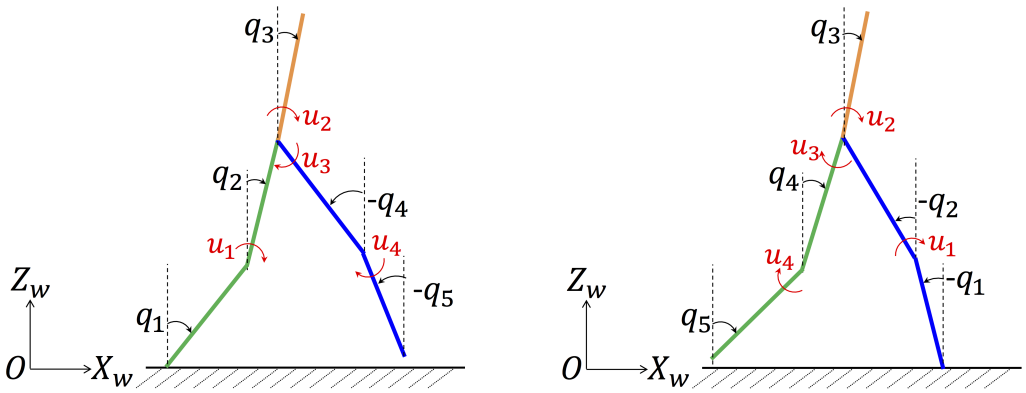

Figure 5.2. An underactuated planar biped represented by the support-swing gait characterization. (a): The right leg is in support. (b): The left leg is in support. (The left leg, the right leg, and the trunk are represented in blue, green, and orange colors, respectively.)

and q_2 are joint positions of the support leg, q_4 and q_5 are joint positions of the swing leg, and q_3 is the joint position of the trunk. Let

$$\mathbf{u} = \begin{bmatrix} u_1 \\ u_2 \\ u_3 \\ u_4 \end{bmatrix} \in \mathbb{R}^4$$

represent the joint-torque vector as illustrated in Fig. 5.2.

The switching surface $S_q(\mathbf{q}, \dot{\mathbf{q}})$ is defined as

$$S(\mathbf{q}, \dot{\mathbf{q}}) := \{(\mathbf{q}, \dot{\mathbf{q}}) \in TQ : z_{sw}(\mathbf{q}) = 0,\ \dot{z}_{sw}(\mathbf{q}, \dot{\mathbf{q}}) < 0\}, \tag{5.2}$$

where $z_{sw}(\mathbf{q})$ is the height of the swing foot above the walking surface and

$$z_{sw}(\mathbf{q}) := l_1 \cos(q_1) + l_2 \cos(q_2) - l_2 \cos(q_4) - l_1 \cos(q_5).$$

The hybrid walking dynamics can be compactly written as:

$$\begin{cases} \mathbf{M}(\mathbf{q})\ddot{\mathbf{q}} + \mathbf{c}(\mathbf{q}, \dot{\mathbf{q}}) = \mathbf{B}_u \mathbf{u}, & \text{if } (\mathbf{q}^-, \dot{\mathbf{q}}^-) \notin S_q(\mathbf{q}, \dot{\mathbf{q}}); \\ [\mathbf{q}^+; \dot{\mathbf{q}}^+] = \boldsymbol{\Delta}(\mathbf{q}^-, \dot{\mathbf{q}}^-), & \text{if } (\mathbf{q}^-, \dot{\mathbf{q}}^-) \in S_q(\mathbf{q}, \dot{\mathbf{q}}); \end{cases} \tag{5.3}$$

where $\mathbf{M} : Q \to \mathbb{R}^{5\times5}$ is the inertia matrix, $\mathbf{c} : Q \to \mathbb{R}^5$ is the sum of the Coriolis, the centrifugal, and the gravitational terms, $\mathbf{B}_u : \mathbb{R}^{5\times4}$ is the input matrix and is full column rank, $\mathbf{u} \in \mathbb{R}^3$ is the joint-torque vector, and $\mathbf{\Delta} : TQ \to \mathbb{R}^{10}$ is the reset map. The expressions of $\mathbf{M}$, $\mathbf{c}$, and $\mathbf{B}_u$ are given in Appendix C.1. Due to space limitation, the derivation instead of the expression of $\mathbf{\Delta}$ is given in Appendix C.2.

5.2.2 A Periodic Symmetric Gait

Before introducing the control law, we shall first describe the desired periodic gait, which corresponds to a periodic orbit in the state space. The desired periodic gait in this study is defined as symmetric. A gait is called symmetric if the relative evolution of joint positions (i.e., walking patterns) characterized by the support and the swing legs is identical for both the left-leg-in-support and the right-leg-in-support phases. However, the proposed controller synthesis in this Chapter can be readily extended from symmetric gaits to asymmetric gaits by recharacterizing the gait with the left and the right legs instead of the support and the swing legs [140].

Suppose that the walking process begins with the initial moment of a single-support phase (SSP) at $t = t_0^+$. Without loss of generality, define $t_0 = 0$. Let $\bar{\mathbf{q}}_d(t)$ denote a set of desired joint position trajectories defined by the desired orbit,

$$\bar{\mathbf{q}}_d(t) := \begin{bmatrix} \bar{q}_{1d}(t) \\ \bar{q}_{2d}(t) \\ \bar{q}_{3d}(t) \\ \bar{q}_{4d}(t) \\ \bar{q}_{5d}(t) \end{bmatrix} \in \mathbb{R}^5, \tag{5.4}$$

and then

$$\bar{\mathbf{q}}_d(t) = \bar{\mathbf{q}}_d(t + k\tau), \forall t > 0, \tag{5.5}$$

where $k \in \{1, 2, ...\}$ and the positive number τ is the least gait cycle of the desired gait. The desired periodic orbit, where $(\bar{\mathbf{q}}_d(t), \dot{\bar{\mathbf{q}}}_d(t))$ resides, can then be formally defined as

$$\Gamma_d := \{(\mathbf{q}, \dot{\mathbf{q}}) \in TQ : \mathbf{q} = \bar{\mathbf{q}}_d(t),\ \dot{\mathbf{q}} = \dot{\bar{\mathbf{q}}}_d(t),\ t > 0\}.$$

Due to the coordinate swap and the rigid impact, $\bar{\mathbf{q}}_d(t)$ is piece-wise continuous with discontinuities caused by the desired swing-foot touchdown at $\tau_k = k\tau$, $k \in \{1,2,...\}$. Without loss of generality, define $\tau_0 = t_0 = 0$.

5.3 Model-based Feedback Control through Input-Output Linearization

Although the control objective is to realize exponential convergence to the desired orbit Γ_d, $\bar{\mathbf{q}}_d(t)$ cannot be directly used to define the output function. The reasons are that the landing moments associated with $\bar{\mathbf{q}}_d(t)$ do not necessarily coincide with the actual ones and that both joint positions and velocities experience sudden jumps upon a swing-foot landing. Therefore, the desired periodic joint trajectories $\bar{\mathbf{q}}_d(t)$ are modified to define the desired time functions $\mathbf{q}_d(t)$,

$$\mathbf{q}_d(t) = \begin{bmatrix} q_{1d}(t) \\ q_{2d}(t) \\ q_{3d}(t) \\ q_{4d}(t) \\ q_{5d}(t) \end{bmatrix} \in \mathbb{R}^5. \tag{5.6}$$

Let T_k ($k \in \{1,2,...\}$) denote the moment of the k^{th} actual swing-foot landing. Without loss of generality, define $T_0 = t_0 = 0$. During the $(k+1)^{th}$ step, the desired time functions $\mathbf{q}_d(t)$ are defined as

$$\mathbf{q}_d(t) := \mathbf{q}_0(t - T_k),\ \forall t \in (T_k, T_{k+1}], \tag{5.7}$$

where $\mathbf{q}_0(t) \in \mathbb{R}^5$ is a smooth extension of $\bar{\mathbf{q}}_d(t)$ from $t \in (0, \tau]$ to $t \in (-\infty, +\infty)$. The definition of $\mathbf{q}_d(t)$ indicates that the discontinuities of $\mathbf{q}_d(t)$ are at T_k ($k \in \{1,2,...\}$) instead of τ_k and that $\mathbf{q}_d(T_k^+) = \bar{\mathbf{q}}_d(\tau_k^+)$. An illustration of $\bar{q}_{2d}(t)$ and $q_{2d}(t)$ is shown in Fig. 5.3.

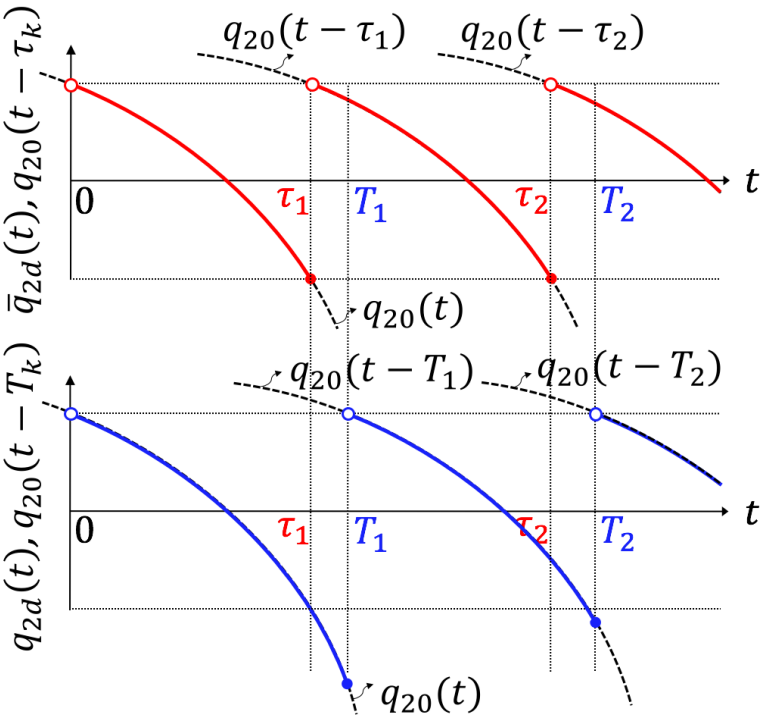

Figure 5.3. An illustration of $\bar{q}_{2d}(t)$ and $q_{2d}(t)$.

In our previous study [142], the lower-limb joint position of the support leg $q_1(t)$ is chosen as the indirectly controlled joint, and the directly controlled joints $\mathbf{q}_a(t)$ are denoted as:

$$\mathbf{q}_a := \begin{bmatrix} q_2 \\ q_3 \\ q_4 \\ q_5 \end{bmatrix} \in \mathcal{Q}_a \subset \mathcal{Q}. \tag{5.8}$$

The output function $\mathbf{y}$ is then defined as

$$\mathbf{y} = \mathbf{q}_a - \mathbf{q}_{ad}(t), \tag{5.9}$$

where

$$\mathbf{q}_{ad}(t) := \begin{bmatrix} q_{2d}(t) \\ q_{3d}(t) \\ q_{4d}(t) \\ q_{5d}(t) \end{bmatrix} \in \mathbb{R}^4. \tag{5.10}$$

This previous definition is limited in the sense that the definition of output functions is fixed and thus cannot be optimized in order to find a stable gait in motion planning. Although the proposed feedback controller can directly drive $\mathbf{y}(t)$ to zero as $t \to \infty$, the stability of internal dynamics caused by the underactuation is also affected by the definition of output function [76]. Therefore, a more general definition of output function is introduced and investigated, from which a systematic optimization method for finding a stable gait will be proposed and presented in Section 5.5.

Introducing the coordinate transformation as

$$\mathbf{q}_T := \begin{bmatrix} q_{T1} \\ q_{T2} \\ q_{T3} \\ q_{T4} \\ q_{T5} \end{bmatrix} = \mathbf{H}_T \mathbf{q}, \tag{5.11}$$

where $\mathbf{H}_T \in \mathbb{R}^{5\times5}$ is a nonsingular matrix, we then design the output function $\mathbf{y}$ as:

$$\mathbf{y} = \mathbf{H}(\mathbf{q}_T - \mathbf{q}_{Td}(t)), \tag{5.12}$$

where $\mathbf{H} \in \mathbb{R}^{4\times 5}$ is full row rank and

$$\mathbf{q}_{Td}(t) = \begin{bmatrix} q_{T1d}(t) \\ q_{T2d}(t) \\ q_{T3d}(t) \\ q_{T4d}(t) \\ q_{T5d}(t) \end{bmatrix}^T = \mathbf{H}_T \mathbf{q}_d(t). \tag{5.13}$$

The continuous-time dynamics during an SSP in Eq. (5.3) becomes

$$\mathbf{M}_T(\mathbf{q}_T)\ddot{\mathbf{q}}_T + \mathbf{c}_T(\mathbf{q}_T, \dot{\mathbf{q}}_T) = \mathbf{B}_u \mathbf{u}, \tag{5.14}$$

where $\mathbf{M}_T(\mathbf{q}_T) := \mathbf{M}(\mathbf{H}_T^{-1}\mathbf{q}_T)\mathbf{H}_T^{-1}$ and $\mathbf{c}_T(\mathbf{q}_T, \dot{\mathbf{q}}_T) := \mathbf{c}(\mathbf{H}_T^{-1}\mathbf{q}_T, \mathbf{H}_T^{-1}\dot{\mathbf{q}}_T)$.

The reset map is obtained as:

$$\mathbf{\Delta}_T(\mathbf{q}_T, \dot{\mathbf{q}}_T) = \mathbf{H}_T \mathbf{\Delta}(\mathbf{H}_T^{-1}\mathbf{q}_T, \mathbf{H}_T^{-1}\dot{\mathbf{q}}_T). \tag{5.15}$$

Without loss of generality, suppose that q_{T1} is not directly controlled. Denote the directly controlled variables as $\mathbf{q}_{Ta}$:

$$\mathbf{q}_{Ta} := \mathbf{H}\mathbf{q}_T = \begin{bmatrix} q_{T2} \\ q_{T3} \\ q_{T4} \\ q_{T5} \end{bmatrix}, \tag{5.16}$$

where

$$\mathbf{H} = \begin{bmatrix} 0 & 1 & 0 & 0 & 0 \\ 0 & 0 & 1 & 0 & 0 \\ 0 & 0 & 0 & 1 & 0 \\ 0 & 0 & 0 & 0 & 1 \end{bmatrix}. \tag{5.17}$$

Accordingly, denote

$$\mathbf{q}_{Tad}(t) := \begin{bmatrix} q_{T2d}(t) \\ q_{T3d}(t) \\ q_{T4d}(t) \\ q_{T5d}(t) \end{bmatrix} := \mathbf{H}\mathbf{q}_{Td}(t). \tag{5.18}$$

From Eq. (5.14), one has

$$\ddot{\mathbf{q}}_T = \mathbf{M}_T^{-1}(\mathbf{B}_u\mathbf{u} - \mathbf{c}_T). \tag{5.19}$$

From Eqs. (5.12) and (5.19), it can be obtained that

$$\ddot{\mathbf{y}} = \mathbf{H}(\mathbf{M}_T^{-1}\mathbf{B}_u\mathbf{u} - (\mathbf{M}_T^{-1}\mathbf{c}_T + \ddot{\mathbf{q}}_{Td}(t))). \tag{5.20}$$

Assume that there are no disturbances or modeling errors and suppose that $\mathbf{H}\mathbf{M}_T^{-1}\mathbf{B}_u$ is globally invertible [50]. Then, input-output linearization is utilized to construct the control law based on Eqs. (5.14) and (5.20),

$$\mathbf{u} = (\mathbf{H}\mathbf{M}_T^{-1}\mathbf{B}_u)^{-1}(\mathbf{v} + \mathbf{H}(\mathbf{M}_T^{-1}\mathbf{c}_T + \ddot{\mathbf{q}}_{Td}(t))), \tag{5.21}$$

which linearizes the nonlinear dynamics in Eq. (5.14) into

$$\ddot{\mathbf{y}} = \mathbf{v} \tag{5.22}$$

during each continuous phase. If $\mathbf{v}$ is chosen as a proportional-derivative (PD) control law,

$$\mathbf{v} = -\mathbf{K}_P\mathbf{y} - \mathbf{K}_D\dot{\mathbf{y}}, \tag{5.23}$$

where $\mathbf{K}_P \in \mathbb{R}^{4\times4}$ and $\mathbf{K}_D \in \mathbb{R}^{4\times4}$ are positive-definite diagonal matrices, one then obtains the following linear dynamics of output function:

$$\begin{bmatrix}\dot{\mathbf{y}}\\ \ddot{\mathbf{y}}\end{bmatrix} = \begin{bmatrix}\mathbf{0}_{4\times4} & \mathbf{I}_{4\times4}\\ -\mathbf{K}_P & -\mathbf{K}_D\end{bmatrix}\begin{bmatrix}\mathbf{y}\\ \dot{\mathbf{y}}\end{bmatrix} := \mathbf{A}(\mathbf{K}_P, \mathbf{K}_D)\begin{bmatrix}\mathbf{y}\\ \dot{\mathbf{y}}\end{bmatrix}, \tag{5.24}$$

where $\mathbf{0}_{4\times4} \in \mathbb{R}^{4\times4}$ is a zero matrix and $\mathbf{I}_{4\times4} \in \mathbb{R}^{4\times4}$ is an identity matrix.

Suppose that $\mathbf{H}\mathbf{M}_T^{-1}\mathbf{B}_u$ is globally invertible [50]. Furthermore, if the PD gains in $\mathbf{K}_P$ and $\mathbf{K}_D$ are designed properly such that $\mathbf{A}$ is Hurwitz, then $\mathbf{y}$ will exponentially converge to zero during each continuous phase, and the convergence rate can be adjusted by tuning $\mathbf{K}_P$ and $\mathbf{K}_D$ [76].

Let χ denote the full state space. Define

$$\mathbf{x} := \begin{bmatrix}\mathbf{x}_1\\ \mathbf{x}_2\end{bmatrix} \in \chi, \tag{5.25}$$

where $\mathbf{x}_1 := \mathbf{q}_T$ and $\mathbf{x}_2 := \dot{\mathbf{q}}_T$. Accordingly, define

$$\bar{\mathbf{x}}_d(t) := \begin{bmatrix} \bar{\mathbf{x}}_{1d}(t) \\ \bar{\mathbf{x}}_{2d}(t) \end{bmatrix} := \begin{bmatrix} \bar{\mathbf{q}}_{Td}(t) \\ \dot{\bar{\mathbf{q}}}_{Td}(t) \end{bmatrix} \in \mathbb{R}^{10}. \tag{5.26}$$

From Eq. (5.2), the switching surface $S(\mathbf{x})$ can be written as:

$$S(\mathbf{x}) := \{\mathbf{x} \in \chi : \psi(\mathbf{x}) = 0,\ \frac{\partial \psi}{\partial \mathbf{x}_1}\mathbf{x}_2 < 0\}, \tag{5.27}$$

where $\psi(\mathbf{x}) := z_{sw}(\mathbf{H}_T^{-1}\mathbf{x}_1)$. From Eqs. (5.12), (5.14), (5.21), (5.23), and (5.27), the closed-loop control system can be rewritten as:

$$\begin{cases} \dot{\mathbf{x}} = \mathbf{f}(t,\mathbf{x}), & \text{if } \mathbf{x} \notin S(\mathbf{x}), \\ \Delta\mathbf{x} = \mathbf{I}(\mathbf{x}), & \text{if } \mathbf{x} \in S(\mathbf{x}), \end{cases} \tag{5.28}$$

where $\Delta\mathbf{x}(t) = \mathbf{x}(t^+) - \mathbf{x}(t)$ and the expressions of $\mathbf{I}(\mathbf{x})$ and $\mathbf{f}(t,\mathbf{x})$ are given in Appendice D. For notational simplicity, left continuity at a switching moment is assumed here, i.e., $\mathbf{x}(t) = \mathbf{x}(t^-)$.

5.4 Closed-Loop Stability Analysis

With the proposed feedback control law, the output function will be driven to zero at an exponential rate determined by the gain matrices $\mathbf{K}_P$ and $\mathbf{K}_D$. However, internal dynamics exist due to the underactuation, which determines the closed-loop stability [76]. It is, therefore, necessary to investigate the sufficient conditions for closed-loop stability. In contrast to previous studies where the internal dynamics are explicitly considered in the stability analysis [50] [77] [102] [103], the stability conditions will need to be derived based on the complete closed-loop control system.

5.4.1 Augmented Autonomous System

The stability of the nonlinear, aperiodically varying, hybrid closed-loop system in Eq. (5.28) is challenging to evaluate. However, it can be converted into an equivalent, autonomous system, based on which the closed-loop stability conditions are established in this section.

Introduce a new variable ρ as

$$\rho = t - T_k,\ \forall t \in (T_k, T_{k+1}],\ k \in \{0,1,2,...\}. \tag{5.29}$$

From Eq. (5.29), ρ can be viewed as a phase indicator of the actual walking process within each step. Another important property of ρ is that it is reset to zero at the initial moment of each step; that is, $\rho(T_k^+) = 0$, $k \in \{0,1,2,...\}$. By its definition, one can obtain the dynamics of ρ as

$$\begin{cases} \dot{\rho} = 1, & \text{if } \mathbf{x} \notin S(\mathbf{x}); \\ \Delta\rho = -\rho, & \text{if } \mathbf{x} \in S(\mathbf{x}); \end{cases} \tag{5.30}$$

where $\Delta\rho(t) := \rho(t^+) - \rho(t)^- = \rho(t^+) - \rho(t)$. When all of the joints follow the desired periodic trajectories $\bar{\mathbf{q}}_d(t)$ exactly, the phase variable ρ will also evolve on its desired periodic trajectory $\bar{\rho}_d(t)$ given by

$$\bar{\rho}_d(t) = t - \tau_k,\ \forall t \in (\tau_k, \tau_{k+1}],\ k \in \{0,1,2,...\}. \tag{5.31}$$

From Eqs. (5.7) and (5.29), $\mathbf{q}_d(t)$ can be rewritten as

$$\mathbf{q}_d(t) := \mathbf{q}_0(\rho). \tag{5.32}$$

Hence, from Eqs. (5.14), (5.21), and (5.32), $\mathbf{f}(t,\mathbf{x})$ can be rewritten as some function $\mathbf{g}(\rho,\mathbf{x})$ during a SSP. The expression of $\mathbf{g}(\rho,\mathbf{x})$ is given in the Appendix E.

Introduce the augmented state $\mathbf{x}_e$ as

$$\mathbf{x}_e := \begin{bmatrix} \rho \\ \mathbf{x} \end{bmatrix} \in \chi_e, \tag{5.33}$$

where $\chi_e \subset \mathbb{R}^{11}$ is the augmented state space. Accordingly, denote

$$\bar{\mathbf{x}}_{ed}(t) := \begin{bmatrix} \bar{\rho}_d(t) \\ \bar{\mathbf{x}}_d(t) \end{bmatrix} \in \mathbb{R}^{11}. \tag{5.34}$$

Then, an autonomous system equivalent to Eq. (5.28) can be obtained as

$$\begin{cases} \dot{\mathbf{x}}_e = \mathbf{g}_e(\mathbf{x}_e), & \text{if } \mathbf{x}_e \notin S_e(\mathbf{x}_e); \\ \Delta\mathbf{x}_e = \mathbf{I}_e(\mathbf{x}_e), & \text{if } \mathbf{x}_e \in S_e(\mathbf{x}_e); \end{cases} \tag{5.35}$$

where

$$\mathbf{g}_e(\mathbf{x}_e) := \begin{bmatrix} 1 \\ \mathbf{g}(\rho, \mathbf{x}) \end{bmatrix}, \ \mathbf{I}_e(\mathbf{x}_e) := \begin{bmatrix} -\rho \\ \mathbf{I}(\mathbf{x}) \end{bmatrix}, \tag{5.36}$$

and the switching surface is defined as

$$S_e(\mathbf{x}_e) := \{\mathbf{x}_e \chi_e : \psi_e(\mathbf{x}_e) := z_{sw}(\mathbf{H}_T^{-1}\mathbf{x}_1) = 0, \ \frac{\partial \psi_e}{\partial \mathbf{x}_e}(\mathbf{x}_e)\mathbf{g}_e(\mathbf{x}_e) < 0\}.$$

The expression of $\mathbf{g}_e(\rho, \mathbf{x})$ is given in Appendix E.

5.4.2 Stability Conditions

Stability of the hybrid periodic orbit Γ_d can be numerically evaluated in two equivalent ways. One is the method of Poincaré section [50], and the other is based on the monodromy matrix of the variational equation [79] [98]. We shall employ the second method to establish the closed-loop stability conditions.

The variational equation of the augmented autonomous system in Eq. (5.35) can be obtained as [79]:

$$\begin{cases} \dfrac{d\mathbf{z}_e}{dt} = \dfrac{\partial \mathbf{g}_e}{\partial \mathbf{x}_e}(\bar{\mathbf{x}}_{ed}(t))\mathbf{z}_e, & \text{if } t \neq \tau_k; \\ \Delta \mathbf{z}_e = \mathbf{M}_{ke}\mathbf{z}_e, & \text{if } t = \tau_k; \end{cases} \tag{5.37}$$

where

$$\mathbf{M}_{ke} = \frac{\partial \mathbf{I}_e}{\partial \mathbf{x}_e} + [\mathbf{g}_e^+ - \mathbf{g}_e - \frac{\partial \mathbf{I}_e}{\partial \mathbf{x}_e}\mathbf{g}_e] \frac{\frac{\partial \psi_e}{\partial \mathbf{x}_e}}{\frac{\partial \psi_e}{\partial \mathbf{x}_e}\mathbf{g}_e} \tag{5.38}$$

and

$$\begin{aligned} &\mathbf{g}_e := \mathbf{g}_e(\bar{\mathbf{x}}_{ed}(\tau_k)), \qquad \mathbf{g}_e^+ := \mathbf{g}_e(\bar{\mathbf{x}}_{ed}(\tau_k^+)), \\ &\frac{\partial \mathbf{I}_e}{\partial \mathbf{x}_e} := \frac{\partial \mathbf{I}_e}{\partial \mathbf{x}_e}(\bar{\mathbf{x}}_{ed}(\tau_k)), \quad \frac{\partial \psi_e}{\partial \mathbf{x}_e} := \frac{\partial \psi_e}{\partial \mathbf{x}_e}(\bar{\mathbf{x}}_{ed}(\tau_k)). \end{aligned} \tag{5.39}$$

The closed-loop stability conditions are now introduced based on the equivalence of the original and the augmented systems.

Theorem 5.1 (Closed-loop Stability) Let the following conditions hold:

(A1) $\dfrac{\partial \psi}{\partial \mathbf{x}}(\bar{\mathbf{x}}_d(\tau_k))\dot{\bar{\mathbf{x}}}_d(\tau_k) \neq 0;$

(A2) There is no beating at a landing impact;

(A3) The monodromy matrix of the linear, periodically varying system in Eq. (5.37) has only one unity-modulus eigenvalue, and the moduli of all the other eigenvalues are strictly less than one.

Then, $\bar{\mathbf{x}}_d(t)$ is a locally orbitally exponentially stable solution of the closed-loop system in Eq. (5.28); that is, the hybrid periodic orbit Γ_d is locally exponentially stable. ■

Proof : The linear system in Eq. (5.37) is the variational equation of the augmented autonomous system in Eq. (5.35) [163]. It can be proved that the biped model in Eq. (5.3) satisfies the following conditions:

1. The function $\mathbf{f} : \mathbb{R} \times \chi \to \mathbb{R}^{2n}$ is piecewise continuous on $t \in \mathbb{R}^+$ and continuously differentiable on $\mathbf{x} \in \chi$;

2. The function $\mathbf{I} : \chi \to \mathbb{R}^{2n}$ is continuously differentiable on χ;

3. The function $z_{sw} : Q \to \mathbb{R}$ is continuously differentiable on Q.

Then, by Theorem 1 in [163], the condition (A3) guarantees that there exists a positive number $\delta > 0$ such that for any $\mathbf{x}_e(0) \in B_\delta(\Gamma)$, where $\Gamma_{ed} := \{\mathbf{x}_e \in \chi_e : \mathbf{x}_e = \bar{\mathbf{x}}_{ed}(t), t > 0\}$, $\mathbf{x}_e(t)$ will converge to the periodic orbit Γ_{ed} exponentially fast for the system in Eq. (5.35). Because the original system in Eq. (5.28) is equivalent to Eq. (5.35) and by the definition of $\bar{\mathbf{x}}_{ed}$ in Eq. (5.34), $\bar{\mathbf{x}}_d(t)$ is a locally orbitally exponentially stable solution of the original closed-loop system in Eq. (5.28). ■

These three conditions are straightforward to evaluate in motion planning. Because we are dealing with orbital stabilization, the monodromy matrix of the variational equation in Eq. (5.37) always has a unity-modulus eigenvalue. Therefore, according to the condition (A3), the eigenvalue with the largest modulus among all the other eigenvalues determines the stability of the hybrid periodic orbit Γ_d and is denoted as λ_s. Also, there is always an eigenvalue zero because ρ is reset to zero upon an impact, and this property will be formally summarized in the next subsection.

5.4.3 Obtaining the Eigenvalues of a Monodromy Matrix

Because applying Theorem 5.1 requires the evaluation of the eigenvalues of the monodromy matrix in the condition (A3), steps to obtaining a monodromy matrix of the variational equation in Eq. (5.37) are explained in details.

Let $\mathbf{Z}_e(t) \in \mathbb{R}^{11\times 11}$ be a fundamental matrix of the linear, periodically varying system in Eq. (5.37). The monodromy matrix $\mathbf{W}_e \in \mathbb{R}^{11\times 11}$ associated with $\mathbf{Z}_e(t)$ is a nonsingular (constant) matrix such that $\mathbf{Z}_e(t+\tau) = \mathbf{Z}_e(t)\mathbf{W}_e$ for $t > 0$ [79]. Note that the monodromy matrices associated with different fundamental matrices are similar, and thus they share the same set of eigenvalues. Therefore, if $\mathbf{Z}_e(0^+)$ is chosen as an identity matrix $\mathbf{I}_{11\times 11} \in \mathbb{R}^{11\times 11}$, one has

$$\mathbf{Z}_e(\tau^+) = \mathbf{Z}_e(0^+)\mathbf{W}_e = \mathbf{W}_e, \tag{5.40}$$

and the monodromy matrix $\mathbf{W}_e$ can be obtained by numerically computing $\mathbf{Z}_e(\tau^+)$. Specifically, let $\mathbf{z}_{e1}(t)$, $\mathbf{z}_{e2}(t)$,..., $\mathbf{z}_{e10}(t)$, and $\mathbf{z}_{e11}(t) \in \mathbb{R}^{11}$ be the solutions of Eq. (5.37) under the initial conditions $\mathbf{z}_{e1}(0^+) = [1,0,0,...,0,0,0]^T$, $\mathbf{z}_{e2}(0^+) = [0,1,0,...,0]^T$, ..., $\mathbf{z}_{e10}(0^+) = [0,0,0,...,0,1,0]^T$, and $\mathbf{z}_{e11}(0^+) = [0,0,0,...,0,0,1]^T$, respectively. Then, one has

$$\mathbf{W}_e = \Big[\mathbf{z}_{e1}(\tau^+), \quad \mathbf{z}_{e2}(\tau^+), \quad ..., \quad \mathbf{z}_{e10}(\tau^+), \quad \mathbf{z}_{e11}(\tau^+)\Big]. \tag{5.41}$$

Note that $\mathbf{z}_{ei}(\tau^+)$ ($i \in \{1,2,...,11\}$) can be computed numerically.

To reduce the computational burden of obtaining the monodromy matrix $\mathbf{W}_e$, it can be analytically decomposed as summarized in Theorem 5.2.

Theorem 5.2 (Analytical Decomposition of Monodromy Matrix) Define

$$\begin{aligned}
\mathbf{M}_k &= \frac{\partial \mathbf{I}}{\partial \mathbf{x}} + [\mathbf{g}^+ - \mathbf{g} - \frac{\partial \mathbf{I}}{\partial \mathbf{x}}\mathbf{g}]\frac{\frac{\partial \psi}{\partial \mathbf{x}}}{\frac{\partial \psi}{\partial \mathbf{x}}\mathbf{g}}, \\
\mathbf{W}_c &= \Big[\mathbf{z}_1(\tau), \quad \mathbf{z}_2(\tau), \quad ..., \quad \mathbf{z}_{10}(\tau)\Big], \\
\mathbf{W}_\rho &= \mathbf{z}_\rho(\tau),
\end{aligned} \tag{5.42}$$

where

$$\begin{aligned}
&\mathbf{g} := \mathbf{g}(\bar{\mathbf{x}}_d(\tau_k)), \qquad \mathbf{g}^+ := \mathbf{g}(\bar{\mathbf{x}}_d(\tau_k^+)), \\
&\frac{\partial \mathbf{I}}{\partial \mathbf{x}} := \frac{\partial \mathbf{I}}{\partial \mathbf{x}}(\bar{\mathbf{x}}_d(\tau_k)), \quad \frac{\partial \psi}{\partial \mathbf{x}} := \frac{\partial \psi}{\partial \mathbf{x}}(\bar{\mathbf{x}}_d(\tau_k)),
\end{aligned} \tag{5.43}$$

$\mathbf{z}_1(t)$, $\mathbf{z}_2(t)$,..., $\mathbf{z}_9(t)$, and $\mathbf{z}_{10}(t) \in \mathbb{R}^{10}$ are the solutions of

$$\frac{d\mathbf{z}}{dt} = \frac{\partial \mathbf{g}}{\partial \mathbf{x}}(\bar{\mathbf{x}}_d(t))\mathbf{z} \tag{5.44}$$

under the initial conditions

$$\mathbf{z}_1(0^+) = [1,0,0,...,0,0]^T,$$

$$\mathbf{z}_2(0^+) = [0,1,0,...,0,0]^T,$$

$$...,$$

$$\mathbf{z}_9(0^+) = [0,1,0,...,1,0]^T,$$

and

$$\mathbf{z}_{10}(0^+) = [0,0,0,...,0,1]^T,$$

respectively, and $\mathbf{z}_\rho(t)$ is the solution of

$$\frac{d\mathbf{z}}{dt} = \frac{\partial \mathbf{g}}{\partial \mathbf{x}}(\bar{\mathbf{x}}_d(t))\mathbf{z} + \frac{\partial \mathbf{g}}{\partial \rho}(\bar{\mathbf{x}}_d(t)) \tag{5.45}$$

under the initial condition $\mathbf{z}_\rho(0^+) = \mathbf{0}_{10\times 1}$.

Then, $\mathbf{W}_e$ in Eq. (5.41) can be decomposed as

$$\mathbf{W}_e = \begin{bmatrix} \frac{\frac{\partial \psi}{\partial \mathbf{x}}}{\frac{\partial \psi}{\partial \mathbf{x}}\mathbf{g}}\mathbf{W}_\rho & \frac{\frac{\partial \psi}{\partial \mathbf{x}}}{\frac{\partial \psi}{\partial \mathbf{x}}\mathbf{g}}\mathbf{W}_c \\ (\mathbf{M}_k + \mathbf{I}_{10\times 10})\mathbf{W}_\rho & (\mathbf{M}_k + \mathbf{I}_{10\times 10})\mathbf{W}_c \end{bmatrix}. \tag{5.46}$$

■

Proof: By the definitions of $\mathbf{M}_{ke}$ and $\mathbf{M}_k$, one obtains

$$\mathbf{M}_{ke} + \mathbf{I}_{11\times 11} = \begin{bmatrix} 0 & \frac{\frac{\partial \psi}{\partial \mathbf{x}}}{\frac{\partial \psi}{\partial \mathbf{x}}\mathbf{g}} \\ \mathbf{0}_{10\times 1} & \mathbf{M}_k + \mathbf{I}_{10\times 10} \end{bmatrix}. \tag{5.47}$$

Denote

$$\mathbf{W}_{ec} := \begin{bmatrix} \mathbf{z}_{e1}(\tau), & \mathbf{z}_{e2}(\tau), & ..., & \mathbf{z}_{e10}(\tau), & \mathbf{z}_{e11}(\tau) \end{bmatrix}. \tag{5.48}$$

Then, by the definition of $\mathbf{z}_{ei}(\tau)$ ($i \in \{1,2,...,11\}$), $\mathbf{W}_\rho$, and $\mathbf{W}_c$, one has

$$\mathbf{W}_{ec} = \begin{bmatrix} 1 & \mathbf{0}_{1\times 10} \\ \mathbf{W}_\rho & \mathbf{W}_c \end{bmatrix}. \tag{5.49}$$

Then, from Eqs. (5.37) and (5.41),

$$\mathbf{W}_e = (\mathbf{M}_{ke} + \mathbf{I}_{11\times 11})\mathbf{W}_{ec}. \tag{5.50}$$

Therefore, from Eqs. (5.47), (5.49), and (5.50), one obtains

$$\mathbf{W}_e = \begin{bmatrix} \frac{\frac{\partial \psi}{\partial \mathbf{x}}}{\frac{\partial \psi}{\partial \mathbf{x}}\mathbf{g}}\mathbf{W}_\rho & \frac{\frac{\partial \psi}{\partial \mathbf{x}}}{\frac{\partial \psi}{\partial \mathbf{x}}\mathbf{g}}\mathbf{W}_c \\ (\mathbf{M}_k + \mathbf{I}_{10\times 10})\mathbf{W}_\rho & (\mathbf{M}_k + \mathbf{I}_{10\times 10})\mathbf{W}_c \end{bmatrix}. \tag{5.51}$$

■

By Theorem 5.2, $\mathbf{W}_e$ can be computed by integrating the 10^{th}-order differential equations in Eqs. (5.44) and (5.45) instead of the 11^{th}-order differential equation in Eq. (5.35), which leads to a relatively lower computational load.

Besides matrix decomposition, another important property of $\mathbf{W}_e$ is summarized in Theorem 5.3.

Theorem 5.3 (Zero-modulus Eigenvalue of Monodromy Matrix) Any monodromy matrix of the variational equation in Eq. (5.37) always has an eigenvalue zero. ■

Proof: From Eq. (5.47), $\mathbf{M}_{ke} + \mathbf{I}_{11\times 11}$ is a singular matrix that possesses an eigenvalue zero. Hence, from Eq. (5.50), $\mathbf{W}_e$ has an eignenvalue zero. Because different monodromy matrices associated with different fundamental matrices are similar and share the same eigenvalues, any monodromy matrix of the variational equation in Eq. (5.37) has an eigenvalue zero. ■

5.5 Systematic Optimization of Output Function Design

In order to find an exponentially stable hybrid orbit Γ_d with desired features, a systematic optimization approach has been developed. There are several reasons why optimization is needed for finding the desired hybrid orbit Γ_d. First, due to the underactuation, Γ_d should satisfy the continuous-time zero dynamics during an SSP as well as the periodicity constraint at switching. Second, the desired gait should meet necessary feasibility constraints, such as torque limits, joint position and velocity limits, and ground-contact constraints. Third, there may be other performance specifications on walking speed, step

length, energy consumption, etc. Last but not the least, the stability conditions in Theorem 5.1 should be satisfied to realize orbitally exponentially stable walking. Note that internal dynamics exist due to the underactuation and that its stability depends on the definition of output function. Therefore, the closed-loop stability is determined by both the feedback controller and the definition of output function.

There are two steps in the proposed systematic optimization. The first step is to find a hybrid periodic orbit that meets necessary constraints. Because the same periodic orbit obtained from the first step may have different stability properties under different definitions of output function, the second step is to guarantee that the orbit obtained from the first step is exponentially stable by optimizing the definition of output function in Eq. (5.12). Specifically, the transformation matrix $\mathbf{H}_T$ in Eq. (5.11) is optimized to ensure the closed-loop stability.

Without loss of generality, the optimization constraints are limited to the following items:

(R1) Periodicity;

(R2) Hybrid walking dynamics in Eq. (5.3);

(R3) Feasibility constraints:

  (a) joint position limit;

  (b) joint velocity limit;

  (c) no scuffing the ground for the swing leg;

(R4) Performance specifications:

  (a) the desired range of step period τ;

  (b) the desired step distance;

(R5) Orbitally exponential stability.

5.5.1 Step 1: Finding Periodic Gaits

The first step of the proposed motion planning is to reach the requirements in (R1) - (R4), which is inspired by the method based on walking pattern encoding [7] [102] [103].

Without loss of generality, choose the lower-limb position q_1 of the support leg as the encoding variable to define the walking pattern of $\mathbf{q}_a$. Then, there exists a unique walking pattern $\mathbf{\Phi}(q_1) \in \mathbb{R}^4$ that corresponds to $\bar{\mathbf{q}}_d(t)$ and satisfies

$$\bar{\mathbf{q}}_{ad}(t) = \mathbf{\Phi}(\bar{q}_{1d}(t)) \tag{5.52}$$

on $t \in (0, \tau]$, where

$$\bar{\mathbf{q}}_{ad}(t) := \begin{bmatrix} \bar{q}_{2d}(t) \\ \bar{q}_{3d}(t) \\ \bar{q}_{4d}(t) \\ \bar{q}_{5d(t)} \end{bmatrix} \in \mathbb{R}^4. \tag{5.53}$$

The walking pattern $\mathbf{\Phi}(q_1)$ can be parameterized by Beziér curves [103]. Here, we choose to use 6^{th}-order Beziér curves ($M = 6$),

$$\mathbf{\Phi}(q_1) := \mathbf{\Psi}(s) := \sum_{k=0}^{M} \mathbf{a}_k \frac{M!}{k!(M-k)!} s^k (1-s)^{M-k} \tag{5.54}$$

with

$$s = \frac{q_1 - a_{64}}{a_{04} - a_{64}}, \tag{5.55}$$

where

$$\mathbf{a}_k := \begin{bmatrix} a_{k1} \\ a_{k2} \\ a_{k3} \\ a_{k4} \end{bmatrix} \in \mathbb{R}^{4\times 1},\ k \in \{0, 1, ..., 6\}, \tag{5.56}$$

is an unknown parameter to be optimized.

Then, $\ddot{\bar{\mathbf{q}}}_{ad}(t)$ can be written as

$$\ddot{\bar{\mathbf{q}}}_{ad}(t) = \frac{\partial^2 \mathbf{\Phi}}{\partial q_1^2}(\bar{q}_{1d})\dot{\bar{q}}_{1d}^2(t) + \frac{\partial \mathbf{\Phi}}{\partial q_1}(\bar{q}_{1d})\ddot{\bar{q}}_{1d}(t), \tag{5.57}$$

on $t \in (0, \tau]$.

Let $\mathbf{B}_u^{\perp}$ denote a 1×5 matrix that satisfies $\mathbf{B}_u^{\perp}\mathbf{B}_u = 0$. Multiplying both sides of Eq. (5.3) by $\mathbf{B}^{\perp}$ and substituting Eq. (5.57) into Eq. (5.3), one obtains

$$\alpha(\bar{q}_{1d}(t))\ddot{\bar{q}}_{1d}(t) + \beta(\bar{q}_{1d}(t))\dot{\bar{q}}_{1d}^2(t) + \gamma(\bar{q}_{1d}(t)) = 0 \tag{5.58}$$

on $t \in (0,\tau]$, where the expressions of α, β, and γ can be derived from Eq. (5.3).

Suppose that $p_1(t)$ $(t>0)$ is a solution of Eq. (5.58) with the initial condition $[\theta_{10},\omega_{10}] := [p_1(0^+),\dot{p}_1(0^+)]$. Define

$$\mathbf{p}(p_1) := \begin{bmatrix} p_1 \\ \mathbf{\Phi}(p_1) \end{bmatrix}. \tag{5.59}$$

If there exists a positive constant τ such that

$$\begin{bmatrix} \mathbf{p}(p_1(\tau)) \\ \dot{\mathbf{p}}(p_1(\tau)) \end{bmatrix} \in S_q(\mathbf{p},\dot{\mathbf{p}}) \tag{5.60}$$

and

$$\begin{aligned} \begin{bmatrix} \mathbf{p}(p_1(\tau^+)) \\ \dot{\mathbf{p}}(p_1(\tau^+)) \end{bmatrix} &:= \begin{bmatrix} \mathbf{p}(p_1(\tau)) \\ \dot{\mathbf{p}}(p_1(\tau)) \end{bmatrix} + \mathbf{I}(\mathbf{p}(p_1(\tau)),\dot{\mathbf{p}}(p_1(\tau))) \\ &= \begin{bmatrix} \mathbf{p}(p_1(0^+)) \\ \dot{\mathbf{p}}(p_1(0^+)) \end{bmatrix} \end{aligned} \tag{5.61}$$

hold, then

$$\bar{\mathbf{q}}_d(t) = \mathbf{p}(t-\tau_k),\ \forall t \in (\tau_k,\tau_{k+1}],\ k \in \{0,1,2,...\}, \tag{5.62}$$

is a periodic solution of the continuous-time zero dynamics and the reset map for $t>0$; that is, $\bar{\mathbf{x}}_d(t) = [\bar{\mathbf{q}}_d(t);\dot{\bar{\mathbf{q}}}_d(t)]$ $(t>0)$ is a periodic solution of the closed-loop dynamics in Eq. (5.3) under the control law in Eqs. (5.21) and (5.23).

In the first step of optimization, the optimization variables are chosen as $\mathbf{a}_n$ $(n \in \{0,1,...,6\})$, θ_{10}, and ω_{10}. To achieve energy-efficient walking, the integral-squared motor torque per step distance is minimized, and the cost function J is defined as [7]:

$$J = \frac{1}{d}\int_0^{\tau} \|\mathbf{u}_d(t)\|^2 dt, \tag{5.63}$$

where d is the step distance and $\mathbf{u}_d$ is defined by substituting $\mathbf{q} = \bar{\mathbf{q}}_d = \mathbf{p}$ and $\dot{\mathbf{q}} = \dot{\bar{\mathbf{q}}}_d = \frac{\partial \mathbf{p}}{\partial p_1}\dot{p}_1$ into Eqs. (5.21) and (5.22). This constrained nonlinear optimization problem can be solved by the MATLAB command *fmincon*.

5.5.2 Step 2: Optimization of Output Function

In Step 2, the objective is to optimize the definition of output function so as to meet the closed-loop stability requirement in (R5). The optimization variables are the elements of $\mathbf{H}_T$. The single constraint in Step 2 is that $\mathbf{H}_T$ should be nonsingular. The MATLAB command *fmincon* is again utilized to optimize the eigenvalues of the monodromy matrix associated with Eq. (5.37) such that there is only one unity-modulus eigenvalue and that the largest modulus $|\lambda_s|$ of all the other eigenvalues is strictly less than one.

Note that the optimization results can be a local optimum instead of a global one. Furthermore, not all of the necessary ground-contact constraints are considered here, for example, the friction-cone and the unilaterality constraints.

5.5.3 Optimization Results

The proposed optimization method is applied to the planar biped model in Fig. 5.1. After the first step of optimization, the energy consumption is minimized to 2134.40 ($N^2 \cdot m \cdot s$), the step length is 0.41 (m), and the walking speed is 0.85 (m/s). The optimization variables are found to be:

$$
\begin{aligned}
\theta_0 &= -0.36 \text{ (rad)}, \\
\omega_0 &= 3.39 \text{ (rad/s)}, \\
\mathbf{a}_0 &= [-0.16, 0.18, 0.23, 0.34]^T, \\
\mathbf{a}_1 &= [-0.27, 0.27, 0.02, 0.67]^T, \\
\mathbf{a}_2 &= [-0.24, 0.19, 0.10, 0.62]^T, \\
\mathbf{a}_3 &= [-0.53, 0.62, -0.34, 1.13]^T, \\
\mathbf{a}_4 &= [-0.38, 0.43, -0.22, -0.11]^T, \\
\mathbf{a}_5 &= [0.61, 0.04, -0.17, -0.56]^T, \\
\mathbf{a}_6 &= [0.23, 0.16, -0.07, -0.34]^T.
\end{aligned}
$$

With the control gains chosen as $\mathbf{K}_P = \text{diag}[40000, 40000, 40000, 40000]$ and $\mathbf{K}_D = \text{diag}[400, 400, 400, 400]$, the stability index λ_s is optimized to be $|\lambda_s| = 0.56$ after the second step of optimization. The moduli of the other eigenvalues are 1.00, 0.53, 0.00, 0.00, 0.00, 0.00, 0.00, 0.00, 0.00, and 0.00. $\mathbf{H}_T$ is found to be

$$\mathbf{H}_T = \begin{bmatrix} 0.10 & 0.03 & 0.11 & 0.01 & -0.05 \\ 0.02 & -0.11 & 0.02 & -0.05 & 0.11 \\ 0.10 & -0.00 & -0.02 & 0.05 & 0.01 \\ -0.01 & 0.10 & -0.02 & 0.06 & 0.09 \\ 0.03 & 0.04 & 0.15 & 0.01 & 0.00 \end{bmatrix}. \tag{5.64}$$

5.6 Simulation Results

The proposed walking control is implemented on a planar biped model (see Fig. 5.2) with the optimization results in Section 5.5. Simulation results show that orbitally exponential stabilization is achieved based on the proposed time-dependent control. Furthermore, the effects of the definition of output function, as well as the PD gains, on the closed-loop stability are illustrated with simulation results.

5.6.1 Orbitally Exponential Stabilization

Based on the output function design in Eqs. (5.12) and (5.64) and the proposed control design, ten steps of walking are simulated with initial conditions and PD gains specified as:

$$\begin{aligned} &\mathbf{q}(0^+) - \mathbf{q}_d(0^+) = \begin{bmatrix} 0.1 \\ -0.1 \\ 0.1 \\ 0.2 \\ -0.2 \end{bmatrix} \text{(rad)}, \ \mathbf{q}(0^+) - \mathbf{q}_d(0^+) = \begin{bmatrix} 0.1 \\ -0.1 \\ -0.1 \\ 0.2 \\ 0.2 \end{bmatrix} \text{(rad/s)}; \\ &\mathbf{K}_P = \text{diag}\begin{bmatrix} 40000, & 40000, & 40000, & 40000 \end{bmatrix}, \\ &\mathbf{K}_D = \text{diag}\begin{bmatrix} 400, & 400, & 400, & 400 \end{bmatrix}. \end{aligned} \tag{5.65}$$

Under the proposed control law with the above PD control gains, the directly controlled variables $\mathbf{q}_{Ta}(t)$ should converge to the desired time functions $\mathbf{q}_{Tad}(t)$ exponentially fast during each continuous phase, which matches the results in Fig. 5.4. Figure 5.4 shows the actual transformed variables $\mathbf{q}_T(t)$ and the desired time functions $\mathbf{q}_{Td}(t)$ during the ten steps of walking. Within each step, the directly controlled variables $\mathbf{q}_{Ta}(t)$ indeed exponentially converge to the desired time functions $\mathbf{q}_{Tad}(t)$, which means that the output function $\mathbf{y}$ converges to zero exponentially fast. This is because the PD gains in Eq. (5.65) guarantee that $\mathbf{A}(\mathbf{K}_P, \mathbf{K}_D)$ in Eq. (5.24) is Hurwitz.

With the proposed optimization method in Section 5.5, the optimized definition of output function in Eqs. (5.12) and (5.64) should ensure the exponential stability of the desired periodic orbit Γ_d. As shown in Fig. 5.5, all of the actual joint trajectories $\mathbf{q}(t)$ do not converge to the desired periodic joint trajectories $\bar{\mathbf{q}}_d(t)$. Instead, they converge to the desired orbit Γ_d where $\bar{\mathbf{x}}_d(t)$ resides. Furthermore, there is a constant steady-state phase delay between $\mathbf{q}(t)$ and $\bar{\mathbf{q}}_d(t)$; that is, there exists a constant number ΔT such that $\mathbf{q}(t) = \bar{\mathbf{q}}_d(t + \Delta T)$ at the steady state. To show the exponential stability of the desired orbit Γ_d clearly, the relative evolution of $\dot{q}_5(t)$ with respect to $q_5(t)$ during the ten steps is shown in Fig. 5.6, which indeed shows the exponential convergence of the actual joint trajectories to the desired orbit Γ_d.

5.6.2 Effects of Output Function Design on Closed-Loop Stability

As discussed previously, the design of output function affects the stability of internal dynamics and is thus optimized in Section 5.5. To illustrate the effects of output function on closed-loop stability, a different design of output function other than the optimized one is applied in the control design, based on which bipedal robotic walking is simulated. Define the output function as in Eq. (5.9), or equivalently, set the coordinate transformation matrix $\mathbf{H}_T$ in Eq. (5.12) as an identity matrix $\mathbf{H}_T = \mathbf{I}_{5\times 5}$. Then, $\mathbf{q}_T = \mathbf{q}$, $\mathbf{q}_{Td} = \mathbf{q}_d$, and $\bar{\mathbf{q}}_{Td} = \bar{\mathbf{q}}_d$.

Since the definition of output function is different from the optimization results, it is expected that the eigenvalues of the monodromy matrix associated with Eq. (5.37) will

also be different. The modulus of λ_s under the output function definition in Eq. (5.9) is calculated as $|\lambda_s| = 3.93$, and the moduli of the other eigenvalues are 1.00, 0.25, 0.00, 0.00, 0.00, 0.00, 0.00, 0.00, and 0.00. Because $|\lambda_s| > 1$, the desired periodic orbit Γ_d obtained in Section 5.5 is unstable under the output function definition in Eq. (5.9). Figure 5.7 shows the divergence of the actual joint trajectories $\mathbf{q}(t)$ from the desired periodic orbit Γ_d. This comparison confirms that the definition of output function can affect the closed-loop stability.

5.6.3 Effects of Proportional-derivative Control Gains on Closed-Loop Stability

The effects of PD gains on the closed-loop stability are also investigated. The PD gains are changed to $\mathbf{K}_P = \text{diag}[400,\ 400,\ 400,\ 400]$ and $\mathbf{K}_D = \text{diag}[40,\ 40,\ 40,\ 40]$. The corresponding $|\lambda_s|$ is computed as $|\lambda_s| = 0.98$, and the moduli of the other ten eigenvalues are calculated to be: 1.00, 0.96, 0.03, 0.00, 0.00, 0.00, 0.00, 0.00, 0.00, and 0.00. The simulation result in Fig. 5.8 shows that the actual joint trajectories $\mathbf{q}(t)$ converge to a small neighborhood of the desired orbit within five steps, while Fig. 5.5 shows the convergence to the same neighborhood in about four steps. The simulation results seemed to indicate that the output function should converge to zero sufficiently fast to guarantee the closed-loop stability. In our future study, the effects of PD gains on the closed-loop stability will be analyzed based on formal theorem proof.

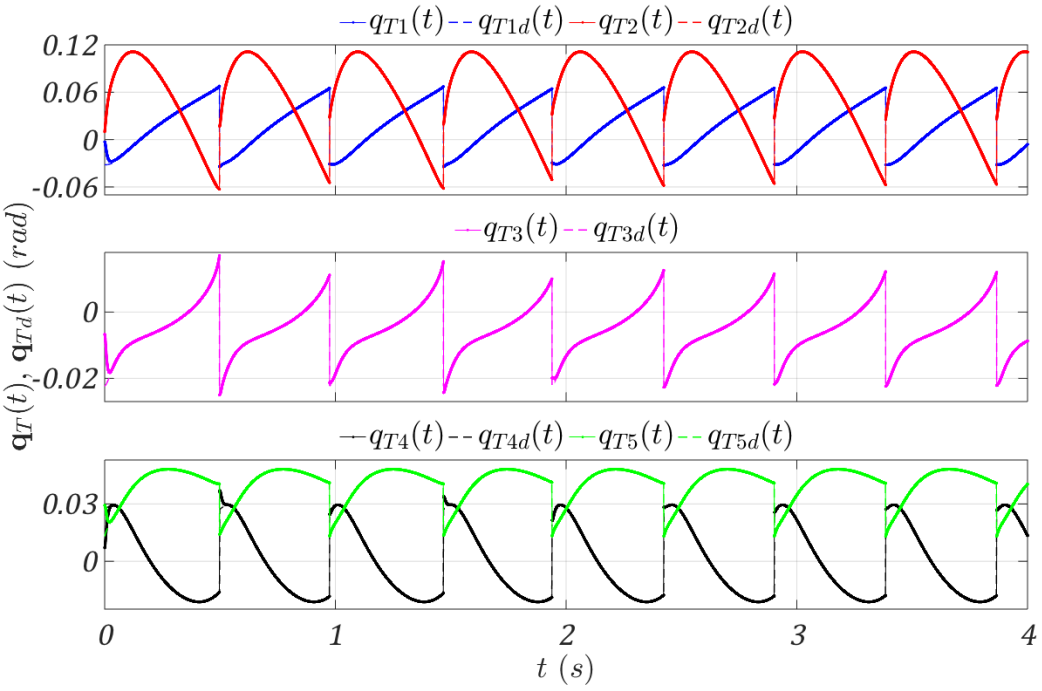

Figure 5.4. Exponential convergence of the actual trajectories $\mathbf{q}_T(t)$ to the desired time functions $\mathbf{q}_{Td}(t)$ during each continuous phase. Control gains: $\mathbf{K}_P$ = diag[40000, 40000,40000,40000]; $\mathbf{K}_D$= diag[400,400,400,400]. Initial conditions: $\mathbf{q}(0)-\mathbf{q}_d(0)= [0.1,-0.1,0.1,0.2,-0.2]^T$(rad); $\dot{\mathbf{q}}(0)-\dot{\mathbf{q}}_d(0)= [0.1,-0.1,-0.1,0.2,0.2]^T$(rad/s).

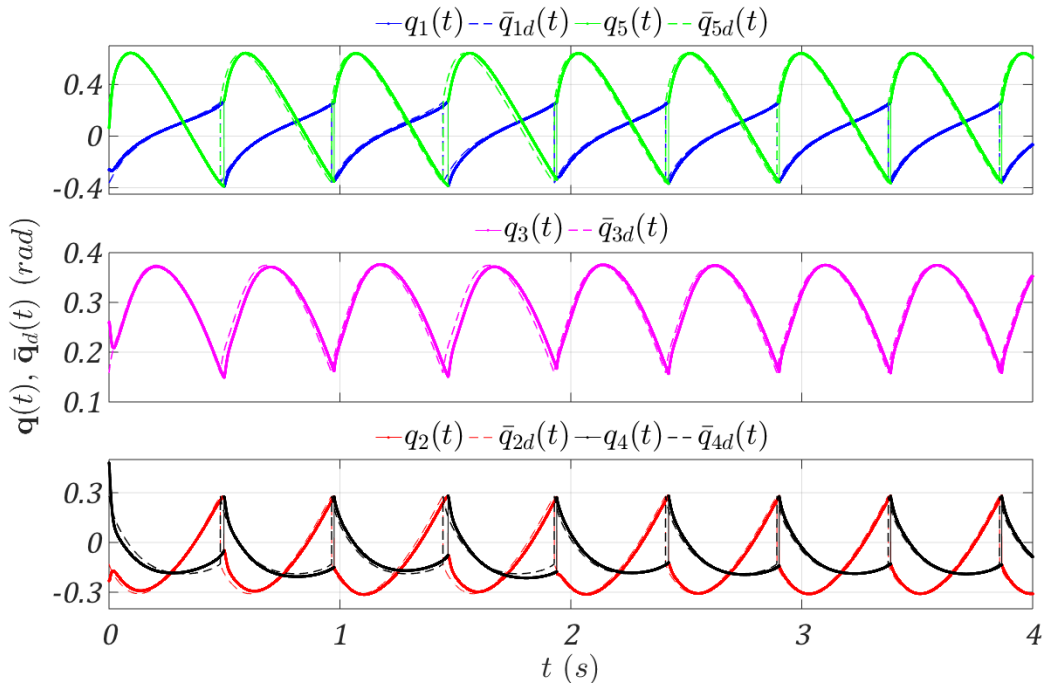

Figure 5.5. Exponential convergence of the actual joint trajectories $\mathbf{q}(t)$ to the desired orbit Γ_d. Control gains: $\mathbf{K}_P = diag[40000, 40000, 40000, 40000]$; $\mathbf{K}_D = diag[400, 400, 400, 400]$. Initial conditions: $\mathbf{q}(0) - \mathbf{q}_d(0) = [0.1, -0.1, 0.1, 0.2, -0.2]^T$(rad); $\dot{\mathbf{q}}(0) - \dot{\mathbf{q}}_d(0) = [0.1, -0.1, -0.1, 0.2, 0.2]^T$(rad/s).

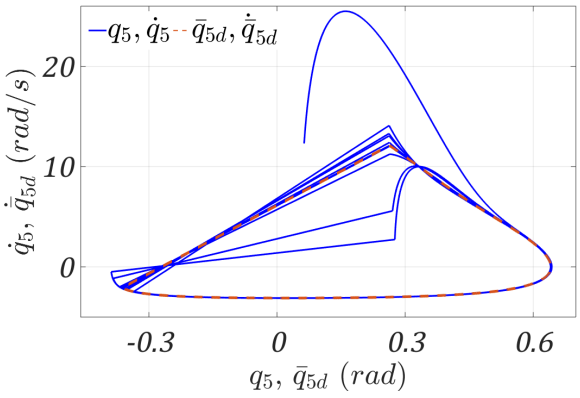

Figure 5.6. Exponential convergence to the desired orbit Γ_d.

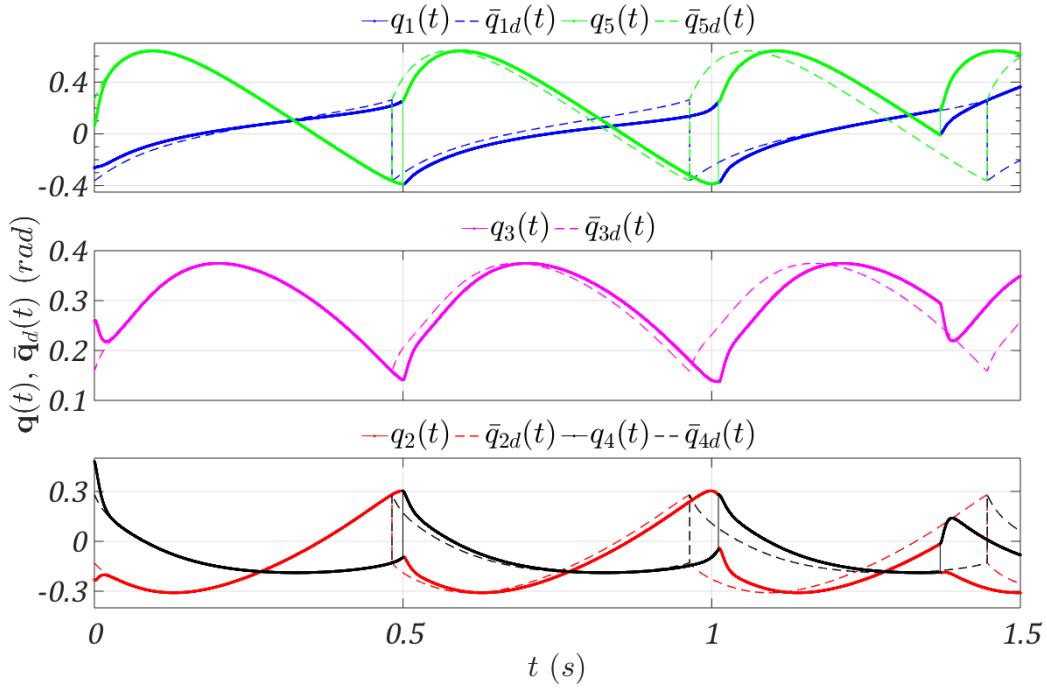

Figure 5.7. Effects of output function on closed-loop stability: divergence of the actual joint trajectories $\mathbf{q}(t)$ from the desired orbit Γ_d. Control gains: $\mathbf{K}_P$ = diag[40000, 40000,40000,40000]; $\mathbf{K}_D$= diag[400,400,400,400]. Initial conditions: $\mathbf{q}(0)-\mathbf{q}_d(0)$= $[0.1,-0.1,0.1,0.2,-0.2]^T$(rad); $\dot{\mathbf{q}}(0)-\dot{\mathbf{q}}_d(0)$= $[0.1,-0.1,-0.1,0.2,\ 0.2]^T$(rad/s).

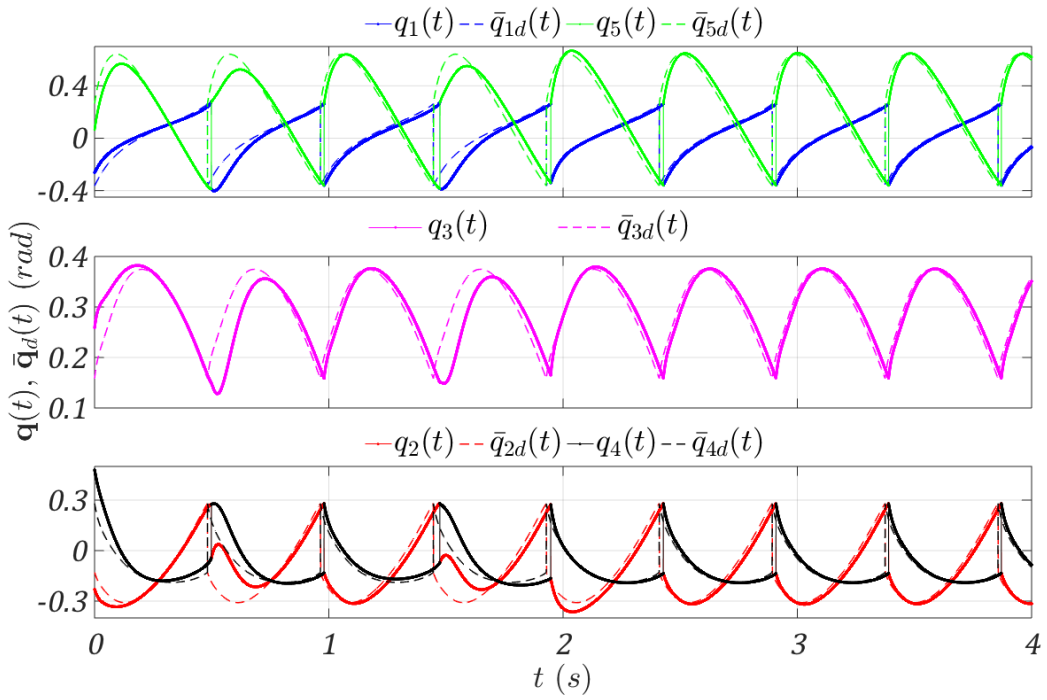

Figure 5.8. Effects of PD gains on closed-loop stability: exponential convergence of the actual joint trajectories $\mathbf{q}(t)$ to the desired orbit Γ_d. Control gains: $\mathbf{K}_P$ = diag[400, 400,400,400]; $\mathbf{K}_D$= diag[40,40,40,40]. Initial conditions: $\mathbf{q}(0)-\mathbf{q}_d(0)$= $[0.1,-0.1,\ 0.1,0.2,-0.2]^T$(rad); $\dot{\mathbf{q}}(0)-\dot{\mathbf{q}}_d(0)$= $[0.1,-0.1,-0.1,0.2,0.2]^T$(rad/s).

5.7 Discussions and Extensions

The proposed walking strategy including motion planning and control design is introduced based on a planar biped model with five revolute joints and point feet. A DSP is assumed to be instantaneous, and there is a single degree of underactuation (DOU) during an SSP. A more general biped model should include more joints, full-sized feet, a finite-time DSP, and high DOU during an SSP. To point out the practicality of the proposed walking strategy, the extension to such a biped model is discussed.

5.7.1 From One to High Degrees of Underactuation

A biped model with a compliant transmission system may have high Degrees of Underactuation (DOU) [103]. Since the incorporation of a compliant transmission system can potentially reduce the energy consumption of robotic walking, it is necessary to extend the proposed strategy to such models. Although the biped model considered in this study has only a single DOU, the proposed motion planning, control design, and stability conditions are general in terms of DOU. Thus, the results of the proposed walking strategy can be applied to bipedal walking with high DOU, as long as the robot is not purely passive. Furthermore, the proposed walking strategy can also be extended to fully actuated walking.

5.7.2 From Planar to Three-dimensional Walking

Since there are no underlying assumptions on the number of degrees of freedom (DOFs) or walking space dimensions in the theoretical analysis, the results of this Chapter are also valid for higher DOFs and three-dimensional (3-D) walking. However, one of the major concerns for practical implementation is that high DOFs can lead to an even heavier computational load in motion planning. It is then necessary to develop efficient searching algorithms to solve this problem, for example, a direct collocation method [164].

5.7.3 From Instantaneous to Finite-time Double-Support Phase

The biped model considered in this study has point feet, and it is thus reasonable to assume that the Double-Support Phase (DSP) is instantaneous. If a biped model has full-sized feet, this assumption will be no longer realistic and a finite-time DSP should be included in the dynamic model. A complete bipedal walking cycle will then include an SSP, a rigid impact with an impulse effect, and a finite-time DSP. This essentially only increases the number of subphases in a complete walking cycle, to which it is straightforward to extend the proposed walking strategy. In fact, because the biped will be overactuated during a DSP when both full-sized feet are in full contact with the ground, the extra degrees

of control freedom due to the overactuation might be advantageous in terms of walking stabilization.

5.8 Summary

In this Chapter, orbitally exponential stabilization of bipedal robotic walking has been realized based on time-dependent feedback control. The desired gait of interest is symmetric and periodic, which defines the desired periodic orbit in the state space. A feedback controller based on input-output linearization was then utilized to exponentially stabilize the desired periodic orbit. Because the moments of swing-foot touchdown associated with the desired periodic joint trajectories do not necessarily coincide with the actual ones and because both joint positions and velocities experience sudden jumps at swing-foot touchdowns, the desired periodic joint trajectories were modified to define the desired time functions that determine the output function. The output function was then designed as linear combinations of the actual joint positions and the desired time functions. The resulting closed-loop system is nonlinear, aperiodically varying, and hybrid with internal dynamics caused by the underactuation. An augmented autonomous system equivalent to the original closed-loop system was constructed, from which the closed-loop stability conditions were established. A systematic optimization method was proposed for finding a stable, periodic gait that satisfies the walking performance specifications and necessary constraints. Specifically, the optimization method involves optimizing the output function definition to guarantee the orbitally exponential stability of the closed-loop system because the stability of the zero dynamics depends on the definition of output function. A planar biped was simulated to confirm the effectiveness of the proposed walking strategy. Through discussions, it was also concluded that the proposed walking strategy can be extended to 3-D biped models that are subject to full actuation and/or underactuation.

6. CONCLUSIONS AND FUTURE RESEARCH

6.1 Summary and Conclusions

Because bipedal robots are capable of highly versatile motion, they will become a very important part of our society in many applications such as disaster response and rescue, space exploration, education and social studies, and personal assistance. However, the walking performance of today's bipedal robots is still far from satisfactory. Therefore, it is critical to developing controller design methodologies for achieving high-performance bipedal robotic walking.

The objective of this research is to study and investigate a controller design methodology that can be applied to both fully actuated and underactuated bipedal robots. Specifically, we have focused on the controller designs of the following three types of bipeds:

1. A fully actuated planar biped with 3 revolute joints and 3 independent actuators (the controller design is effective for any fully actuated planar bipeds);

2. A fully actuated 3-D biped with 9 revolute joints and 9 independent actuators (the controller design is effective for any fully actuated 3-D bipeds);

3. An underactuated biped with 5 revolute joints and 4 independent actuators (the controller design is effective for any underactuated bipeds).

The characteristics of the proposed controller design methodology include:

1. Modeling of full-order hybrid walking dynamics;

2. Motion planning based on optimization techniques that minimize the energy cost of walking under necessary constraints and conditions such as joint limit, actuator limit, and ground-contract constraints;

3. Model-based feedback control design based on nonlinear control theories and formal stability analysis.

Among these three characteristics, the key difference between our proposed controller design and the previous controller designs based on Hybrid Zero Dynamics is that our controller design is explicitly time-dependent while the HZD framework utilizes time-invariant controller designs. This difference is caused by the fact that our output function design is explicitly time-dependent instead of time-invariant as in HZD framework. A time-dependent design of output function opens up many opportunities in defining complex tasks such as position tracking in Cartesian space. It can also be utilized to achieve high walking robustness.

With these characteristics of the proposed control strategy, the impact and contributions of this research are listed as follows:

1. We have achieved provably stable walking for both fully actuated and underactuated bipeds based on time-dependent walking control design. Because our controller design is time-dependent, the overall closed-loop control system is accordingly time-varying. It is challenging to evaluate the stability of a time-varying control system, but we have established sufficient conditions for such evaluation based on nonlinear control theories and formal stability analysis;

2. We have achieved highly versatile walking for fully actuated, planar bipeds. Because fully actuated bipeds can directly control each of its joints, high walking versatility is potentially achievable for fully actuated planar bipeds. The capability of position tracking in Cartesian space is crucial to accomplishing complex tasks such as multi-agent coordination, but global position tracking has not been fully studied in previous studies on model-based walking control. In this dissertation, we have developed the *first* walking controller design that utilizes formal stability analysis to achieve position tracking in Cartesian space for fully actuated planar bipeds [140] [141]. Furthermore, we have realized exponential tracking of asymmetric gaits, which is potentially meaningful for walking control of impaired human walking.

3. We have achieved highly versatile walking for fully actuated, 3-D bipeds. In comparison with a planar biped, walking control of a 3-D biped is much more difficult because of its extra degree of freedom on the walking surface. Although velocity tracking in Cartesian space has been studied for fully actuated 3-D bipeds under the HZD framework, position tracking in Cartesian space has not been explored. In this dissertation, exponential tracking of a straight-line path on the walking surface has been achieved for fully actuated 3-D bipeds, which greatly improves the walking versatility as compared with previous work. Potential applications of this controller design include complex tasks such as multi-agent coordination and obstacle avoidance.

4. We have achieved robust walking for underactuated bipeds. Due to the lack of actuators to directly control each joint, underactuated bipeds are difficult to stabilize, especially under a time-dependent controller design methodology. This dissertation research has established the *first* set of sufficient conditions for orbitally exponential stabilization of underactuated walking [142] [143]. This controller design can achieve improved robustness of bipedal robotic walking as compared with the HZD framework. Furthermore, the proposed walking strategy can be applied to any degrees of underactuation as well as any types of actuation including full actuation.

A comparison with previous work on bipedal walking control for fully actuated and underactuated bipeds is shown in Tables 6.1 and 6.2, respectively.

Table 6.1.
Comparisons with previous controller designs for fully actuated walking.

Walking strategies	Provable stability	High versatility	High speed	High efficiency
The ZMP approach	×	✓	×	×
The HZD framework	✓	×	✓	✓
Proposed control design	✓	✓	✓	✓

Table 6.2.
Comparisons with previous controller designs for underactuated walking.

Walking strategies	Provable stability	High robustness	High speed	High efficiency
The ZMP approach	NA	NA	NA	NA
The HZD framework	✓	✓/×	✓	✓
Proposed control design	✓	✓	✓	✓

6.2 Future Research

There are several limitations of the proposed controller design methodology. To fully leverage the effectiveness of our proposed controller design methodology, these limitations will be addressed in our future research listed as follows.

- **General Contour Tracking**: One limitation of the developed contour tracking controller for fully actuated walking is that the controller is developed for straight-line contours alone. To realize the satisfactory tracking of a general contour on the walking surface, the current control law needs to be extended. One promising solution is to design transition gaits that piece together straight-line contours so that the biped

can access the entire walking surface. Furthermore, a high-level motion planner can be developed to determine the transition gaits. Because the proposed controller can track any feasible motion along a straight-line on the walking surface, it can be conveniently integrated with a high-level planner. Future investigations will include online motion planning and control design for achieving satisfactory tracking of a general contour on the walking surface.

- **Construction of Time-dependent Hybrid Zero Dynamics**: One weakness of the developed time-dependent orbital stabilization is that the motion planning has a high computational load. For example, to plan the desired periodic orbit for underactuated walking, it involves the numerical integration of the variational equation of the full-order closed-loop dynamics, which can be highly computationally expensive. For example, the state space of a bipedal model with five revolute joints is 10^{th} dimensional when the support foot maintains full, static contact with the ground. With the proposed decomposition of the monodromy matrix, finding the monodromy matrix requires integration of the 10×10 matrix over the least gait cycle. A promising solution to significantly reduce the computational load is to construct hybrid zero dynamics for the time-dependent feedback control system.

- **Time-dependent Multi-Domain Control**: In this dissertation study, bipedal walking control of underactuated bipeds and fully actuated bipeds are addressed separately. Our ultimate goal is to incorporate phases of both full actuation and underactuation in a complete gait cycle.

  Observations of human walking show that there are several advantages of integrating both actuation types in a complete bipedal gait: a biped can be significantly accelerated by lifting the toe of its support foot during the take-off phase, and a biped can be re-stabilized during a finite-time double-support phase when both feet are in support. Inspired by human walking, it will be interesting to explore the possibility of utilizing the underactuated take-off phase to efficiently accelerate a biped. Also, the

finite-time double-support phase may be the key to realizing contour tracking even in the presence of underactuated phases within a complete gait.

REFERENCES

REFERENCES

[1] I. Kato, S. Ohteru, H. Kobayashi, K. Shirai, and A. Uchiyama. Information-power machine with senses and limbs. In *On Theory and Practice of Robots and Manipulators*, pages 11–24. Springer, 1974.

[2] K. Byl and R. Tedrake. Metastable walking on stochastically rough terrain. *Proc. of Robotics: Science and Systems IV*, pages 6490–6495, 2008.

[3] E. R. Westervelt, J. W. Grizzle, C. Chevallereau, J. H. Choi, and B. Morris. *Feedback control of dynamic bipedal robot locomotion*, volume 28. CRC press, 2007.

[4] B. Stephens. *Push recovery control for force-controlled humanoid robots*. PhD thesis, Carnegie Mellon University, 2011.

[5] N. A. Radford, P. Strawser, K. Hambuchen, J. S. Mehling, W. K. Verdeyen, A. S. Donnan, J. Holley, J. Sanchez, V. Nguyen, L. Bridgwater, et al. Valkyrie: NASA's first bipedal humanoid robot. *Journal of Field Robotics*, 32(3):397–419, 2015.

[6] J. E. Pratt and R. Tedrake. Velocity-based stability margins for fast bipedal walking. In *Fast Motions in Biomechanics and Robotics*, pages 299–324. Springer, 2006.

[7] J. W. Grizzle, C. Chevallereau, R. W. Sinnet, and A. D. Ames. Models, feedback control, and open problems of 3D bipedal robotic walking. *Automatica*, 50(8):1955–1988, 2014.

[8] G. Nelson, A. Saunders, N. Neville, B. Swilling, J. Bondaryk, D. Billings, C. Lee, R. Playter, and M. Raibert. Petman: A humanoid robot for testing chemical protective clothing. *ł*, 30(4):372–377, 2012.

[9] A. Ramezani, J. W. Hurst, K. A. Hamed, and J. W. Grizzle. Performance analysis and feedback control of ATRIAS, a three-dimensional bipedal robot. *Journal of Dynamic Systems, Measurement, and Control*, 136(2):021012, 2014.

[10] B. G. Buss, A. Ramezani, K. A. Hamed, B. A. Griffin, K. S. Galloway, and J. W. Grizzle. Preliminary walking experiments with underactuated 3D bipedal robot MARLO. In *Proc. of IEEE International Conference on Intelligent Robots and Systems*, pages 2529–2536, 2014.

[11] Y. Sakagami, R. Watanabe, C. Aoyama, S. Matsunaga, N. Higaki, and K. Fujimura. The intelligent ASIMO: System overview and integration. In *Proc. of IEEE International Conference on Intelligent Robots and Systems*, volume 3, pages 2478–2483, 2002.

[12] K. Kaneko, F. Kanehiro, M. Morisawa, K. Akachi, G. Miyamori, A. Hayashi, and N. Kanehira. Humanoid robot HRP-4 - Humanoid robotics platform with lightweight and slim body. In *Proc. of IEEE International Conference on Intelligent Robots and Systems*, pages 4400–4407, 2011.

[13] I. Park, J. Kim, J. Lee, and J. Oh. Mechanical design of humanoid robot platform KHR-3 (KAIST humanoid robot 3: HUBO). In *Proc. of IEEE-RAS International Conference on Humanoid Robots*, pages 321–326, 2005.

[14] Y. Gu, C. S. G. Lee, and B. Yao. Feasible center of mass dynamic manipulability of humanoid robots. In *Proc. of IEEE International Conference on Robotics and Automation*, pages 5082–5087, 2015.

[15] Y. Hurmuzlu, F. Génot, and B. Brogliato. Modeling, stability and control of biped robots - A general framework. *Automatica*, 40(10):1647–1664, 2004.

[16] Marc H Raibert. *Legged robots that balance*. MIT press, 1986.

[17] M. H. Raibert, H. B. Brown Jr, and M. Chepponis. Experiments in balance with a 3D one-legged hopping machine. *The International Journal of Robotics Research*, 3(2):75–92, 1984.

[18] J. Pratt, C. Chew, A. Torres, P. Dilworth, and G. Pratt. Virtual model control: An intuitive approach for bipedal locomotion. *The International Journal of Robotics Research*, 20(2):129–143, 2001.

[19] M. W. Spong and F. Bullo. Controlled symmetries and passive walking. *IEEE Transactions on Automatic Control*, 50(7):1025–1031, 2005.

[20] M. W. Spong. Passivity based control of the compass gait biped. In *Proc. pf IFAC World Congress*, volume 3, pages 19–23, 1999.

[21] R. Tedrake, T. W. Zhang, and H. S. Seung. Learning to walk in 20 minutes. In *Proc. of Fourteenth Yale Workshop on Adaptive and Learning Systems*, volume 95585, pages 1939–1412, 2005.

[22] R. Tedrake, T. W. Zhang, and H. S. Seung. Stochastic policy gradient reinforcement learning on a simple 3D biped. In *Proc. of IEEE International Conference on Intelligent Robots and Systems*, volume 3, pages 2849–2854, 2004.

[23] A. D. Ames, R. D. Gregg, and M. W. Spong. A geometric approach to three-dimensional hipped bipedal robotic walking. In *Proc. of IEEE Conference on Decision and Control*, pages 5123–5130, 2007.

[24] R. D. Gregg and M. W. Spong. Reduction-based control of three-dimensional bipedal walking robots. *The International Journal of Robotics Research*, 29(6):680–702, 2010.

[25] R. D. Gregg and M. W. Spong. Reduction-based control with application to three-dimensional bipedal walking robots. In *Proc. of American Control Conference*, pages 880–887, 2008.

[26] A. D. Ames and R. D. Gregg. Stably extending two-dimensional bipedal walking to three dimensions. In *Proc. of American Control Conference*, pages 2848–2854, 2007.

[27] J. Seipel and P. Holmes. A simple model for clock-actuated legged locomotion. *Regular and Chaotic Dynamics*, 12(5):502–520, 2007.

[28] S. Rezazadeh and J. W. Hurst. Toward step-by-step synthesis of stable gaits for underactuated compliant legged robots. In *Proc. of IEEE International Conference on Robotics and Automation*, pages 4532–4538, 2015.

[29] M. Posa, M. Tobenkin, and R. Tedrake. Lyapunov analysis of rigid body systems with impacts and friction via sums-of-squares. In *Proc. of International Conference on Hybrid Systems: Computation and Control*, pages 63–72, 2013.

[30] A. Majumdar, A. A. Ahmadi, and R. Tedrake. Control design along trajectories with sums of squares programming. In *Proc. of IEEE International Conference on Robotics and Automation*, pages 4054–4061, 2013.

[31] K. Byl and R. Tedrake. Approximate optimal control of the compass gait on rough terrain. In *Proc. of IEEE International Conference on Robotics and Automation*, pages 1258–1263, 2008.

[32] K. Byl and R. Tedrake. Metastable walking machines. *The International Journal of Robotics Research*, 28(8):1040–1064, 2009.

[33] H. Dai and R. Tedrake. Optimizing robust limit cycles for legged locomotion on unknown terrain. In *Proc. of IEEE Conference on Decision and Control*, pages 1207–1213, 2012.

[34] H. Dai and R. Tedrake. L2-gain optimization for robust bipedal walking on unknown terrain. In *Proc. of IEEE International Conference on Robotics and Automation*, pages 3116–3123, 2013.

[35] S. Kuindersma, F. Permenter, and R. Tedrake. An efficiently solvable quadratic program for stabilizing dynamic locomotion. In *Proc. of IEEE International Conference on Robotics and Automation*, pages 2589–2594, 2014.

[36] S. Kuindersma, R. Deits, M. Fallon, A. Valenzuela, H. Dai, F. Permenter, T. Koolen, P. Marion, and R. Tedrake. Optimization-based locomotion planning, estimation, and control design for the Atlas humanoid robot. *Autonomous Robots*, 40(3):429–455, 2016.

[37] P. B. Wieber. On the stability of walking systems. In *Proc. of International Workshop on Humanoid and Human Friendly Robotics*, pages 53–59, 2002.

[38] J. P. Aubin. *Viability theory*. Springer, 2009.

[39] M. Wisse and D. G. E. Hobbelen. *Limit Cycle Walking*. I-Tech Education and Publishing, 2007.

[40] M. Vukobratovic, A. A. Frank, and D. Juricic. On the stability of biped locomotion. *IEEE Transactions on Biomedical Engineering*, (1):25–36, 1970.

[41] M. Vukobratović and B. Borovac. Zero-Moment Point - thirty five years of its life. *International Journal of Humanoid Robotics*, 1(01):157–173, 2004.

[42] H. Hirukawa, S. Hattori, K. Harada, S. Kajita, K. Kaneko, F. Kanehiro, K. Fujiwara, and M. Morisawa. A universal stability criterion of the foot contact of legged robots-adios ZMP. In *Proc. of IEEE International Conference on Robotics and Automation*, pages 1976–1983, 2006.

[43] K. Kaneko, K. Harada, F. Kanehiro, G. Miyamori, and K. Akachi. Humanoid robot HRP-3. In *Proc. of IEEE International Conference on Intelligent Robots and Systems*, pages 2471–2478, 2008.

[44] A. Goswami. Foot rotation indicator (FRI) point: A new gait planning tool to evaluate postural stability of biped robots. In *Proc. of IEEE International Conference on Robotics and Automation*, pages 47–52, 1999.

[45] A. Goswami. Postural stability of biped robots and the foot-rotation indicator (FRI) point. *The International Journal of Robotics Research*, 18(6):523–533, 1999.

[46] A. Goswami and V. Kallem. Rate of change of angular momentum and balance maintenance of biped robots. In *Proc. of IEEE International Conference on Robotics and Automation*, pages 3785–3790, 2004.

[47] H. Herr and M. Popovic. Angular momentum in human walking. *Journal of Experimental Biology*, 211(4):467–481, 2008.

[48] A. Hofmann, M. Popovic, and H. Herr. Exploiting angular momentum to enhance bipedal center-of-mass control. In *Proc. of IEEE International Conference on Robotics and Automation*, pages 4423–4429, 2009.

[49] J. E. Pratt, J. Carff, S. Drakunov, and A. Goswami. Capture point: A step toward humanoid push recovery. In *Proc. of IEEE International Conference on Humanoid Robots*, pages 200–207, 2006.

[50] J. Grizzle, G. Abba, and P. Plestan. Asymptotically stable walking for biped robots: Analysis via systems with impulse effects. *IEEE Transaction on Automatic Control*, 46(1):51–64, 2001.

[51] Y. C. Pai and J. Patton. Center of mass velocity-position predictions for balance control. *Journal of Biomechanics*, 30(4):347–354, 1997.

[52] J. M. Haddad, J. L. Gagnon, C. J. Hasson, R. E. Van Emmerik, and J. Hamill. Evaluation of time-to-contact measures for assessing postural stability. *Journal of Applied Biomechanics*, 22(2), 2006.

[53] A. L. Hof. The equations of motion for a standing human reveal three mechanisms for balance. *Journal of Biomechanics*, 40(2):451–457, 2007.

[54] S. Bierbaum. *Proactive and reactive adaptability of elderly adults with respect to dynamic stability*. PhD thesis, Humboldt-Universität zu Berlin, Philosophische Fakultät IV, 2013.

[55] S. Kajita and K. Tani. Study of dynamic biped locomotion on rugged terrain-derivation and application of the linear inverted pendulum mode. In *Proc. of IEEE International Conference on Robotics and Automation*, pages 1405–1411, 1991.

[56] K. Nishiwaki, S. Kagami, Y. Kuniyoshi, M. Inaba, and H. Inoue. Online generation of humanoid walking motion based on a fast generation method of motion pattern that follows desired ZMP. In *Proc. of IEEE International Conference on Intelligent Robots and Systems*, volume 3, pages 2684–2689, 2002.

[57] E. Yoshida, C. Esteves, T. Sakaguchi, J.-P. Laumond, and K. Yokoi. Smooth collision avoidance: Practical issues in dynamic humanoid motion. In *Proc. of IEEE International Conference on Intelligent Robots and Systems*, pages 827–832, 2006.

[58] J. Park and Y. Youm. General ZMP preview control for bipedal walking. In *Proc. of IEEE International Conference on Robotics and Automation*, pages 2682–2687, 2007.

[59] W. Huang, C.-M. Chew, Y. Zheng, and G.-S. Hong. Pattern generation for bipedal walking on slopes and stairs. In *Proc. of IEEE International Conference on Humanoid Robots*, pages 205–210, 2008.

[60] K. Yamane and J. Hodgins. Simultaneous tracking and balancing of humanoid robots for imitating human motion capture data. In *Proc. of IEEE International Conference on Intelligent Robots and Systems*, pages 2510–2517. IEEE, 2009.

[61] B. J. Stephens and C. G. Atkeson. Dynamic balance force control for compliant humanoid robots. In *Proc. of IEEE International Conference on Intelligent Robots and Systems*, pages 1248–1255, 2010.

[62] C. Ott, M. A. Roa, and G. Hirzinger. Posture and balance control for biped robots based on contact force optimization. In *Proc. of IEEE International Conference on Humanoid Robots*, pages 26–33, 2011.

[63] Z. Li, B. Vanderborght, N. G. Tsagarakis, L. Colasanto, and D. G. Caldwell. Stabilization for the compliant humanoid robot COMAN exploiting intrinsic and controlled compliance. In *Proc. of IEEE International Conference on Robotics and Automation*, pages 2000–2006, 2012.

[64] G. Garofalo, C. Ott, and A. Albu-Schäffer. Walking control of fully actuated robots based on the bipedal SLIP model. In *Proc. of IEEE International Conference on Robotics and Automation*, pages 1456–1463, 2012.

[65] A. D. Kuo. Choosing your steps carefully. *IEEE Robotics & Automation Magazine*, 14(2):18–29, 2007.

[66] M. B. Popovic, A. Goswami, and H. Herr. Ground reference points in legged locomotion: Definitions, biological trajectories and control implications. *The International Journal of Robotics Research*, 24(12):1013–1032, 2005.

[67] A. D. Kuo. Energetics of actively powered locomotion using the simplest walking model. *Journal of Biomechanical Engineering*, 124(1):113–120, 2002.

[68] T. Koolen, T. De Boer, J. Rebula, A. Goswami, and J. E. Pratt. Capturability-based analysis and control of legged locomotion, Part 1: Theory and application to three simple gait models. *The International Journal of Robotics Research*, 31(9):1094–1113, 2012.

[69] J.E. Pratt, T. Koolen, T. De Boer, J. Rebula, S. Cotton, J. Carff, M. Johnson, and P. Neuhaus. Capturability-based analysis and control of legged locomotion, Part2: Application to M2V2, a lower-body humanoid. *The International Journal of Robotics Research*, 31(10):1117–1133, 2012.

[70] J. Englsberger, C. Ott, and A. Albu-Schäffer. Three-dimensional bipedal walking control using divergent component of motion. In *Proc. of IEEE International Conference on Intelligent Robots and Systems*, pages 2600–2607, 2013.

[71] A. L. Hof, M. G. J. Gazendam, and W. E. Sinke. The condition for dynamic stability. *Journal of Biomechanics*, 38(1):1–8, 2005.

[72] A. L. Hof. The extrapolated center of mass concept suggests a simple control of balance in walking. *Human Movement Science*, 27(1):112–125, 2008.

[73] S. M. Bruijn, O. G. Meijer, P. J. Beek, and J. H. Van Dieën. Assessing the stability of human locomotion: A review of current measures. *Journal of The Royal Society Interface*, 10(83):20120999, 2013.

[74] Y. Hurmuzlu and C. Basdogan. On the measurement of dynamic stability of human locomotion. *Journal of Biomechanical Engineering*, 116(1):30–36, 1994.

[75] F. B. Horak, L. M. Nashner, et al. Central programming of postural movements: Adaptation to altered support-surface configurations. *Journal of Neurophysiology*, 55(6):1369–1381, 1986.

[76] H. K. Khalil. *Nonlinear control*. Prentice Hall, 1996.

[77] I. R. Manchester, U. Mettin, F. Iida, and R. Tedrake. Stable dynamic walking over uneven terrain. *The International Journal of Robotics Research*, pages 265–279, 2011.

[78] Y. Hürmüzlü and G. D. Moskowitz. The role of impact in the stability of bipedal locomotion. *Dynamics and Stability of Systems*, 1(3):217–234, 1986.

[79] D. D Bainov and P. S. Simeonov. *Impulsive differential equations: Periodic solutions and applications*, volume 66. CRC Press, 1993.

[80] A. Goswami, B. Thuilot, and B. Espiau. A study of the passive gait of a compass-like biped robot: Symmetry and chaos. *The International Journal of Robotics Research*, 17(12):1282–1301, 1998.

[81] S. H. Collins, M. Wisse, and A. Ruina. A three-dimensional passive-dynamic walking robot with two legs and knees. *The International Journal of Robotics Research*, 20(7):607–615, 2001.

[82] M. Wisse, A. L. Schwab, and F. C. T. van der Helm. Passive dynamic walking model with upper body. *Robotica*, 22(06):681–688, 2004.

[83] F. Asano and Z. Luo. On energy-efficient and high-speed dynamic biped locomotion with semicircular feet. In *Proc. of IEEE International Conference on Intelligent Robots and Systems*, pages 5901–5906, 2006.

[84] M. Wisse and A. L. Schwab. A 3D passive dynamic biped with yaw and roll compensation. *Robotica*, 19(03):275–284, 2001.

[85] I. Fumiya and T. Russ. Minimalistic control of biped walking in rough terrain. *Autonomous Robot*, 28(1):355–368, 2010.

[86] D. G. E. Hobbelen and M. Wisse. Ankle actuation for limit cycle walkers. *The International Journal of Robotics Research*, 27(6):709–735, 2008.

[87] D. Hobbelen, T. de Boer, and M. Wisse. System overview of bipedal robots Flame and TUlip: Tailor-made for limit cycle walking. In *Proc. of IEEE International Conference on Intelligent Robots and Systems*, pages 2486–2491, 2008.

[88] M. Wisse and J. Van Frankenhuyzen. Design and construction of MIKE: A 2-D autonomous biped based on passive dynamic walking. In *Adaptive motion of animals and machines*, pages 143–154. 2006.

[89] A. Goswami, B. Espiau, and A. Keramane. Limit cycles and their stability in a passive bipedal gait. In *Proc. of IEEE International Conference on Robotics and Automation*, volume 1, pages 246–251, 1996.

[90] S. H. Collins and A. Ruina. A bipedal walking robot with efficient and human-like gait. In *Proc. of IEEE International Conference on Robotics and Automation*, pages 1983–1988, 2005.

[91] S. Collins, A. Ruina, R. Tedrake, and M. Wisse. Efficient bipedal robots based on passive-dynamic walkers. *Science*, 307(5712):1082–1085, 2005.

[92] C. Canudas-de Wit, B. Espiau, and C. Urrea. Orbital stabilization of underactuated mechanical systems. In *Proc. of IFAC World Congress*, 2002.

[93] A. Shiriaev, J. W. Perram, and C. Canudas-de Wit. Constructive tool for orbital stabilization of underactuated nonlinear systems: Virtual constraints approach. *IEEE Transactions on Automatic Control*, 50(8):1164–1176, 2005.

[94] G. Song and M. Zefran. Underactuated dynamic three-dimensional bipedal walking. In *Proc. of IEEE International Conference on Robotics and Automation*, pages 854–859, 2006.

[95] A. S. Shiriaev, L. B. Freidovich, and I. R. Manchester. Can we make a robot ballerina perform a pirouette? Orbital stabilization of periodic motions of underactuated mechanical systems. *Annual Reviews in Control*, 32(2):200–211, 2008.

[96] K. D. Mombaur, H. G. Bock, J. P. Schloder, and R. W. Longman. Human-like actuated walking that is asymptotically stable without feedback. In *Proc. of IEEE International Conference on Robotics and Automation*, volume 4, pages 4128–4133, 2001.

[97] K. D. Mombaur, H. G. Bock, J. P. Schlöder, and R. W. Longman. Open-loop stable solutions of periodic optimal control problems in robotics. *ZAMM-Journal of Applied Mathematics and Mechanics/Zeitschrift für Angewandte Mathematik und Mechanik*, 85(7):499–515, 2005.

[98] K. Mombaur. Using optimization to create self-stable human-like running. *Robotica*, 27(03):321–330, 2009.

[99] F. Plestan, J. W. Grizzle, E. R. Westervelt, and G. Abba. Stable walking of a 7-DOF biped robot. *IEEE Transactions on Robotics and Automation*, 19(4):653–668, 2003.

[100] C. Chevallereau, G. Abba, Y. Aoustin, F. Plestan, E. Westervelt, C. Canudas-de Wit, and J. W. Grizzle. Rabbit: A testbed for advanced control theory. *IEEE Control Systems Magazine*, 23(5):57–79, 2003.

[101] K. Sreenath, H.-W. Park, I. Poulakakis, and J. W. Grizzle. A compliant hybrid zero dynamics controller for stable, efficient and fast bipedal walking on MABEL. *The International Journal of Robotics Research*, 30(9):1170–1193, 2011.

[102] E. R. Westervelt, J. W. Grizzle, and D. E. Koditschek. Hybrid zero dynamics of planar biped walkers. *IEEE Transaction on Automatic Control*, 48(1):42–56, 2003.

[103] B. Morris and J. W. Grizzle. Hybrid invariant manifolds in systems with impulse effects with application to periodic locomotion in bipedal robots. *IEEE Transactions on Automatic Control*, 54(8):1751–1764, 2009.

[104] P. Bézier. *Numerical control: Mathematics and applications*. John Wiley & Sons, 1972.

[105] X. Da, O. Harib, R. Hartley, B. Griffin, and J. W. Grizzle. From 2D design of underactuated bipedal gaits to 3D implementation: Walking with speed tracking. *IEEE Access*, 4:3469–3478, 2016.

[106] B. Griffin and J. Grizzle. Nonholonomic virtual constraints for dynamic walking. In *Proc. IEEE Conference on Decision and Control*, pages 4053–4060, 2015.

[107] S. Kolathaya, A. Hereid, and A. D. Ames. Time dependent control Lyapunov functions and hybrid zero dynamics for stable robotic locomotion. In *Proc.of American Control Conference*, pages 3916–3921, 2016.

[108] B. Morris and J. W. Grizzle. A restricted Poincaré map for determining exponentially stable periodic orbits in systems with impulse effects: Application to bipedal robots. In *Proc. of IEEE International Conference on Decision and Control*, pages 4199–4206, 2005.

[109] B. Morris and J. W. Grizzle. Hybrid invariance in bipedal robots with series compliant actuators. In *Proc. of IEEE Conference on Decision and Control*, pages 4793–4800, 2006.

[110] A. D. Ames, K. Galloway, K. Sreenath, and J. W. Grizzle. Rapidly exponentially stabilizing control Lyapunov functions and hybrid zero dynamics. *IEEE Transaction on Automatic Control*, 59(4):876–891, 2014.

[111] A. D. Ames, E. A. Cousineau, and M. J. Powell. Dynamically stable bipedal robotic walking with NAO via human-inspired hybrid zero dynamics. In *Proc. of International Conference on Hybrid Systems: Computation and Control*, pages 135–144, 2012.

[112] A. D. Ames. Human-inspired control of bipedal walking robots. *IEEE Transactions on Automatic Control*, 59(5):1115–1130, 2014.

[113] A. D. Ames. First steps toward automatically generating bipedal robotic walking from human data. In *Robot Motion and Control*, pages 89–116. Springer, 2012.

[114] I. Poulakakis and J. W. Grizzle. The spring loaded inverted pendulum as the hybrid zero dynamics of an asymmetric hopper. *IEEE Transactions on Automatic Control*, 54(8):1779–1793, 2009.

[115] I. Poulakakis and J. W. Grizzle. Modeling and control of the monopedal robot thumper. In *Proc. of IEEE International Conference on Robotics and Automation*, pages 3327–3334, 2009.

[116] I. Poulakakis. *Stabilizing monopedal robot running: Reduction-by-feedback and compliant hybrid zero dynamics*. PhD thesis, University of Michigan, 2009.

[117] B. Morris, E. R. Westervelt, C. Chevallereau, G. Buche, and J. W. Grizzle. Achieving bipedal running with RABBIT: Six steps toward infinity. In *Fast Motions in Biomechanics and Robotics*, pages 277–297. Springer, 2006.

[118] K. Sreenath, H.-W. Park, I. Poulakakis, and J. W. Grizzle. Embedding active force control within the compliant hybrid zero dynamics to achieve stable, fast running on MABEL. *The International Journal of Robotics Research*, 32(3):324–345, 2013.

[119] J. W. Grizzle, C. Chevallereau, and C.-L. Shih. HZD-based control of a five-link underactuated 3D bipedal robot. In *Proc. of IEEE Conference on Decision and Control*, pages 5206–5213, 2008.

[120] J. W. Grizzle, C. Chevallereau, A. D. Ames, and R. W. Sinnet. 3D bipedal robotic walking: Models, feedback control, and open problems. *IFAC Proceedings Volumes*, 43(14):505–532, 2010.

[121] C. Chevallereau, J. W. Grizzle, and C.-L. Shih. Steering of a 3D bipedal robot with an underactuated ankle. In *Proc. of IEEE International Conference on Intelligent Robots and Systems*, pages 1242–1247, 2010.

[122] C. Chevallereau, J. W. Grizzle, and C.-L. Shih. Asymptotically stable walking of a five-link underactuated 3-d bipedal robot. *IEEE Transactions on Robotics*, 25(1):37–50, 2009.

[123] C.-L. Shih, J. W. Grizzle, and C. Chevallereau. From stable walking to steering of a 3D bipedal robot with passive point feet. *Robotica*, 30(07):1119–1130, 2012.

[124] K. A. Hamed and J. W. Grizzle. Event-based stabilization of periodic orbits for underactuated 3-D bipedal robots with left-right symmetry. *IEEE Transactions on Robotics*, 30(2):365–381, 2014.

[125] T Yang, E. R. Westervelt, and A. Serrani. A framework for the control of stable aperiodic walking in underactuated planar bipeds. In *Proc. of IEEE International Conference on Robotics and Automation*, pages 4661–4666, 2007.

[126] S. N. Yadukumar, M. Pasupuleti, and A. D. Ames. Human-inspired underactuated bipedal robotic walking with AMBER on flat-ground, up-slope and uneven terrain. In *Proc. of IEEE International Conference on Intelligent Robots and Systems*, pages 2478–2483, 2012.

[127] S. Kolathaya and A. D. Ames. Achieving bipedal locomotion on rough terrain through human-inspired control. In *Proc. of IEEE International Symposium on Safety, Security, and Rescue Robotics*, pages 1–6, 2012.

[128] H.-W. Park, A. Ramezani, and J. W. Grizzle. A finite-state machine for accommodating unexpected large ground-height variations in bipedal robot walking. *IEEE Transactions on Robotics*, 29(2):331–345, 2013.

[129] B. Griffin and J. Grizzle. Walking gait optimization for accommodation of unknown terrain height variations. In *Proc. of American Control Conference*, pages 4810–4817, 2015.

[130] A. Hereid, S. Kolathaya, M. S. Jones, J. Van Why, J. W. Hurst, and A. D. Ames. Dynamic multi-domain bipedal walking with ATRIAS through SLIP based human-inspired control. In *Proc. of International Conference on Hybrid Systems: Computation and Control*, pages 263–272, 2014.

[131] J. H. Choi and J. W. Grizzle. Planar bipedal walking with foot rotation. In *Proc. of American Control Conference*, pages 4909–4916, 2005.

[132] J. H. Choi and J. W. Grizzle. Feedback control of an underactuated planar bipedal robot with impulsive foot action. *Robotica*, 23(05):567–580, 2005.

[133] C. Chevallereau, D. Djoudi, and J. W. Grizzle. Stable bipedal walking with foot rotation through direct regulation of the Zero Moment Point. *IEEE Transactions on Robotics*, 24(2):390–401, 2008.

[134] A. E. Martin, D. C. Post, and J. P. Schmiedeler. Design and experimental implementation of a hybrid zero dynamics-based controller for planar bipeds with curved feet. *The International Journal of Robotics Research*, 33(7):988–1005, 2014.

[135] R. D. Gregg, T. Lenzi, L. J. Hargrove, and J. W. Sensinger. Virtual constraint control of a powered prosthetic leg: From simulation to experiments with transfemoral amputees. *IEEE Transactions on Robotics*, 30(6):1455–1471, 2014.

[136] A. E. Martin, D. C. Post, and J. P. Schmiedeler. The effects of foot geometric properties on the gait of planar bipeds walking under HZD-based control. *The International Journal of Robotics Research*, 33(12):1530–1543, 2014.

[137] A. Agrawal, O. Harib, A. Hereid, S. Finet, M. Masselin, L. Praly, A. Ames, K. Sreenath, and J. Grizzle. First steps towards translating HZD control of bipedal robots to decentralized control of exoskeletons. *IEEE Access*, 2017.

[138] K. Galloway, K. Sreenath, A. D. Ames, and J. W. Grizzle. Torque saturation in bipedal robotic walking through control Lyapunov function-based quadratic programs. *IEEE Access*, 3:323–332, 2015.

[139] T. Yang, E. R. Westervelt, and A. Serrani. A framework for the control of stable aperiodic walking in underactuated planar bipeds. In *Proc. of IEEE International Conference on Robotics and Automation*, pages 4661–4666, 2007.

[140] Y. Gu, B. Yao, and C. S. G Lee. Bipedal gait recharacterization and walking encoding generalization for stable dynamic walking. In *Proc. of IEEE International Conference on Robotics and Automation*, pages 1788–1793, 2016.

[141] Y. Gu, B. Yao, and C. S. G Lee. Exponential stabilization of fully actuated planar bipedal robotic walking with global position tracking capabilities. *Journal of Dynamic Systems, Measurement, and Control (submitted)*, 2017.

[142] Yan Gu, Bin Yao, and C. S. George Lee. Time-dependent orbital stabilization of underactuated bipedal walking. In *Proc. of American Control Conference*, pages 4858–4863, 2017.

[143] Y. Gu, B. Yao, and C. S. G Lee. Time-dependent orbital stabilization of underactuated bipedal walking. In *Automatica (submitted)*, 2017.

[144] K. A. Hamed, B. G. Buss, and J. W. Grizzle. Exponentially stabilizing continuous-time controllers for periodic orbits of hybrid systems: Application to bipedal locomotion with ground height variations. *The International Journal of Robotics Research*, 35(8):977–999, 2016.

[145] N. Naksuk and C. S. G. Lee. Zero Moment Point manipulability ellipsoid. In *Proc. of IEEE International Conference on Robotics and Automation*, pages 1970–1975, 2006.

[146] S. Cotton, P. Fraisse, and A. P. Murray. On the manipulability of the center of mass of humanoid robots: Application to design. In *Proc. of ASME International Design Engineering Technical Conferences and Computers and Information in Engineering Conference*, pages 1259–1267, 2010.

[147] T. Yoshikawa. Dynamic manipulability of robot manipulators. In *Proc. of IEEE International Conference on Robotics and Automation*, pages 1033–1038, 1985.

[148] T. J. Graettinger and B. H. Krogh. The acceleration radius: A global performance measure for robotic manipulators. *IEEE Journal of Robotics and Automation*, 4(1):60–69, 1988.

[149] P. Chiacchio, S. Chiaverini, L. Sciavicco, and B. Siciliano. Influence of gravity on the manipulability ellipsoid for robot arms. *Journal of Dynamic Systems, Measurement, and Control*, 114(4):723–727, 1992.

[150] P. Chiacchio. A new dynamic manipulability ellipsoid for redundant manipulators. *Robotica*, 18(04):381–387, 2000.

[151] M. T. Rosenstein and R. A. Grupen. Velocity-dependent dynamic manipulability. In *Proc. of IEEE International Conference on Robotics and Automation*, pages 2424–2429, 2002.

[152] A. Bowling and C. H. Kim. Dynamic performance analysis for non-redundant robotic manipulators in contact. In *Proc. of IEEE International Conference on Robotics and Automation*, pages 4048–4053, 2003.

[153] C. H. Kim and A. Bowling. Influence of end-effector velocities on robotic manipulator dynamic performance: An analytical approach. In *Proc. of ASME International Design Engineering Technical Conferences and Computers and Information in Engineering Conference*, pages 1231–1237, 2003.

[154] T. Yamawaki and M. Yashima. Effect of gravity on manipulation performance of a robotic arm. In *Proc. of IEEE International Conference on Robotics and Automation*, pages 4407–4413, 2007.

[155] Y. C. Pai and K. Iqbal. Simulated movement termination for balance recovery: Can movement strategies be sought to maintain stability in the presence of slipping or forced sliding? *Journal of Biomechanics*, 32(8):779–786, 1999.

[156] M. S. Branicky. Multiple Lyapunov functions and other analysis tools for switched and hybrid systems. *IEEE Transaction on Automatic Control*, 43(4):475–482, 1998.

[157] B. Yao, C. Hu, and Q. Wang. An orthogonal global task coordinate frame for contouring control of biaxial systems. *IEEE Transaction on Mechatronics*, 17(4):622–634, 2012.

[158] S. Kajita, F. Kanehiro, K. Kaneko, K. Fujiwara, K. Harada, K. Yokoi, and H. Hirukawa. Biped walking pattern generation by using preview control of Zero-Moment Point. In *Proc. of IEEE International Conference on Robotics and Automation*, pages 1620–1626, 2003.

[159] C. Hu, B. Yao, Q. Wang, Z. Chen, and C. Li. Experimental investigation on high-performance coordinated motion control of high-speed biaxial systems for contouring tasks. *International Journal of Machine Tools and Manufacture*, 51(9):677–686, 2011.

[160] C. Hu, B. Yao, and Q. Wang. Global task coordinate frame-based contouring control of linear-motor-driven biaxial systems with accurate parameter estimations. *IEEE Transactions on Industrial Electronics*, 58(11):5195–5205, 2011.

[161] A. D. Ames, P. Tabuada, A. Jones, W. L. Ma, M. Rungger, B. Schürmann, S. Kolathaya, and J. W. Grizzle. First steps toward formal controller synthesis for bipedal robots with experimental implementation. *Nonlinear Analysis: Hybrid Systems*, 2017.

[162] T. Wang and C. Chevallereau. Stability analysis and time-varying walking control for an under-actuated planar biped robot. *Robotics and Autonomous Systems*, 59(6):444–456, 2011.

[163] P. S. Simeonov and D. D. Bainov. Exponential stability of the solutions of the initial-value problem for systems with impulse effect. *Journal of Computational and Applied Mathematics*, 23(3):353–365, 1988.

[164] A. Hereid, E. A. Cousineau, C. M. Hubicki, and A. D. Ames. 3D dynamic walking with underactuated humanoid robots: A direct collocation framework for optimizing hybrid zero dynamics. In *Proc. of IEEE International Conference on Robotics and Automation*, pages 1447–1454, 2016.

APPENDICES

A. PLANAR WALKING MODEL WITH THREE REVOLUATE JOINTS UNDER LEFT-RIGHT GAIT CHARACTERIZATION

The following denotations are used here:

$$S_i := \sin q_i,$$
$$C_i := \cos q_i,$$
$$S_{ij} := \sin(q_i - q_j),$$
$$C_{ij} := \cos(q_i - q_j),$$

where $i, j \in \{1,2,3\}$.

A.1 Continuous-Time Dynamics

The dynamic matrices in Eq. (3.4) can be derived based on the Lagrange's equations [50]. Details of the model derivation can be found in the reference [50].

The dynamic matrices are given as follows:

$$\mathbf{M}_L(\mathbf{q}) = \begin{bmatrix} (\frac{5}{4}m + M_T + M_H)r^2 & -\frac{1}{2}mr^2C_{12} & M_T rlC_{13} \\ -\frac{1}{2}mr^2C_{12} & \frac{1}{4}mr^2 & 0 \\ M_T rlC_{13} & 0 & M_T l^2 \end{bmatrix},$$

$$\mathbf{c}_L(\mathbf{q}, \dot{\mathbf{q}}) = \begin{bmatrix} -\frac{1}{2}mr^2S_{12}\dot{q}_2^2 + M_T rlS_{13}\dot{q}_3^2 - (\frac{3}{2}m + M_T + M_H)grS_1 \\ \frac{1}{2}mr^2S_{12}\dot{q}_1^2 + \frac{1}{2}mgrS_2 \\ -M_T rlS_{13}\dot{q}_1^2 - M_T glS_3 \end{bmatrix},$$

$$\mathbf{B}_{uL} = \begin{bmatrix} 1 & 0 & -1 \\ 0 & 1 & 0 \\ 0 & -1 & 1 \end{bmatrix},$$

$$\mathbf{u}_L = \begin{bmatrix} u_1 \\ u_3 \\ u_4 \end{bmatrix};$$

$$\mathbf{M}_R(\mathbf{q}) = \begin{bmatrix} -\frac{1}{2}mr^2C_{12} & (\frac{5}{4}m + M_T + M_H)r^2 & M_T rlC_{23} \\ \frac{1}{4}mr^2 & -\frac{1}{2}mr^2C_{12} & 0 \\ 0 & M_T rlC_{23} & M_T l^2 \end{bmatrix},$$

$$\mathbf{c}_R(\mathbf{q}, \dot{\mathbf{q}}) = \begin{bmatrix} \frac{1}{2}mr^2S_{12}\dot{q}_1^2 + M_T rlS_{23}\dot{q}_3^2 - (\frac{3}{2}m + M_T + M_H)grS_2 \\ -\frac{1}{2}mr^2S_{12}\dot{q}_2^2 + \frac{1}{2}mgrS_1 \\ -M_T rlS_{23}\dot{q}_2^2 - M_T glS_3 \end{bmatrix},$$

$$\mathbf{B}_{uR} = \begin{bmatrix} 0 & 0 & -1 \\ 1 & 1 & 0 \\ 0 & -1 & 1 \end{bmatrix},$$

$$\mathbf{u}_R = \begin{bmatrix} u_2 \\ u_3 \\ u_4 \end{bmatrix}.$$

A.2 Reset Map

Derivation of the reset map $\mathbf{\Delta}_i(\mathbf{q}, \dot{\mathbf{q}})$ ($i \in \{L, R\}$) in Eq. (3.4) can be found in the reference [50]. Its expression is given as:

$$\begin{bmatrix} \mathbf{q}^+ \\ \dot{\mathbf{q}}^+ \end{bmatrix} = \mathbf{\Delta}_L(\mathbf{q}^-, \dot{\mathbf{q}}^-) = \begin{bmatrix} q_1^- \\ q_2^- \\ q_3^- \\ \omega_{1L}^+(\mathbf{q}^-, \dot{\mathbf{q}}^-) \\ \omega_{2L}^+(\mathbf{q}^-, \dot{\mathbf{q}}^-) \\ \omega_{3L}^+(\mathbf{q}^-, \dot{\mathbf{q}}^-) \end{bmatrix},$$

where

$$\begin{aligned}
\omega_{1L}^{+}(\mathbf{q},\dot{\mathbf{q}}) =& \frac{1}{a}[m\dot{q}_1 - (4m+4M_H+2M_T)\dot{q}_1\cos(2q_1-2q_2) \\
&+ 2M_T\dot{q}_1\cos(2q_1-2q_3) + 2m\dot{q}_2C_{12}], \\
\omega_{2L}^{+}(\mathbf{q},\dot{\mathbf{q}}) =& \frac{1}{a}[2M_T\dot{q}_1\cos(-q_1+2q_3-q_2) \\
&- (2m+4M_H+2M_T)\dot{q}_1C_{12} + m\dot{q}_2], \\
\omega_{3L}^{+}(\mathbf{q},\dot{\mathbf{q}}) =& \frac{1}{al}[(2mr+2M_Hr+2M_Tr)\dot{q}_1\cos(q_3+q_1-2q_2) \\
&- 2M_Hr\dot{q}_1C_{13} - (2mr+2M_Hr)\dot{q}_1C_{13} \\
&+ mr\dot{q}_1\cos(-3q_1+2q_2+q_3) - rm\dot{q}_2C_{23} \\
&- (3ml+4M_Hl+2M_Tl)\dot{q}_3 + 2ml\dot{q}_3\cos(2q_1-2q_2) \\
&+ 2M_Tl\dot{q}_3cos(-2q_2+2q_3)] \\
a =& -3m-4M_H-2M_T+2m\cos(2q_1-2q_2) \\
&+ 2M_T\cos(-2q_2+2q_3);
\end{aligned}$$

$$\begin{bmatrix}\mathbf{q}^{+}\\ \dot{\mathbf{q}}^{+}\end{bmatrix} = \boldsymbol{\Delta}_R(\mathbf{q}^{-},\dot{\mathbf{q}}^{-}) = \begin{bmatrix} q_1^{-} \\ q_2^{-} \\ q_3^{-} \\ \omega_{1R}^{+}(\mathbf{q}^{-},\dot{\mathbf{q}}^{-}) \\ \omega_{2R}^{+}(\mathbf{q}^{-},\dot{\mathbf{q}}^{-}) \\ \omega_{3R}^{+}(\mathbf{q}^{-},\dot{\mathbf{q}}^{-}) \end{bmatrix}, \tag{A.1}$$

where

$$\begin{aligned}
\omega_{1R}^{+}(\mathbf{q},\dot{\mathbf{q}}) =& \frac{1}{a}[m\dot{q}_2 - (4m+4M_H+2M_T)\dot{q}_2\cos(2q_1-2q_2) \\
&+ 2M_T\dot{q}_2\cos(2q_2-2q_3) + 2m\dot{q}_1C_{12}], \\
\omega_{2R}^{+}(\mathbf{q},\dot{\mathbf{q}}) =& \frac{1}{a}[2M_T\dot{q}_2\cos(-q_2+2q_3-q_1) \\
&- (2m+4M_H+2M_T)\dot{q}_2C_{12} + m\dot{q}_1],
\end{aligned}$$

$$
\begin{aligned}
\omega_{3R}^{+}(\mathbf{q},\dot{\mathbf{q}}) =& \frac{1}{al}[(2mr+2M_Hr+2M_Tr)\dot{q}_2\cos(q_3+q_2-2q_1) \\
& -2M_Hr\dot{q}_2C_{23}-(2mr+2M_Tr)\dot{q}_2C_{23} \\
& +mr\dot{q}_2\cos(-3q_2+2q_1+q_3)-rm\dot{q}_1C_{13} \\
& -(3ml+4M_Hl+2M_Tl)\dot{q}_3+2ml\dot{q}_3\cos(2q_1-2q_2) \\
& +2M_Tl\dot{q}_3\cos(-2q_1+2q_3)], \\
a =& -3m-4M_H-2M_T+2m\cos(2q_1-2q_2) \\
& +2M_T\cos(-2q_1+2q_3).
\end{aligned}
$$

B. INPUT-OUTPUT LINEARIZATION

The expressions of $\mathbf{P}_i$ and $\mathbf{z}_i$, $i \in \{L, R\}$, in Eq. (3.13) are given as follows:

$$\mathbf{P}_L = \begin{bmatrix} 1 & 0 & 0 \\ -\frac{d\tilde{\phi}_{1L}}{dq_1} & 1 & 0 \\ -\frac{d\tilde{\phi}_{2L}}{dq_1} & 0 & 1 \end{bmatrix};$$

$$\mathbf{z}_L = \begin{bmatrix} \ddot{q}_{1d} \\ \frac{d^2\tilde{\phi}_{1L}}{dq_1^2}\dot{q}_1^2 \\ \frac{d^2\tilde{\phi}_{2L}}{dq_1^2}\dot{q}_1^2 \end{bmatrix};$$

$$\mathbf{P}_R = \begin{bmatrix} 1 & -\frac{d\tilde{\phi}_{1R}}{dq_2} & 0 \\ 0 & 1 & 0 \\ 0 & -\frac{d\tilde{\phi}_{2R}}{dq_2} & 1 \end{bmatrix};$$

$$\mathbf{z}_R = \begin{bmatrix} \frac{d^2\tilde{\phi}_{1R}}{dq_2^2}\dot{q}_2^2 \\ \ddot{q}_{2d} \\ \frac{d^2\tilde{\phi}_{2R}}{dq_2^2}\dot{q}_2^2 \end{bmatrix}.$$

C. PLANAR WALKING MODEL WITH FIVE REVOLUATE JOINTS UNDER SUPPORT-SWING GAIT CHARACTERIZATION

The following denotations are used in this section:

$$S_i := \sin q_i,$$
$$C_i := \cos q_i,$$
$$S_{ij} := \sin(q_i - q_j),$$
$$C_{ij} := \cos(q_i - q_j),$$

where $i, j \in \{1, 2, ..., 5\}$.

C.1 Continuous-Time Dynamics

The dynamic matrices in Eq. (5.3) can be derived based on the Lagrange's equations [50]. Their expressions are given as follows.

$$\mathbf{M}(\mathbf{q}) = [m_{ij}(\mathbf{q})],\ i, j \in \{1, 2, ..., 5\}, \tag{C.1}$$

where

$$\begin{aligned}
m_{11} &= \frac{1}{4}(5m_1 + 8m_2 + 4M_H + 4M_T)l_1^2, \\
m_{12} = m_{21} &= \frac{1}{2}(2m_1 + 3m_2 + 2M_H + 2M_T)l_1 l_2 C_{12}, \\
m_{13} = m_{31} &= \frac{1}{2}M_T r l_1 C_{13}, \\
m_{14} = m_{41} &= -\frac{1}{2}(2m_1 + m_2)l_1 l_2 C_{14}, \\
m_{15} = m_{51} &= -\frac{1}{2}m_1 l_1^2 C_{15}, \\
m_{22} &= \frac{1}{4}(4m_1 + 5m_2 + 4M_H + 4M_T)l_2^2,
\end{aligned}$$

$$
\begin{aligned}
m_{23} &= m_{32} = \frac{1}{2} M_T r l_2 C_{23}, \\
m_{24} &= m_{42} = -\frac{1}{2}(2m_1 + m_2) l_2^2 C_{24}, \\
m_{25} &= m_{52} = -\frac{1}{2} m_1 l_1 l_2 C_{25}, \\
m_{33} &= \frac{1}{4} M_T r^2, \\
m_{34} &= m_{43} = 0, \\
m_{35} &= m_{53} = 0, \\
m_{44} &= \frac{1}{4}(4m_1 + m_2) l_2^2, \\
m_{45} &= m_{54} = \frac{1}{2} m_1 l_1 l_2 C_{45}, \\
m_{55} &= \frac{1}{4} m_1 l_1^2.
\end{aligned}
$$

$$
\mathbf{c}(\mathbf{q}, \dot{\mathbf{q}}) = \mathbf{C}(\dot{\mathbf{q}})\dot{\mathbf{q}} + \mathbf{G}(\mathbf{q}),\ i \in \{1, 2, ..., 5\}, \tag{C.2}
$$

where

$$
\mathbf{C}(\mathbf{q}) = [c_{ij}(\mathbf{q})],\ i, j \in \{1, 2, ..., 5\}, \tag{C.3}
$$

with

$$
\begin{aligned}
c_{11} &= 0, \\
c_{12} &= \frac{1}{2}(2m_1 + 3m_2 + 2M_H + 2M_T) l_1 l_2 S_{12} \dot{q}_2, \\
c_{13} &= \frac{1}{2} M_T r l_1 S_{13} \dot{q}_3, \\
c_{14} &= -\frac{1}{2}(2m_1 l_2 + m_2 l_2) 1_1 S_{14} \dot{q}_4, \\
c_{15} &= -\frac{1}{2} m_1 l_1^2 S_{15} \dot{q}_5, \\
c_{21} &= -\frac{1}{2}(2m_1 + 3m_2 + 2M_H + 2M_T) l_1 l_2 S_{12} \dot{q}_1, \\
c_{22} &= 0, \\
c_{23} &= \frac{1}{2} M_T r l_2 S_{23} \dot{q}_3, \\
c_{24} &= -\frac{1}{2}(2m_1 + m_2) l_2^2 S_{24} \dot{q}_4,
\end{aligned}
$$

$$
\begin{aligned}
c_{25} &= -\frac{1}{2} m_1 l_1 l_2 S_{25} \dot{q}_5, \\
c_{31} &= -\frac{1}{2} M_T r l_1 S_{13} \dot{q}_1, \\
c_{32} &= -\frac{1}{2} M_T r l_2 S_{23} \dot{q}_2, \\
c_{33} &= 0, \\
c_{34} &= 0, \\
c_{35} &= 0, \\
c_{41} &= \frac{1}{2} (2m_1 + m_2) l_1 l_2 S_{14} \dot{q}_1, \\
c_{42} &= \frac{1}{2} (2m_1 + m_2) l_2^2 S_{24} \dot{q}_2, \\
c_{43} &= 0, \\
c_{44} &= 0, \\
c_{45} &= \frac{1}{2} m_1 l_1 l_2 S_{45} \dot{q}_5, \\
c_{51} &= \frac{1}{2} m_1 l_1^2 S_{15} \dot{q}_1, \\
c_{52} &= \frac{1}{2} m_1 l_1 l_2 S_{25} \dot{q}_2, \\
c_{53} &= 0, \\
c_{54} &= -\frac{1}{2} m_1 l_1 l_2 S_{45} \dot{q}_4, \\
c_{55} &= 0,
\end{aligned}
$$

and

$$
\mathbf{G} = \begin{bmatrix}
-\frac{1}{2}(3m_1 + 4m_2 + 2M_H + 2M_T) g l_1 \sin(q_1) \\
-\frac{1}{2}(2m_1 + 3m_2 + 2M_H + 2M_T) g l_2 \sin(q_2) \\
-\frac{1}{2} M_T g r \sin(q_3) \\
\frac{1}{2}(2m_1 + m_2) g l_2 \sin(q_4) \\
\frac{1}{2} m_1 g l_1 \sin(q_5)
\end{bmatrix}.
$$

$$\mathbf{B}_u = \begin{bmatrix} 1 & 0 & 0 & 0 \\ -1 & 1 & 0 & 0 \\ 0 & -1 & 1 & 0 \\ 0 & 0 & -1 & 1 \\ 0 & 0 & 0 & -1 \end{bmatrix}. \tag{C.4}$$

C.2 Reset Map

The reset map $\boldsymbol{\Delta}(\mathbf{q}, \dot{\mathbf{q}})$ in Eq. (5.3) includes a coordinate swap and the rigid-body impact dynamics. Because the impact involves the motion of the point feet, an extended set of generalized coordinates are needed to derive $\boldsymbol{\Delta}(\mathbf{q}, \dot{\mathbf{q}})$, which includes the support foot's position $\mathbf{p} = (p_x, p_z)$ in the world coordinate frame $X_w O Z_w$ in Fig. 5.2. Let $Q_e \subset \mathbb{R}^7$ be the extended configuration space. Let $\mathbf{q}_e \in Q_e$ be the extended generalized coordinates:

$$\mathbf{q}_e = \begin{bmatrix} \mathbf{q} \\ p_x \\ p_z \end{bmatrix} := \begin{bmatrix} \mathbf{q} \\ \mathbf{p} \end{bmatrix}.$$

The impact is assumed to be instant with an impulse effect, and the swing foot remains in static contact with the ground upon impact. Based on the derivations in the previous study [50], one has

$$\begin{bmatrix} \boldsymbol{\omega}_e^+ \\ \mathbf{F}_{sw} \end{bmatrix} = \begin{bmatrix} \mathbf{M}_e(\mathbf{q}) & -\mathbf{J}_{sw}^T(\mathbf{q}) \\ \mathbf{J}_{sw}(\mathbf{q}) & \mathbf{0}_{2\times 2} \end{bmatrix}^{-1} \begin{bmatrix} \mathbf{M}_e(\mathbf{q})\dot{\mathbf{q}}_e \\ \mathbf{0}_{2\times 1} \end{bmatrix}, \tag{C.5}$$

where $\boldsymbol{\omega}_e^+$ represents the first derivatives of the extended coordinates right after an impact, $\mathbf{F}_{sw} \in \mathbb{R}^2$ is the impulse force at the swing foot, $\mathbf{M}_e : Q \to \mathbb{R}^{7\times 7}$ is the extended inertia matrix, and $\mathbf{J}_{sw} : Q \to \mathbb{R}^{2\times 7}$ is the Jacobian matrix relating $\dot{\mathbf{q}}_e$ to the swing foot velocity. The upper-left 5×5 block of $\mathbf{M}_e = [m_{ij}]$ $(i, j \in \{1, 2, ..., 7\})$ is $\mathbf{M}$, and the other elements are:

$$m_{16} = m_{61} = \frac{1}{2}(3M_1 + 4M_2 + 2M_H + 2M_T) l_1 C_1,$$
$$m_{17} = m_{71} = -\frac{1}{2}(3M_1 + 4M_2 + 2M_H + 2M_T) l_1 S_1,$$

$$
\begin{aligned}
m_{26} &= m_{62} = \frac{1}{2}(2m_1 + 3m_2 + 2M_H + 2M_T) l_2 C_2, \\
m_{27} &= m_{72} = -\frac{1}{2}(2m_1 + 3m_2 + 2M_H + 2M_T) l_2 S_2, \\
m_{36} &= m_{64} = m_{63} = \frac{1}{2} M_T r C_3, \\
m_{37} &= m_{73} = -\frac{1}{2} M_T r S_3, \\
m_{46} &= -\frac{1}{2}(2m_1 + m_2) l_2 C_4, \\
m_{47} &= m_{74} = \frac{1}{2}(2m_1 + m_2) l_2 S_4, \\
m_{56} &= m_{65} = -\frac{1}{2} m_1 l_1 C_5, \\
m_{57} &= m_{75} = \frac{1}{2} m_1 l_1 S_5, \\
m_{66} &= 2m_1 + 2m_2 + M_H + M_T, \\
m_{67} &= m_{76} = 0, \\
m_{77} &= 2m_1 + 2m_2 + M_H + M_T.
\end{aligned}
$$

The Jacobian matrix $\mathbf{J}_{sw}$ is defined as

$$
\mathbf{J}_{sw} = \begin{bmatrix} l_1 C_1 & l_2 C_2 & 0 & -l_2 C_4 & -l_1 C_5 & 1 & 0 \\ -l_1 S_1 & -l_2 S_2 & 0 & l_2 C_4 & l_1 C_5 & 0 & 1 \end{bmatrix}. \tag{C.6}
$$

Then, the reset map $\boldsymbol{\Delta}(\mathbf{q}, \dot{\mathbf{q}})$ is defined as

$$
\boldsymbol{\Delta}(\mathbf{q}, \dot{\mathbf{q}}) = \begin{bmatrix} \mathbf{R} & \mathbf{0}_{5\times 5} \\ \mathbf{0}_{5\times 5} & \mathbf{R} \end{bmatrix} \begin{bmatrix} \mathbf{q} \\ \boldsymbol{\omega}^+ \end{bmatrix}, \tag{C.7}
$$

where

$$
\mathbf{R} = \begin{bmatrix} 0 & 0 & 0 & 0 & 1 \\ 0 & 0 & 0 & 1 & 0 \\ 0 & 0 & 1 & 0 & 0 \\ 0 & 1 & 0 & 0 & 0 \\ 1 & 0 & 0 & 0 & 0 \end{bmatrix} \tag{C.8}
$$

represents the coordinate swap caused by the role switching between the support and the swing legs and $\boldsymbol{\omega}$ is the vector of the first seven elements of $\boldsymbol{\omega}_e$.

D. STATE-SPACE REPRESENTATION OF CLOSED-LOOP DYNAMICS

The expression of $\mathbf{f}(t,\mathbf{x})$ in Eq. (5.28) is given as follows:

$$\mathbf{f}(t,\mathbf{x}) := \begin{bmatrix} \mathbf{f}_1(t,\mathbf{x}) \\ \mathbf{f}_2(t,\mathbf{x}) \end{bmatrix} \tag{D.1}$$

with

$$\begin{aligned} \mathbf{f}_1(t,\mathbf{x}) :=& \mathbf{x}_2, \\ \mathbf{f}_2(t,\mathbf{x}) :=& \mathbf{M}_T^{-1}[\mathbf{B}_u(\mathbf{H}\mathbf{M}_T^{-1}\mathbf{B}_u)^{-1}(-\mathbf{K}_P\mathbf{H}(\mathbf{x}_1 - \mathbf{q}_{Td}) \\ & - \mathbf{K}_D\mathbf{H}(\mathbf{x}_2 - \dot{\mathbf{q}}_{Td}) + \mathbf{H}(\mathbf{M}_T^{-1}\mathbf{h}_T + \ddot{\mathbf{q}}_{Td}) - \mathbf{h}_T]. \end{aligned} \tag{D.2}$$

Define $\mathbf{I}_q(\mathbf{q},\dot{\mathbf{q}})$ as

$$\mathbf{I}_q(\mathbf{q},\dot{\mathbf{q}}) = \boldsymbol{\Delta}(\mathbf{q},\dot{\mathbf{q}}) - \begin{bmatrix} \mathbf{q} \\ \dot{\mathbf{q}} \end{bmatrix}. \tag{D.3}$$

Then, the reset map $\mathbf{I}(\mathbf{x})$ can be obtained from $\mathbf{I}_q(\mathbf{q},\dot{\mathbf{q}})$ as

$$\mathbf{I}(\mathbf{x}) := \begin{bmatrix} \mathbf{H}_T & \mathbf{0}_{5\times5} \\ \mathbf{0}_{5\times5} & \mathbf{H}_T \end{bmatrix} \mathbf{I}_q(\mathbf{H}_T^{-1}\mathbf{x}_1, \mathbf{H}_T^{-1}\mathbf{x}_2). \tag{D.4}$$

E. AUGMENTED AUTONOMOUS SYSTEM

The function $\mathbf{g}(\rho,\mathbf{x})$ in Eq. (5.36) is defined as:

$$\mathbf{g}(\rho,\mathbf{x}) := \begin{bmatrix} \mathbf{g}_1(\rho,\mathbf{x}) \\ \mathbf{g}_2(\rho,\mathbf{x}) \end{bmatrix} \tag{E.1}$$

with

$$\begin{aligned} \mathbf{g}_1(\rho,\mathbf{x}) :=& \mathbf{x}_2, \\ \mathbf{g}_2(\rho,\mathbf{x}) :=& \mathbf{M}_T^{-1}[\mathbf{B}_u(\mathbf{H}\mathbf{M}_T^{-1}\mathbf{B}_u)^{-1}(-\mathbf{K}_P\mathbf{H}(\mathbf{x}_1-\mathbf{H}_T\mathbf{q}_0(\rho)) \\ & -\mathbf{K}_D\mathbf{H}(\mathbf{x}_2-\mathbf{H}_T\dot{\mathbf{q}}_0(\rho))+\mathbf{H}(\mathbf{M}_T^{-1}\mathbf{h}_T+\mathbf{H}_T\ddot{\mathbf{q}}_0(\rho)) \\ & -\mathbf{h}_T], \end{aligned} \tag{E.2}$$

where $\dot{\mathbf{q}}_0(\rho)=\frac{\partial \mathbf{q}_0(\rho)}{\partial \rho}\dot{\rho}$ and $\ddot{\mathbf{q}}_0(\rho)=\frac{\partial^2 \mathbf{q}_0(\rho)}{\partial \rho^2}\dot{\rho}^2+\frac{\partial \mathbf{q}_0(\rho)}{\partial \rho}\ddot{\rho}$.

VITA

VITA

Yan Gu was born on November 10th, 1988 in Handan, China. She received a B.S. degree in Mechanical Engineering from Zhejiang University (Hangzhou, China) in 2011. After her undergraduate studies, Yan was admitted to the direct Ph.D. program in the School of Mechanical Engineering at Purdue University. After graduating with her Ph.D. degree, Yan will join the faculty of the Department of Mechanical Engineering at the University of Massachusetts Lowell in September 2017.